OIL FILM BEARINGS APPLIED TO HEAVY DUTY ROLLING MILL DRIVE COUPLINGS.

by

J. F. Perez Gomez BSc. Mech. Eng.

being a thesis submited for the CNAA degree of

MASTER OF PHILOSOPHY

Department of Mechanical &
Production Engineering
Sheffield City Polytechnic
and the collaborating
establishment
Davy Loewy Ltd. Sheffield.

June 1982

ProQuest LLC.
789 East Eisenhower Parkway
P.O. Box 1346
Ann Arbor, MI 48106 – 1346

A C K N O W L E D G E M E N T S.

I am greatly indebted to Davy Loewy Ltd. for being given the opportunity to work on this project and for the financial support, also to CONACYT (Consejo Nacional de Ciencia y Tecnologia, Mexico) for the scholarship enjoyed during the period of study.

I acknowledge the valuable assistance of my principal supervisor Mr. G. Cockerham B.Tech (Hons), M.Phil, CEng MIMechE. and to Dr. G. R. Symmons BSc. PhD. MIMechE. CEng. and Mr. D. R. Howard B.Eng. CEng. MIMechE. who have kindly read the entire manuscript and contributed useful comments. Special thanks are due to Mr. F. Clarke for his efforts in making the test rig, to Mr. R. Teasdale, Chief Technician for his kind cooperation, to Mr. R. Wilkinson for preparing the electronic equipment and to Mr. L. Evans for supplying and assembling the hydraulic system. Also, to Mobil-Oil Co. Ltd for supplying the test lubricant.

My sincere gratitude together with that of my family is expresed to Mr. D. R. Howard, Manager of Research and Development at Davy Loewy Ltd. for his always generous aid, since without it this invaluable experience acquired for us in this country, would never have been achieved.

Lastly this thesis is dedicated: to the memory of my grandmother Celica and my son Francisco, to my parents Jose and Lilia, to my parents in law Efrain and Ma. Victoria, to my brothers and sisters, to my brothers in law, to my children Jorge and Patricia and to my wife Patricia for her encouraging support, patience and also for typing the present work.

Heavy Duty Rolling Mill Drive Couplings

J F Perez Gomez

SUMMARY

The present work describes an investigation related to rolling mill drive-lines in the Steel Industry with special reference to Hooke's joint couplings. This coupling transmits the torque and the rotational motion, required for the rolling process, and contains four bearings which are under oscillating motion. Together with the impact loads often found in rolling mills this provides a severe operating environment which has been simulated to permit an experimental investigation of the suitability of oil film bearings for such applications.

In the rig, displacements of the shaft centre, i.e. locus path or eccentricity, have been recorded versus load levels and frequencies of oscillation or rotational speeds for constant oil inlet pressure. Three different types of oil lubricant bearings have been tested under the adverse conditions of dynamic load and oscillating motion, but less severe tests for conditions of continuous motion and static load were also carried out to give reference of the behaviour of such bearings.

Comparisons have been obtained between hydrodynamic bearings with axial and circumferential grooving and slot entry hybrid bearings, showing the latter to be suited to the particular application considered. Results have been compared with existing design procedures suitably modified to take account of the adverse operating conditions.

C O N T E N T S

LIST OF FIGURES

N O M E N C L A T U R E

Unless otherwise specified, the following symbols are used in the text:

$C_{d,r}$	Bearing diametral and radial clearance
D	Bearing diameter
L	Bearing length
N	Shaft rotational speed
$\bar{N}$	Average oscillating speed
P	Rolling load
P_s	Supply pressure
U	Bearing sliding speed
V	Tangential velocity
W	Bearing load
$\bar{W}$	Fuller number $= \dfrac{W}{P_s LD}$
a	Bearing axial land width
e	Eccentricity between bearing and the shaft centres
h	Oil film thickness
p	Fluid film pressure
q	Lubrication supply flow rate
α_1	Angular acceleration of output shaft
α_2	Angular coordinate of the arc of contact
δ	Angle between shafts
Δ	Ocvirk number or capacity number $= \dfrac{W}{\pi \eta NLD} \left(\dfrac{C_d}{D}\right)^2 \left(\dfrac{D}{L}\right)^2$
$\bar{\Delta}$	Ocvirk number for oscillating bearing $= \dfrac{W}{\pi \eta LD\bar{N}} \left(\dfrac{C_d}{D}\right)^2 \left(\dfrac{D}{L}\right)^2$

ϵ	Eccentricity ratio ($= 2e/C_d$)
η	Dynamic viscosity
θ	Angular displacement of the input shaft
θ_1	Angular position round bearing circumference
ϕ_1	Angular displacement of the output shaft
ϕ	Attitude angle
ψ	Pin-angular displacement
ω	Angular velocity of the input (driving) shaft
ω_1	Angular velocity of the output (driven) shaft

CHAPTER 1. INTRODUCTION.

1.1 Background to investigation.

It is apparent that the use of universal or Hooke joints for the transfer of high power in rolling mill drives has significant advantages over the existing coupling designs. Development of this joint is less than a decade old and much work is still being undertaken (1)*.

A common feature of these joints is the use of needle or roller bearings to support the cross-pin or trunnions. However, under certain operating conditions such as severe dynamic and transient effects present in the rolling mill transmission, these roller bearings may give rise to problems such as brinneling fatigue. It is for this reason that the collaborating company Davy-Loewy Ltd, has proposed the potential use of oil film bearings in such joints as an alternative solution to extend the life of the bearing and the coupling. In addition needle bearings have lower torque capacity than similar-sized plain bearings joints, and needle bearings are more expensive than the simpler plain bearings.

Thus, after the joint is adequately designed for all its stresses -static and dynamic-, it becomes a matter of application of the bearings. Roller bearings for this type of application are difficult to specify, so the universal joint industry has had to develop its own dynamic factor for trunnion bearings by running many hundreds of hours of tests on many joints.

---

* Numerical references are listed in chapter 7.

This has been done by testing complete universal joints on four square testing machines under actual running conditions (2).

The universal joint is considered generally to have the weakest point at the cross-pin and it is well known that the life of the bearing will determine the life of the joint (3). The bearings represent a special problem because of the nature of the relative motion between the cross-pin and the bearings, which reverses twice per revolution of the joint. A study of oscillating bearings is an essential preliminary to any attempt to predict the performance of these components.

Much theoretical and experimental work has been carried out for hydrodynamic bearings under steady/dynamic loading and continuous motion (4), (5), (6), but less effort has been directed to this particular case of a bearing loaded in a complex dynamic mode together with oscillating motion, such as occurs in a universal coupling in rolling mill transmision.

In such a case the plain bearing life could be limited by material fatigue, and it is probable that a knowledge of the hydrodynamic performance of the bearing would enable designers to reduce the peak stresses in the material by increasing the minimum oil film thickness.

It might happen that a fully hydrodynamic lubrication will breakdown at a certain minimum film thickness, determined by the surface irregularities, suspended particles and cavitation within the lubricant and physical properties of lubricant. A further reduction of oil-

film thickness will make the bearing work under boundary lubrication.

If the bearing is exposed to a dynamic loading another effect will become more apparent. When the load is increased, the two bearing surfaces will approach each other, and the lubricant between them will be "squeezed" outwards. As a consequence, a pressure will be created, the magnitude of which depends on the rate at which the load is applied, the geometry of the surfaces and the viscosity of the lubricant. This effect, sometimes denoted "squeeze-film effect", may substantially increase the load-carrying capacity of the bearing, and is believed under favourable conditions to prevent sliding surfaces of an oscillating bearing from coming into appreciable metallic contact at all, even though the relative tangential motion of these surfaces becomes momentarily zero (7).

Similarly in an oscillating bearing under dynamic loading the same effect may be created when the tangential velocity is rapidly decreasing, causing a relatively rapid radial velocity to be built up, again creating squeeze-film effect.

1.2 Application of Drive Couplings in the Steel Industry.

1.2.1 General.

The initial breakdown of steel ingots into blooms, slabs or billets is generally done by hot-rolling, although these products may also be obtained by continuous casting, followed by further hot-rolling into plate, sheet, rod, bar, pipes, etc.(13).

Cold rolling is also used to produce sheet, strip and foil with good surface finish and increased mechanical strength.

A typical hot-strip mill basically comprises a primary mill or scalebreaker followed by the roughing stands and the finishing tandem mill train (see fig. 1.1).

The material or stock is processed semi-continuosly. It is first heated to rolling temperatures which depend upon the composition of the material and then progressively fed through the stands, emerging as a finished or semi-finished product.

The material enters the first stand at a low speed and travels through the finishing stands, reducing in thickness and increasing in speed, which might be up to 12 m/s when it leaves the last finishing stand.

Rolling mills as single units or stands are classified with respect to the number and arrangement of rolls. A brief description of the most important arrangements is given below and schematically shown in fig. 1.2 (14).

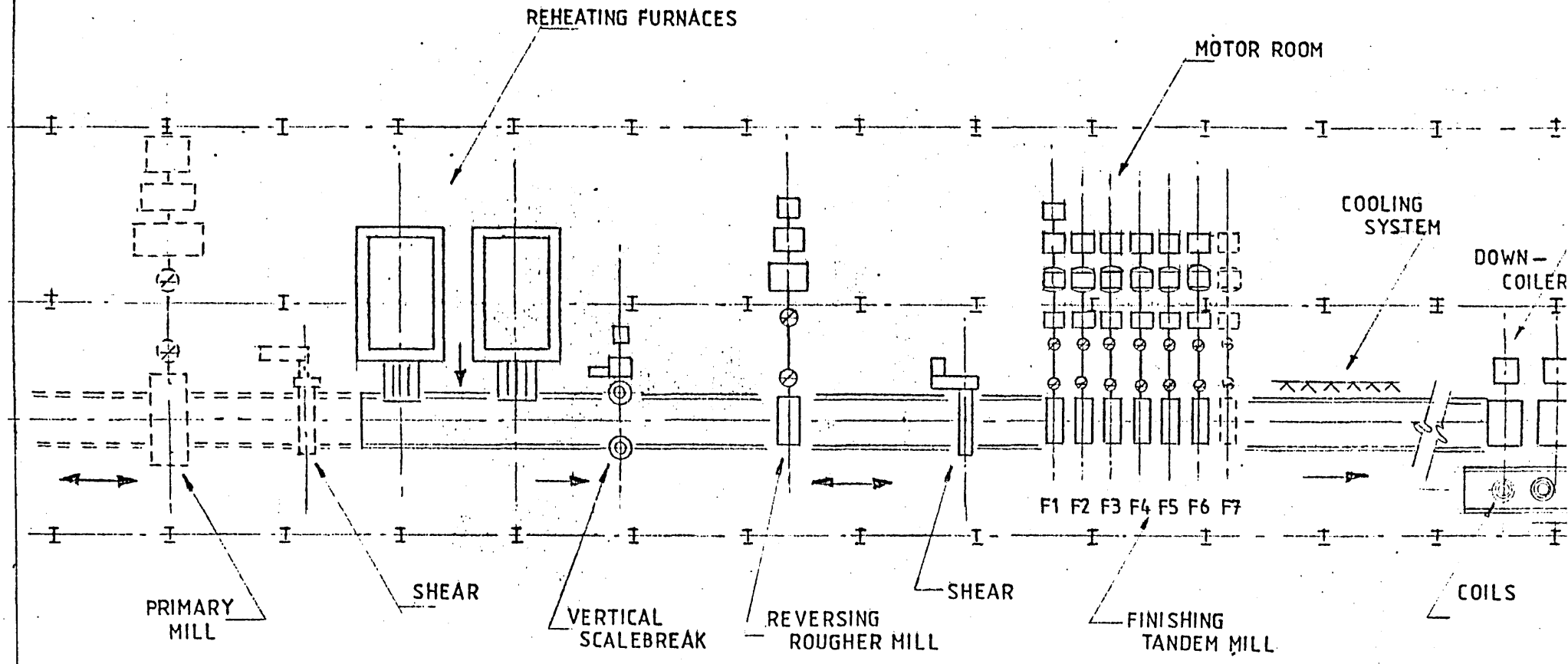

FIG.1.1 TYPICAL HOT STRIP MILL LAYOUT

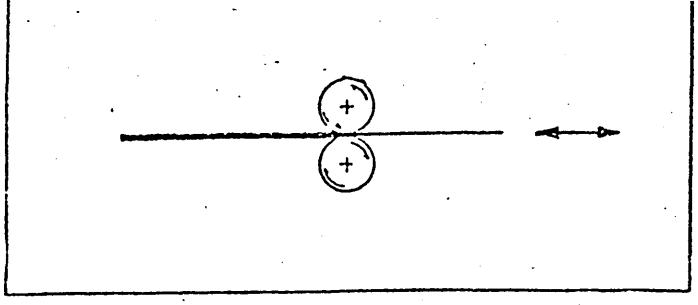

PRIMARY MILL

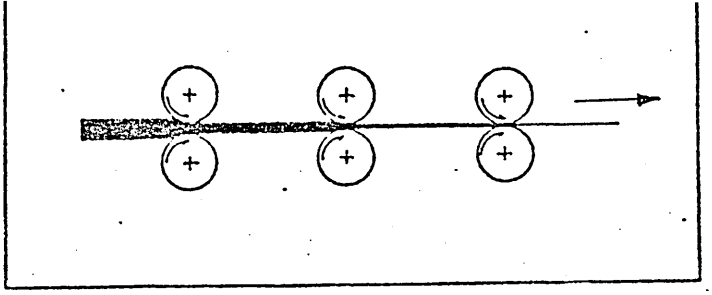

CONTINUOUS 2-HIGH MILLS

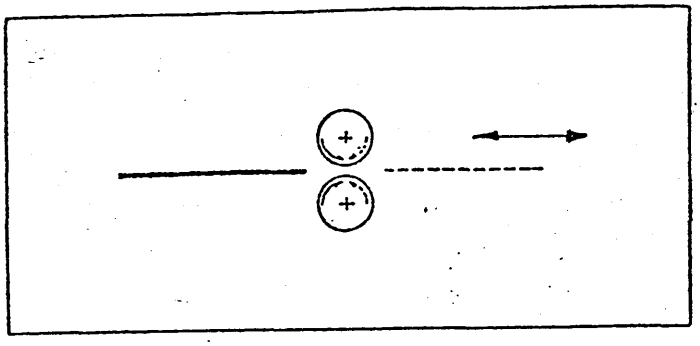

REVERSING 2-HIGH MILL

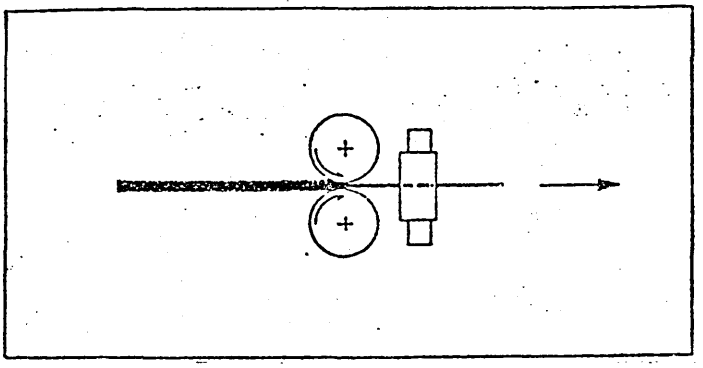

UNIVERSAL MILL

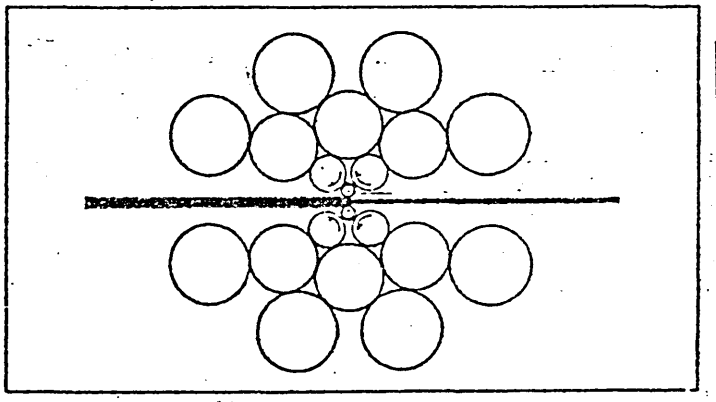

SENDZIMIR MILL

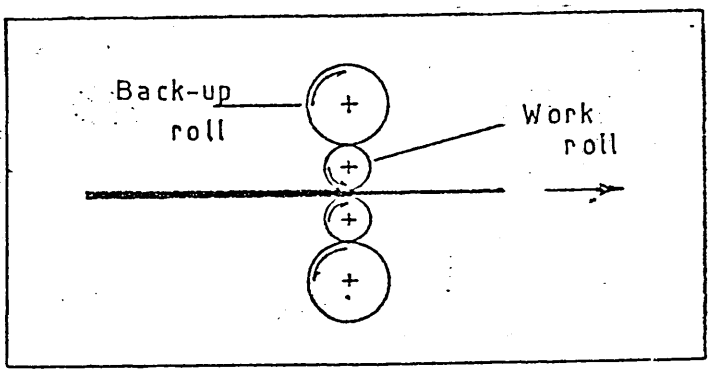

4-HIGH MILL

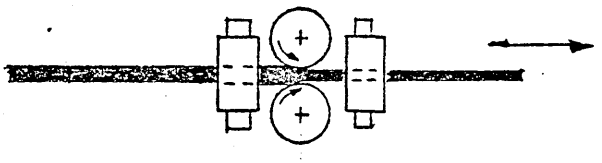

TRIPLET MILL

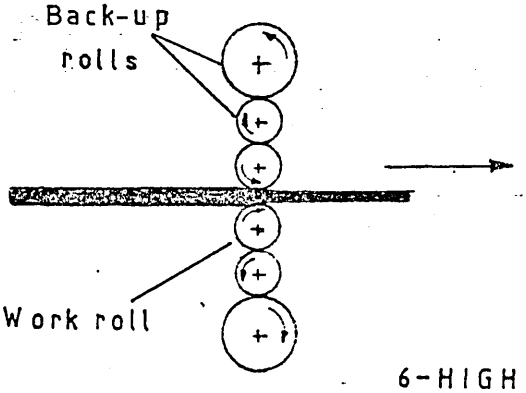

6-HIGH MILL

FIG. 1.2 DIAGRAMATIC ARRANGEMENT OF ROLLING MILLS.

i) Two high mill.- This is the simplest and most common; rolls of equal size are rotated only in one direction. The stock is returned to the entrance of the rolls for further reduction.

ii) Two-high reversing mill.- To improve speed the stock is passed backwards and forwards by the rolls, which change direction of rotation.

iii) Three high mill.- Consists of upper and lower driven rolls and a middle roll which rotates by friction.

iv) Four high mill.- Due to the reduced diameter of the work rolls energy is saved, but they are susceptible to bending and should be supported by large back-up rolls.

v) Cluster/sendzimir mill.- To roll very thin sheet to very close tolerances, by using small rolls, two work rolls and a set of back-up rolls are used. The sendzimir is a modification of the cluster, useful for rolling thin sheet or foil from high-strength alloys.

vi) Triplet mill.- This is a new development for rolling slabs on edge through a vertical-horizontal-vertical reversing mill combination (16).

vii) Six-high mill.- Also a new development, consisting of two work rolls, two intermediate rolls and two back-up rolls. The intermediate rolls may be moved axially to change the effective length of the back-up roll which supports the work roll (17).

1.2.2 Rolling-mill drive system description.

The layout of a stand can of course take many different forms, depending on the type of mill, the means of transmission and the type of rolling process being undertaken. Typical variations are continuous or semicontinuous mills compared with single stand, reversing mills, and the types of transmissions can involve a single motor driving the mill or each stand with its own motor, with the orientation of the drive being from above, below or from the side of the roll stand (13).

Thus, a rolling mill drive consists basically of a pair of rolls. i.e. work rolls,driven by a D. C. motor through a gear box, pinion stand and two drive shafts or spindles interconnected by means of universal couplings. A diagramatic arrangement of the system is shown in fig. 1.3.

The aim of the drive-line is to provide a work roll peripheral velocity sufficient to perform the work reduction. The requirements of the spindle and coupling might generally be described as a means of transmitting a flexible drive between the pinion box and the roll assembly, allowing for variable angular and axial displacements whilst remaining torsionally rigid to prevent slack or play instigating transmission wind up leading to "roll chatter" (18).

Adjacent to the roll is a universal coupling with an adaptor sleeve, which allows the necessary variation in horizontal alignment to accommodate automatic roll changing equipment. The spindle follows the universal coupling, which can be self-supporting or supported by a permanent or movable assembly, depending on the particular stand requirements.

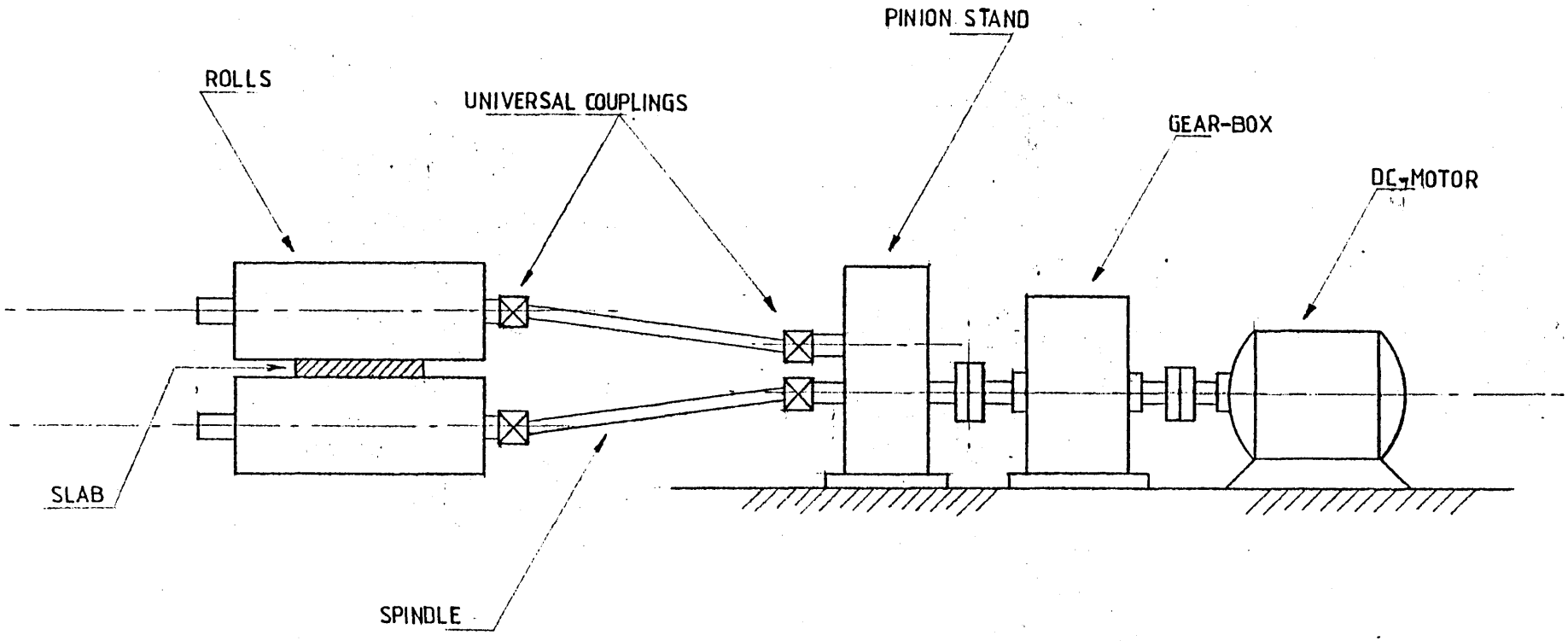

FIG.1.3 BLOCK DIAGRAM OF THE MILL DRIVE SYSTEM.

1.2.3 Rolling principles and operating conditions.

Rolling is the process of plastically deforming metal by passing it between rolls, producing high compressive stresses from the squeezing action of the rolls and surface shear stresses as a result of the friction between the rolls and the metal. The friction forces also cause the metal to be drawn into the rolls. (see fig. 1.4). (13).

The roll load or separating load is the summation of the vertical components of the forces described. This load forces the rolls apart, which results in "mill spring" (19) involving bending of the rolls, compression of the bearings-chucks-screws, stretching of the housing and much more relevant to the present work, the transmission of a transient load to the drive-line and components i.e. the universal couplings. From this load the rolling torque is determined.

The load is also affected by the following conditions:

i) Temperature of stock.

ii) Chemical composition of the material being rolled.

iii) The rolling speed.

iv) The roll diameter.

An additional dynamic effect, which is also important from the transmission point of view, is the "shock-loading" input as the ingot, slab or strip enters and exits from the rolls (20).

When drafting very heavily in a slabbing mill the main motors will often hesitate and even stop momentarily as the ingot enters the rolls (21). The motor current shows an overload and as the speed drops, the torque will reach

BASIC TORQUE FOR THE REDUCTION

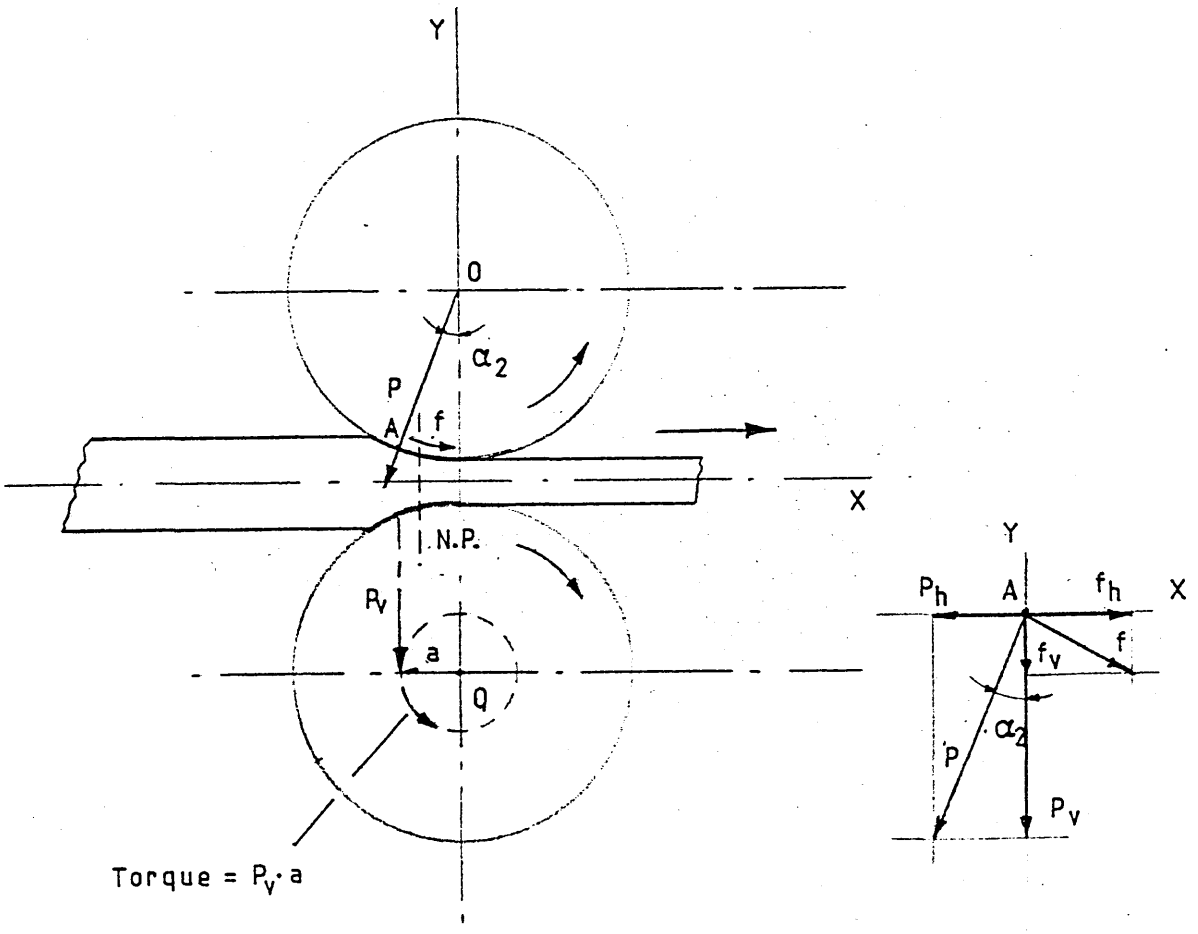

LOAD TRANSMITTED TO THE ROLL NECK

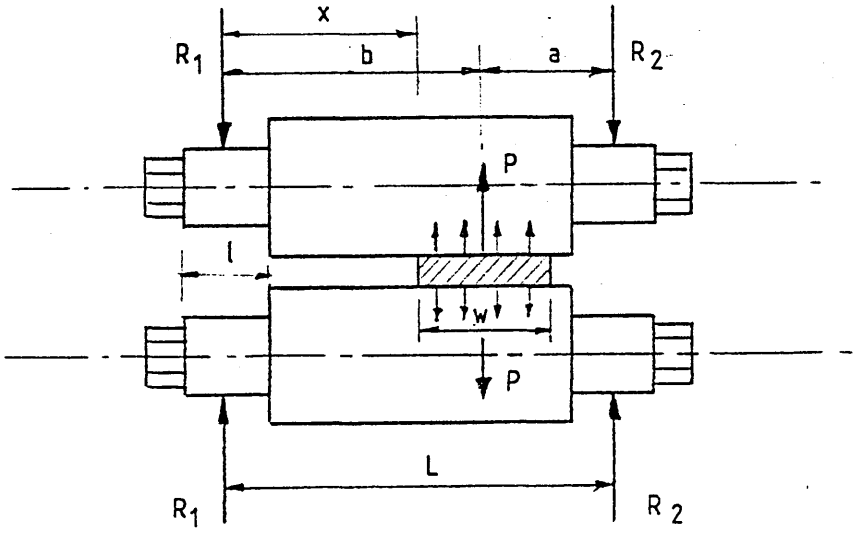

FIG. 1.4 SCHEMATIC REPRESENTATION OF THE LOADS DURING ROLLING PROCESS.

a very high value. This phenomenon is always present in the rolling mills to some extent depending on the type of mill. The effect causes momentary peak torques which may be several times the corresponding steady state rolling values. These peak torques must be considered in the design and protection of the mill and its drive line.

Another, significant feature in the mills is the presence of backlash. This tends to be most pronounced in roll-neck couplings, and occurs at this point in the system because of the necessity to accommodate large variations in horizontal alignment. Backlash also occurs because of wear or manufacturing tolerances in couplings, gears, etc. (22) Unfortunately, the backlash can also aggravate the transient loading on the system. This torque amplification also takes place with slippage of the material in the roll gap. It is also strongly influenced by the degree of head and crop shear imposed on the entering bar.

A typical chart of the torque amplification factor, defined as the ratio of the peak torque to the mean input torque, is shown in fig.1.5 and typical characteristics of rolling mills including torque values are also tabulated in tables 1 and 2 (23).

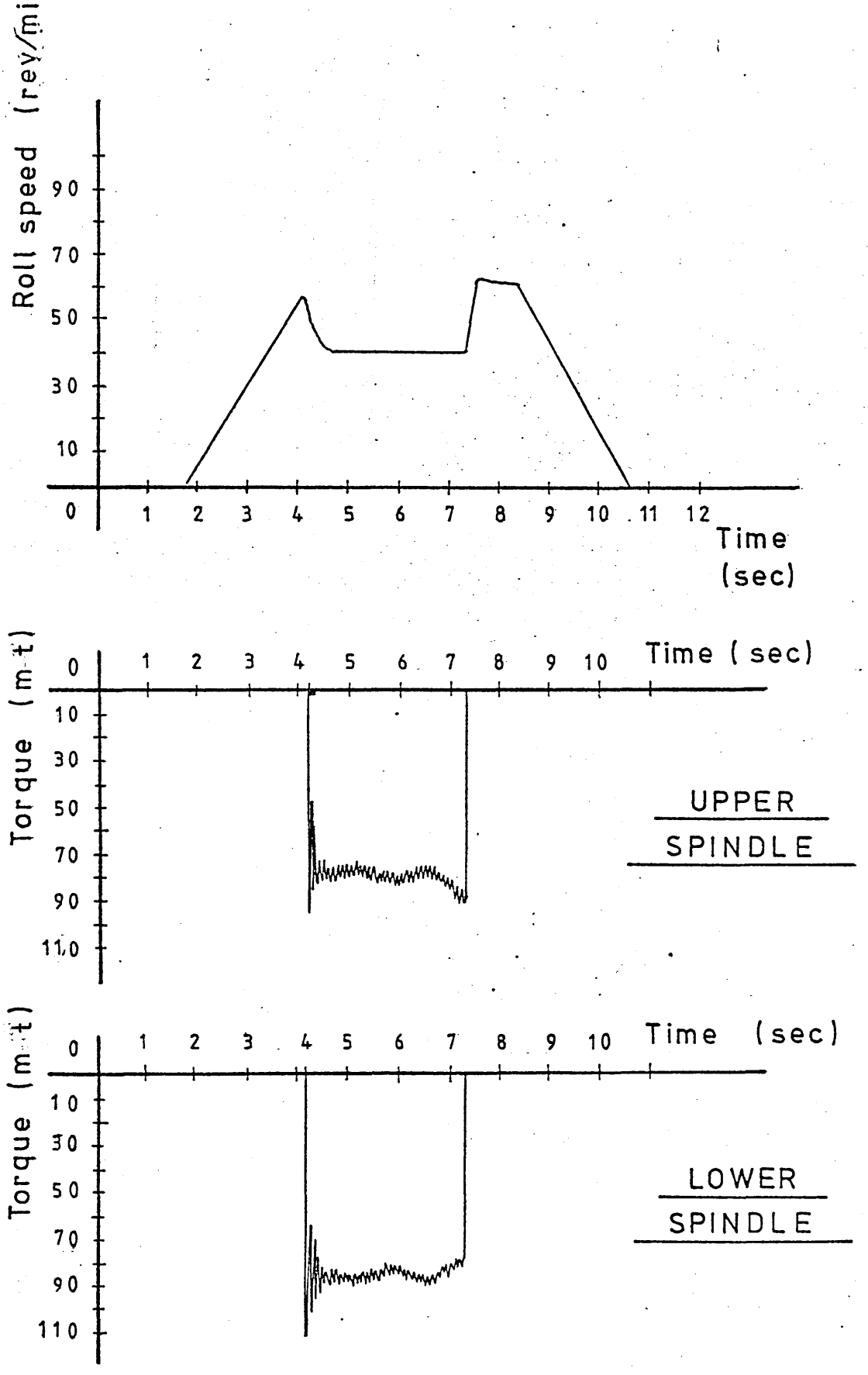

Fig. 1.5 Typical torque traces for mill rolling aluminium slabs to plate. (Swiss aluminium)

TABLE 1. TYPICAL CHARACTERISTICS OF A HOT STRIP MILL (Nippon - Steel, ref. 1).

Stand	Motor Power kW	Speed rev/min	Service Torque kNm	Peak Torque kNm	Steady Torque kNm
Rev. Roughing	2 x 2250	40/100	1611	1880	537
F1	3750	175/400	616	1848	503
F2	4400	120/310	495	1488	403
F3	4400	120/310	294	882	240
F4	4400	120/310	214	428	175
F5	3750	180/415	127	365	99
F6	2600	170/450	94	268	73

TABLE 2. TYPICAL LOAD VALUES IN ROLLING MILLS.

Works	Type of Mill	Peak Torque kNm	Steady Torque kNm
Muroran (Nippon Steel)	Hot reversing Plate rougher	1880	1611
Nisshin Seiko Co. Ltd. Kure	Hot reversing Plate rougher	2220	1863
Appleby - Frodingham (B. S. C.)	Secondary Blooming	1832	1145
Aldwarke (B. S. C.)	Primary	2994	1247

1.2.4 Various types of drive couplings.

The drive couplings currently used in rolling mills drives, are classified in four groups. Their aim is to provide a torsionally stiff, precise and positive drive. The following list is laid out in chronological order of development.

1. Wobbler couplings
2. Slipper spindles
3. Gear couplings
4. Universal or Hooke's Joint

1. Wobbler couplings.- This is the oldest coupling design and consists of a cruciform connection between the pinion box shaft and roll end by means of a loose fitting cast iron box, which provides a simple non-uniform, slow drive. It allows for low angularity and takes up axial displacements. Wobbler couplings have been replaced by slipper spindles, since they do not lend themselves to large angularities and high speed operations but are still widely used in older mills. A representation of this coupling is given in fig. 1.6

2.- Slipper spindle.- The spade and claw combination with intermediate movable pads allows for large angular and axial displacements. Angularities up to 10^{o} can be accommodated between the roll and the spindle axis. However spindle support is required when roll changing and on the larger or heavier applications, the spindles need supporting during operation. Currently, this coupling is used most frequently in application such as blooming, slabbing, primary, plate, tube, strip and cold rolling mills. However, is not suitable for very high speed operation because of its non-sealed

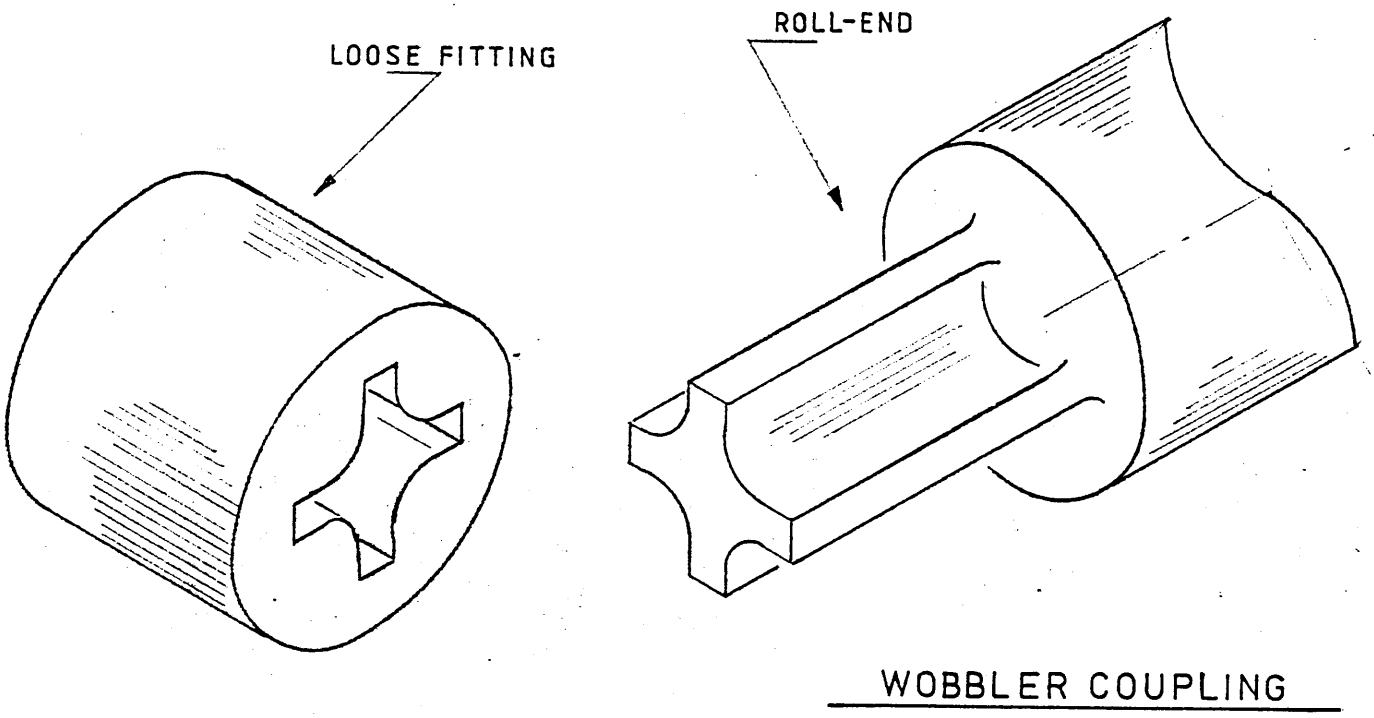

WOBBLER COUPLING

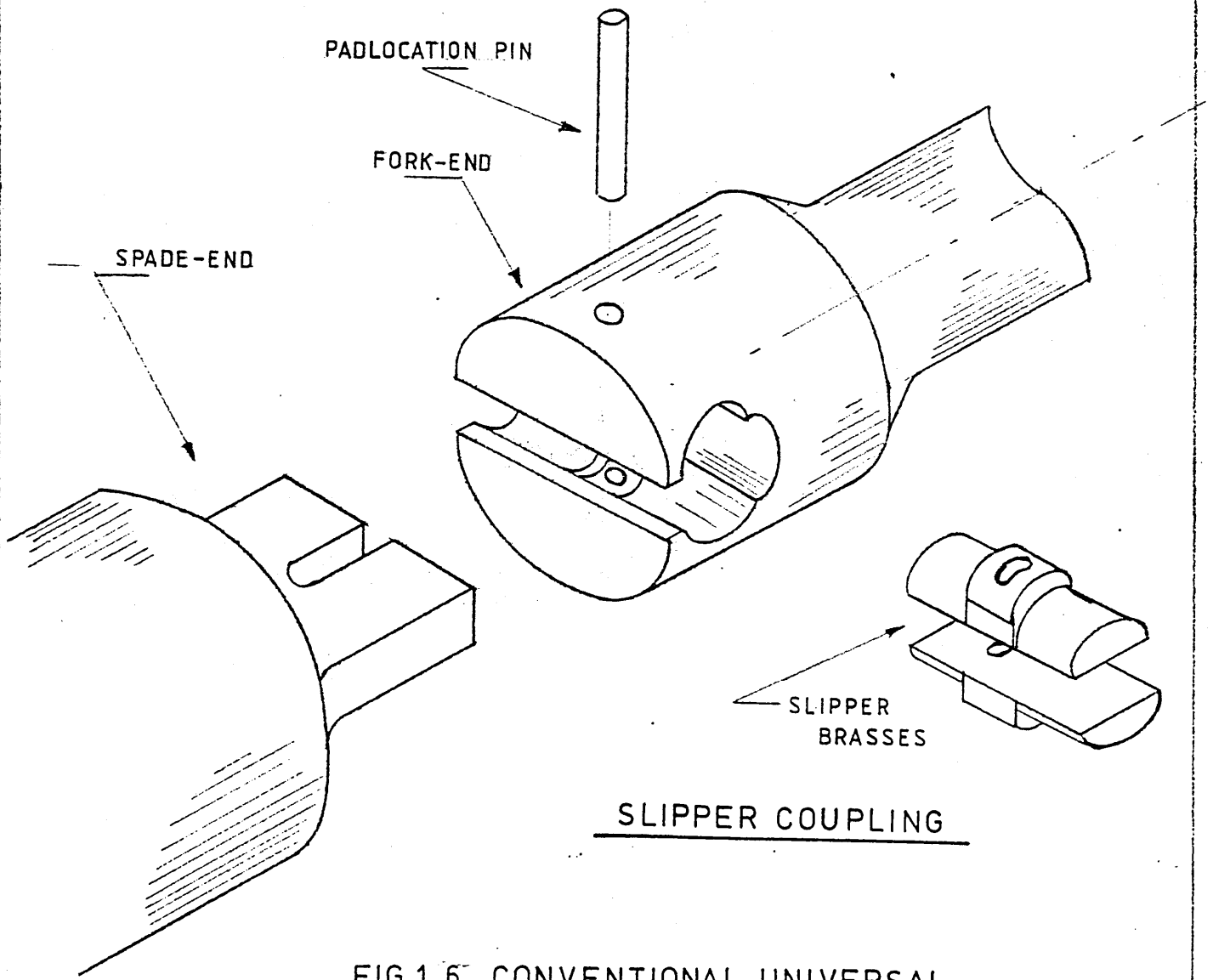

SLIPPER COUPLING

FIG.1.6 CONVENTIONAL UNIVERSAL COUPLINGS.

lubrication system. Also, for low torque operations it is replaced by gear couplings. (see fig. 1.7).

3.- Gear couplings.- They are produced by means of a pair of gears assembled together, one being a plain internal gear with a crown and bevelled external spur gear, with a small clearance between them. Axial sliding is unrestricted, except by friction, whilst angular misalignment is permitted by tilting between the teeth. Since gear couplings transmit smaller torques effectively, this coupling is used for low torque stands in rolling mills frequently in combination with a slipper spindle. However, a separate roll end coupling is required together with spindle support during roll change. The angularity is restricted to 2° and a splined spindle is required if the axial displacement is large compared with coupling diameter. They are applied mainly to hot and cold tandem mills.

4.- Universal or Hooke's joint.- The Hooke's joint, provided with roller bearing mounting of the yokes onto the cross-pin has been developed for rolling mill drive applications. The complementary spindle must be splined to take up axial movement, and spindle support for roll change is essential.

The application of this type of coupling to rolling mill drives has been actively promoted by three companies in recent years. In Germany by G. W. B. (Gelenk Wellen Bau) in Essen and Voith in Heidenheim and by Koyo Seiko in Osaka Japan (24).

The torque capacity for a given swing diameter (the maximum diameter of the circular path described by a rotating universal joint) has been increased significantly in recent years to meet the stringent demands of rolling mill drives.

The size is up to 1.5m swing diameter couplings. On the other hand G. W. B. have the longest experience installing rolling mill drives since 1958 and with a diversity of application as wide as Koyo s, they do not have the same size range. Blooming mills, billet mills, continuous casting plants and section mills are all fitted with universal joints up to 12.7m. long. Finally, Voith has been providing a well considered joint and spline suitable for the mill environment.

A useful graph for classification of different universal couplings applied in rolling mill drives, on the basis of spindle torque and spindle diameter is shown in fig. 1.7. This graph is taken from a Koyo publication (25) and so should not be regarded as giving anything more than an indication of the relative torque capacities of the various types of coupling.

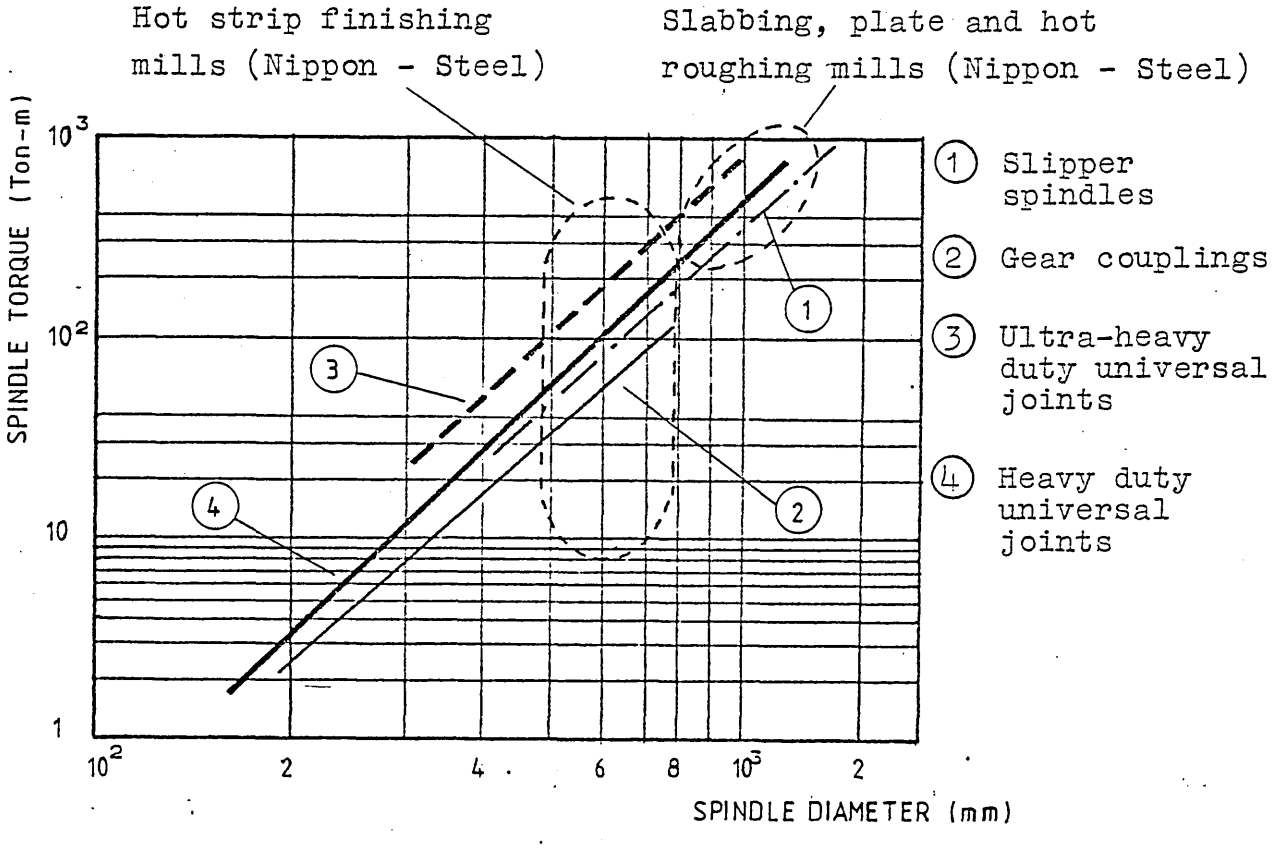

Fig. 1.7 Classification of different universal couplings applied in rolling mill drives.

Bearings are effectively sealed and bearing deterioration and wear rate are therefore minimized, thus improving the reliability of the coupling and reducing maintenance costs.

The new universal joints have been successfully applied at Japanese steel plants, such as Nippon Steel's Muroran works in 1974, where the slipper couplings were replaced by universal joints-ultra-heavy duty type, which were developed jointly with Koyo-Seiko Co. (see fig. 1.8) (26).

As part of a research program with a view to increasing the load capacity in the rolling-mill, they developed a high-capacity drive shaft, which required a new high strength coupling as well. The aim of this new series of universal joints was to satisfy the severe conditions present in the rolling mill drive.

At Muroran works the most severe requirement for the universal joint was the No. 1 stand of the hot-strip mill; which has a maximum torque of 185 ton·m, with a maximum swing diameter of 590mm. A vast programme of tests were also carried out in the No. 4 stand, and were more encouraging, with little wear and a drastic reduction in vibration compared with the original slipper couplings. The coupling performed well for over 20 months, and it was suggested that they would run for 90 months (1).

In claiming that problems do not exist or that field applications have been successful, the three manufacturers have quoted their experiences; for instance, Koyo-couplings have been fitted to a whole range of mill drives from reversing primary mills, hot-strip mills, bar and rod mills to cold mills (25).

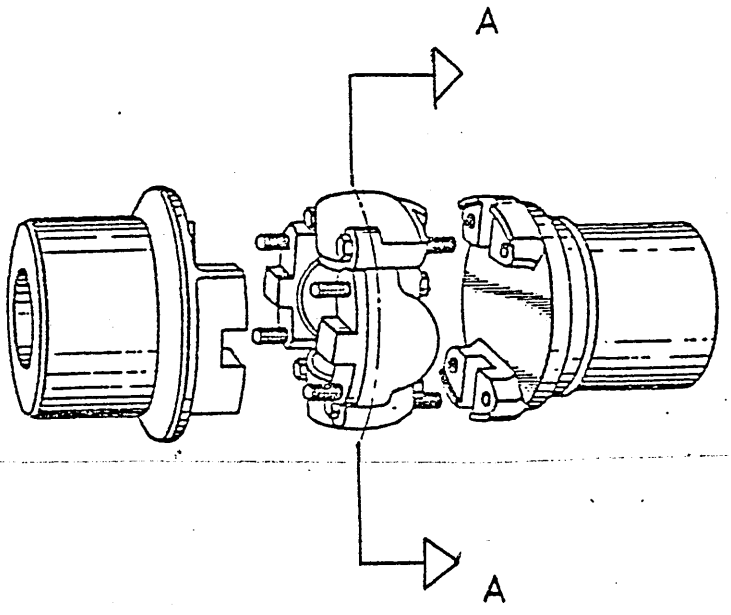

A-A SECTION

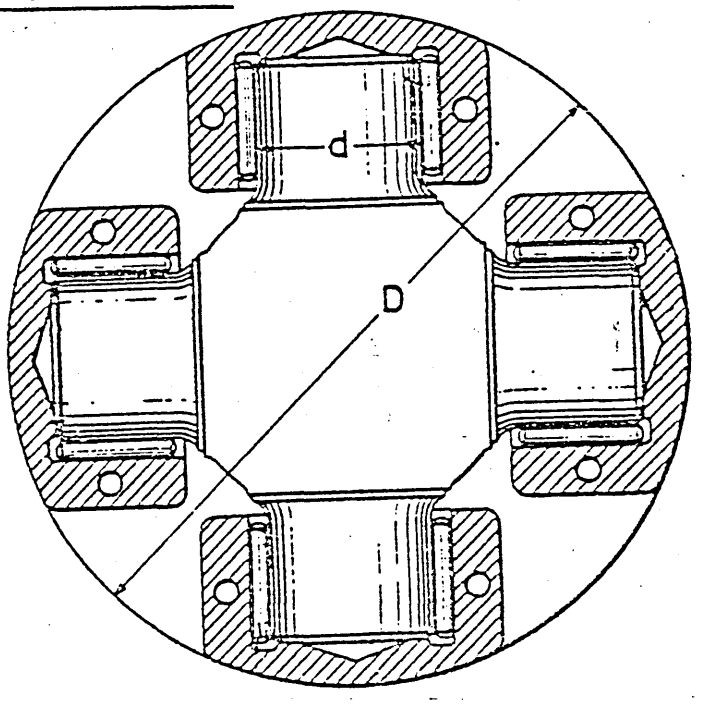

FIG. 1.8 UNIVERSAL JOINT

KOYO DESIGN.

1.2.5 Comparison of the universal joint with traditional couplings.

A slipper coupling cannot be precision manufactured of material with high hardness because of its inherent contruction features. The universal joint consists of a cross-pin and needle bearing made of high Ni Cr steel and precision ground on every contacting face eliminating play and minimizing wear.

Compared to gear couplings, universal joints require substantially less downtime; they have higher misalignment capability, up to 30° in some cases, compared with 3° for a gear type coupling. Once fitted, they require no realignment during normal operation. They are easily and quickly disassembled and reinstalled without disturbing drive and driven units. Manufacturers also claim that universal joints have longer life than gear couplings because they can operate at much greater angularities and have a bearing connection with low-wear rolling action. Gear couplings have a friction gear connection with greater wearing metal-to-metal contact. Universal couplings also have higher power transmitting efficiency than gear couplings therefore the energy is reduced and power savings of 5 to 15 % are obtainable. Another great advantage of the universal couplings is that can be selected according to life requirements because their service life can be accurately predicted (1).

The reduced play produces less vibration, about 1/30 of that of a slipper coupling. Vibration is an important factor in improving quality of the product, and the use of a universal joint eliminates the chatter marks sometimes present when slipper couplings are used.

Noise levels can be reduced, for example at levels of 100 dB with slipper couplings noise was reduced to about 70 dB after installation of universal joints in one instance (1).

The universal joint with its precision seal practically eliminates leakage, reducing grease consumption and providing a clear environment. Whereas slipper coupling has no effective sealing, requiring great amounts of grease (approximate 1 ton/month) for each finishing stand of a hot-strip mill and about the same quantity of solvent for cleaning the expelled grease (1). In addition production is increased as the universal joint provides an opportunity to increase the rolling speed as well as reduce rejections. In summary benefits could be categorized as:

i) Annual saving in grease
ii) Saving on maintenance
iii) Increased power transmission
iv) Increased speed

It is considered by some rolling mill manufacturers that possible inadequancies in universal joints may be associated with the failure of the rolling element bearings between pin and yoke. It is well known that all rolling element bearings have a finite life and are susceptible to occasional early failure.

In addition, the severe dynamic and transient effects present in some rolling mill drives may exacerbate the brinnelling fatigue effects in the bearings. It is for this reason that the current project has been carried out; to investigate the potential for the use of oil film bearings in such couplings with the intention of extending the life of the bearing and the coupling.

1.3 Review of Universal-Couplings.

1.3.1 General

A universal joint is a mechanical device which can transmit torque and-or rotational motion from one shaft to another at fixed or varying angles of intersection of the shaft axes. It accommodates much larger values of misalignment than can be tolerated by the other types of flexible couplings e. g. shaft angles up to 30° may be used. (2)

Generally, the initial interest in any universal joint is its motion transmission characteristic, which can be either non-uniform or uniform.

i) A non-uniform motion or non constant velocity universal joint transmits motion with varying ratios of instantaneous angular velocity between output and input members, when operating at joint angles greater than zero. The average angular-velocity ratio is unity over one complete revolution.

ii) A uniform motion or constant velocity universal joint transmits motion with an angular velocity ratio of unity between output and input members. (8)

Universal joints are also classified with regard to their supporting capabilities:

i) A self-supporting universal joint is supported by internal means and hence requires location at only one shaft; which can be either the driving or the driven member of the joint.

ii) A nonself supporting universal joint requires a means of external support at both driving and driven members in order to maintain the proper alignment of joint components.

In addition, universal joints can be described with regard to directional capabilities of power transmission. Most universal joints are bi-directional and therefore transmit torque from either joint to the other, with equal efficiency and capacity (9).

1.3.2 Design of the Universal Coupling.

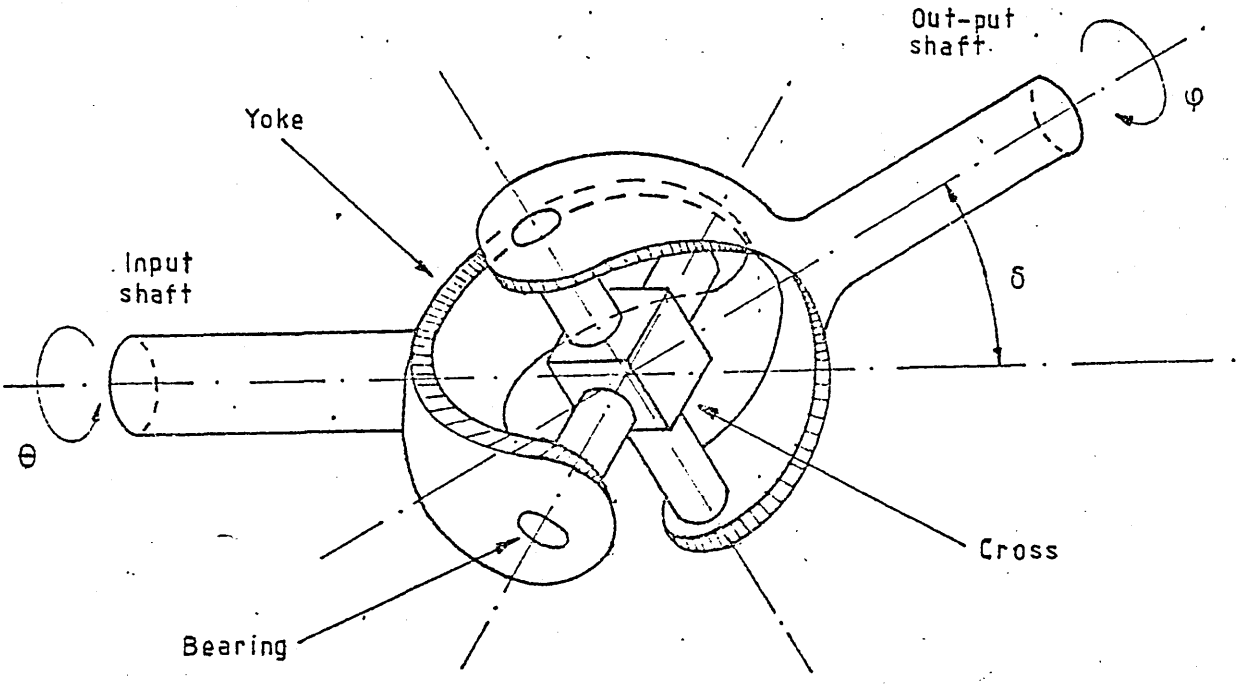

Fig. 1.9 Universal Coupling. Main Components.

The basic design is quite old, dating back to the Greeks however, it has only been since the advent of the automobile that its design was improved and only recently has it found application in the steel industry (3).

Robert Hooke (in 1636) used the joint to drive a rotating shaft, Cardan (in 1501) having first described the principles. From 1700 to 1900 there was little in the way of development of the joint. With the advent of the automobile the development of the Cardan joint accelerated (3).

In Germany after World war II, rapid devolpment of the diesel-hydraulic locomotive required Cardan joints to transmit the drive from the power unit to the axles. This required a bigger and better joint than that used by the automotive industry and led to the evolution of joints with up to 6800 N·m capacity and with 10,000 to 20,000 hr B-10 life (9).

Other applications have been in aircraft, marine, agricultural, industrial and stationary drive system installations.

The German steel industry after World war II used these joints in many applications. By 1950 joints up to 24.5×10^3 N·m capacity were used for steel mill drives. Currently, they are made in sizes up to 2.72×10^5 N·m, and are used for reeler drives on tube mills, edge roll drives, pinch roll drives, continuous casting machine drives, strightener roll drives, leveller drives, etc. These large joints were first introduced in the U. S. in 1958 and are now well accepted (3).

The universal joint has been most generally used as a self supporting joint, in conventional, open-type drive-line constructions.

The principal advantages of the universal joint are its cost to manufacture as well as simple and robust construction, combined with long life and ease of serviceability.

In addition to providing the necessary torque capacity in a limited operating space, the joint has the thrust capability to withstand relatively high, externally imposed axial forces which may be produced e. g. by sliding spline when shaft length changes are required.

Further, the joint offers the versatility and flexibility to permit the design of numerous yoke and bearing constructions to meet the functional and durability requirements of a large variety of applications.

In summary, the four basic functions e. g. torque, rotation, misalignment and length changes demanded in a driveline are satisfied.

1.3.3 Motion characteristics.

The kinematics of motion of a Hooke's joint are quite unusual. Whenever it operates at an angle, non-uniform motion is developed (2).

When the driving yoke of the coupling is operating at a uniform rotational velocity the driven yoke rotates nonuniformly with respect to angular displacement, velocity and acceleration.

Equations of motion

The equations of motion of a universal coupling have been developed according to the following analysis (11):

Fig 1.9 shows the basic angular relationship of a universal joint operating at an angle.

Then, the angular displacement of the driven shaft is determined as follows:

$$\text{Tan}\,\varphi = \text{Tan}\,\theta\,\cos\delta \qquad \ldots\ldots(1.1)$$

By differentiating this expression with respect to time, and simplifying, the output angular velocity of the driven shaft can be found as follows:

$$\omega_1 = \frac{\omega\cos\delta}{1 - \sin^2\delta\,\sin^2\theta} \qquad \ldots\ldots(1.2)$$

The output angular acceleration of the driven shaft can be found by differentiating the velocity equation with respect to time and simplifying as follows:

$$\alpha_1 = \frac{d\omega_1}{dt} = \frac{\omega^2\,\sin^2\delta\,\cos\delta\,\sin 2\theta}{(1 - \sin^2\delta\,\sin^2\theta)^2} \qquad \ldots\ldots(1.3)$$

These equations describe the displacement, velocity and acceleration characteristics of a universal joint operating at an angle.

These motion characteristics are illustrated in fig. 1.10 for a universal coupling operating at a 10° joint angle and at 120 rpm.

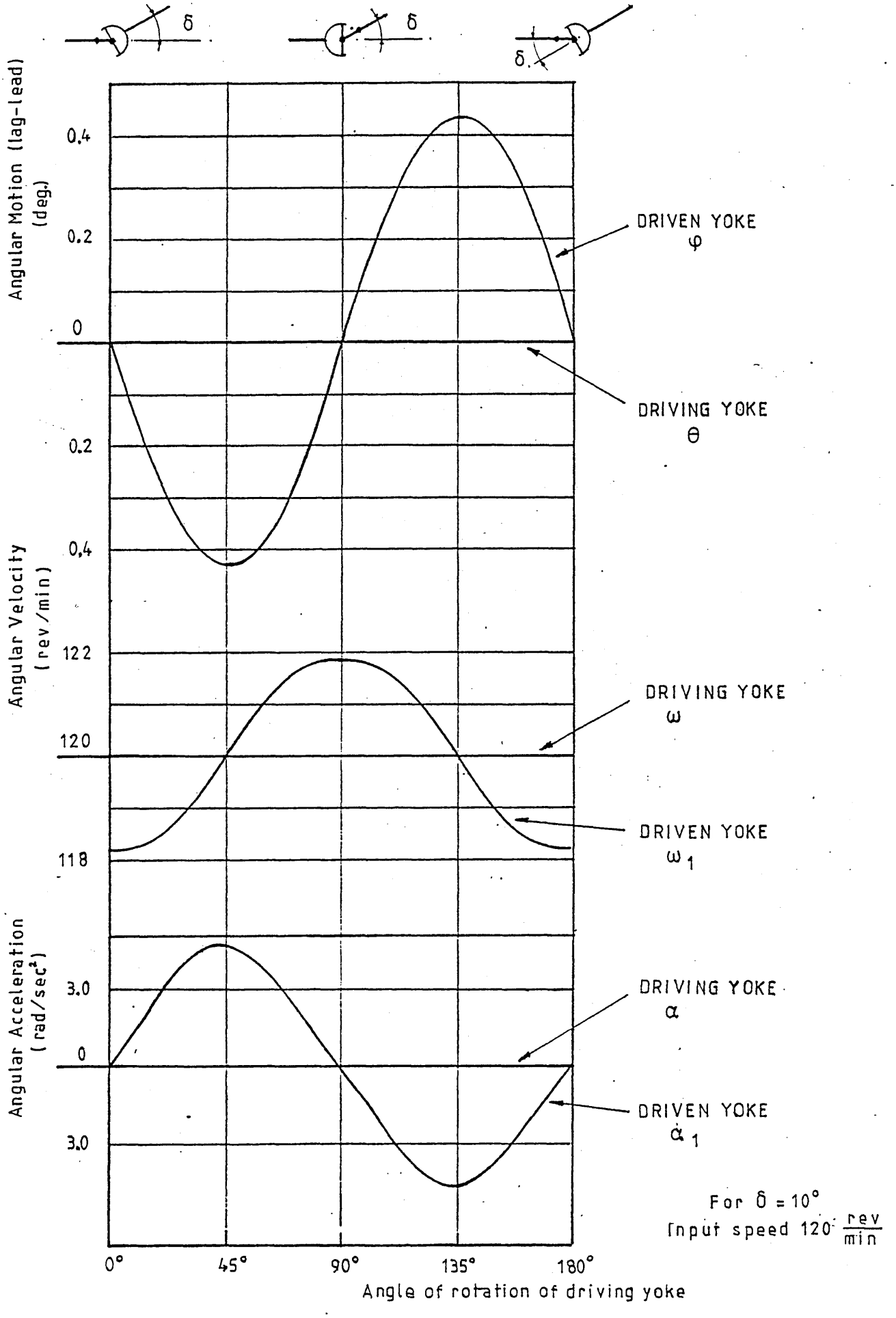

FIG.1.10 UNIVERSAL JOINT MOTION CHARACTERISTICS

A simplified derivation of the universal coupling non-constant velocity characteristics is shown in fig. 1.11.

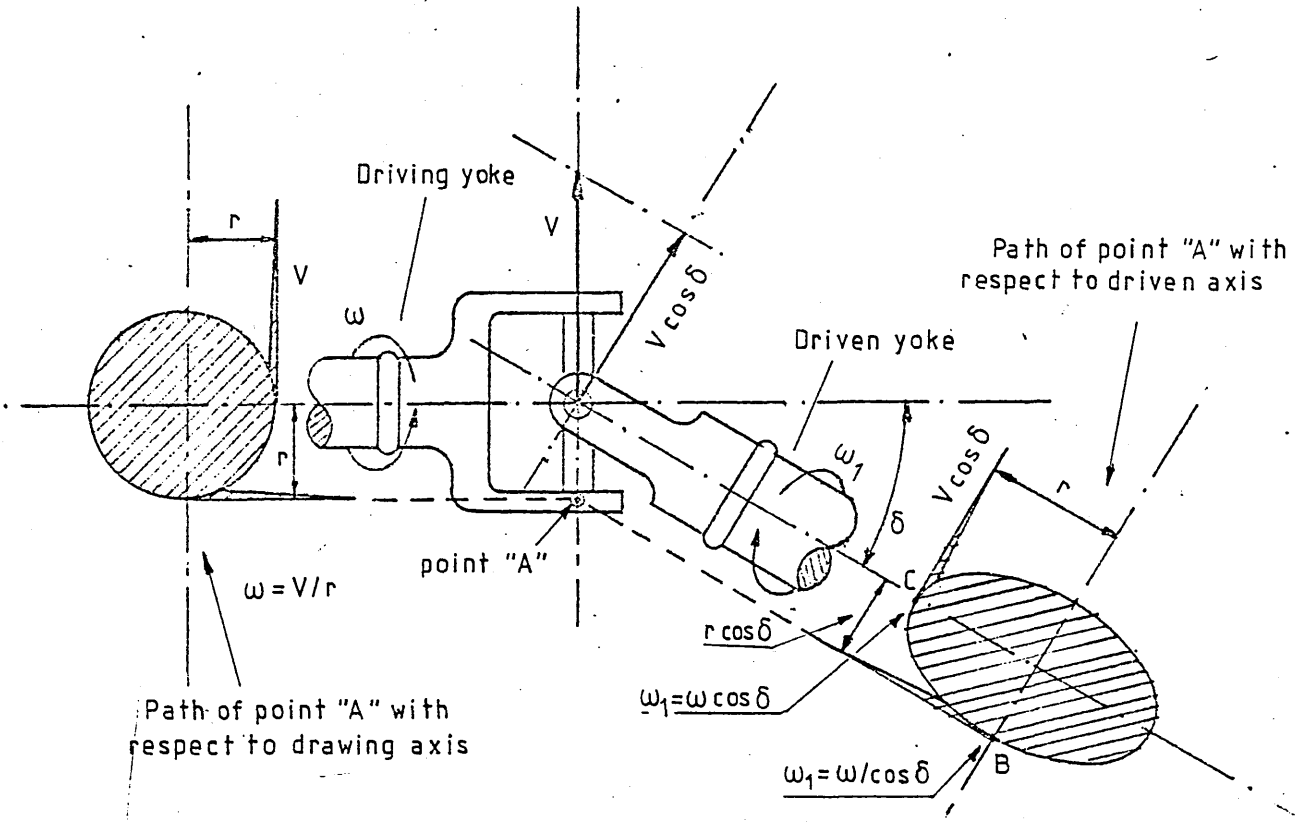

Fig 1.11 Universal coupling motion characteristics.

The analysis is done by considering the speed of a point on the cross trunnion, point A. So point A rotates around the driving yoke axis in a circular path of radius "r" and at a constant speed.

Therefore, the input angular velocity of the driving-yoke is:

$$\omega = \frac{V}{r} \qquad \ldots\ldots(1.4)$$

When viewed along the driven-yoke rotational axis, the path of point A appears as an ellipse with a major axis radius of r and a minor axis radius of r cos δ . Therefore the rotational speed of the driven yoke varies from ω/Cos δ to ω Cosδ as A moves from B to C.

Hence, the output angular velocity varies continuously and produces two complete cycles of speed variation for every revolution of the driving yoke.

A polar diagram is shown in fig.1.12 which shows the angular velocity of both the driving and driven yokes for one complete revolution of the universal coupling (11).

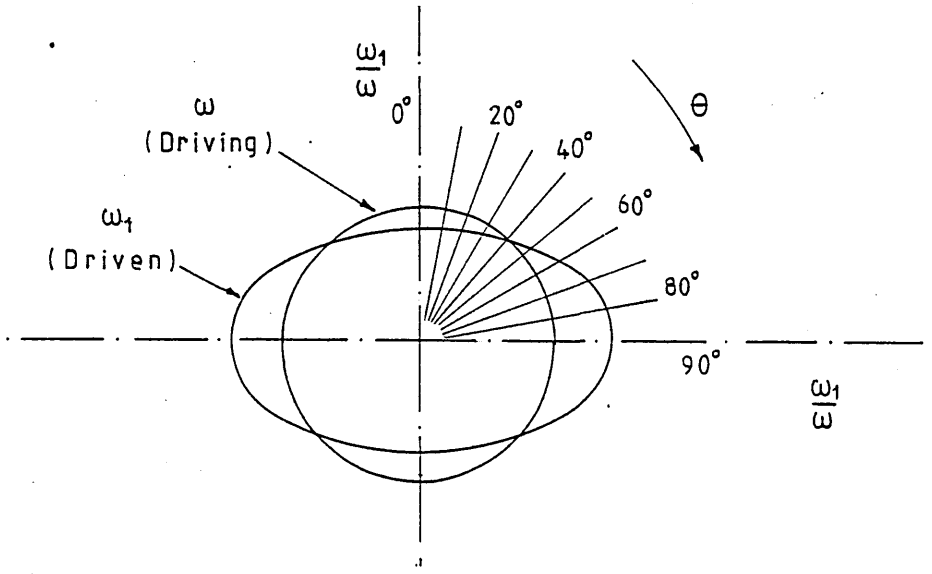

Fig. 1.12 Polar diagram for universal coupling angular velocity.

Since the driving yoke is assumed to have a constant angular velocity, its polar diagram is a circle.

However, the diagram for the driven yoke is an ellipse which intersects the circle at four places. This means that there are four instantaneous positions during a single rotation where the angular velocities of both yokes are equal. This has the effect of causing the movement of the pin with respect to the claw to be oscillatory and will be examined in detail in section 4.1.

1.3.4 Analysis of the torque transmitted through the universal coupling.

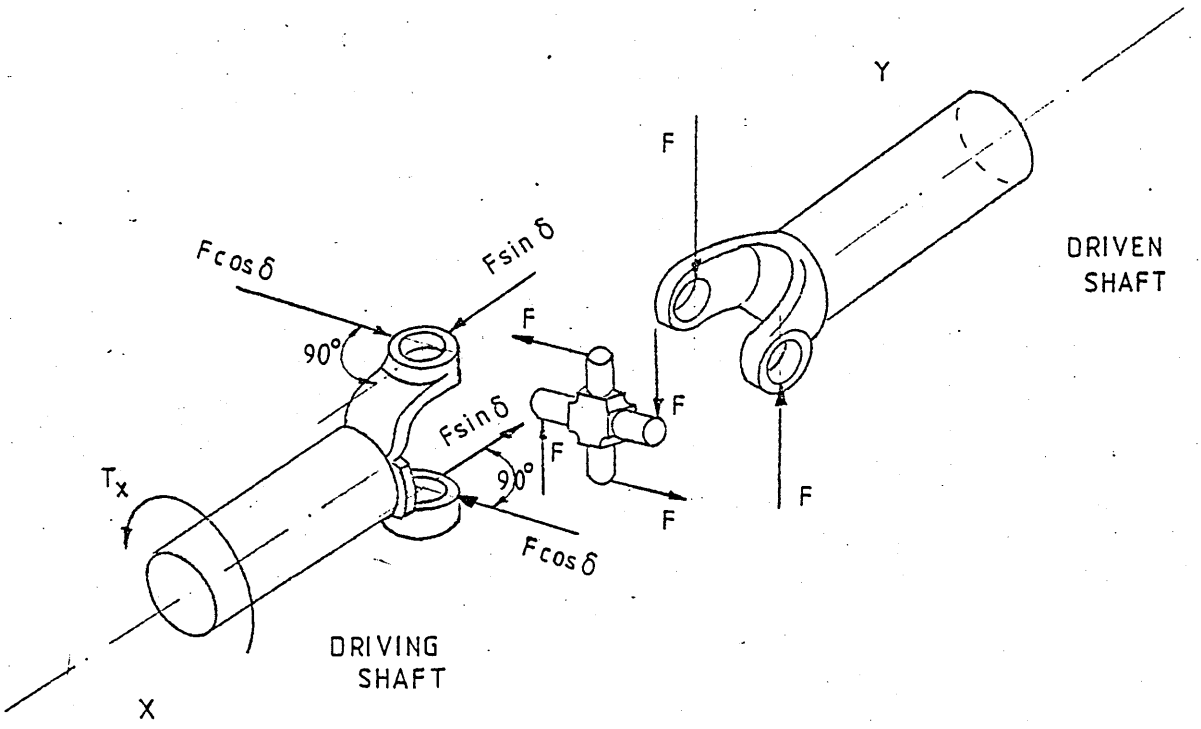

Fig. 1.13 Universal Joint.

The torque on the driven shaft "Y" can be determined in several ways (see fig. 1.13 above). One method is the application of the equations of equilibrium to determine that the only forces which can be applied to it are as shown in the plane of the cross. Each of the forces acting on the cross trunnions are designated F (12).

The two components of F acting on the yoke of driving shaft "X" are:

$$F_b = F \cos \delta \quad \text{.....(1.6)}$$

which is perpendicular to the rotational axis.

And $$F_a = F \sin \delta \quad \text{.....(1.7)}$$

which is axially in line with the rotational axis.

The torque acting on the yoke of the driving shaft "X" due to the action of the cross is:

$$T_x = F_b\,(2\,R) = F\cos\delta\;(2\,R) \qquad \ldots\ldots\ldots(1.8)$$

Where:

T_x = Torque on yoke of driving shaft (X).

F = Couple force on cross trunnion.

R = Torque radius of couple force.

δ = Joint angle.

The solution for the force can be obtained by re-arranging equation (8) and substituing as follows:

$$F = \frac{T_x}{\cos\delta\;(2R)} \qquad \ldots\ldots\ldots(1.9)$$

And the torque on the driven shaft Y is:

$$T_y = F\,(2R) \qquad \ldots\ldots\ldots(1.10)$$

A second method that can be used to obtain the output torque of the coupling is based on the condition that the power-in must be equal to the power-out, when no friction loss is assumed in the joint and the relationship of angular speeds are taken into account,

$$T_x\,\omega_x = T_y\,\omega_y \qquad \ldots\ldots\ldots(1.11)$$

and,

$$\omega_y = \frac{\omega_x\cos\delta}{1 - \sin^2\delta\,\sin^2\theta} \qquad \ldots\ldots\ldots(1.12)$$

Where:

ω_y = Rotational speed of the driven shaft yoke.

ω_x = Rotational speed of the driving shaft yoke.

δ = Joint angle, angle between the axes of the driving, and driven shafts.

θ = Angle of rotation of the driving shaft yoke from the position where it is perpendicular to the plane of the joint angle.

Then, substituting:

$$T_x \omega_y = T_y \frac{\omega_x \cos\delta}{1 - \sin^2\delta \sin^2\theta} \quad \ldots\ldots\ldots(1.13)$$

Then by arranging this equation, the torque on the driven shaft Y can be expressed as follows:

$$T_y = T_x \frac{1 - \sin^2\delta \sin^2}{\cos\delta} \quad \ldots\ldots\ldots(1.14)$$

Therefore,

$$T_{y(max)} = \frac{T_x}{\cos\delta} \quad \ldots\ldots\ldots(1.15)$$

When $\theta = 0^\circ, 180^\circ$

$$T_{y(min)} = T_x \cos\delta \quad \ldots\ldots\ldots(1.16)$$

When $\theta = 90^\circ, 270^\circ$

1.3.5 Double Universal Joint.

As has been mentioned in section 1.2 the angular velocity ratio for two shafts connected by one universal joint is not constant, but it may be made constant by use of an intermediate shaft installing a second universal joint with the same shaft angles as the first joint and properly phased, i.e. yoke ears must be inclined on the centre shaft connecting the two joints. By means of this arrangement the uneven angular velocity caused by the first joint of a drive will be cancelled out by the second joint. Actually, this is the normal practice, found in the drive-line in the rolling mills, having the universal couplings installed in pairs.

So, one typical arrangement of double joints is the parallel shaft system (see fig.1.14), where the joint angles shown are true angles, since the input and output shafts as well as the connecting, shaft lies in the same plane when seen in the plan view (2).

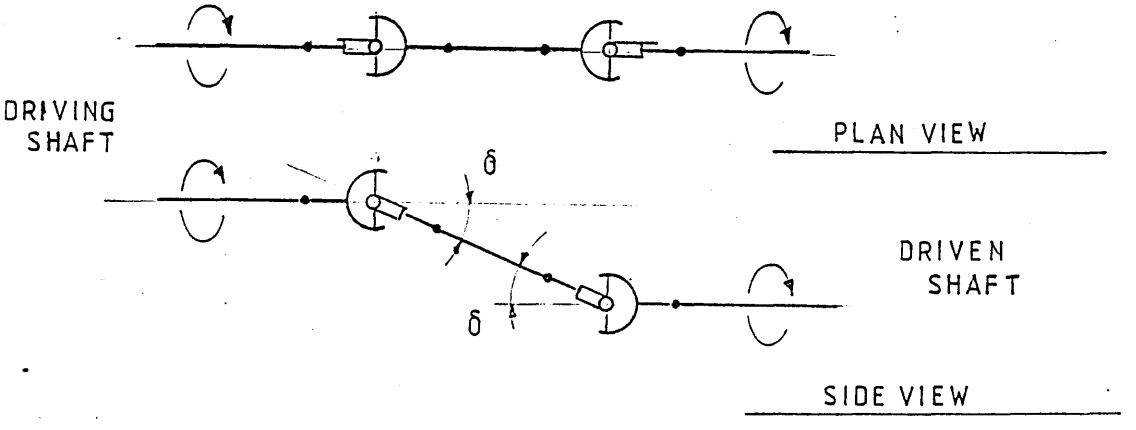

Fig.1.14 Parallel shaft arrangement.

Another system is the case where the shafts do not lie in the same plane, the yokes on the intermediate shaft can be rotated at an angle equal to the angle between the planes of the shafts to provide uniform angular velocity of the driven shaft (see fig. 1.15).

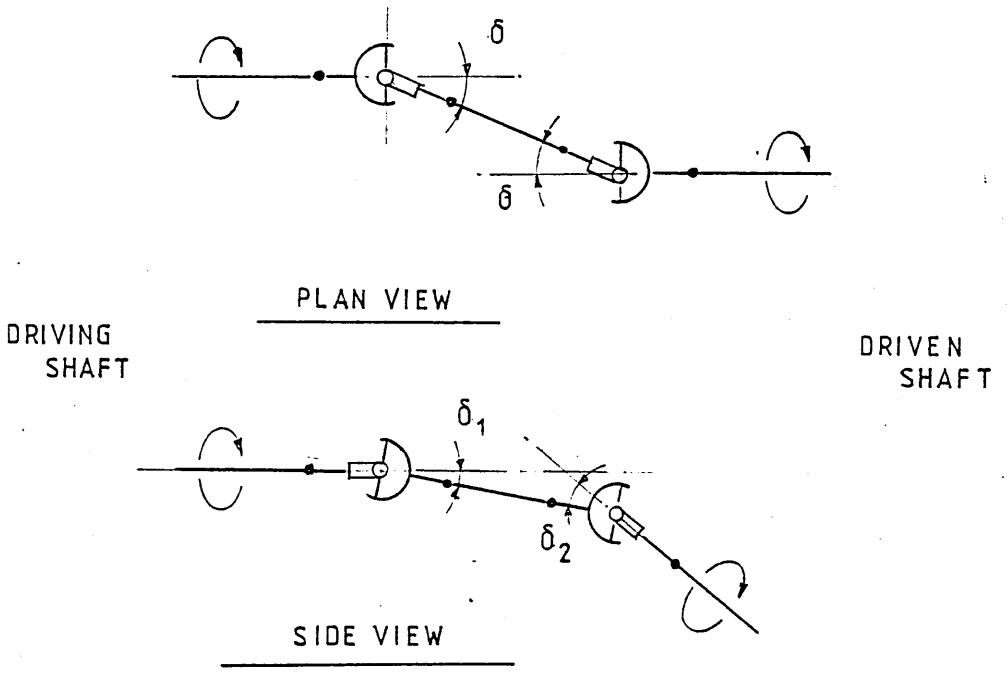

Fig.1.15 General two-joint shaft system.

The same considerations apply in applications where the centre shaft must telescope to accommodate end movement between driving and driven shafts, where as a single joint is locked tight. Therefore, that end movement must be provided by a slipping connection between the joints, by allowing an end fitting yoke to move freely on its shaft, by using a sliding coupling at one end of a shaft opposite the joint or by using a splined shaft (2).

CHAPTER 2. REVIEW OF PREVIOUS WORK.

2.1 Hydrodynamic bearings.

All theoretical work concerning hydrodynamic bearings in this field is fundamentally related to the flow and shearing forces of the lubricant based on the work of Reynolds (28).

The solution for a particular application is produced by applying boundary conditions, to provide exact and approximate solutions of the Reynolds' equation, for infinitely long and infinitely short bearings as well as those with finite dimensions.

The three types of boundary conditions used for radial bearings are as follows:

i) The pressure function and its derivative are continuous, analytical functions over the total range of the bearing. The calculations yield a negative pressure zone in the bearing.

ii) The pressure gradient is discontinuous in the bearing and the negative pressure zone is considered to be zero.

iii) Same as assumption (ii), but discontinuity is avoided, by putting the pressure gradient as well as the pressure equal to zero, where the pressure according to assumption (i) would have been negative. This condition yields results that compare favourably with practice.

2.1.1 Plain bearings with continuous motion subjected to static and dynamic loading.

Bearings with constant angular velocity subjected to a constant load are very well covered in the literature and their performance has been theoretically predicted with an acceptable degree of accuracy (29), (30).

The basic work, covering analytical and numerical solutions has been done by several scientists, including Sommerfeld (31), Gumbel (32), Raimondi and Boyd (4), Michell and Cardullo (33), Dubois and Ocvirk (5). They are based on assumption (iii), considering bearings with infinite and finite width.

On the other hand, publications of plain bearings subjected to dynamic loading are very numerous in practice but still no general solution has been established to provide a design procedure for the prediction of the journal locus, peak pressures and oil flow for a proposed geometry and loading.

The problem was investigated by Swift (34), one of the pioneers in this field and his analysis assumes an infinitely long bearing i.e. no-side leakage, and within this restriction the work is very complete. Although his results are somewhat unrealistic due to the fact that he considered no-oil film disruption i.e. continuous pressure gradient, including negative pressure, the approach was valid and provided a valuable guide for subsequent workers. Burwell (35)

extended the knowledge of dynamically loaded bearings and somewhat generalized the analysis of Swift, by considering an infinitely long bearing solution. He applied it to a diesel engine crankpin and calculated the path of the pin centre, peak oil film pressure, oil flow and the temperature rise across the bearing.

Later, he also assumed an infinitely long bearing (36) and an infinitely short bearing (37) with a correction for side leakage.

Hahn (38) also extended the use of the numerical methods to dynamically loaded bearings by considering the oil-film disruption pressure and a Runge-Kutta integration technique to obtain the journal locus.

Hornshell and Mc Callion (39) also utilized numerical methods to obtain such loci and used more realistic but complicated boundary conditions. However, Lloyd, Hornshell and Mc Callion (40) later refined the technique used by Hahn, this utilizing a high-speed digital computer and computed for any loading pattern the journal centre locus, oil flow, friction work done and traces of the positions and magnitudes of peak pressures and positions of the disrupted zone for any axisymetric bearing. A very good correlation was later obtained between those predictions and the experimental work carried out by Middleton, Dudley, and Mc Callion (41).

The squeeze film effect has also been studied by Archibald (42). However this study assumes only a radial velocity and it is therefore of little value for the more general case, as the effect may not be superimposed on the

tangential effect, due to the non-linear nature of the problem.

Experiments with radial bearings subjected to dynamic loading have also been carried out by Radermacher (43) in order to measure the path of the centre of the shaft. He found reasonable correlations between a variety of theoretical predictions and real engine-bearing behaviour, by measurements carried out on the fast running diesel engines, but pointed out that the possibility of comparison was limited by the restrictions imposed on the theory. These included constant viscosity, rigid bearing components, ideal bearing geometry, etc. A conclusion which Carl (44) also arrived at, when he measured the pressure distribution in a radial bearing and the path of the journal centre under sinusoidal loading.

Further, Simons (45) found several discrepancies when comparing experimental work on dynamically loaded radial bearings, with mathematical investigations. All of which require a number of questionable assumptions, particularly the "continuous film" assumption, and journal position when started from rest.

White (46) also suggested from results obtained for a squeeze film bearing, that when operating at high eccentricity ratios with a constant rotating load, cavities occur throughout the film, leading to a loss of load-carrying capacity.

2.1.2 Plain bearings under oscillating motion.

So far, only work in relation to radial bearings with constant angular velocity has been mentioned because very little information has been published in the field of bearings with oscillating motion.

Although, it might be that there are many applications for oscillating bearings it seems that most of the work done in this field has been directed to the gudgeon-pin or top-end bearings of marine diesel engines. Such is the case for the investigations carried by F. T. Barwell (7), Jakobsen (47) , Blount and De Guerin (48). Glaeser and Duframe (49) also studied the performance of heavily loaded oscillating bearings but with particular reference to "air frame" application. Early attempts were also made by Fogg and Jakeman 1938 (50), as an extension of studies on the apparatus originally designed by Sir Thomas Stanton in the course of investigations of boundary friction.

Barwell (7) has shown that the shape and position of oil grooves as well as the oil supply are of major importance for the performance of a bearing with oscillating motion. Further, that contrary to the case of bearings in which the shaft revolves continuosly, the presence of oil grooves in the loaded region may improve lubrication.

He found that a plain bearing both with a central hole in the loaded region and with two oil holes located just outside the arc of contact, are unsuitable for use under oscillating motion. However, he found succesful results for bearings having axial grooves in the loaded area,

indicating also that an improvement may be obtained under certain conditions, if the central groove is replaced by a helical groove. In the former case the angular pitch of the axial grooves was less than the angle of oscillation, and these oil grooves were fed from two circumferential grooves cut eccentrically so as to fade out half way round the bush. This showed excessive wear rate together with slight pick-up of white metal at the edges of the bearing. The circumferial grooves were replaced by a single helical groove and extra small axial grooves. According to Wilcock and Booser (51) this is almost the type of groove arrangement found in practice for crosshead bearings, where the usual arrangement of oil grooves is a central-circumferential groove, through which axial grooves are spaced with an arc slightly less than the angle of oscillation all around the bearing.

Barwell (7) experiments also showed that under static loads and at low speed, friction was constant through out the stroke - this term is used here to denote the relative movement of shaft and bearing -, indicative of "boundary conditions". He pointed out that the selection of bearing materials is very important under these conditions, which is the same conclusion as Glaeser and Dufrane (49) arrived at, from their results of experimental work in which plain bearings of various materials were operated under oscillating motion and heavy static loads.

Barwell also demostrated that a compatibility exists between the materials and the lubricants used, so that a leaded-bonze bearing working with a compounded oil was

satisfactory but not working with an uncompounded oil. Similarly tin-base white metals operated more satisfactorily with compounded than with uncompounded lubricants.

On the other hand, Blount and De Guerin (48) found that the nature of the load function influenced the performance of the bearing in their experiments carried out in a test machine to simulate the operating conditions of small-end bearings in a two stroke engine. They have confirmed that the bearing will support a higher average load if the load applied is of a dynamic nature, largely due to the squeeze effect. They also found that better conformity between the oscillating shaft and the bearing at running conditions reduces the bearing temperature and increases load carrying capacity. A perfect conformity was achieved in this experiment by machining a shallow scallop in the bearing, so that over an arc of 120° the radius of the bearing and that of the journal were equal. Since 360° bearings were used, this allowed expansion of the journal during operation without causing seizure.

Further, they concluded that the load-carrying capacity is directly affected by the surface finish of the journal with the effect becoming more pronounced as the finish improves.

Jakobsen(47) has contributed to the understanding of this problem, from his experiments carried out on a very comprehensive testing machine, which was designed to simulate the conditions of a crosshead bearing in large supercharged two-stroke marine diesel engines, where the load is uni-directional and pulsating. He found that, even in a bearing

in which the relative motion between journal and bearing is of an oscillating nature, it is possible under certain conditions, to obtain mainly hydrodynamic conditions of lubrication, provided the bearing temperature is kept below a certain critical limit. He also suggested that there are at least two stable modes of lubrication apart from the pure hydrodynamic and boundary modes, which occur either side of what is usually denoted "mixed lubrication". The transition from one of these modes into the other may or may not be abrupt and might be associated with a large temperature rise in the bearing, depending at least on the surface finish and lubricant viscosity.

The importance of cooling is thereby strongly accentuated, and temperature warning equipment is advisable.

Jakobsen (47) also found that the journal as well as the bearing surface may experience a considerable degree of running-in, even if the hardness of the former may be of one order of magnitude higher than the latter. He also found that the loaded areas i.e. top and bottom, represent the areas of maximun wear and the horizontal side positions, the areas of least wear, from a series of surface roughness profile charts of the tested journal. However, he did not find a satisfactory explanation for the wear phenomenon of the journal.

From the above review it is concluded that most of the work carried out so far has been focussed in particular on the running-in characteristics of dynamically loaded bearings. Usually this is achieved by endurance tests considering the variation of temperature, coefficient of friction, rate of

wear with the passage of time. However, results for real measurements of oil film thickness have not been published. Barwell (1955) attempted to measure the relative displacement of journal and bush during the cycle of oscillation by using capacitive type probes but he pointed out that those measurements should be regarded as explorative only, due to poor measuring technique available at that time for this purpose.

2.2 Hybrid bearings.

The self-acting nature, compactness and reasonably cheap lubrication system provided by the hydrodynamic plain bearing makes it attractive for high load carrying capacities at appropriate speeds. However, a novel type of externally pressurized bearing has emerged, proving to be very succesful for adverse conditions such as low speeds and shock loadings. Recent theoretical and experimental work has been carried out by Rowe W. R., Koshal D., Stout K. J. (52) on these bearings.

The system combines the advantages of the extra-load support from the fluid-film due to hydrodynamic effects when a hydrostatic bearing operates at certain speed levels, so the bearing is said to operate in a "hybrid" manner. The supporting fluid is fed to the bearing gap through strategically positioned discrete slots, as opposed to orifices or capillaries. This concept was conceived after a fairly comprehensive study of the problems associated with the orifice design of bearings, carried out by Rowe and co-workers (52). They suggested that the features of this type of bearings include good load capacity and

stiffness independent of speed, low start-up torque and absence of wear, high accuracy of location and smoothness of motion, good dynamic stability and cool operation. They also found that the hybrid bearings are superior to both axial groove and circumferential groove hydrodynamic bearings when heavy dynamic loading is applied in widely varying directions.

2.3 Purpose of the investigation.

The current project is concerned with the application of oil film bearings to universal couplings used in the drive line of a rolling mill. Such bearings, operating under dynamic loads and oscillating motion cannot be adequately designed at present and the purpose of the work is to experimentally simulate the operating characteristics of such bearings and evaluate their performance.

It is not within the scope of this work to theoretically analyse such bearings but simple analyses for both hydrodynamic and hydrostatic systems are given in section 3 to provide a basis for the presentation of the experimental results.

CHAPTER 3. TRIBOLOGICAL ANALYSIS.

3.1 General.

The type of universal joint to be analyzed in the current work relies on plain-bearing action at the cross-pin and yoke interfaces to support sliding motion with oil film lubrication. This represents a tribomechanical system, which has to satisfy the following primary functions:

i) Guidance transmission of motion.

ii) Transmission of work or power.

In this system wear leads to property changes and losses from the cross-pin and bearings which are subjected to severe working conditions such as shock load and oscillating motion.

In the ideal bearing, hydrodynamic forces arising from the viscous nature of the applied lubricant are made to separate the surfaces involved in the tribo-mechanical system eliminating wear and reducing the tangential frictional force. But such hydrodynamic forces only are generated when circumstances are favourable, whereas in the present system such conditions may not be achieved, due to the fact that the movement of the bearing from rest through an angle less than 20^{o} to rest again may not provide an opportunity for the formation of the Reynolds' wedge. However, there are indications that "quasi-hydrodynamic" conditions as suggested by Barwell, may exist in this type of bearing. (7).

The design of any successful bearing must take account of many factors-service conditions, type of load, amount of load, shaft speed and its variations, oil supply, shaft hardness, cost, fatigue strength and compressive strength of bearing

materials, ease of fabrication and replacement and antiseizure characteristics. These factors are common to most applications but the list is by no means exhaustive and the importance of each factor will change according to the particular application.

In the case of the universal joint, the plain journal bearing is an attractive alternative to the rolling element bearing because of its lower cost, smoother operation and greater ability to absorb shock loads. If one could be guaranteed that the bearing was always going to operate in a fully hydrodynamic mode the design would be relatively straightforward but the service conditions imposed on the universal joint are such that the bearing may be forced to operate in any of the three zones of the well known Stribeck diagram.

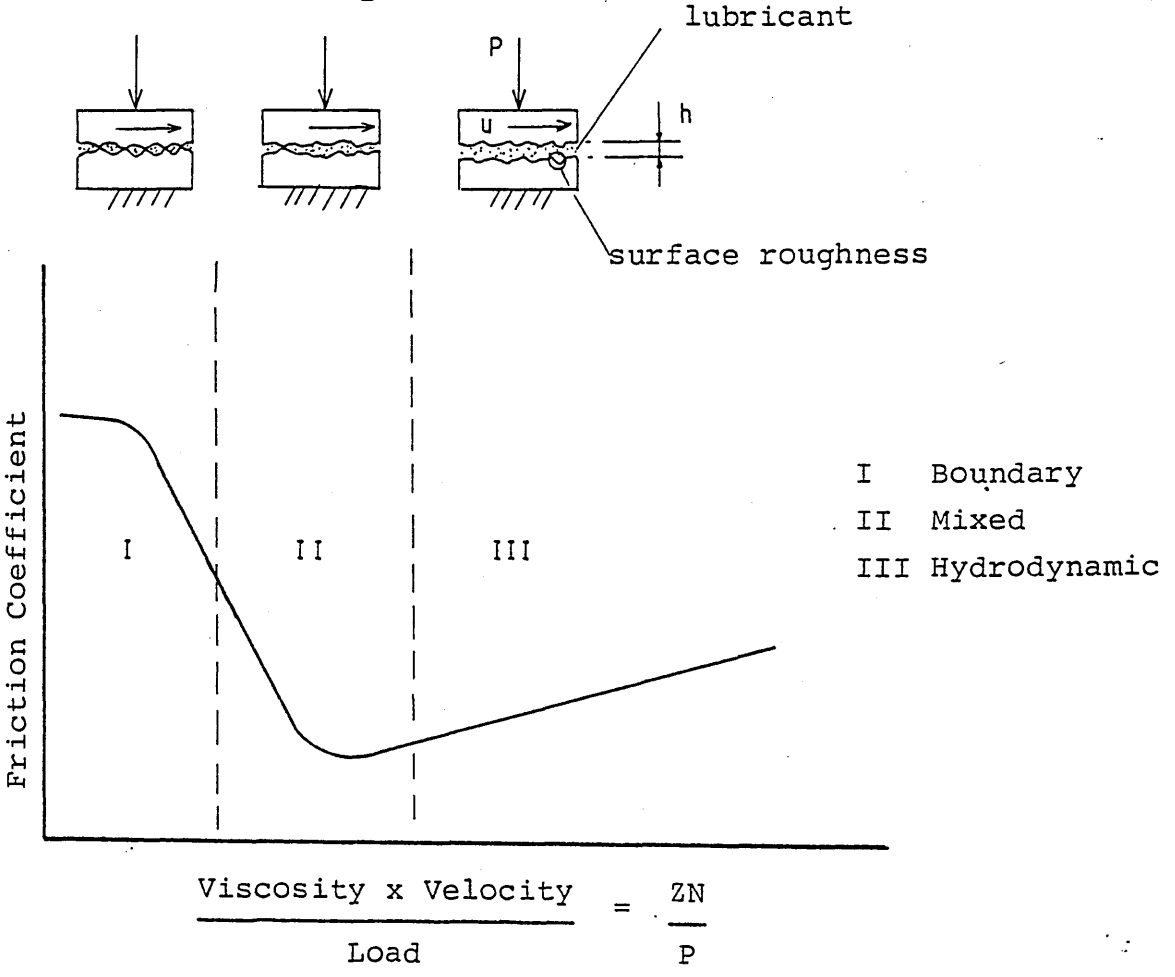

Fig. 3.1 Different Modes of Lubrication

(The Stribeck Diagram)

When a universal joint is used to drive the rolls of a rolling mill there will be occasions when the axis of the roll and the axis of the drive spindle are very nearly in line. In this situation the value of "N" will momentarily be zero and the bearing will be operating in the boundary region. On other occasions the rolls will be set well apart and there will be a large angle between the roll axis and the axis on the drive spindle. In this situation the average "N" will be finite and "P" will change from a very small value when the mill is empty with rolls turning, to a relatively large value when the product is being rolled.

Thus the average value of "N/P" will change from a high value to a relatively low value and the operating point of the bearing will move through regions III and II on the diagram. Evidently the variation of "N/P" will be even greater if the instantaneous values of "N" are considered.

In practice the loads on the bearings are even more complex. When the product enters the mill the rolls spring apart and transmit additional impact forces to the bearings because of the inertia of the spindle itself. Similarly when the product leaves the mill the rolls are suddenly brought closer together under the effect of the mill spring.

Even when the drive spindle is idling the weight of the spindle, which may be several tons in a large mill, produces a bearing load which varies in its direction from radial to axial as the spindle rotates and this load is combined with the oscillatory angular motion of the cross pin journal within the bearing bush.

In view of the great complexity of the magnitude and direction of the loading combined with the oscillatory nature of the motion it is unrealistic to expect that the established theory of hydrodynamic lubrication can provide anything more than a very general guide to the behaviour of a bearing in a universal joint. In spite of this reservation a simplified approach to hydrodynamic lubrication is presented in the following section as a basis for studying the behaviour of the test bearing.

3.2 Hydrodynamic lubrication.

The tribological behaviour of this particular bearing-journal system under a hydrodynamic lubrication mode is determined by the two following features (54):

i) The resistance to motion is given by the "internal friction" of fluid i.e. the shear resistance or viscosity of the fluid film.

ii) Wear is eliminated if the geometry of the surface is such that a load-carrying pressure is generated in the lubricant film during the motion of the surfaces leading to a complete separation of the surfaces.

So, in (i) the flow mechanism is presented by the known equations of Couette and Poiseuille. Thus, the surfaces separated by a distance h, with velocities U_1 and U_2, the entrained flow is given by, (see fig. 3.2a).

$$q_c = \tfrac{1}{2} (U_1 + U_2) h \qquad \ldots\ldots(3.1)$$

For two surfaces at rest separated by a distance h, where there is a pressure gradient (see fig. 3.2b), for a fluid with a coefficient of viscosity η , the velocity distribution is parabolic.

Therefore, volume rate of flow per unit width is:

$$q_p = -\frac{h^3}{12\eta}\frac{dp}{dx} \qquad \text{.....(3.2)}$$

If there is no variation in density,(velocity distribution parabolic superimposed upon linear profile) then the continuity for flow through the bearing is the volume rate of flow per unity width:

$$q = q_c + q_p = \text{constant.}$$

or

$$1/2\ (U_1 + U_2)\ h - \frac{h^3}{12\eta}\frac{dp}{dx} = \text{constant.....(3.3)}$$

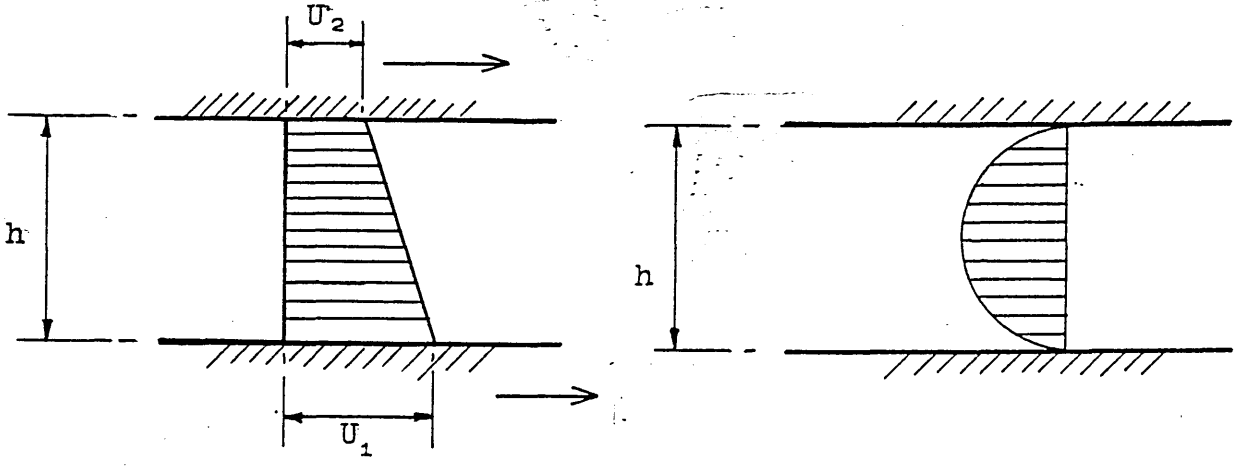

$q_c = (U_1 + U_2)\frac{h}{2}$ $\qquad$ $q_p = \frac{h^3\eta}{12}\frac{dp}{dx}$

a) Couette flow - Surface motion

b) Poiseuille flow - Pressure gradient

Fig. 3.2 Viscous Drag between two parallel plates.

As regards point (ii), for the generation of a load carrying pressure the formation of a converging, wedge-shaped film is necessary, as demonstrated by Osborne Reynolds (1886) (28).

Thus, the most important pressure generating mechanisms in self-acting fluid film bearing are the physical wedge and squeeze film (55).

If at some point in the bearing the pressure is a maximum (see fig. 3.3),

Then $dp/dx = 0$ and if $h = ho$ at this point.

Thus,

$$q = 1/2\ (U_1 + U_2)\ ho$$

and

$$1/2\ (U_1 + U_2)\ h - \frac{h^3}{12\eta}\ \frac{dp}{dx} = 1/2(U_1 + U_2)\ ho$$

therefore,

$$\frac{dp}{dx} = 6\eta\ (U_1 + U_2)\ \frac{h - ho}{h^3} \qquad \ldots\ldots(3.4)$$

Considering the general form of bearing from fig. 3.3 when the upper pad is stationary and the lower moves with velocity U ; i.e.

$$U_1 = 0, \quad U_2 = U,$$

then,

$$\frac{dp}{dx} = 6\eta\ U\ \frac{h - ho}{h^3} \qquad \ldots\ldots(3.5)$$

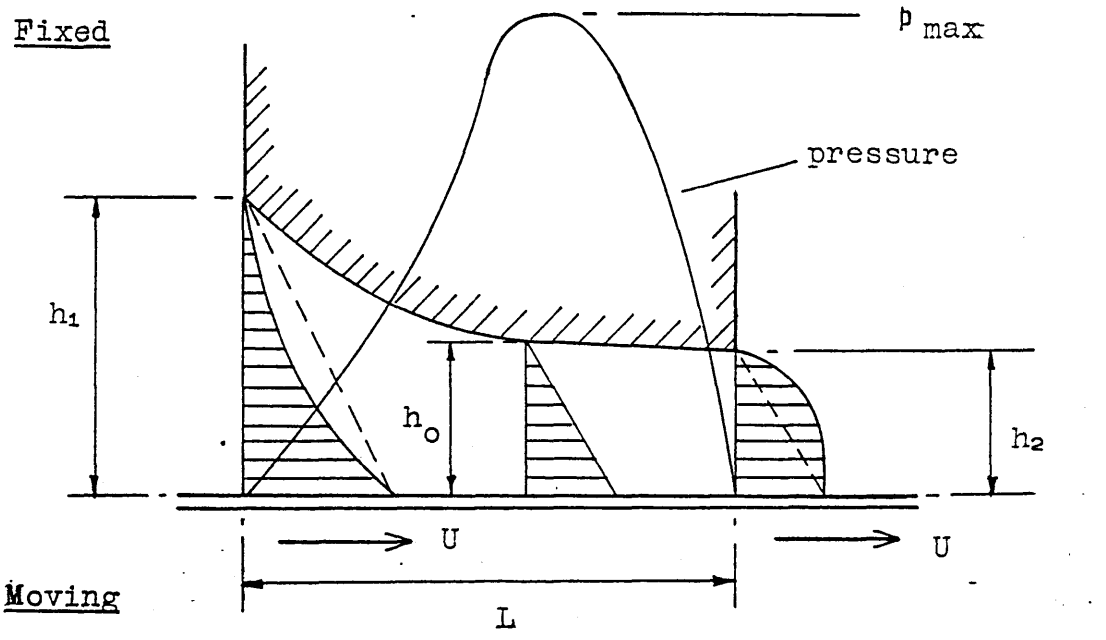

Fig. 3.3 Velocity profile in converging wedge with pressure.

Clearly this treatment is very simplified, ideally a full statement of the assumptions made in deriving the Reynolds' equation from the fundamental equations of motion for a viscous fluid i.e. the Navier-Stokes equations, should be given; these are:

1. The fluid is Newtonian.
2. The fluid flow is laminar.
3. The fluid adheres to the bearing surfaces.
4. The fluid inertia can be neglected.
5. The fluid weight can be neglected.
6. The fluid pressure is constant across the thickness of the fluid film.
7. The fluid is incompressible.

From the above assumptions the full Reynolds' differential equation can be written as:

$$\underset{(A)}{\frac{1}{6}\left\{\frac{\partial}{\partial x}\left(\frac{h^3}{\eta}\frac{\partial p}{\partial x}\right)\right.} + \underset{(B)}{\left.\frac{\partial}{\partial z}\left(\frac{h^3}{\eta}\frac{\partial p}{\partial z}\right)\right\}} \qquad \ldots\ldots(3.6)$$

$$= (U_1 - U_2)\frac{\partial h}{\partial x} \qquad \text{"wedge" term}$$

$$+ h\frac{\partial (U_1 + U_2)}{\partial x} \qquad \text{"stretch" term}$$

$$+ 2\frac{\partial h}{\partial t} \qquad \text{"squeeze" term}$$

The right hand side of this equation contains three terms of different physical significance:

i) Wedge term.- This contribution is caused by the shape of the fluid film, $\partial h/\partial x$, and the relative velocity $(U_1 - U_2)$ of the surfaces.

ii) Stretch term.- This term requires that the sum of the velocities in the x- direction change as h function of x-location. This term never exists in rigid plane-slider bearings but is applicable to special cases of dynamically loaded journal bearings.

iii) Squeeze term.- This effect arises when fluid is trapped between approaching surfaces. When the films are as thin as normal lubricants films, this action provides a valuable cushioning effect when excessive loads are applied for short intervals of time.

Solution of Reynolds' equation leads to the pressure distribution. Solutions, often termed approximate solutions, have been realized by considering the first term (A) or the second term (B) of the left hand side of the equation (3.6), equal to zero. But they are also called exact solutions in the sense that they satisfy equation (3.6), for the case of a bearing of an infinite axial length and for the infinitely short bearing. However, they are regarded as approximate solutions when used to determine the pressure distribution in bearings of finite length.

Sommerfeld (31) presented a solution for journal bearings by assumming $\partial p/\partial z = 0$, thus eliminating the second of the left hand terms of Reynolds equation, in other words the variation of oil pressure in the longitudinal or axial direction is zero, i.e. no-endwise flow, as in the case of an infinitely long bearing.

Another analysis, the short-bearing theory was originated by Michell and Cardullo, which has been amplified both experimentally and theoretically by Dubois and Ocvirk (5). They presented this solution as giving the pressure distibution in journal bearings of finite lengths, which are more common in engineering practice. In this solution the effect of the variation of pressure on oil flow in the circumferential direction is assumed to be zero i.e. $\partial p/\partial x = 0$.

The Summerfeld solution is too complex, and the accuracy of Ocvirks solution is questionable. However, for reasonable length-diameter ratios, i.e. L/D up to 1, Ocvirks solution

gives results which are well within experimental error, according with R. G. Woolacott (56) and certainly within what can be accepted from manufacturing tolerances (55).

3.2.2 Short - bearing solution (Ocvirks solution).

As has been pointed out this assumption includes endwise flow Z-axis according to fig. 3.4 and also that part of the circumferential flow which is proportional to journal surface velocity and varying film thickness but neglects the effect of oil film pressure on the circumferential flow (fig. 3.4).

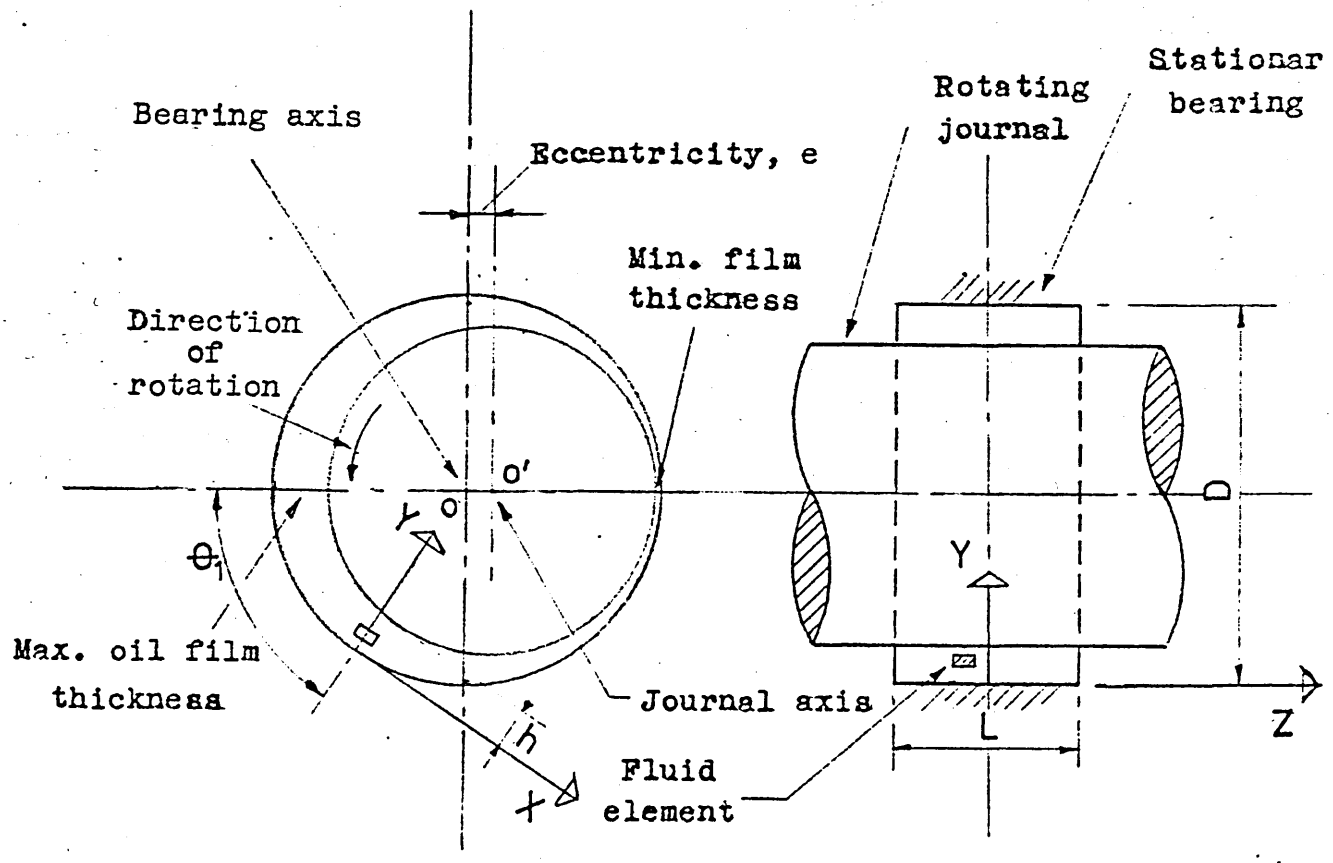

Fig. 3.4 Fluid element in converging oil film of cylindrical bearing with endwise flow.

Another important simplification is that the pressure film is assumed to commence at $\theta_1 = 0$ and to terminate when $\theta_1 = \pi$, according with fig.3.5. In other words the pressure is positive throughout the converging portion of the clearance volume and zero throughout the diverging portion.

This short-bearing application makes available formulas relating eccentricity ratio to applied load, attitude angle, angular position of peak film pressure, friction, required oil flow. Basic non-dimensional quantities called the load number, the capacity number, the friction ratio and the oil flow factor are derived, which simplify the prediction of short-bearing performance.

Thus, neglecting the first term (A), Reynolds equation can be rearranged and written:

$$\frac{d}{dz}\left(h^3 \frac{dp}{dz}\right) = 6\eta U \frac{dh}{dx} \qquad \ldots\ldots(3.7)$$

Since h is not a function of z - equation (3.7) can be written:

$$\frac{d^2p}{dz^2} = \frac{6\eta U}{h^3} \frac{dh}{dx}$$

As the variables have now been separated it can be integrated to give the pressure.

Thus, on one integration

$$\frac{dp}{dz} = 6\eta U \frac{dh/dx}{h^3} z + c, \qquad \ldots\ldots(3.8)$$

and on the second,

$$p = \frac{6\,\eta\,U}{h^3}\,\frac{dh}{dx}\,\frac{z^2}{2} + C_1 z + C_2 \qquad \ldots\ldots(3.9)$$

From fig. 3.4 the pressure p must be zero at either edge of the bearing, when $Z = \pm L/2$, also the same figure shows that there is symmetry about $Z = 0$, so $dp/dz = 0$ at $Z = 0$.

This means $C_1 = 0$ from equation (3.8), and from equation (3.9), C_2 is determined,

$$C_2 = -\frac{3\,\eta\,U}{h^3}\,\frac{dh}{dx}\,\frac{L^2}{4}$$

Therefore, the pressure distribution as a function of X and Z is given by,

$$p = \frac{3\,\eta\,U}{h^3}\,\frac{dh}{dx}\,z^2 - \frac{L^2}{4} \qquad \ldots\ldots(3.10)$$

Since, $dx = r\,d\theta_1$, from fig. 3.5 equation (3.10) may be given in polar coordinates.

$$p = \frac{3\,\eta\,U}{rh^3}\,\frac{dh}{d\theta_1}\,z^2 - \frac{L^2}{4} \qquad \ldots\ldots(3.11)$$

For the journal axis displaced "e" with respect to the bearing axis, the film thickness is considered to be:

$$h = C_r + e\cos\theta_1 = C_r(1 + \varepsilon\cos\theta_1) \ldots\ldots(3.12)$$

As shown in fig. 3.5, θ_1 is measured from the point where the film is of maximun thickness thus,

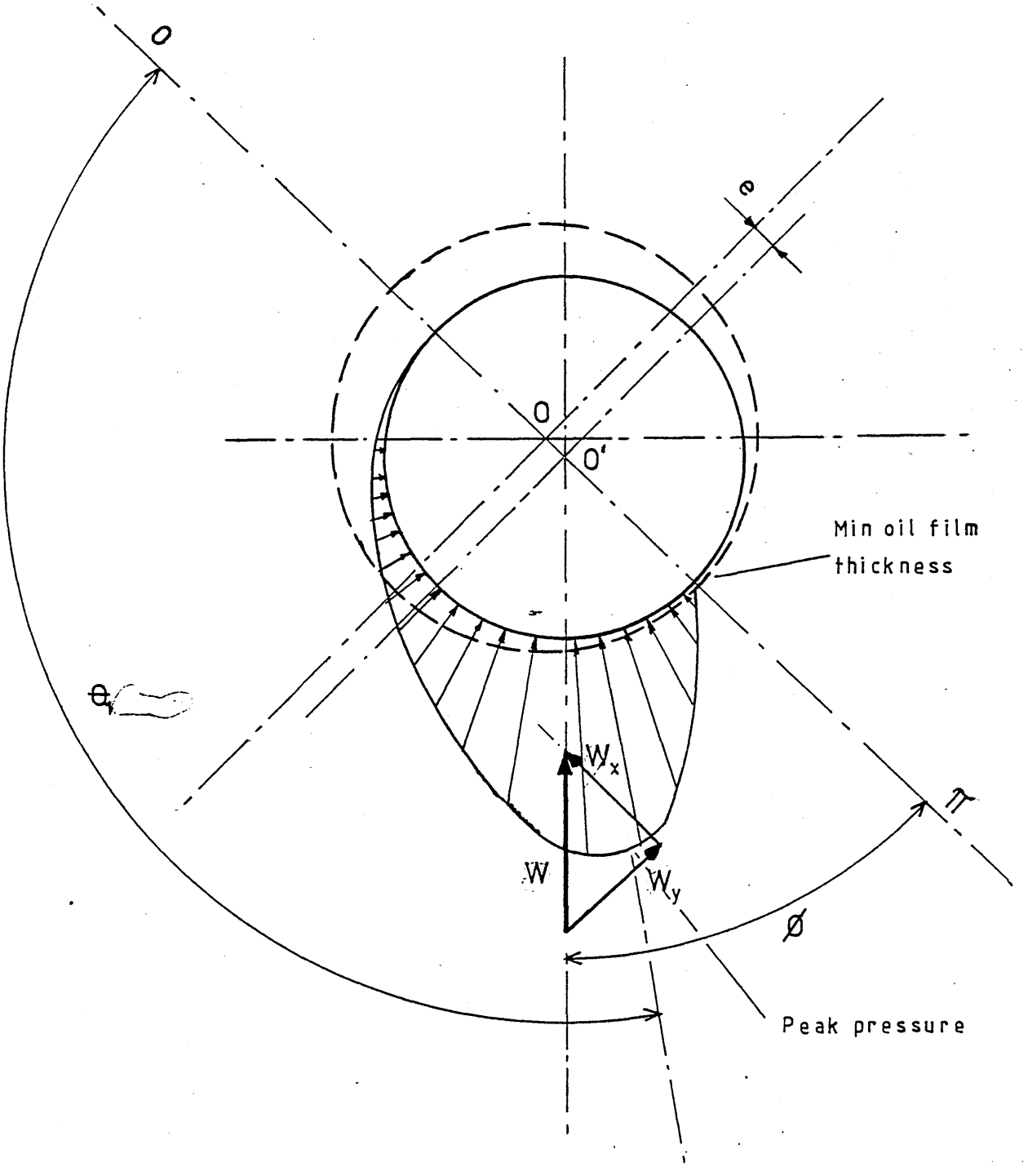

FIG. 3.5 DIAGRAM SHOWING ATTITUDE ANGLE Ø AND MAXIMUM PRESSURE.

$$\frac{dh}{d\theta_1} = - C_r \varepsilon \sin\theta_1 \qquad \text{.....(3.13)}$$

Substituting equations (3.12) and (3.13) in equation (3.11).

$$p = \frac{3 \eta U}{r C_r^2} \frac{L^2}{4} - Z^2 \frac{\varepsilon \sin \theta_1}{(1 + \varepsilon \cos \theta)^3} \qquad \text{.....(3.14)}$$

This equation shows that the pressure distribution is parabolic in the Z - direction and sinusoidal in the circumferential direction giving zero pressures at $Z = \pm L/2$ and $\theta_1 = \pi$, which are represented in fig. 3.6 below.

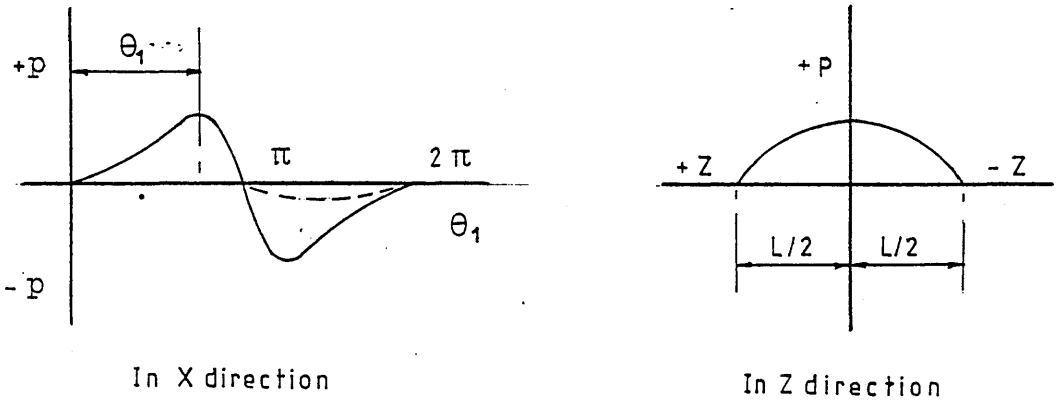

Fig. 3.6 Pressure Distribution in a full Cylindrical Bearing.

So, the external load W may be related to pressures induced in the oil film by performing certain integrations. Thus, from fig.3.5 the integrations of pressures on the journal in the directions of X - and Y - axes will give components W_X and W_Y of the resultant force which is equal to P.

$$W_x = -2 \int_0^{\pi} \int_{-L/2}^{L/2} pr \cos\theta_1 \, d\theta_1 \, dz$$

$$W_y = 2 \int_0^{\pi} \int_{-L/2}^{L/2} pr \sin\theta_1 \, d\theta_1 \, dz$$

Employing Sommerfelds' mathematical approach, the integrations with respect to θ_1 yield:

$$W_x = \frac{\eta U L^3}{C_r^2} \quad \frac{\varepsilon^2}{(1-\varepsilon^2)} \qquad \ldots\ldots(3.15)$$

and

$$W_y = \frac{\eta U L^3}{4C_r^2} \quad \frac{\pi\varepsilon}{(1-\varepsilon^2)^{3/2}} \qquad \ldots\ldots(3.16)$$

The applied load is given by

$$W = (W_x^2 + W_y^2)^{1/2}$$

$$W = \frac{\eta U L^3}{4C_r^2} \quad \frac{\varepsilon}{(1-\varepsilon^2)^2} [\pi^2 (1-\varepsilon^2) + 16\varepsilon^2]^{1/2}$$

$\ldots\ldots(3.17)$

Substituting, $U = \pi DN/2$ and rearranging gives

$$\frac{\pi L D \eta N}{W} \left(\frac{D}{C_d}\right)^2 \left(\frac{L}{D}\right)^2 = \frac{2(1-\varepsilon^2)^2}{\varepsilon} \left[\frac{1}{\pi^2(1-\varepsilon^2) + 16\varepsilon^2}\right]^{1/2}$$

$\ldots\ldots(3.18)$

The left hand term is a grouping of bearing variables in nondimensional form and is clearly seen to be dependant upon the eccentricity ratio, or attitude, ε . The reciprocal of this group will be used as the Ocvirk Number Δ throughout the rest of this thesis.

Both of the hydrodynamic bearings used in this work have central circumferential grooves requiring the modification of the Ocvirk number by considering the bearing to be in two equal halves, each with a half load capacity. If the width of the groove is "g", then the width of each half bearing is given by (L - g)/2 which, together with a half load capacity of W/2 gives an Ocvirk number of:

$$\frac{(W/2)}{\pi \eta N (L - g)/2 D} \left(\frac{C_d}{D}\right)^2 \left[\frac{D}{(L - g)/2}\right]^2$$

Therefore,

$$\Delta = \frac{4 W}{\pi \eta N (L - g) D} \left(\frac{C_d}{D}\right)^2 \left[\frac{D}{(L - g)}\right]^2$$

Attitude angle (ϕ).- This is another useful factor in examining the behaviour of narrow bearings which relates the angular position of the line of action of the load W with respect to the location of the minimum film thickness, or point of closest approach, as shown in fig. 3.5. The attitude angle is determined from,

$$\text{Tan } \phi = \frac{W_y}{W_x} = \frac{\pi}{4} \frac{(1 - \varepsilon^2)^{1/2}}{\varepsilon} \qquad \ldots\ldots(3.20)$$

So, the attitude angle depends directly on eccentricity ratio such that a simple polar curve of ε against ϕ applies for different L/D ratios.

3.3 Hydrostatic Lubrication.

3.3.1 General.

As it has been pointed out, a break down of the natural protective film carried by the surface may occur in this type of bearings i.e. hydrodynamic plain bearing, which might cause metal to metal contact. So, in order to ensure that the surfaces will be separated, an external source will provide a film of lubricant at high pressure. Under this condition the bearing is then said to work by hydrostatic lubrication. The pressures in the bearing film are controlled so that the highest pressure acts to oppose the applied load (57).

Although, hydrostatic bearings may require relatively expensive and complex fluid supply equipment, they offer the following advantages:

i) No metal to metal contact, i.e. no wear, at any operating velocity (including U = 0) or at any load for all types of relative motion.

ii) Low friction determined only by the internal friction of the fluid.

iii) Predictable functional performance.

A hydrostatic bearing esentially involves two resistances in series. The fluid flows through an orifice restrictor (or other control resistance) and then through the resistance formed by the bearing clearance. The basic principle of a hydrostatic bearing is illustrated in fig. 3.7. A fixed displacement pump supplies oil to a capillary restrictor at a constant supply pressure Ps which is controlled

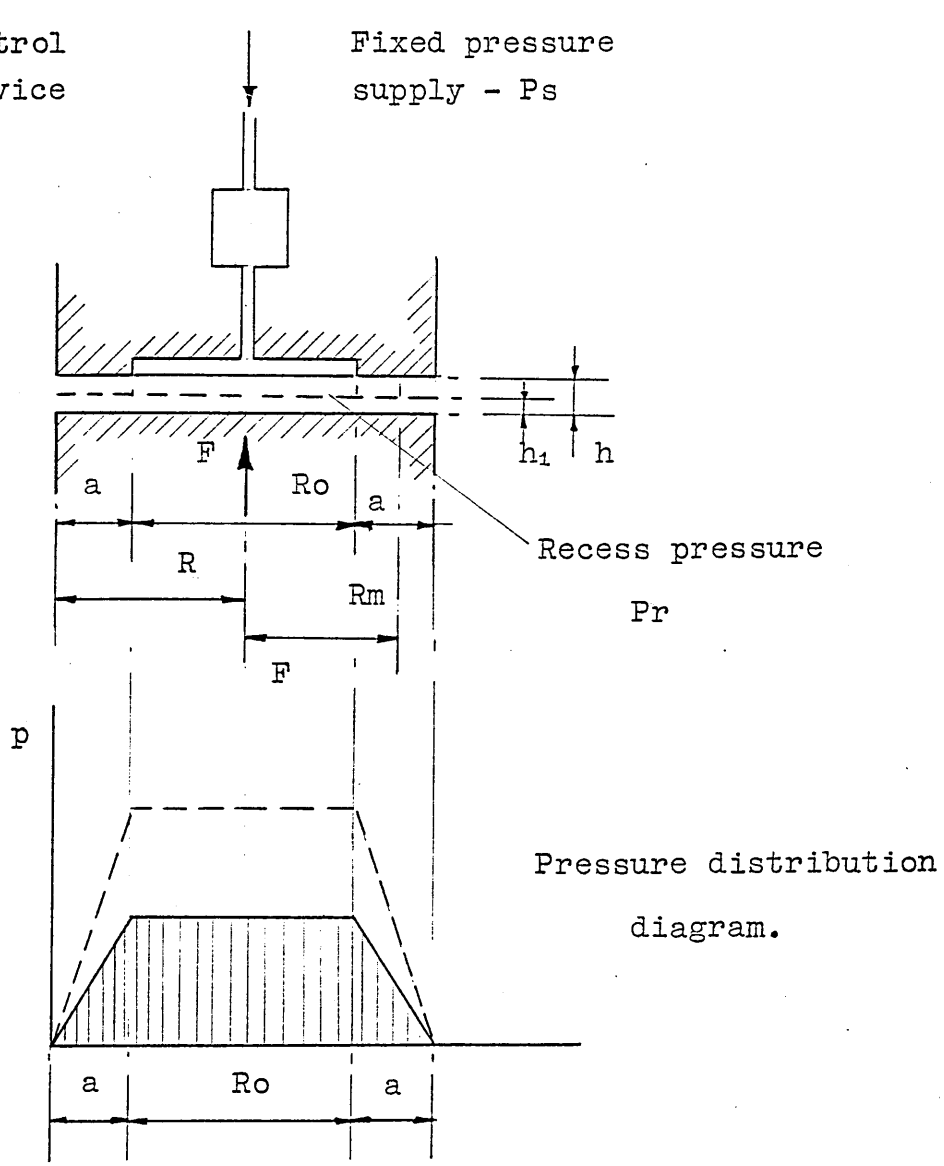

Fig. 3.7 Basic Hydrostatic Bearing.

by a relief valve. The pressure is reduced through the capillary and arrives at the entry to the bearing at recess pressure Pr (58).

The pressure further reduces as the oil flows through the restriction caused by the bearing gap or clearance "h". If the bearing clearance closes up a distance "h_1" the restriction to flow through the bearing increases and the recess pressure increases.

The relationship between bearing clearance and recess pressure will depend on such features as the nature of the control device, in this case a capillary, and parameters such as the supply pressure and the oil viscosity.

From the figure 3.7 , of a typical hydrostatic thrust bearing, it is seen that hydrostatic bearings can operate with uniform oil film thickness, h = constant, in contrast to hydrodyanmic bearings and also with no-relative tangential motion.

Therefore, in the Reynolds equation, the right hand side becomes zero, since Uo, U_1, h/ t may be put equal to zero (59).

Hence, the Reynolds equation reduces to :

$$\frac{\partial^2 p}{\partial X^2} + \frac{\partial^2 p}{\partial Z^2} = 0 \qquad \ldots\ldots(3.25)$$

Which can be solved for the particular geometry of the bearing under consideration. So, for this case the pump pressure P_s in the recess needed for the support of the load F is determined by

$$P_s = \frac{2\,F}{\pi\, D_m\, a} \ln \frac{D_o}{D} \qquad \ldots\ldots(3.26)$$

And the flow rate q and film thickness are related by means of the following equation:

$$q = \frac{F\, h^3}{3\,\eta\, D_m\, a} \qquad \ldots\ldots(3.27)$$

where the terms P_s and q determine the requirements of the pump.

Similarly the very simple capillary control can be analysed to yield results for non-dimensional stiffness.

3.3.2 Slot-entry Hybrid Bearing.

This is another type of hydrostatic bearing, which has been used for the present work. In this, the conventional orifice is replaced by an almost continuous slot which induces axial laminar flow to the bearing gap and avoids recesses for maximum hydrodynamic effect (60).

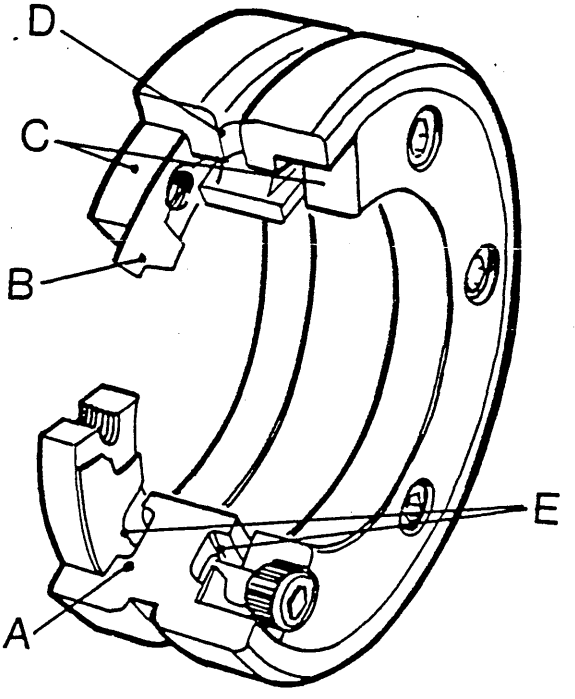

Fig. 3.8 Illustration of a standard modular bearing.

Figure 3.8, above, shows the arrangement of a slot-entry bearing having a double row of radial slots. The bearing consists of a bearing body - A, which is recessed on either side. These recesses accept a preformed shim ring - B, which provides the slot configuration, when clamped between the body and the retaining rings - C. The operating fluid enters via holes - D in the outer radial groove and reaches the annular fluid chamber - E.

Then, when the shaft becomes eccentric the bearing film thickness is reduced on one side of the bearing bore and increased on the diametrically opposite side. The presence of the supply restrictors as indicated in fig. 3.9, causes the supply pressure P_s to increase in the region of the reduced film thickness and to reduce in the region of the increased film thickness.

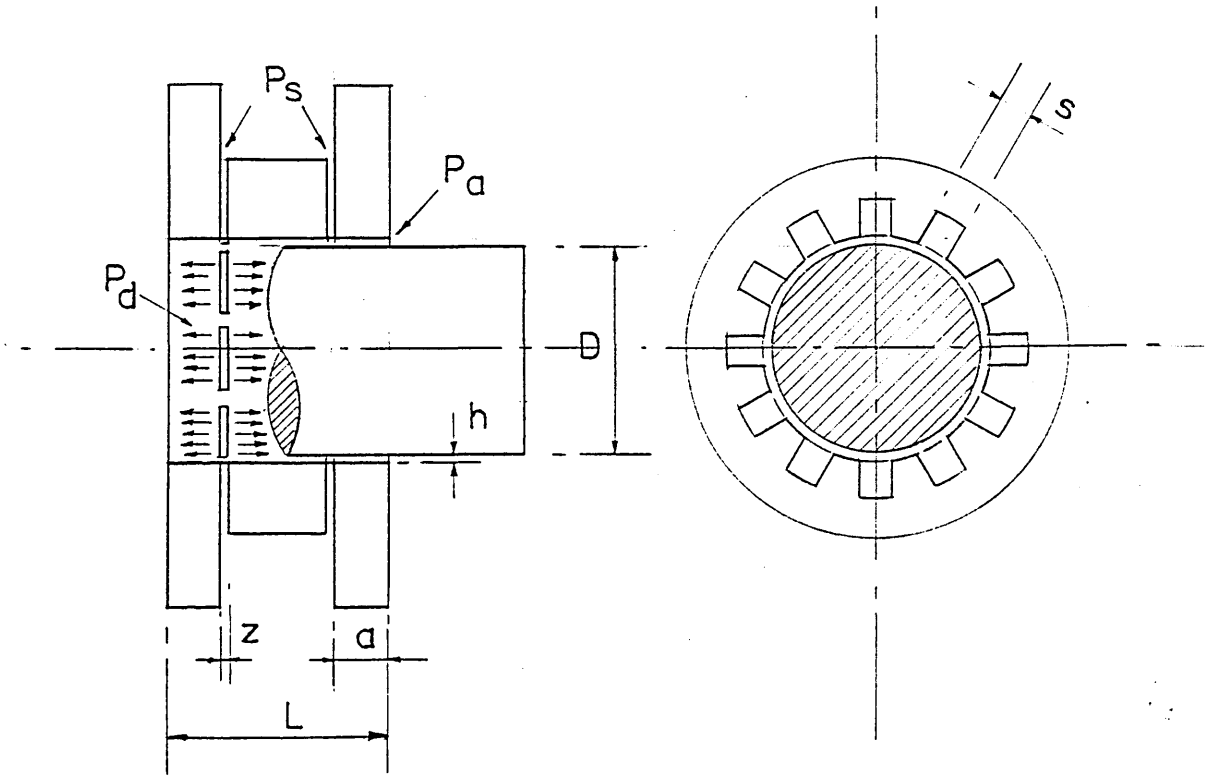

Fig. 3.9 Diagram of slot fed journal bearing.

This simple principle is the basis by which a hydrostatic journal bearing provides stiffness and load - capacity at zero speed. At speed, rotation of the shaft drags the lubricant around the bearing clearance; as the shaft becomes eccentric the lubricant is forced into the converging film thickness region causing an increase of pressure in that area - P_d. The lubricant is also forced out from the diverging film thickness region loading to a reduction in pressure down to atmospheric pressure - P_a.

So, the oil pumped into the bearing will efectively "float" the shaft enabling a wedge or thick film to develop under running conditions. Therefore, this effect raises the load - carrying capacity. The relationship between the load parameter with the supply pressure and bearing area has been described by Fuller.(57), which is called Fuller number and defined as follows:

$$\overline{W} = \frac{W}{P_s LD} \qquad \text{.....(3.28)}$$

This is the parameter used in the present work in the graphical representation of the results against the eccentricity ratio.

4.1 Hooke's Joint Model.

4.1.1 Kinematic Analysis of the Numerical Joint Pin.

The universal or Hooke's joint has a cross-pin supported with bearings at each of its ends. When the angle between the two shafts is non-zero, i.e. when misalignment exists, the cross-pin will move with oscillating motion. The total angular displacement (ψ) will be twice the misalignment angle (δ), so

$$\psi = 2\,\delta$$

A kinematic analysis of the cross-pin is necessary in order to find the pin velocity, which in conjuction with the load applied will be the main parameters for determing the performance of the bearings.

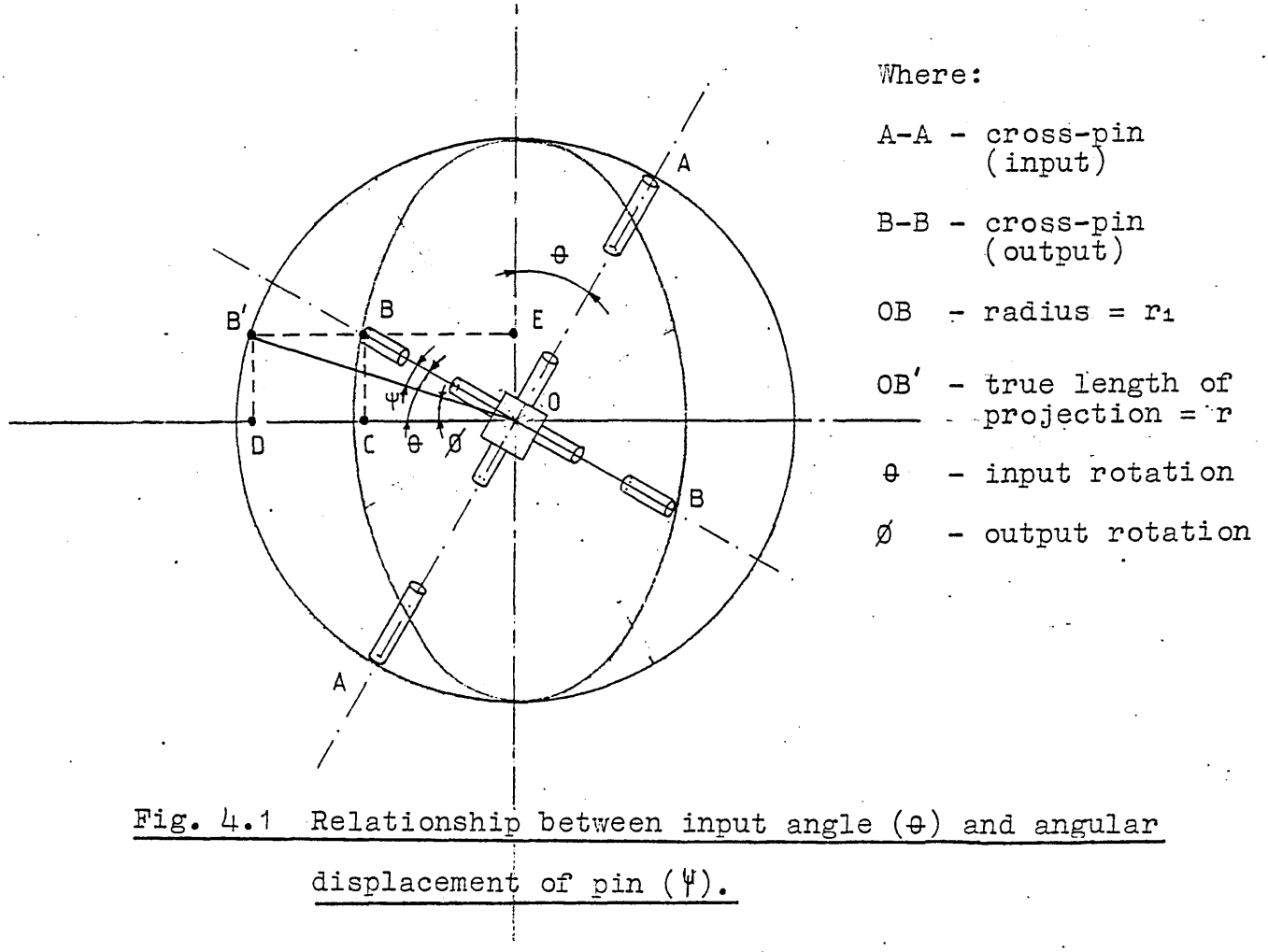

Fig. 4.1 Relationship between input angle (θ) and angular displacement of pin (ψ).

Consider fig. 4.1 which shows the circular path of the cross-pins of the driving shaft "A" and the circular path of the cross-pin connected to the out-put shaft "B".

When the cross-pin of shaft "A" rotates through an angle θ in plane A the corresponding rotation in plane B will be through an angle ϕ , which is produced only by the projection of θ imparted to the cross-pin of shaft "B".

Then, the pin angular displacement is determined by trigonometry as follows:

Rotation of pin is ψ which is found from fig 4.1 as:

$$\cos \psi = \frac{r_1}{r} \qquad \ldots\ldots(4.1)$$

Applying the properties of the ellipse:

$$\cos \delta = \frac{\overline{EB}}{\overline{EB''}} \qquad \ldots\ldots(4.2)$$

where:

$$EB = r_1 \cos \theta \quad \text{and} \quad EB'' = r \cos \phi$$

therefore,

$$\frac{\overline{EB}}{\overline{EB''}} = \frac{r_1 \cos \theta}{r \cos \phi} = \cos \psi \; ; \; \frac{\cos \theta}{\cos \phi} = \cos \delta \qquad \ldots\ldots(4.3)$$

but,

$$\tan \phi = \frac{\overline{DB''}}{\overline{OD}} = \frac{CB}{EB''}$$

and

$$\overline{EB''} = \frac{\cos \delta}{\overline{EB}}$$

substituting,

$$\tan \phi = \frac{\overline{CB}}{\overline{EB''}} \cos \delta$$

finally,

$$\tan \phi = \tan \theta \cos \delta \qquad \ldots\ldots(4.4)$$

which represented in a right-angled triangle gives,

opposite side $a = \tan \theta \cos \delta$

adjacent side $b = 1$

hypoteneuse $c = (1 + \tan^2 \theta \cos^2 \delta)^{1/2}$

from this, $\cos \phi$ is defined as:

$$\cos \phi = \frac{1}{(1 + \tan^2 \theta \cos^2 \delta)^{1/2}} \qquad \ldots\ldots(4.5)$$

sustituting (4.5) in (4.3) gives:

$$\cos \psi = \frac{\cos \delta}{\cos \theta} \cos \phi$$

therefore,

$$\cos \psi = \frac{\cos \delta}{\cos \theta} \frac{1}{(1 + \tan^2 \theta \cos^2 \delta)^{1/2}} \qquad \ldots\ldots(4.6)$$

squaring the above equation and substituting:

$$\cos^2 \theta + \sin^2 \theta = 1$$

and

$$\cos^2 \delta + \sin^2 \delta = 1$$

gives,

$$\cos^2 \psi = \frac{\cos^2 \delta}{1 - \sin^2 \theta \quad \sin^2 \delta} \qquad \ldots\ldots(4.7)$$

finally the pin displacement may be expressed as follows:

$$\cos \psi = \frac{\cos \delta}{(1 - \sin^2 \theta \quad \sin^2 \delta)^{1/2}} \qquad \ldots\ldots(4.8)$$

simplifying and differentiating equation 4.7 with respect to time, the angular velocity of the cross-pin relative to the yoke is given by,

$$\frac{d\psi}{dt} = - \frac{\sin 2\theta \quad \sin 2\delta}{4 (1 - \sin^2 \theta \quad \sin^2 \delta) \cos \theta} \quad \frac{d\theta}{dt} \qquad \ldots\ldots(4.9)$$

The pin-angular acceleration is found by differentiating the velocity equation with respect to time, giving the following equation:

$$\frac{d^2 \psi}{dt^2} = - \cos\theta \tan \delta (\sec^2 \delta + \tan^2 \delta \quad \sin^2 \theta)$$

$$(1 + \cos^2 \theta \tan^2 \delta)^{-2} \quad \left(\frac{d\theta}{dt} \right)^2 \qquad \ldots\ldots(4.10)$$

4.1.2 Cross-pin angular displacement experimental measurement.

The analytical solution of the pin displacement (ψ) in relation to the shaft input angle (θ) was verified by means of a working model, which is shown in fig. 4.2. The model consists of an input shaft and an output shaft connected by universal couplings. The misalignment between the shafts can be altered, and angles from 0° to 45° are obtainable.

FIG.4.2 MODEL FOR TESTING HOOKE'S JOINT.

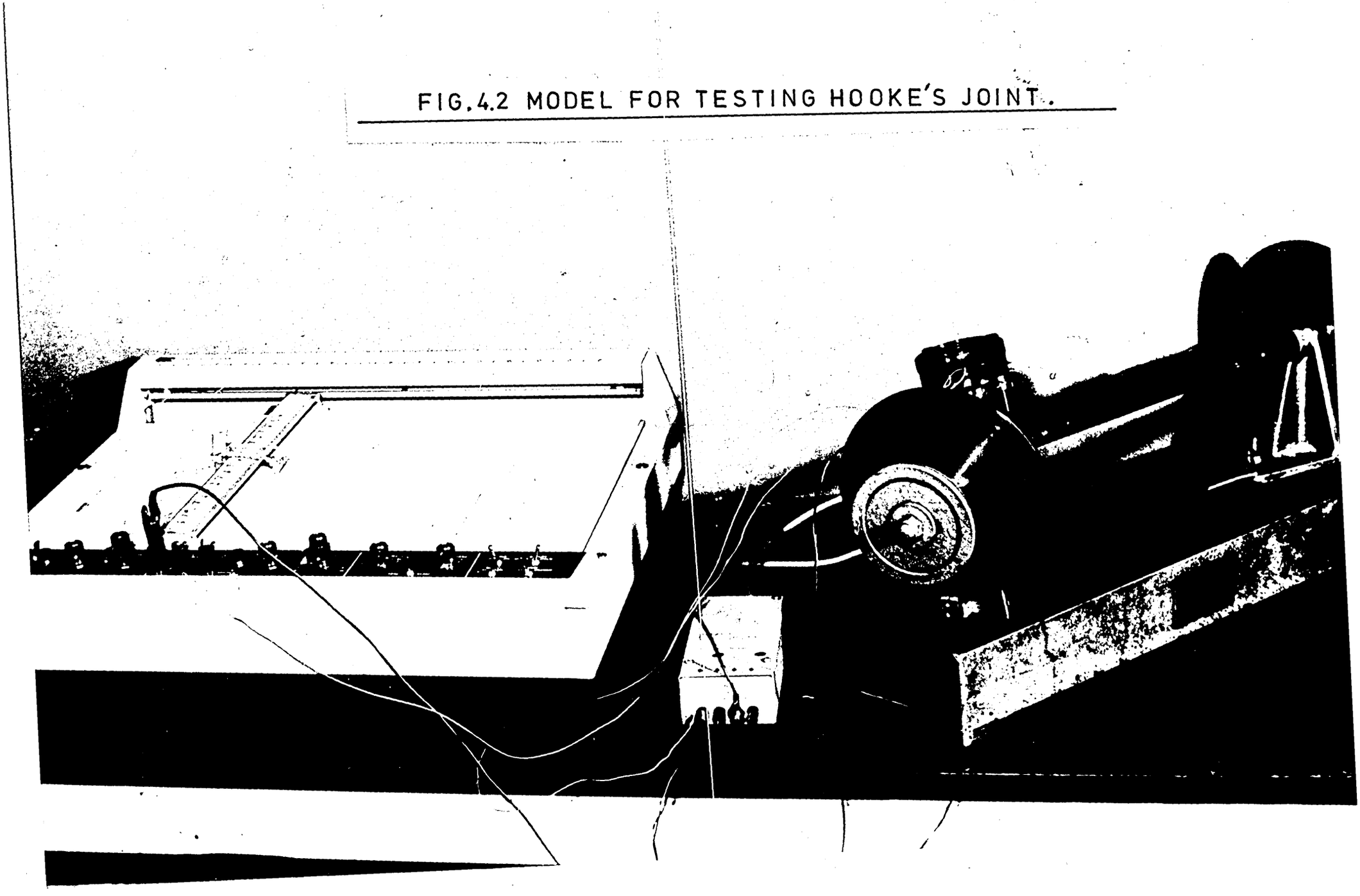

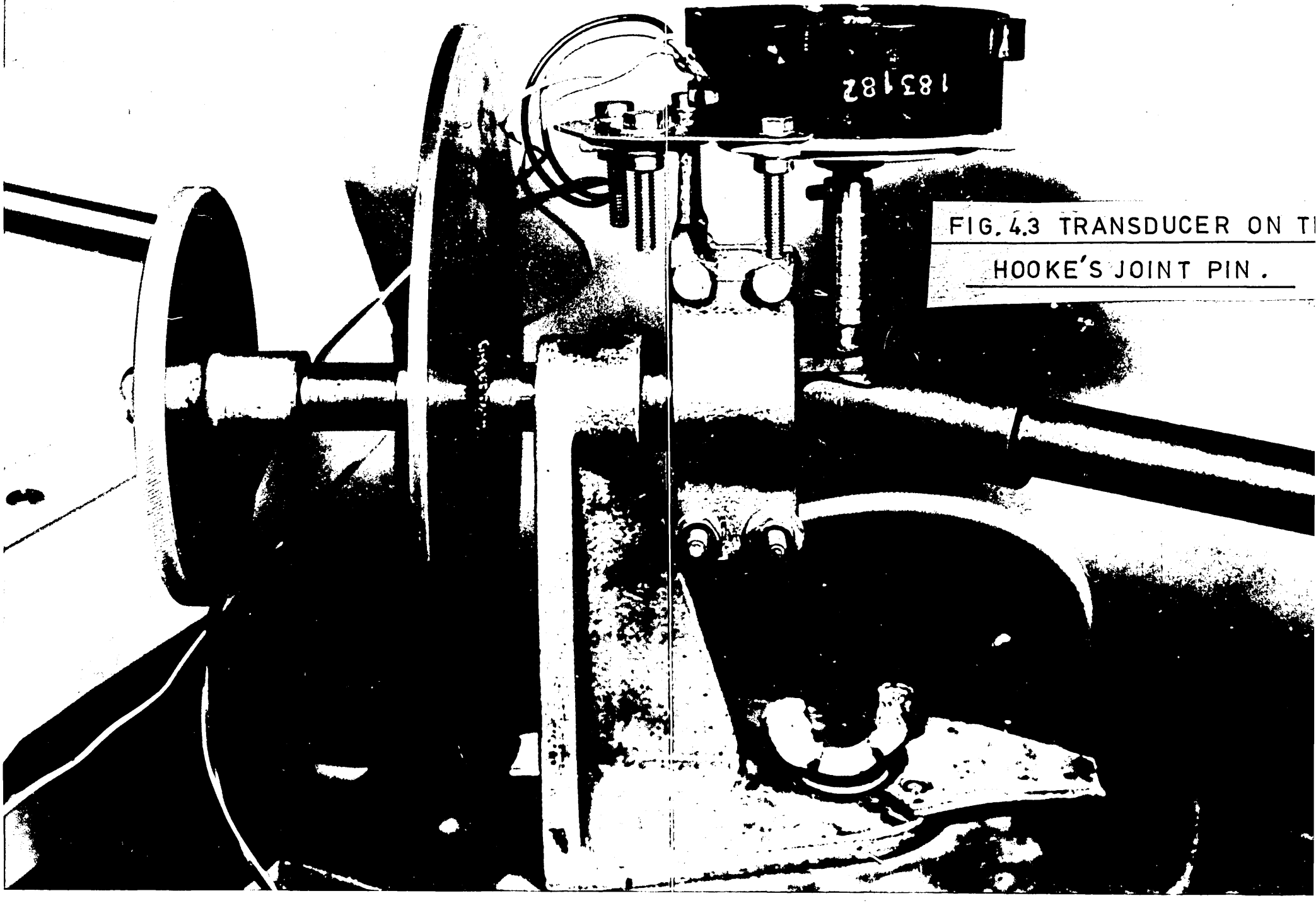

FIG. 4.3 TRANSDUCER ON T
HOOKE'S JOINT PIN.

The crosspin angular displacement relative to the yoke was measured by means of a rotary potentiometer, which was fitted directly to the pin end (see fig. 4.3).

The transducer was firmly supported in relation to the input shaft via a bracket, allowing the whole of the transducer to move through the same angle as the input shaft.

The transducer was connected to an X - Y recorder providing a record of angular pin displacement against input shaft rotation for a particular setting of misalignment between the shafts.

The circuit used to obtain the pin displacement is shown diagramatically in fig. 4.4 below.

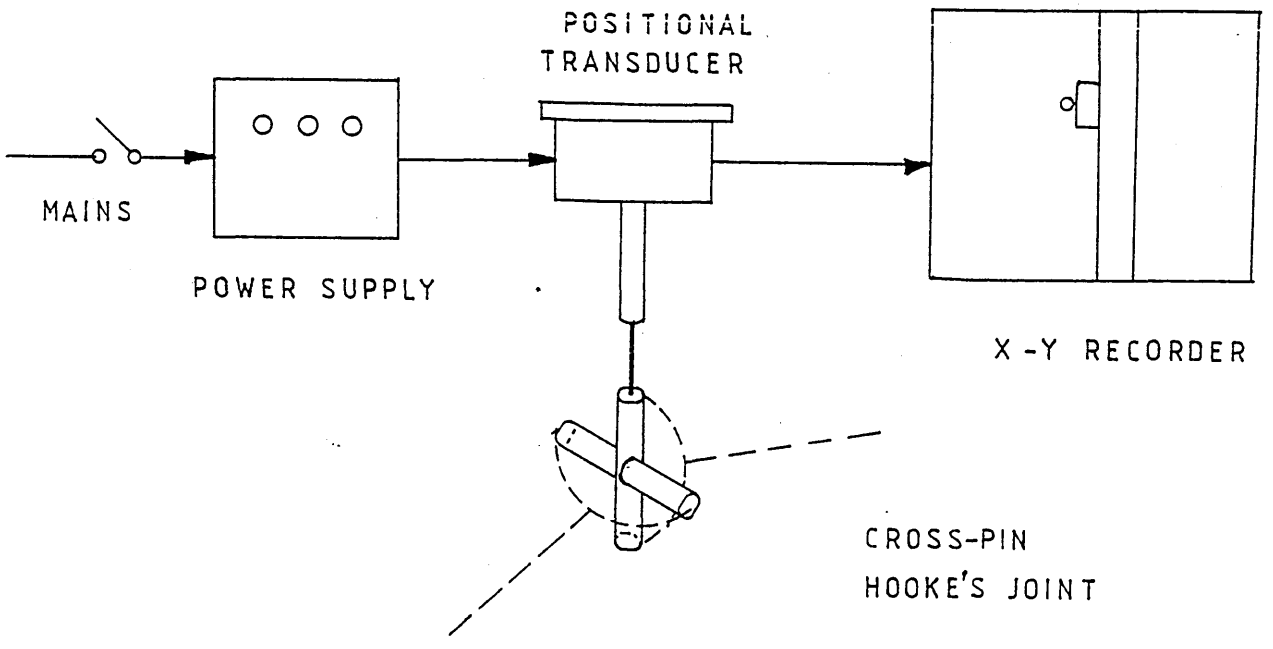

Fig. 4.4 Diagram of the experimental apparatus.

The results obtained are plotted in fig. 4.5 where close correlation between the theoretical and experimental values was obtained.

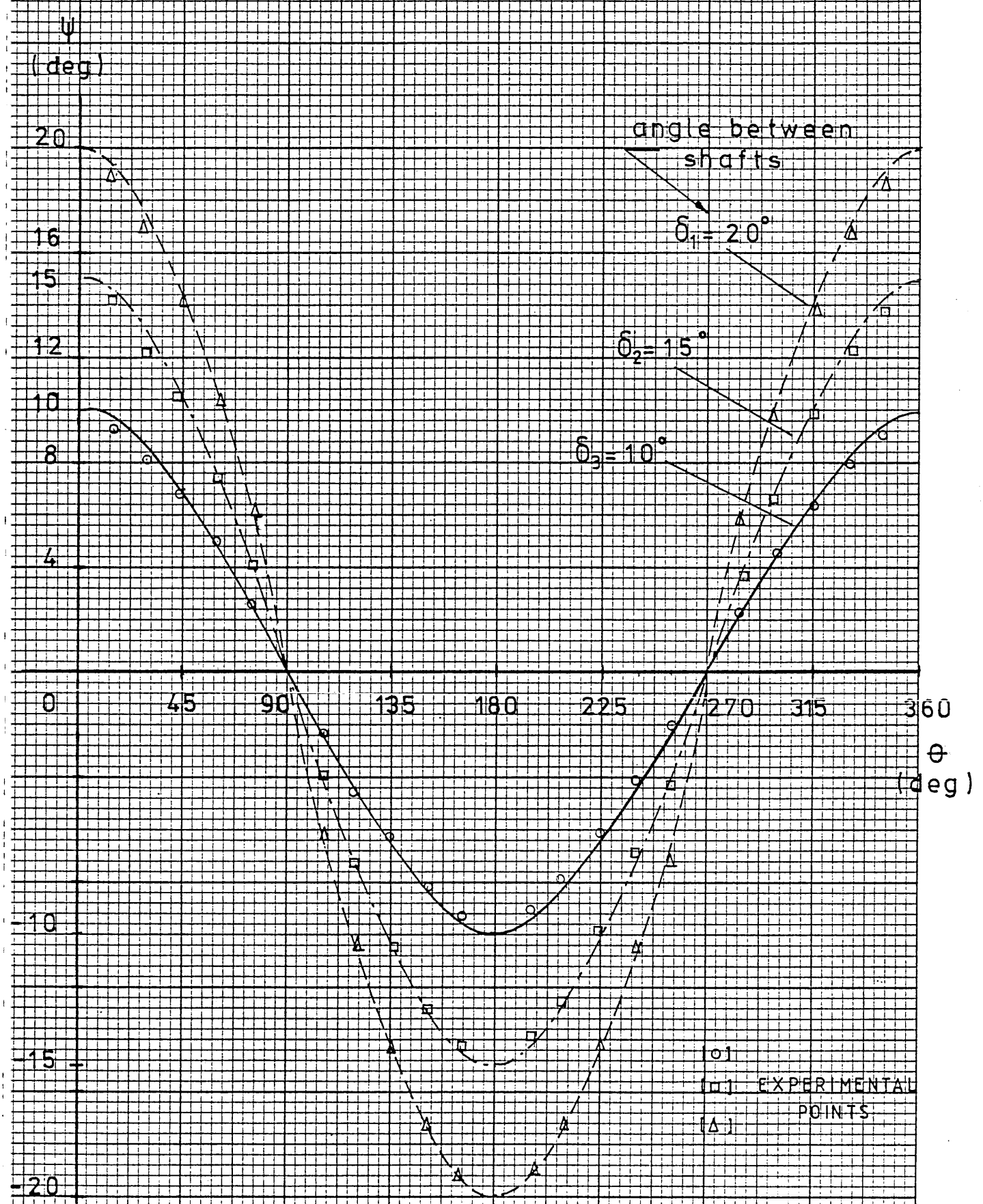

FIG. 4.5 GRAPH OF PIN DISPLACEMENT (ψ) AGAINST INPUT SHAFT ROTATION (θ).

4.2 Experimental rig.

4.2.1 Selection of parameters.

The objective of the present test rig, which simulates the universal coupling bearing conditions in the rolling mill drive-line, is to provide a means of laboratory investigation of those parameters which are expected to affect the life of such machine components.

The general design of the apparatus is given by the arrangement drawing shown in appendix D, detail drawings of each individual component are also included.

The model similarity was fundamentally done in accordance with the data sheets formulated by the Institution of Mechanical Engineers - ESDU - item No. 66023. This is (61) a standard method based largely on a computer numerical analysis. The model similarity is described in section 4.2.3.

The parameters listed below are likely to influence the performance of the bearings to be analyzed.

1. Dynamic considerations.

i) The shape and magnitude of the load applied.

ii) The phasing between angle of oscillation and the load.

iii) Frequency of oscillation.

iv) Angle of oscillation.

2. Geometric considerations.

i) Radial clearance.

ii) The length-diameter ratio of the bearing.

iii) Shape and position of oil grooves and oil supply.

iv) The rigidity of the bearing.

v) Deflection of the journal.

vi) Surface roughness.

3. Lubrication.

i) Viscosity of lubricant.

ii) Lubricant inlet pressure.

iii) Lubricant inlet temperature.

iv) Viscosity as a function of temperature.

v) Condition of the lubricant.

4. Physical properties of bearing and journal.

i) Choice of bearing material.

ii) Choice of shaft material.

iii) Surface hardness of shaft.

<u>Dynamic considerations.</u>

Dynamic loading will tend to promote the formation of hydrodynamic pressure films, due to the squeeze film effect.

The oscillating motion will induce zero velocity at reversal which is likely to be detrimental to the formation of a hydrodynamic film sufficiently to cause the journal to ground. However this will only be an instantaneous effect and the fluctuation of sliding velocity throughout oscillation may well promote the film formation and mantain a reasonable bearing performance.

Also, the phase of peak load relative to the oscillating motion may be significant i.e. if the peak load coincides with the velocity reversal of the journal, being momentarily zero, a degree of metallic contact may occur.

Geometric considerations.

In the majority of cases the main dimensions of the bearing are fixed by other considerations in the machine design. For instance the diameter is usually fixed by considerations of cross-pin rigidity and strength, and bearing length is normally limited by the space available, but it is advisable to adopt a reasonable length-diameter ratio (L/D) on the basis that increasing diameter will have the result of high tangential speed therefore encouraging hydrodynamic conditions which, coupled with the shortness of the pin will considerably reduce the pin deformations resulting in less risk of failure.

The clearance between the bearing and journal is a very critical factor in hydrodynamic bearings in order to obtain an adequate oil flow, but also generate a satisfactory pressure.

A rule of thumb of 1/1000 of the diameter has been found reliable. The grooving to be used, is the axial and circumferential arrangement, which is the best adapted to the type of loading and type of service for this bearing as it has been shown in previous work.

Another consideration is that a good surface finish will improve the load-carrying capacity and the effect becomes greater as the finish is improved (48).

Lubrication.

The flow of the lubricant will be dependant upon radial clearance, supply pressure, viscocity. High pressure will be supplied in order to improve the load carrying-capacity of the bearing by increasing the oil flow and to form a hydrostatic pressure in the bearing.

Physical properties of bearing.

The bearing and shaft materials have been considered from those used in previous experiments. Bronze, according to M. J. Neale (54) is an advisable material in oscillatory journal bearings with small rubbing velocity and shock loading.

4.2.2 Bearing performance.

It has already been mentioned in section 4.2.1, some of the main parameters which are expected to influence the performance of the test bearings. By varying each of these in turn an appreciation of their significance will be

established. In assessing the performance of the bearing the variation of radial clearance will be measured and used, in conjunction with non-dimensional parameter groups suggested in the theoretical section to present experimental information.

Thus, the choice of these parameters in order to define the frame of the present investigation has been made as indicated below.

For a series of different bearing loads, frequencies of oscillation and oil supply pressure the following quantities will be determined experimentally:

i) Shaft centre displacement - eccentricity.

ii) Bearing temperatures.

iii) Shape and magnitude of loading.

iv) Shape and amplitude of the oscillating motion mode of the shaft.

4.2.3 Model Similarity.

The design of plain oil film bearing for the cross-pin of the universal coupling applied to a plate rolling mill, was originally attempted as a possible reference for the design of the present test rig.

The performance of such a bearing was determined by the guidelines laid down in the data sheets issued by the Institution of Mechanical Engineers, ESDU - item No. 66023 (61) This is a standard method based largely on a computer numerical analysis, to design steadily loaded bearings, which predicts the position of the journal centre quite easily with the aid of the load carrying capacity/eccentricity relationship. The ESDU solution was used with the following design conditions:

i) Steady load W = 1.4 MN

ii) Maximum speed N = 120 rev/min

iii) Cross-pin diameter D = 200 mm

iv) Length / Diameter ratio L/D = 0.66

v) Oil viscosity η = 0.4 N s / m^2

With the above information and with the help of the charts the following procedure was carried out:

From figure 4.6

a) Draw J - K line for a L/D = 0.66.

b) Draw A - B line for speed limitation of

N = 2 rev/sec

And from figure 4.7, the safe oil thickness is determined for a bearing diameter D = 200 mm and N = 2.0 rev/sec then,

$$hs = 0.0089 \text{ mm}$$

On the other hand, the deflection of the cross-pin due to the applied load should be determined in order to consider the minimum oil film thickness.

$$\delta' = \frac{8 W L^3}{\pi E D^4}$$

$$\delta' = \frac{8 \times 1.4 \times 10^6 \times 0.66^3}{\pi \times 200 \times 10^9 \times 0.20}$$

Therefore,

$$\delta' = 0.025 \times 10^{-3} \text{m (total)}$$

Then the minimum oil film is calculated as follows:

$$h \text{ min} = h \text{ safe} + \delta'' \text{ at the centre}$$

$$h \text{ min} = 0.0089 \times 10^{-3} + 0.0125 \times 10^{-3}$$

Hence,

$$h \text{ min} = 0.0214 \times 10^{-3} \text{ m}$$

Then the ratio below can be calculated using the values already known,

$$\frac{W^{1/2} \quad h \text{ min}}{D^2} = \frac{(1.4 \times 10^6)^{1/2} \times 0.0214 \times 10^{-3}}{0.2^2} = 0.633$$

So, in figure 4.6, this value indicated by the line X - Y is well above the line A - B of speed limitation;

therefore this method suggests that bearings of this type are not suitable for the real application.

But assuming that all data are known in the formula of the duty parameter W' e.g. Sommerfeld number, another attempt can be made to calculate the bearing load capacity (under static loading and constant velocity):

$$W' = \frac{W}{\eta N D L} \left(\frac{Cd}{D} \right)^2$$

$$= \frac{1.400 \times 10^3}{0.4 \times 2 \times 0.2 \times 0.132} (0.001)^2$$

$$W' = 66$$

This value is out of the scale in the vertical axis of fig. 4.8, from which it is concluded that such bearings cannot be determined by this method either.

Therefore, it was decided to examine the performance of a model bearing designed within the recommendations of the ESDU - charts and laboratory limitations, in order to establish a reasonable eccentricity ratio.

It was felt that a load of 5000 N was the maximum which could be satisfactorily applied and that a pin diameter of 38 mm would provide sufficient clearance to enable sensible eccentricity measurements to be made. Also the pin speed was kept around that likely to be found in practice i.e. 120 rev/ min.

Again, using the ESDU charts the design of the test rig is determined as follows

1) From figure 4.6

a) Space limitation maximum $\frac{b}{d} = 0.66$

draw J - K line.

b) Speed limitation N = 2.0 rev/sec

draw A - B line.

2) From figure 4.7

a) Film thickness limitations

for d = 38 mm N = 2.0 rev/sec

Therefore,

$hs = 4.1 \times 10^{-6} m$

b) Deflection of the shaft due to the load:

$$\delta' = \frac{8 W b^3}{\pi E d^4}$$

for, b/d = 0.66 and $E = 200 \times 10^9 \ N/m^2$

therefore,

$$\delta' = \frac{8 \times 5000 \times (0.66 \times 0.038)^3}{\pi \times 200 \times 10^9 \times 0.038^4}$$

$$\delta' = 1.1 \times 10^{-6} \ m \ \text{(total)}$$

hence,

$h \ min = [illegible] = 4.65 \times 10^{-6} m$

and the ratio:

$$\frac{W^{1/2} h \ min}{d^2} = \frac{5000^{1/2} \times 4.65 \times 10^{-6} m}{0.038^2} = 0.22$$

Hence draw A - D line in figure 4.6.

c) Choice of lubricant:

Draw D - C line which gives oil No. 4.

d) Guide to minimun clearance:

for oil No. 4

N = 2.0 rev/sec point B must lie to left hand side of guide line (oil No. 4)

therefore B is selected at $\frac{Cd}{d} = 1.2 \times 10^{-3}$

e) Check clearance limitation

$$\frac{Cd}{d} = \frac{h\ min}{d} \quad \frac{25}{(11 - d/b)}$$

$$\frac{Cd}{d} = \frac{4.66 \times 10^{-6} \times 25}{0.038\ (11 - 38/25)} = 3.23 \times 10^{-4}$$

Cd/d should not be less than the above value.

f) From point C:

$\theta max - \theta min = 30^{\circ}$ C

θ min for oil 4 = 40° C

therefore,

$\theta max = 70^{\circ}$ C

g) From line C-D the oil viscosity is defined:

$\eta e = 0.35$ N - S/m^2

3) From figure 4.8, the load capacity is determined:

$$W' = \frac{W}{\eta e \quad N \quad b \quad d} \left(\frac{Cd}{d}\right)^2$$

$$W' = \frac{5000}{0.35 \times 2.0 \times 0.038 \times 0.025} (1.2 \times 10^{-3})^2$$

$$W' = 10.83$$

With the above value and b/d = 0.66, the eccentricity ratio is determined in fig. 4.8.

Hence,

$$\epsilon = 0.75$$

Which lies within the recommended area.

Summary of design:

1) Diameter and width ratio: L/D = 0.66, D = 38 mm

2) Minimum film thickness: h min = 4.65 μm

3) Diametral clearance : Cd = 0.045 mm (=0.0015 inch).

4) Maximum temperature: $\theta_{max} = 70^{\circ}$ C

5) Oil viscosity: $\eta_e = 0.35$ N - S / m^2

6) Eccentricity ratio: $\epsilon = 0.75$

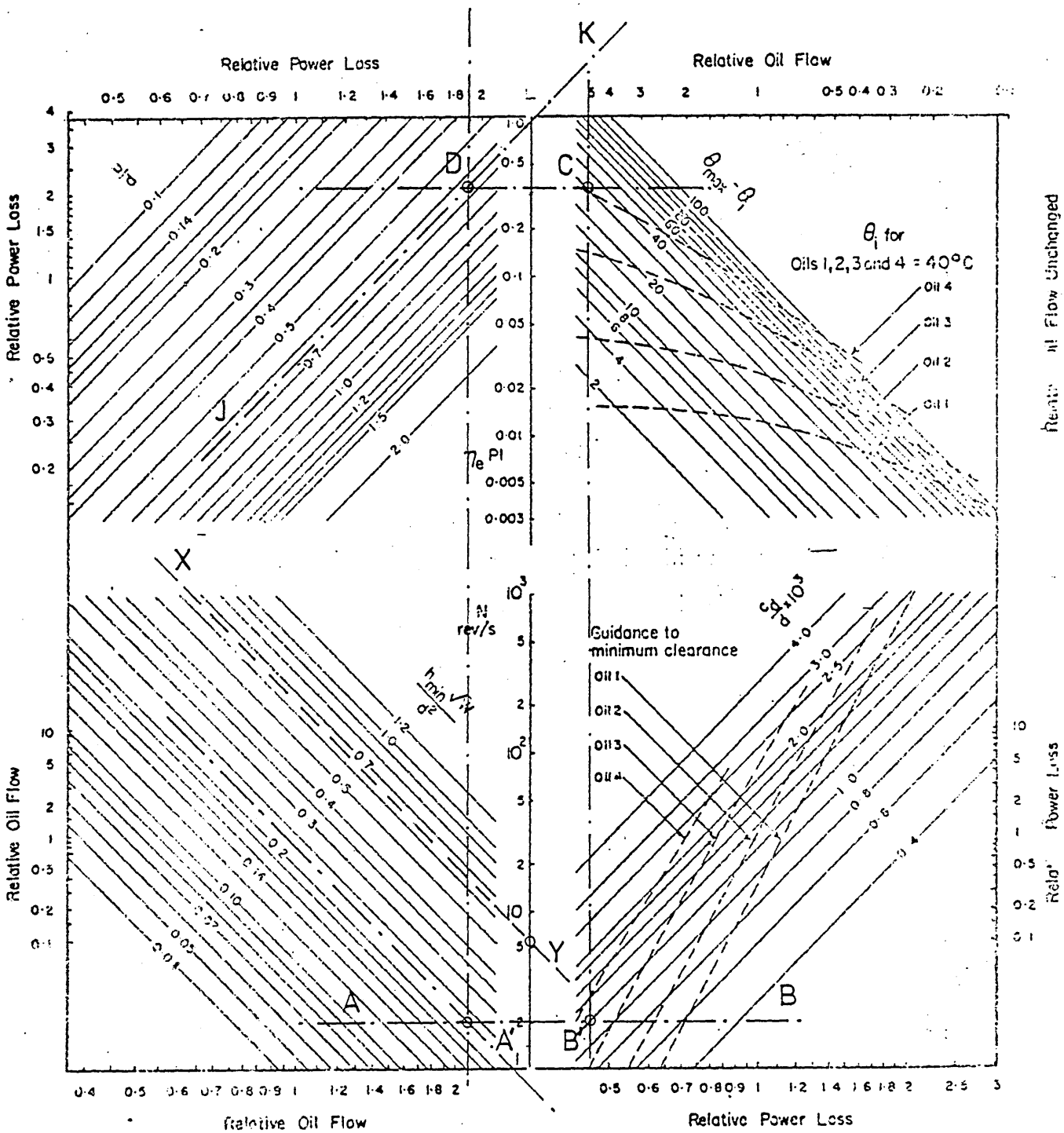

APPROXIMATE DESIGN CHART, SI UNITS

FIGURE 4.6

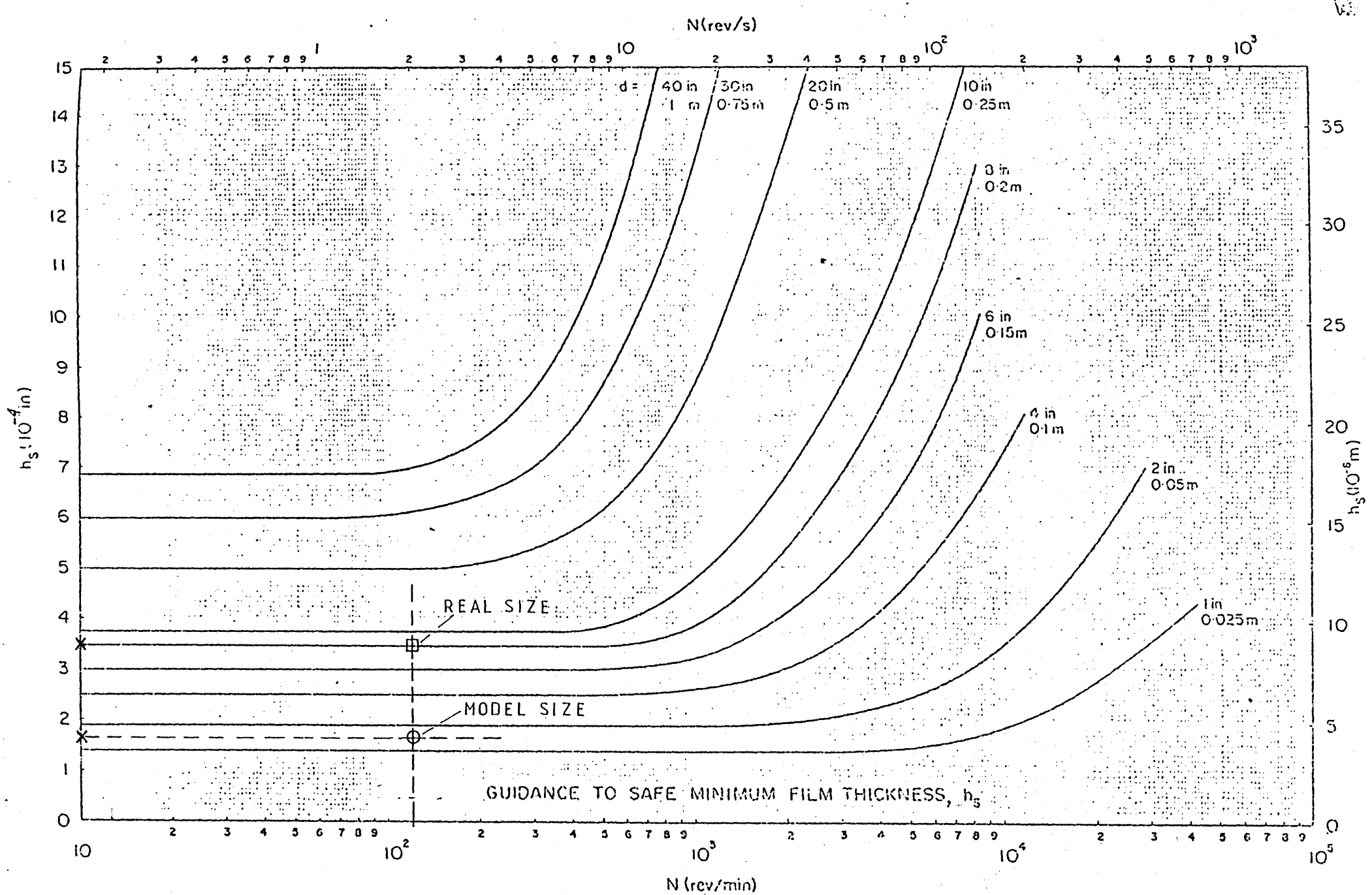
N(rev/s)
d =
40 in
1 m
30in
0·75m
20in
0·5m
10in
0·25m
8 in
0·2m
6 in
0·15m
4 in
0·1m
2 in
0·05m
1 in
0·025m
REAL SIZE
MODEL SIZE
GUIDANCE TO SAFE MINIMUM FILM THICKNESS, h_s
h_s (10^{-4} in)
h_s (10^{-6} m)
N (rev/min)

FIGURE 4.7

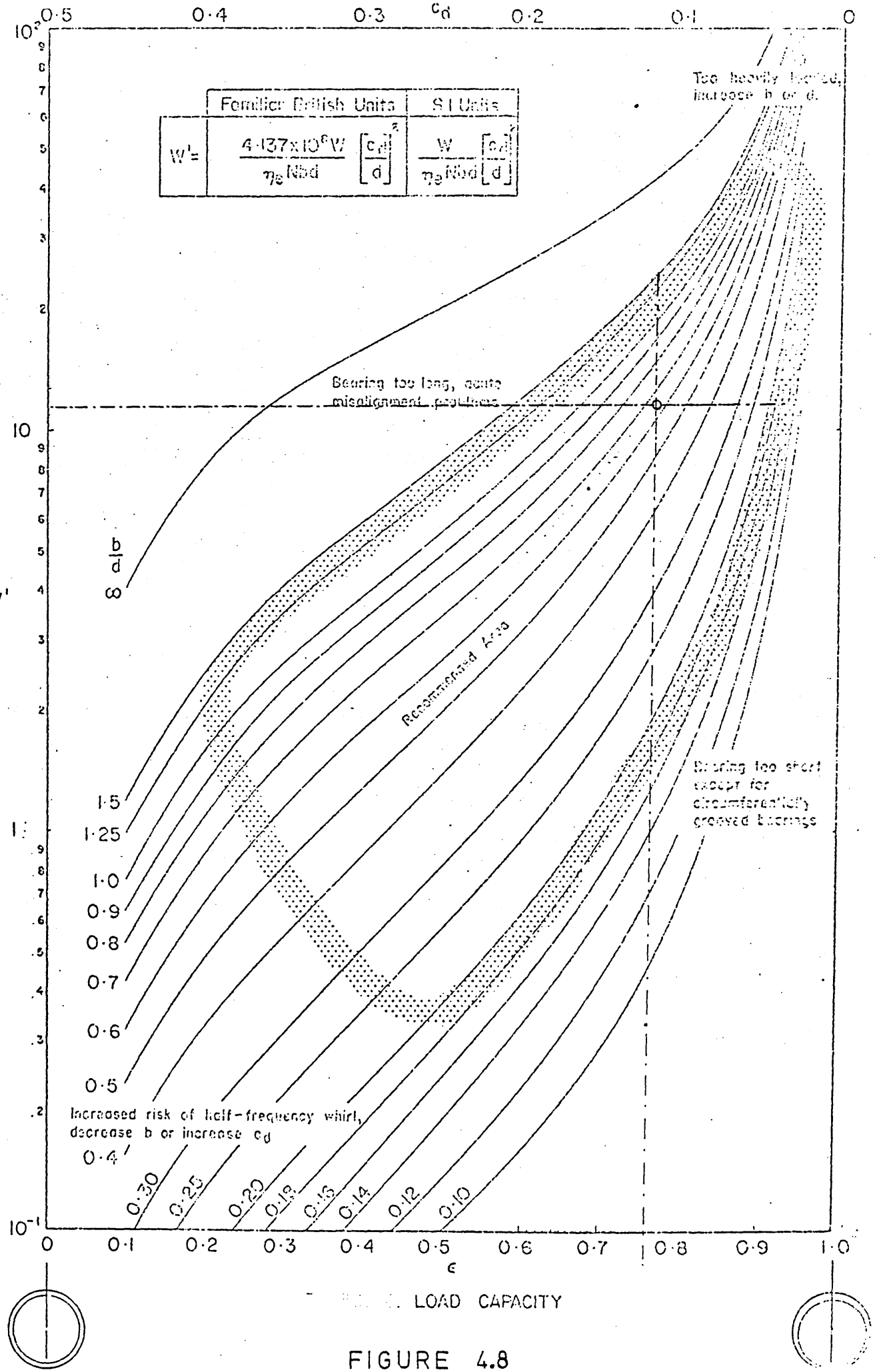
0·5
0·4
0·3
c_d
0·2
0·1
0
Familiar British Units
SI Units
$W' = \frac{4{\cdot}137\times10^6 W}{\eta_e N b d}\left[\frac{c_d}{d}\right]^2$
$\frac{W}{\eta_e N b d}\left[\frac{c_d}{d}\right]^2$
Too heavily loaded, increase b or d.
Bearing too long, acute misalignment problems
$\frac{b}{d}$ ∞
W'
Recommended Area
Bearing too short except for circumferentially grooved bearings
1·5
1·25
1·0
0·9
0·8
0·7
0·6
0·5
Increased risk of half-frequency whirl, decrease b or increase c_d
0·4
0·30
0·25
0·20
0·18
0·16
0·14
0·12
0·10
10
1
10^{-1}
0
0·1
0·2
0·3
0·4
0·5
0·6
0·7
0·8
0·9
1·0
ε
LOAD CAPACITY

FIGURE 4.8

4.2.4 Mechanical components.

The test rig basically consists of the following main parts:

i) Bearing unit.

ii) Loading system.

iii) Drive unit.

iv) Lubrication system.

A schematic arrangement of the rig is shown in fig. 4.9 and, figs. 4.10 and 4.11 give a general view of the equipment.

The bearing and loading unit were mounted on a heavy steel base plate supported on a fabricated steel frame, with rubber pad mountings. Concrete blocks were used to provide structural rigidity and prevent vibrations being transmitted to the test bearing; further, the driven unit was placed on a separate bench for the same purpose. The shaft is supported at each end by the test bearings, with the load being transmitted by a pneumatic cylinder through a central selfaligning double roller bearing. The oscillating motion of the bearing shaft is achieved by a crank-mechanism driven by a variable speed motor, connected to a secondary shaft supported by two pillow blocks and coupled to the test shaft by a flexible coupling.

These main parts will be described in detail.

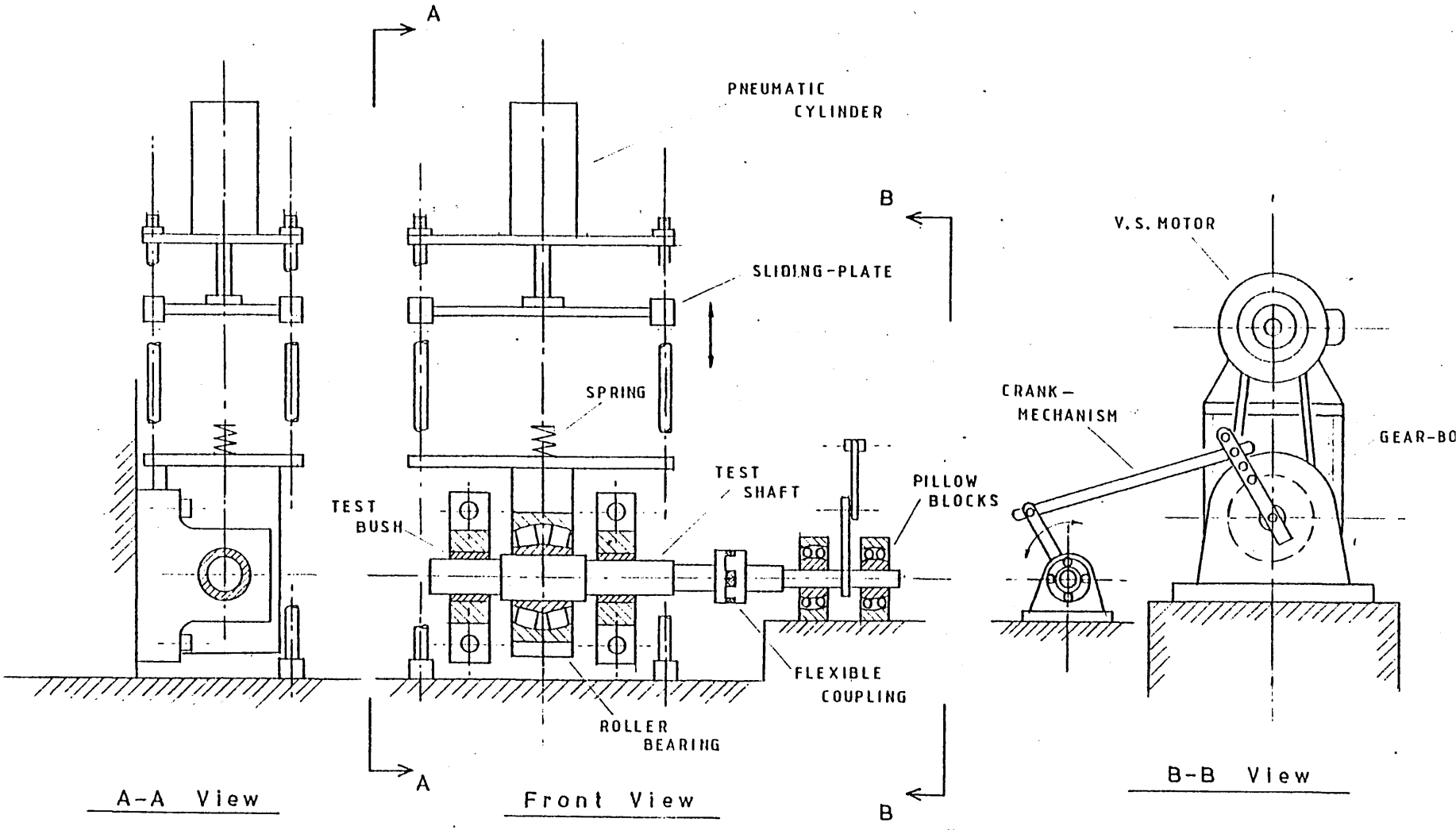

FIG. 4.9 SCHEMATIC DIAGRAM OF THE OSCILLATING BEARING TEST RIG.

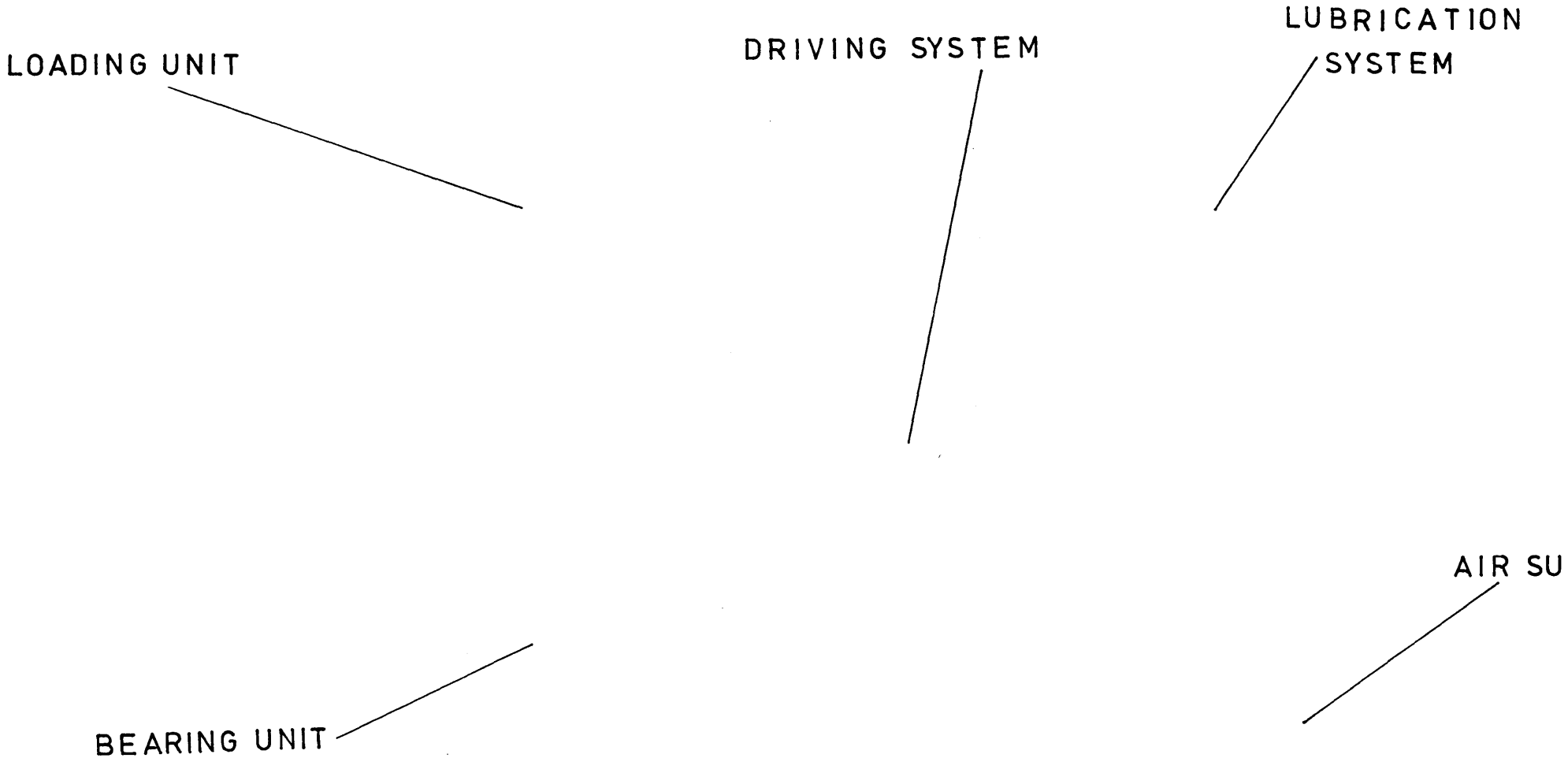

FIG. 4.10 GENERAL VIEW OF THE TEST RIG.

FIG.4.10 GENERAL VIEW OF THE TEST RIG.

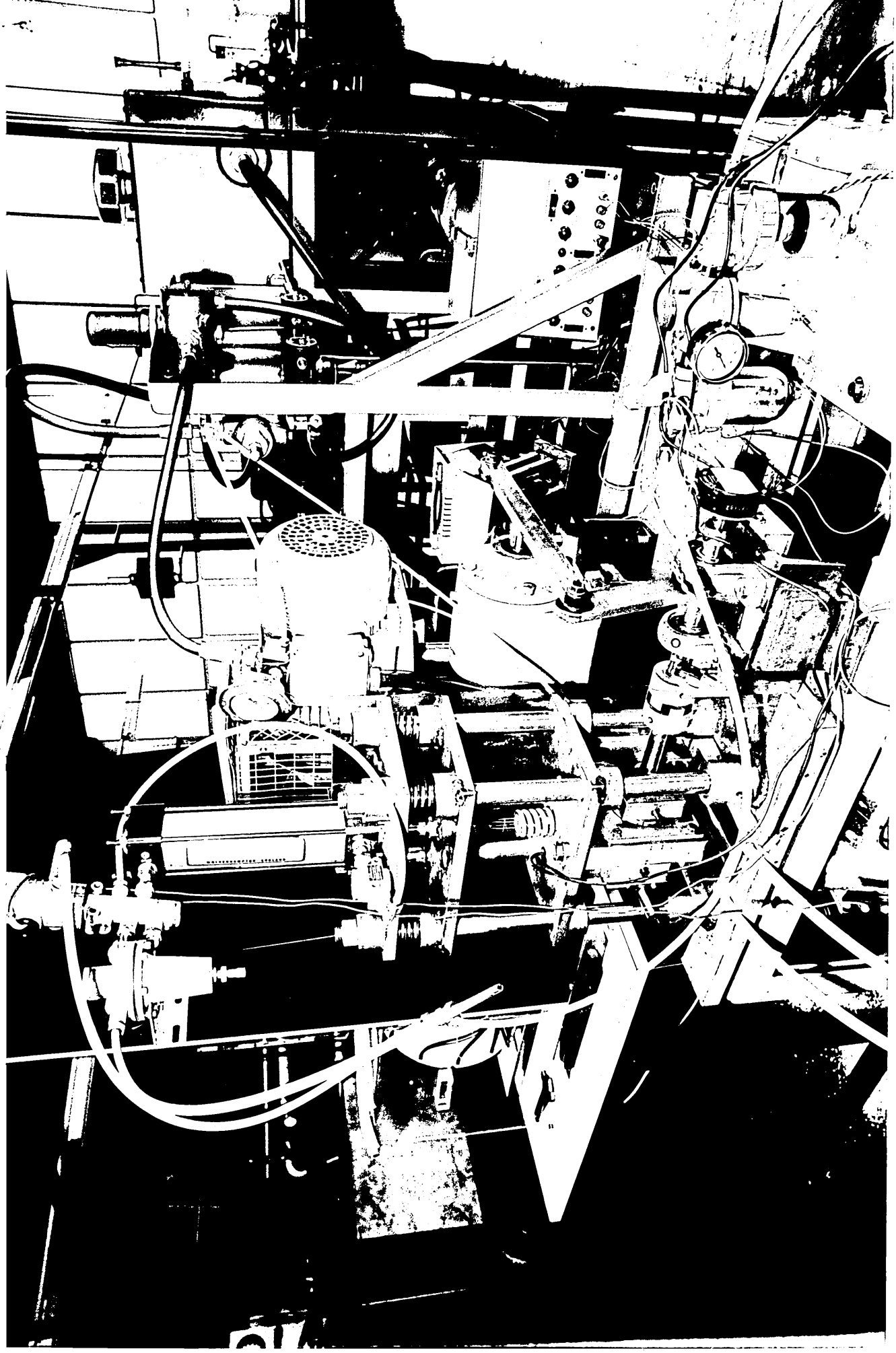

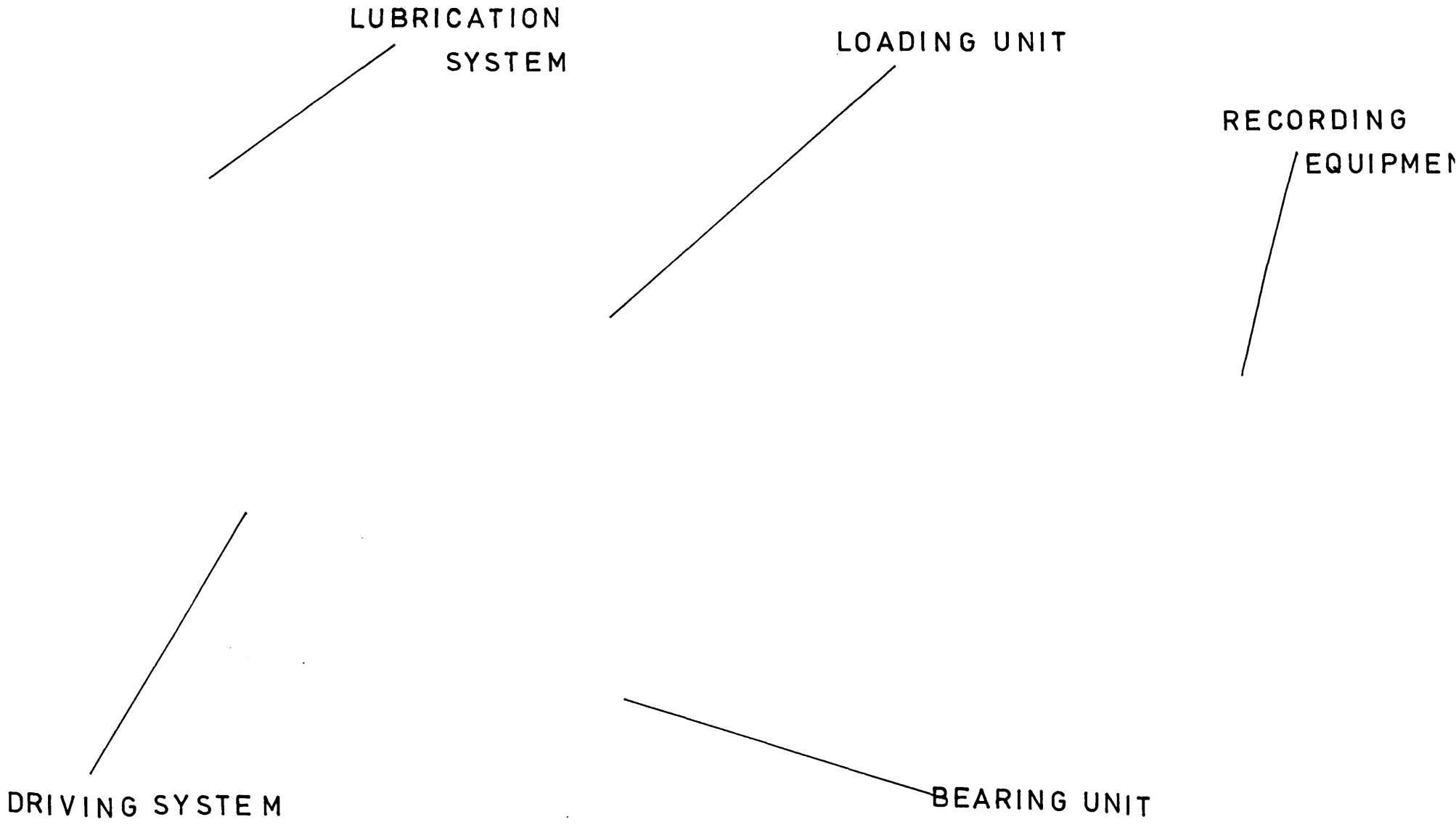

FIG. 4.11 GENERAL VIEW OF THE TEST RIG.

FIG. 1 GENERAL VIEW OF THE TEST RIG.

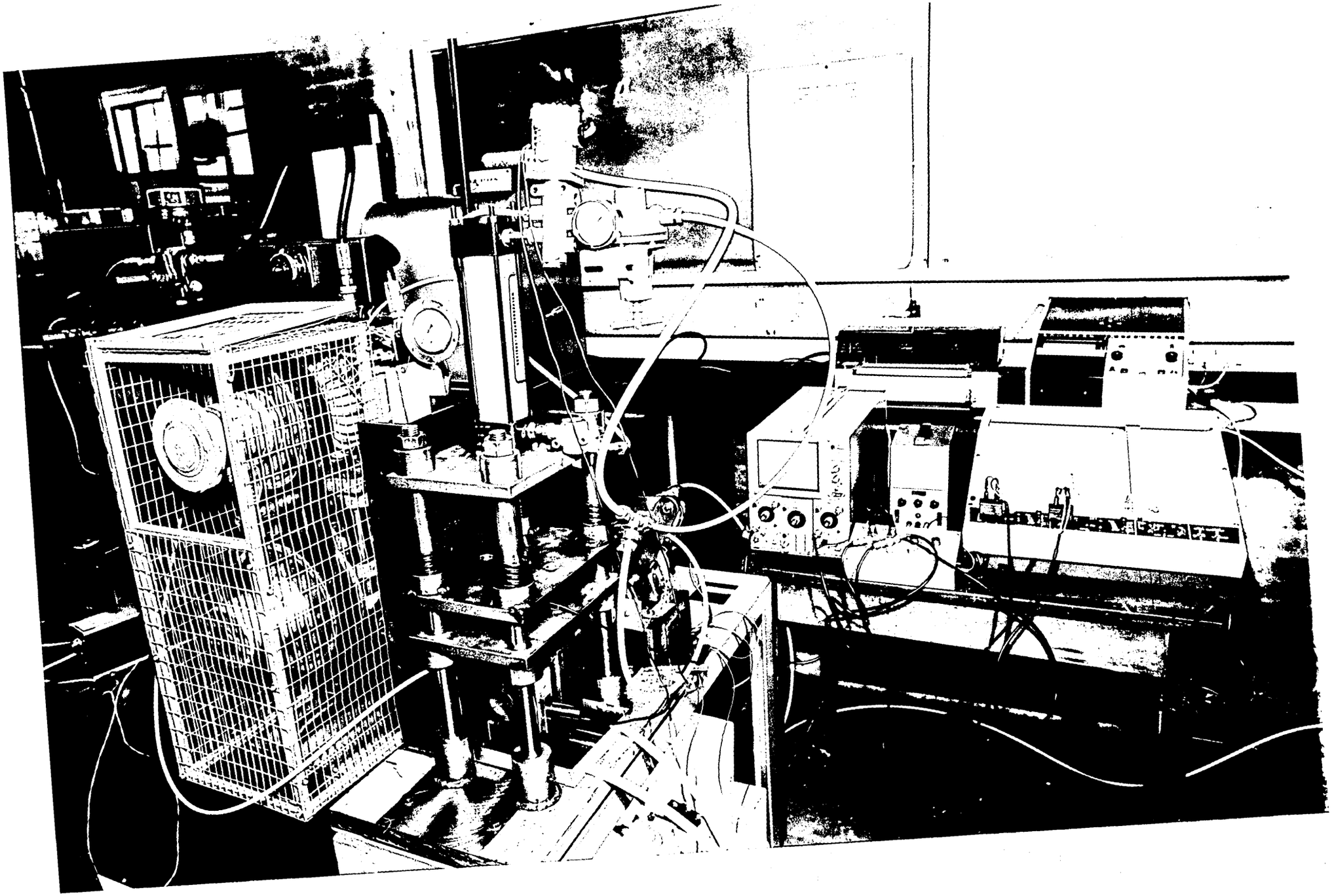

4.2.4.1 Bearing System.

Three different oil film bearing types have been tested. The first two are hydrodynamic and differ only in the oil groove arrangement. The third one is an externally pressurized hybrid bearing.

The test bearings were located as near as possible to the centre bearing in order to minimize deflections and bending stresses in the test shaft. A detail drawing of this arrangement is shown in fig. 4.12. Brief description of each of one of the components of the unit, is given below.

1) Designed test bearings.

a) Bearing type I

Bearing bore = 38 mm (nominal).

Bearing width = 25 mm.

Length/diameter = 0.66.

Grooves: 1 central circumferential groove 3 mm wide.

Material: bronze.

Bearing clearance: 0.050 mm (nominal).

Surface roughness: 2.5 μm, ovality:2.4 μm see fig. 4.13

b) Bearing type II

Bearing bore = 38 mm (nominal).

Bearing width = 25 mm.

Length/diameter = 0.66.

Grooves: 6 axial grooves and 1 central circumferential groove.

Material: bronze

Bearing clearance: 0.038 mm (nominal).

Surface roughness: 3.4 μm, ovality:2.0 μm see fig. 4.13

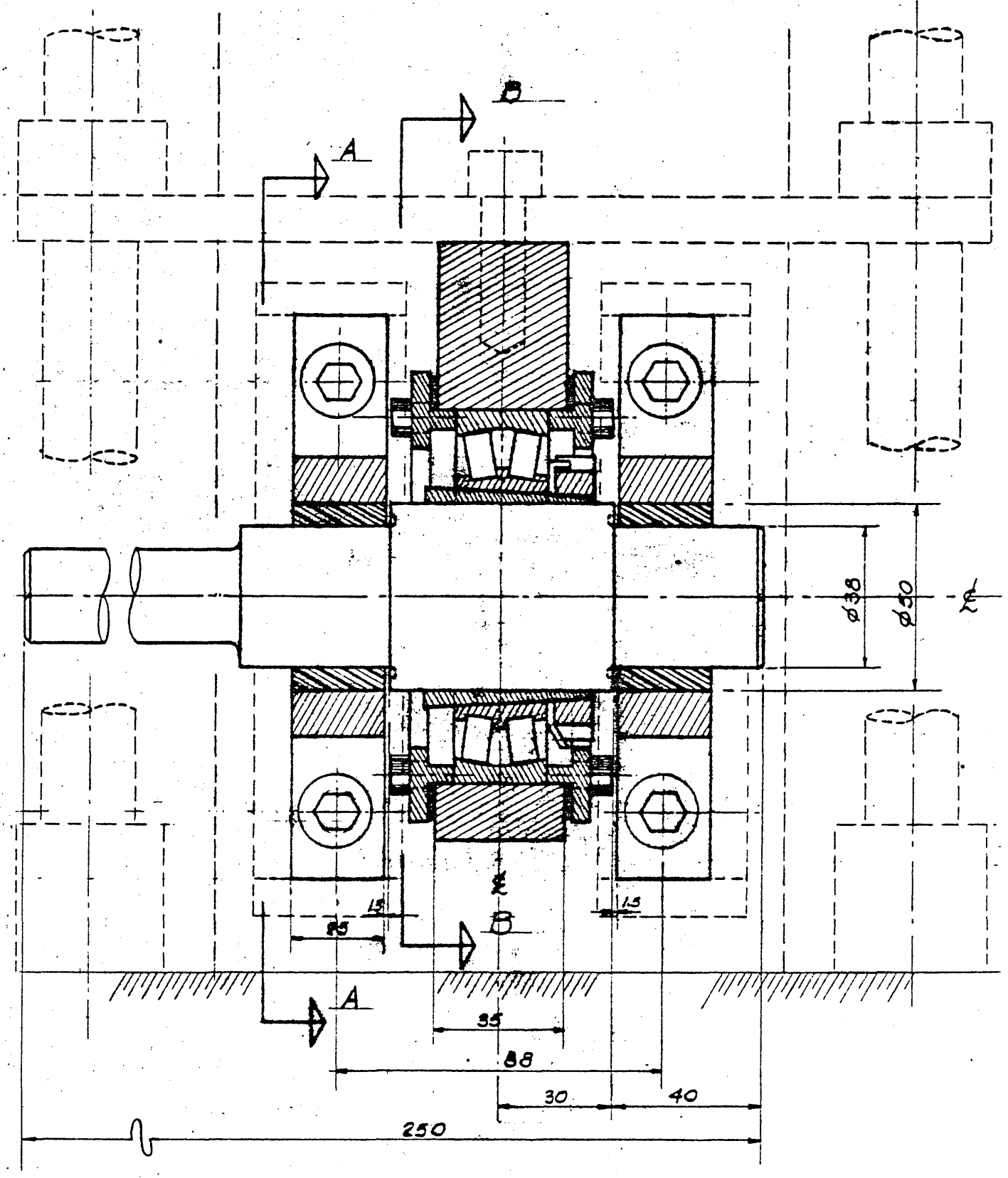

FIG. 4.12 DETAIL DRAWING OF THE BEARING UNIT.

TEST BEARING I

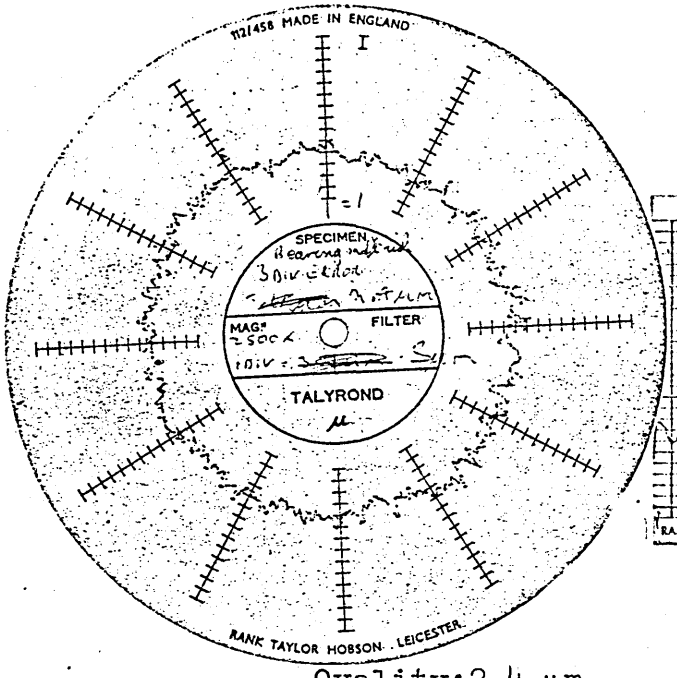

Ovality: 2.4 μm.

(Magnification on Talyrond Diagram: 2500)

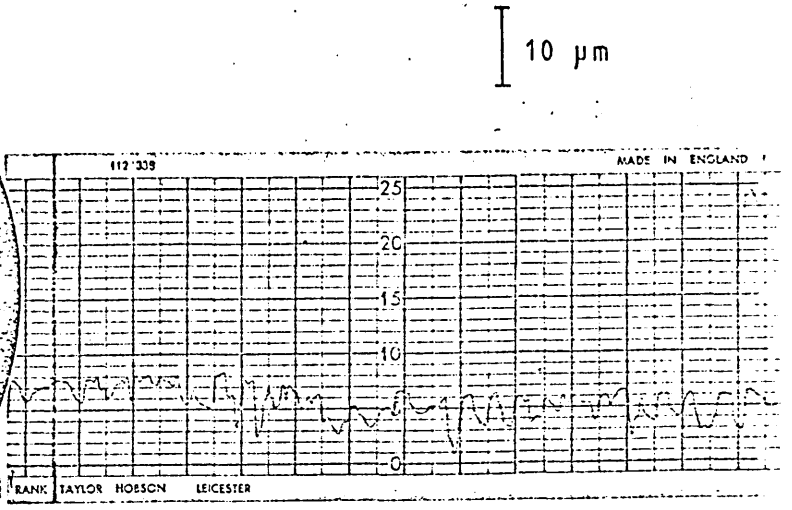

R_a = 2.5 μm

(Vertical/Horizontal Magnification of Talysurf chart 2000/100)

TEST BEARING II

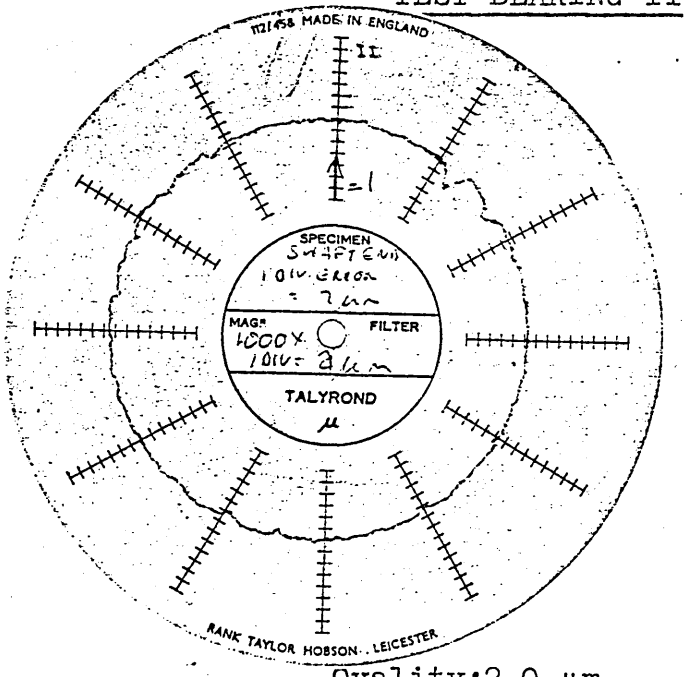

Ovality: 2.0 μm

(Magnification on Talyround Diagram: 1000)

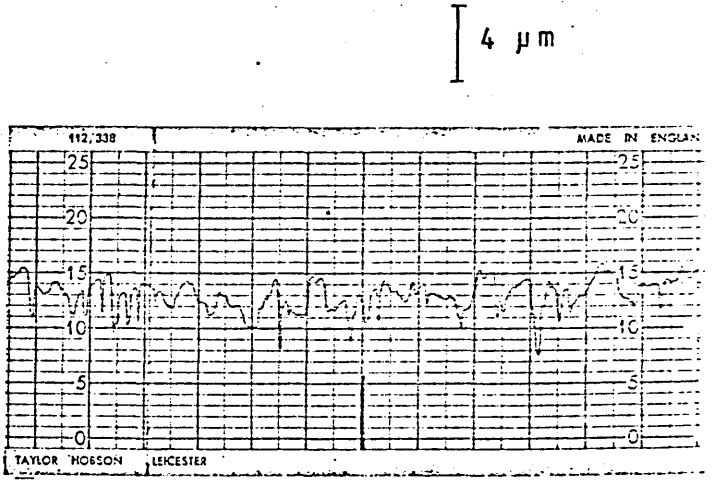

R_a = 3.4 μm

(Vertical/Horizontal Magnification of Talysuf chart 5000/100)

Fig 4.13 Test Bearing Surface Roughness and Ovality Charts.

In order to get geometry as perfect as possible the housings of the test bearings were machined out, and a thick bronze-bush (6 mm) was pressed in. These bushes were finally bored out in their housings already mounted in the rig to ensure concentricity and alignment.

The grooving arrangement was that best adapted to the current conditions applied to the test bush i.e. dynamic loads and oscillating motion, according to experiences described in section 2.2. Thus, a central circumferential groove was used to feed oil to a series of axial grooves spaced with 25° intervals in the working area of the bearing.

The cross-section of the axial grooves is of a semi-circular shape, the diameter of which is 2 mm, however the edge of the groove is rounded off as shown by the drawing in fig. 4.14.

2. Standard test bearing.

c) Bearing type III - Hybrid bearing - slot entry.
Horstmann Gauge Ltd. (type A-030).
Bearing bore = 30 mm (nominal).
Bearing length = 22 mm.
Bearing outside diameter = 62 mm.
Bearing clearance = 0.063 mm.
Load capacity = 1903 N (at 68 bar).

This bearing is a line-source plain hybrid bearing which is a standard bearing developed by Horstmann Gauge Ltd. It consists of a body which has been recessed on either

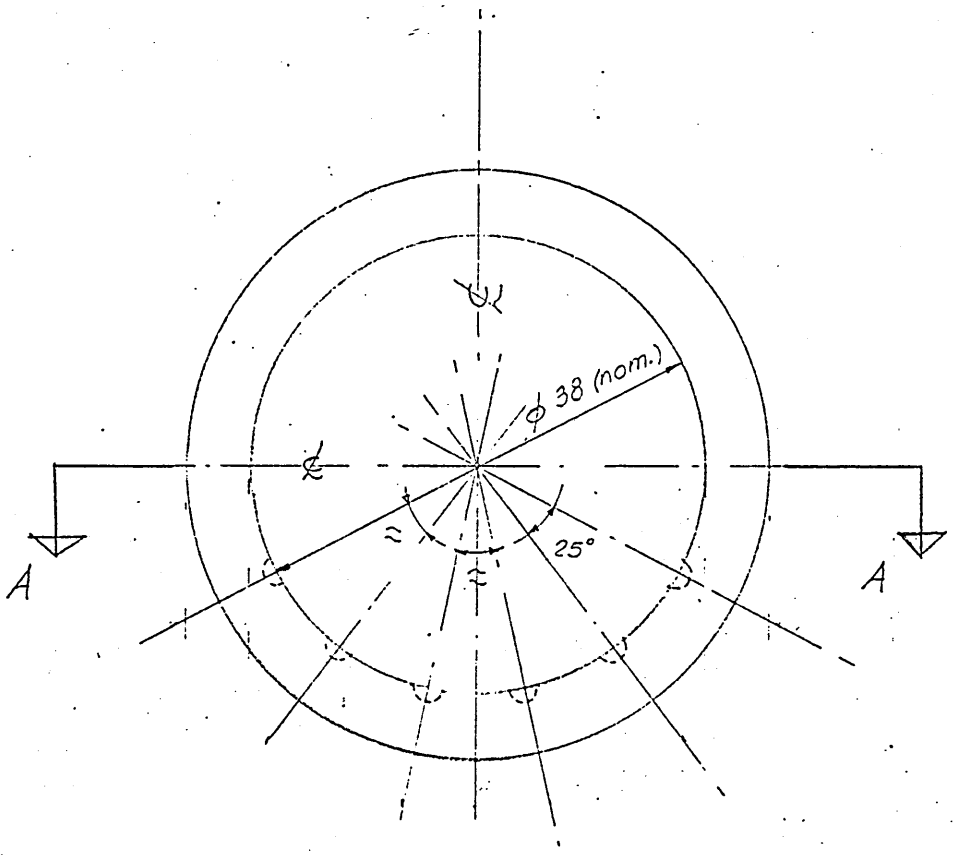

A-A SECTION

DIMENSIONS: mm

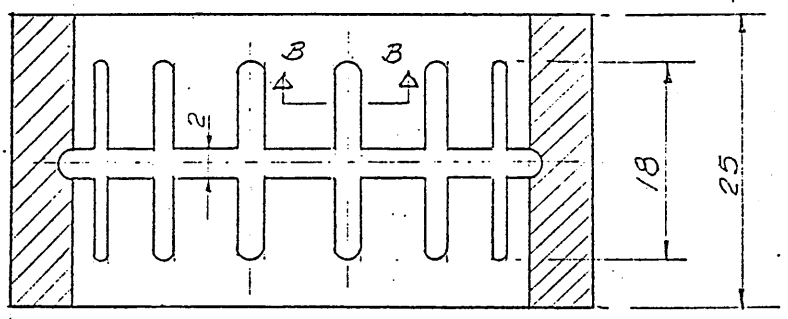

B-B SECTION

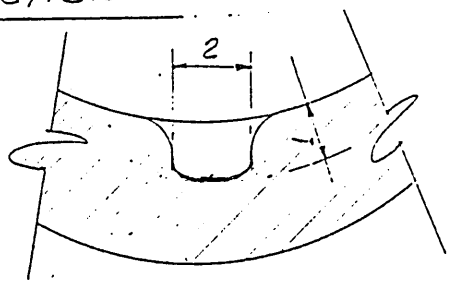

Fig. 4.14 Test Bush Type II.

side to accommodate slotted shims. The shims are held in position by retaining rings. The assembly is clamped together with bolts which pass through the body and the side retaining rings. The oil enters through holes leading into an annulus and passes through slots, which act as laminar restrictors, into the bearing clearance.

The three types of bearings above mentioned are shown in the photograph, fig. 4.15.

3. Standard central bearing.

The centre bearing is a standard selfaligning double row spherical roller bearing with an adapter sleeve manufactured by Ransome Hoffmann Pollard Ltd (type RHP 222-10), size 50 mm bore and 18 mm width. It was chosen on the basis that its dynamic capacity should be very much higher that the loading test conditions ensuring an effective safety factor and also to be selfaligned in order to accomodate shaft deflections during loading (63).

4. Test journal.

Two test journals were used during the experiments, one for the hydrodynamic bearings and the other for the hybrid bearing. A detail drawing is given in appendix D . They were made of steel E N - 8, having a surface hardness in the range of 260-290 BHN, obtained by heat treatment, finally ground with surface roughness varying from 0.4 to 0.7 μm C. L. A. Ovality, i.e. the maximum diameter difference was in the range of 0.4 to 0.6 μm. Typical Talysurf charts of shaft surface roughness measurements are shown in fig. 4.16

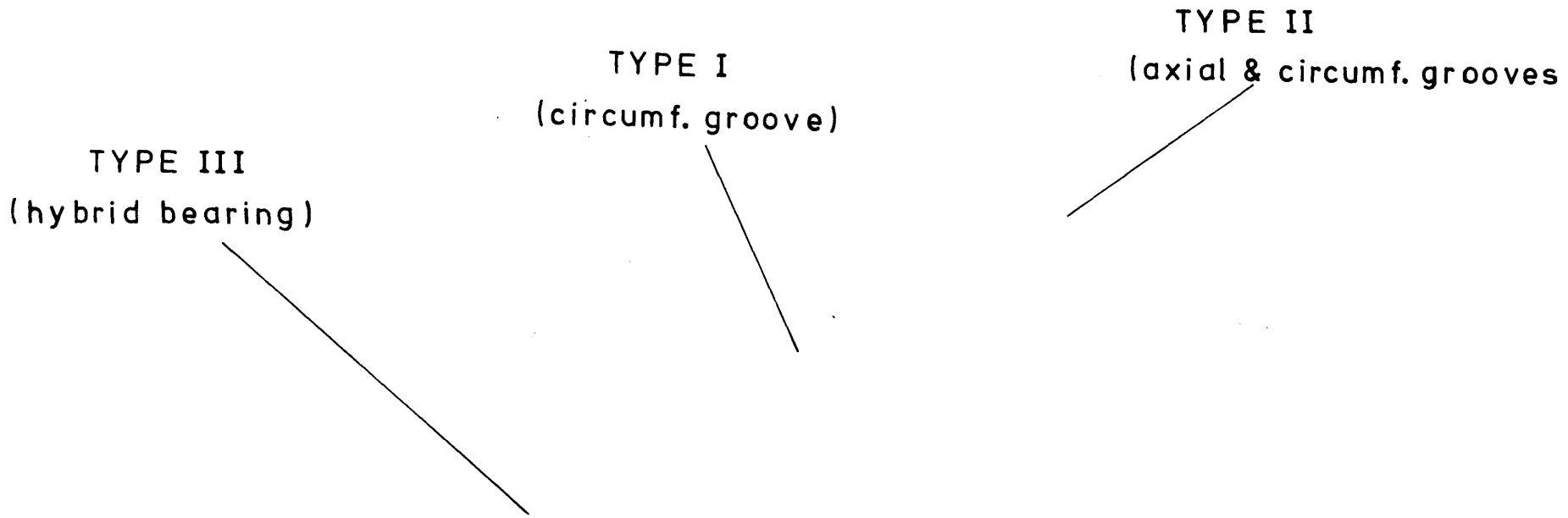

FIG. 4.18 TEST BEARINGS.

FIG. 1.18 BEARING TEST.

TEST SHAFT II

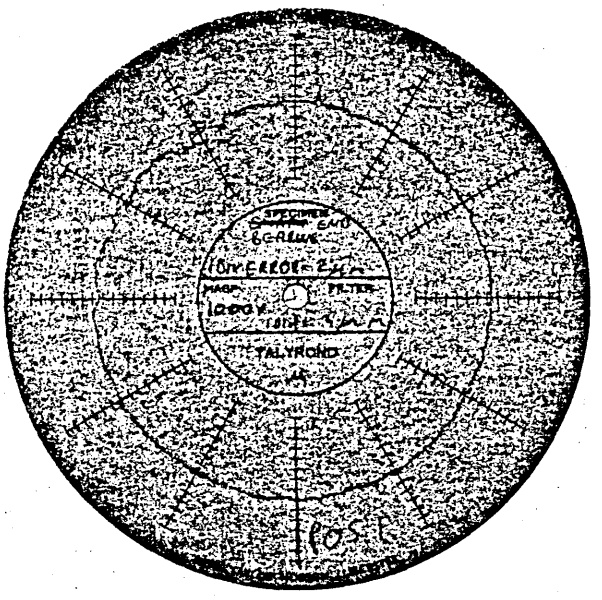

Ovality: 2 μm.

TEST SHAFT III

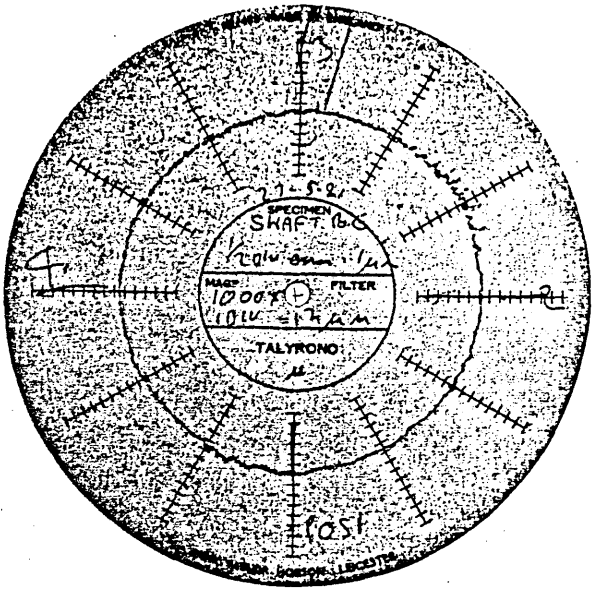

Ovality: 0.5 μm.

(Magnification on Talyrond Diagram: 1000)

TEST SHAFT II - Ra = 0.556 μm

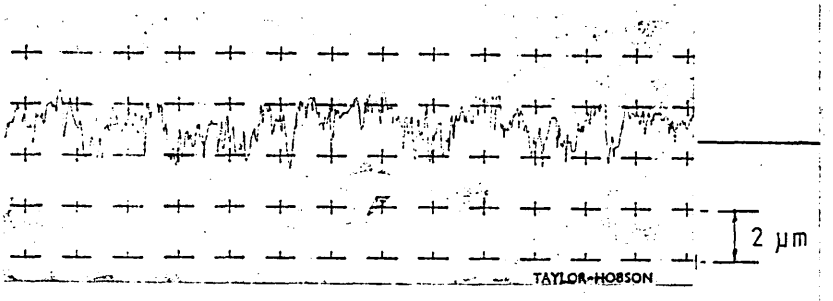

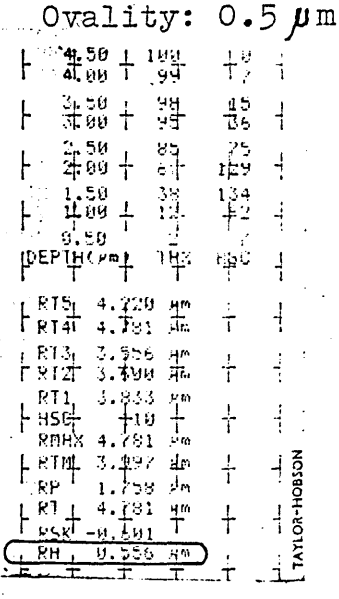

(Vertical/Horizontal Magnification of Talysurf Chart: 5000/100)

TEST SHAFT III - Ra = 0.477 μm

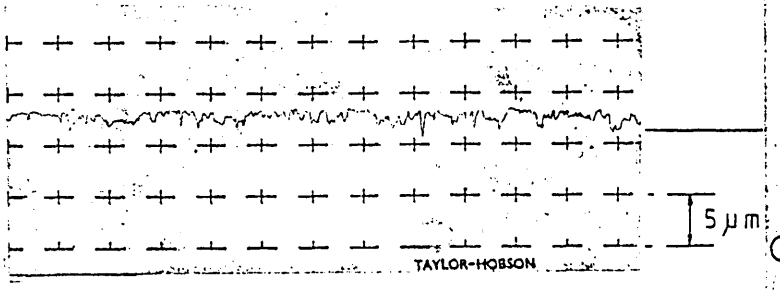

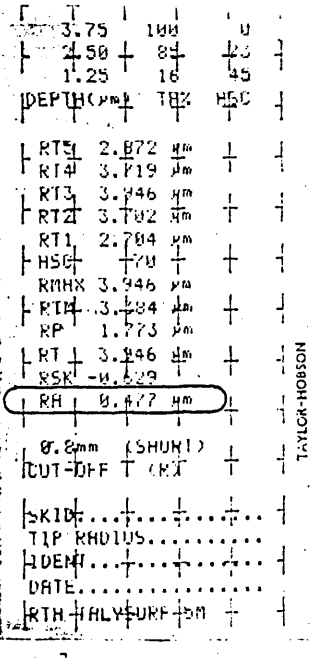

(Vertical/Horizontal Magnification of Talysurt Chart: 2000/100)

Fig. 4.16 Test Shaft Surface Roughness and Ovality Charts.

An exploded view of the bearing unit showing all the components above mentioned is given in photograph, fig. 4.17.

4.2.4.2 Load system.

A dynamic load is applied to the central bearing by means of a sliding plate operated with a pneumatic cylinder of 56 mm diameter and 150 mm stroke. The plate hammers a spring fitted on the top of the central housing. This load is then transmitted to each of the side housings providing the desired load function on the test bearings. A maximum compression of the spring initially occurs by the effect of the piston force and also due to the kinetic energy of the mass during its travel. This is followed by an oscillating spring recovery to a position which corresponds to the piston static force. Thus, with this loading sequence the pattern of the real load in the rolling-mill drive is simulated. It has the capability to be able to simulate a wide range of load values in a very simple way, such as changing the spring stiffness or the mass of the sliding plate and by applying different pressures to the cylinder. Typical dynamic loading diagrams are shown in fig. 4.18, recorded by means of a X - Y recorder.

This system is fully automatic in operation using solenoid valves, electrical timers and microswitches to synchronize the impact load to any position of the testing shaft during the cycle of oscillation see the circuit in fig. 4.19.

A front view drawing of the bearing unit and load system is shown in fig. 4.20.

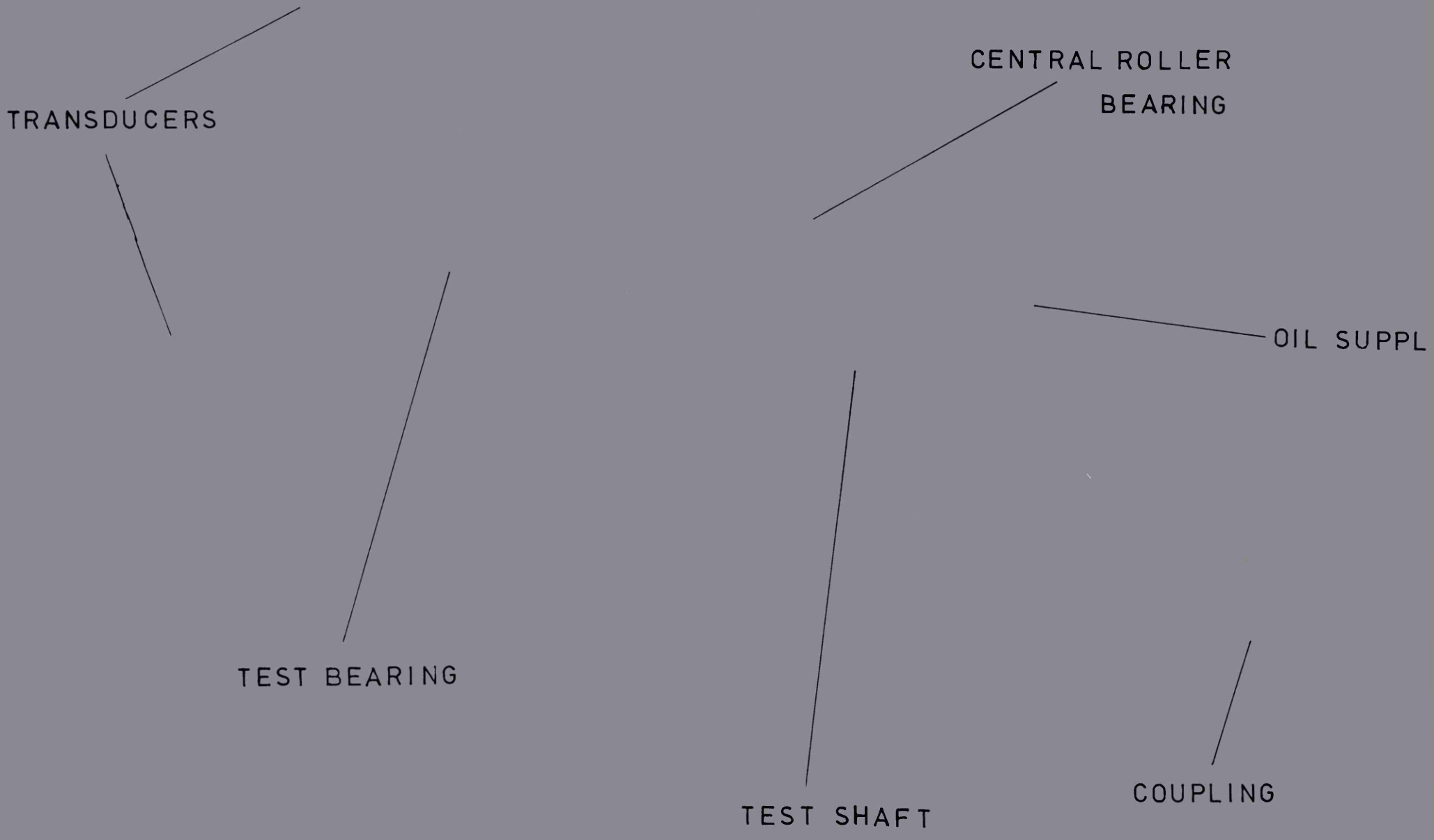

FIG. 4.17 TEST BEARING UNIT VIEW

FIG.4.7 TEST BEARING UNIT VIEW

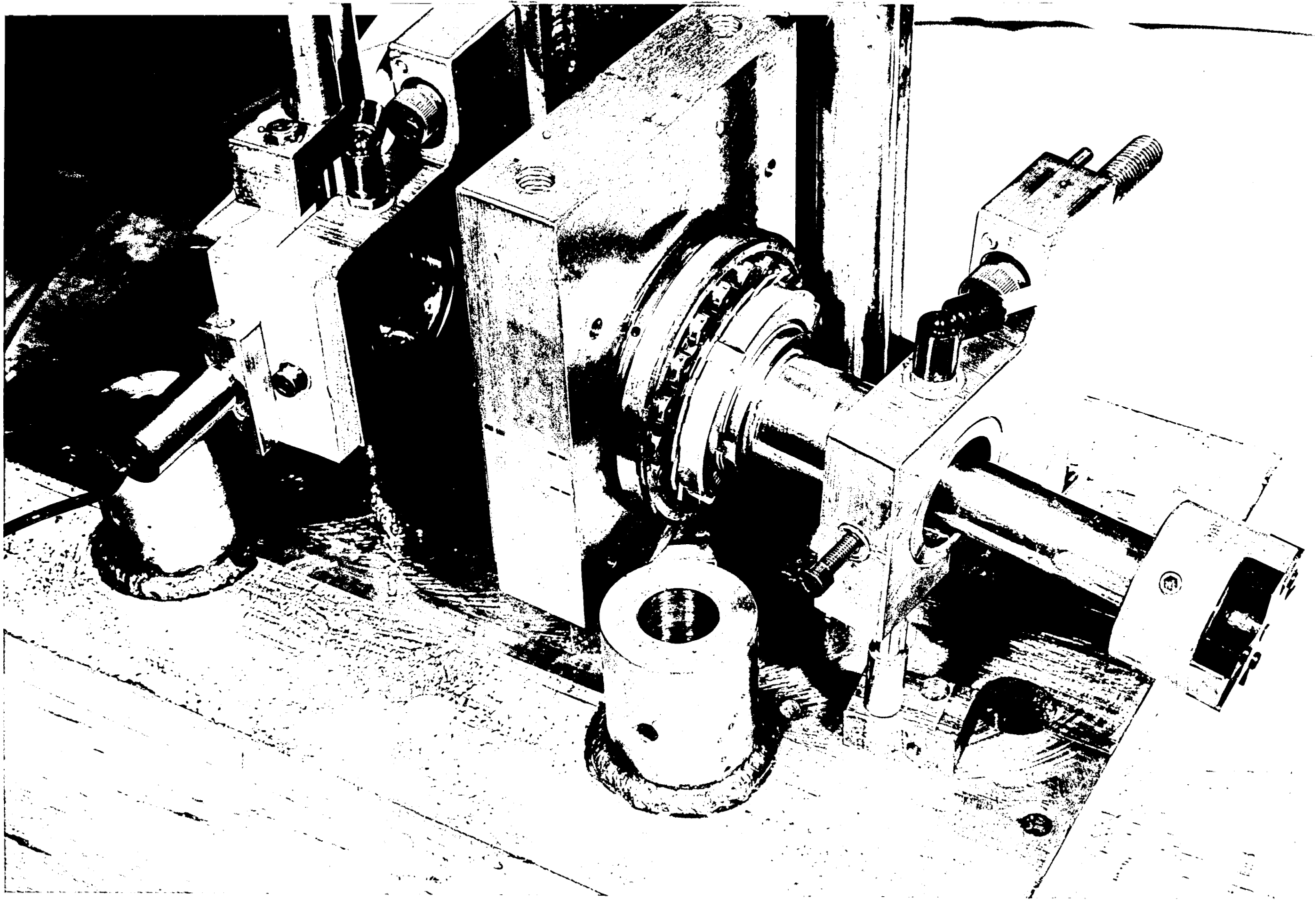

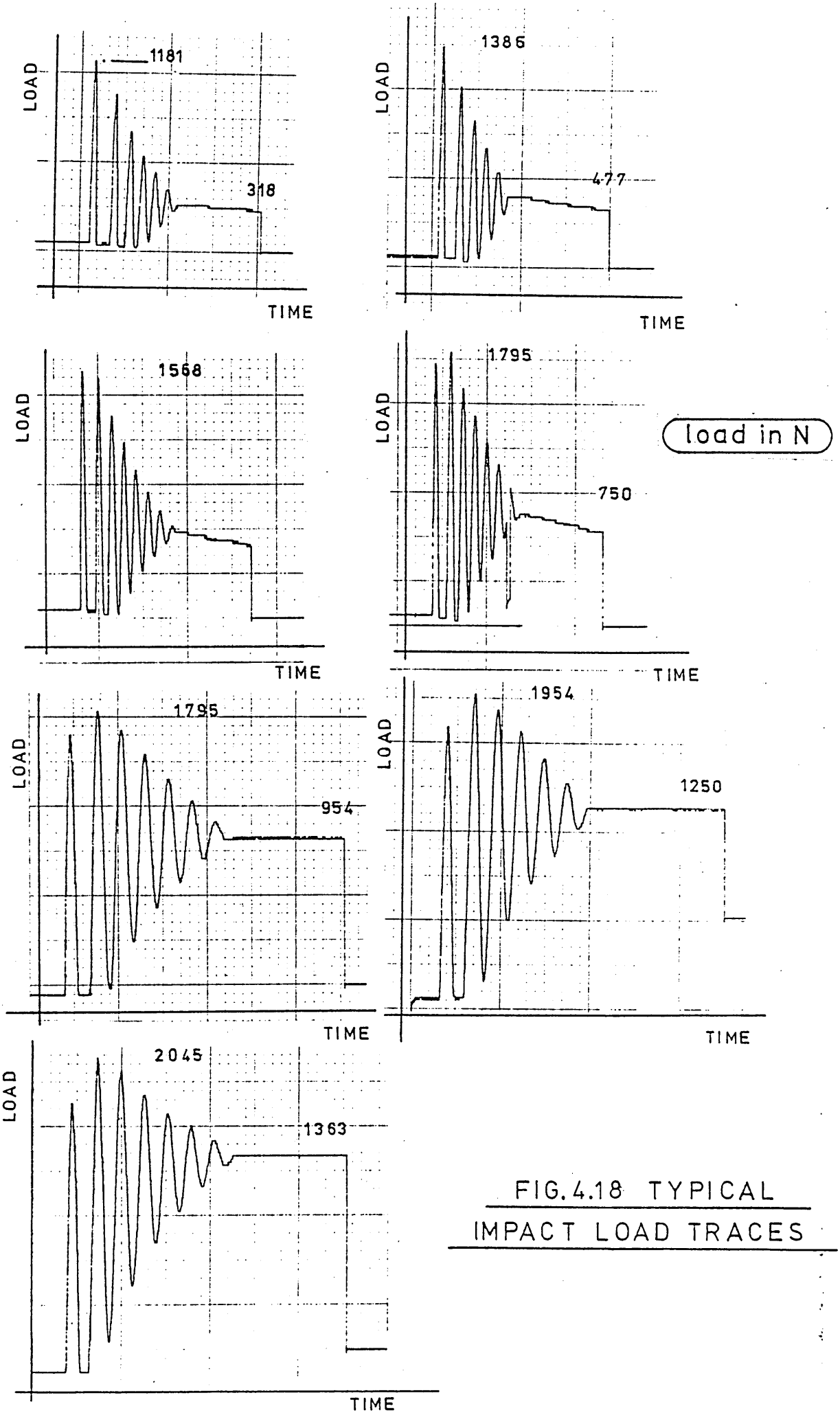

FIG. 4.18 TYPICAL IMPACT LOAD TRACES

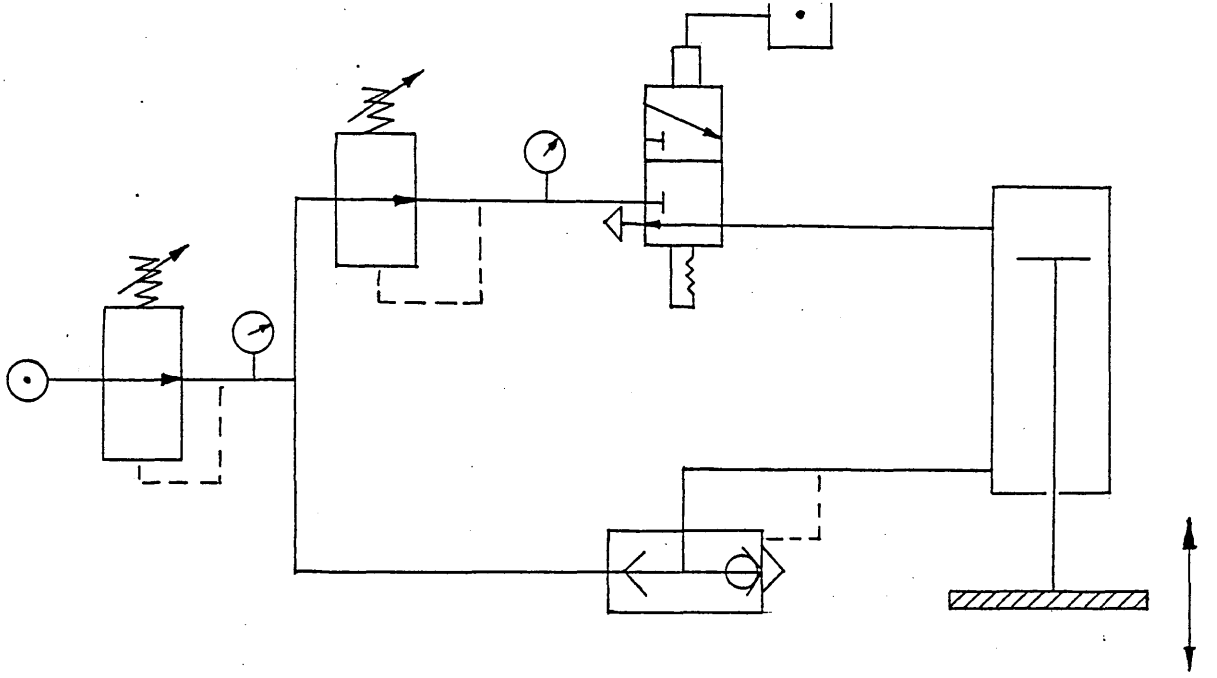

Fig. 4.19 Pneumatic Circuit for the load system.

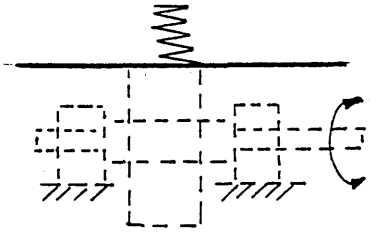

4.2.4.3 Drive unit.

The oscillating motion of the test shaft is produced by an electric variable speed motor of 1½ HP capacity with speed range between 20 to 130 rev/min, driving a four bar linkage mechanism. This mechanism consists of a crank, a connecting rod and a rocker, transmitting its movement to a secondary shaft in the machine. This shaft is supported by two selfaligning plummer blocks (Croft type - 20 mm diameter).

A flexible coupling (Essex coupling - Fenner of 24 mm bore) is fitted between the secondary shaft and the test shaft in order to eliminate any effect due to the transmission and catering for incidental angular, parallel and axial misalignment.

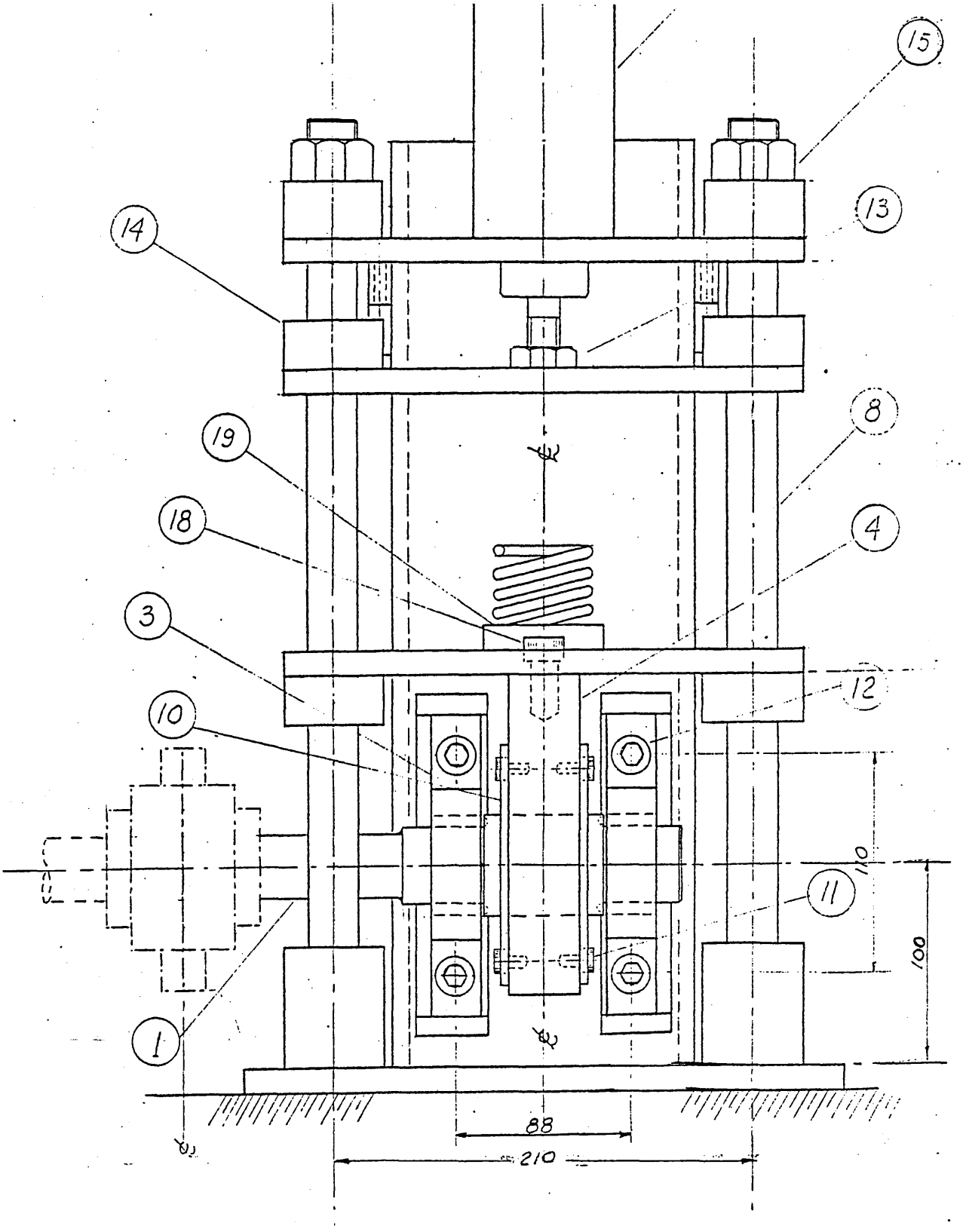

FIG. 4.20 BEARING UNIT AND LOAD SYSTEM.

The schematic arrangement and the general dimensions of the four-bar linkage mechanism are shown in fig. 4.21 below.

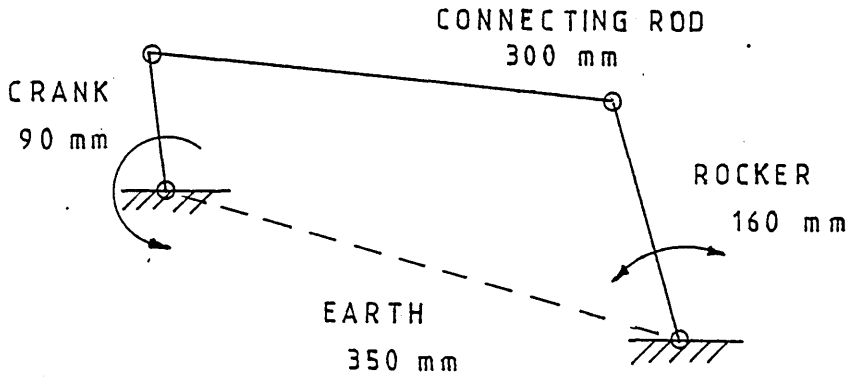

FIG. 4.21 OSCILLATING MECHANISM DIAGRAM.

The dimensions were determined by a computer package (64) developed to analyze a four-bar linkage mechanism. The mechanism was designed such that the oscillation of the rocker can be varied from 0° to 70° by changing the crank length. This maximum angle of oscillation would correspond to a shaft separation angle of 35° in the actual universal coupling. Typical graphs of the computing results are shown in fig.4.22. For different angle of shaft oscillation also measurement results are indicated.

All linkage connections are fitted with bolts, nuts and separating washers to allow free movement of the links which have also bronze bushes at their end to reduce friction as much as possible.

Final dimensions are given in appendix.

4.2.4.4 Lubrication system.

Oil pressure fed was applied for the testing bearings, using a mobil DTE oil - extra heavy. The oil viscosity was determined by means of a Redwood viscometer, as shown in fig. 4.23 (65).

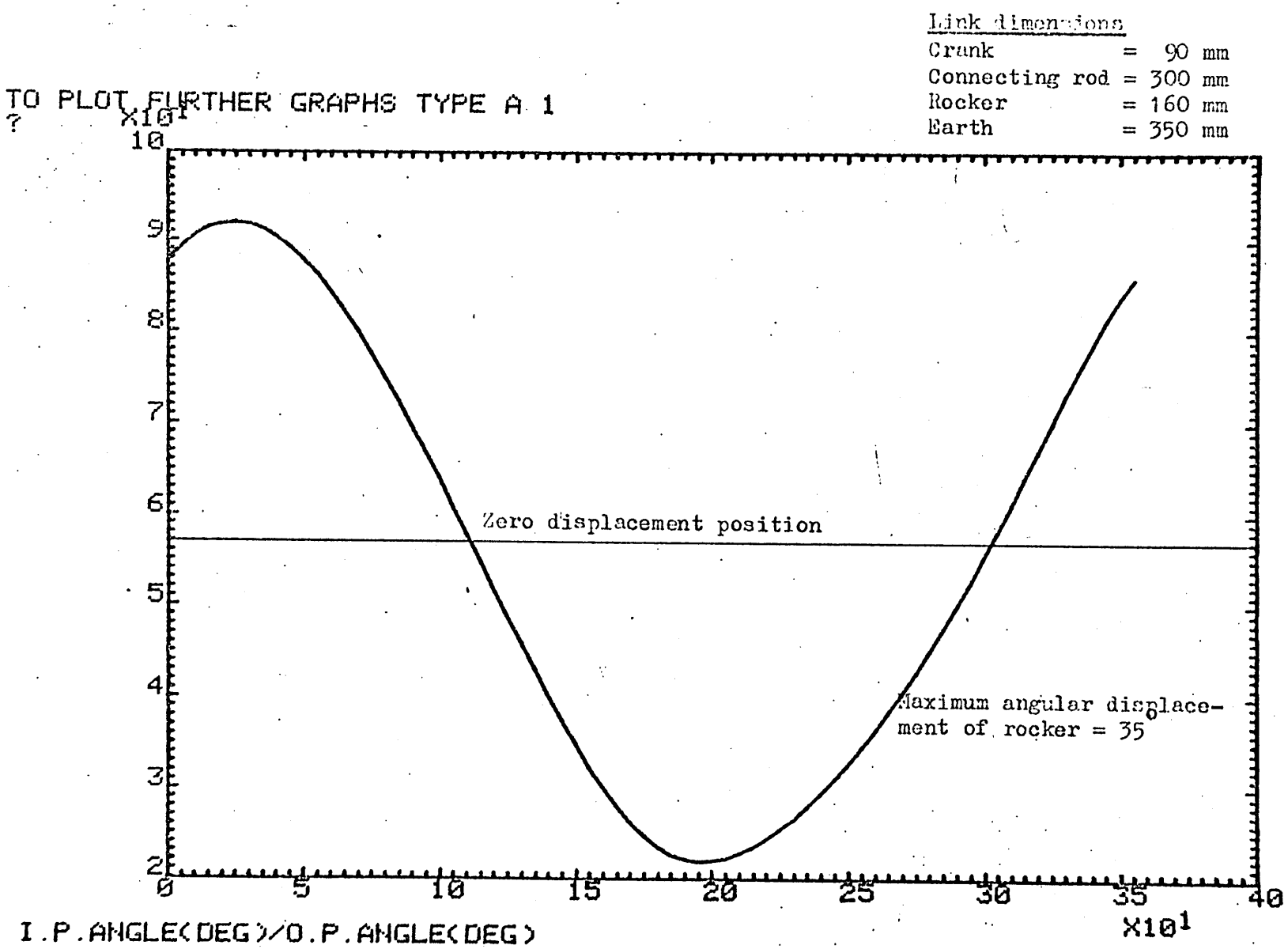

FIG. 4.22 COMPUTER RESULT OF THE LINK MECHANISM ANGULAR DISPLACEMENT.

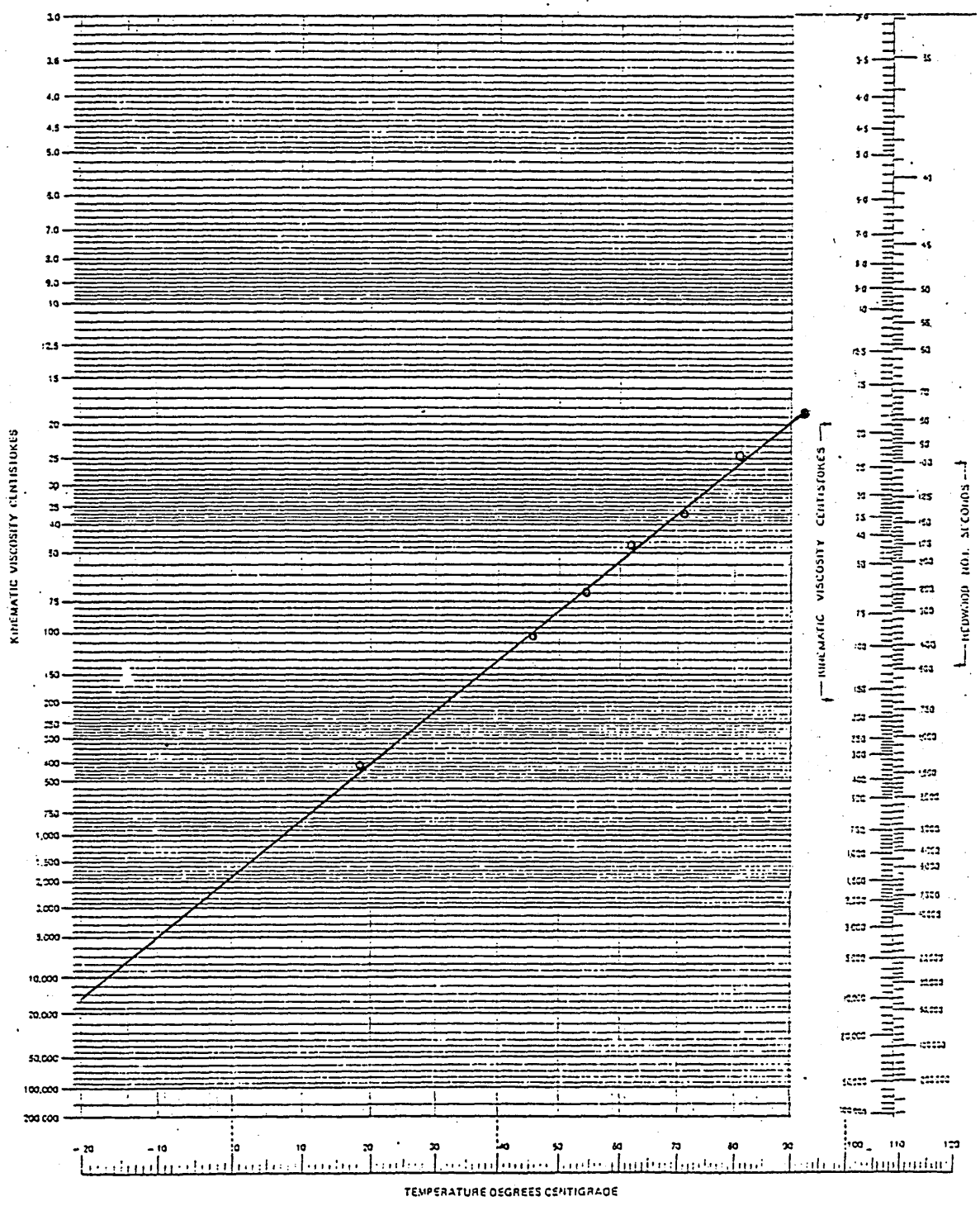

Fig. 4.23 Viscosity - Temperature chart of Mobil - DTE oil (extra - heavy).

Two different lubrication systems were employed depending on the bearing type to be tested.

For the hydrodynamic bearings the system schematically shown in fig. 4.24 below was used.

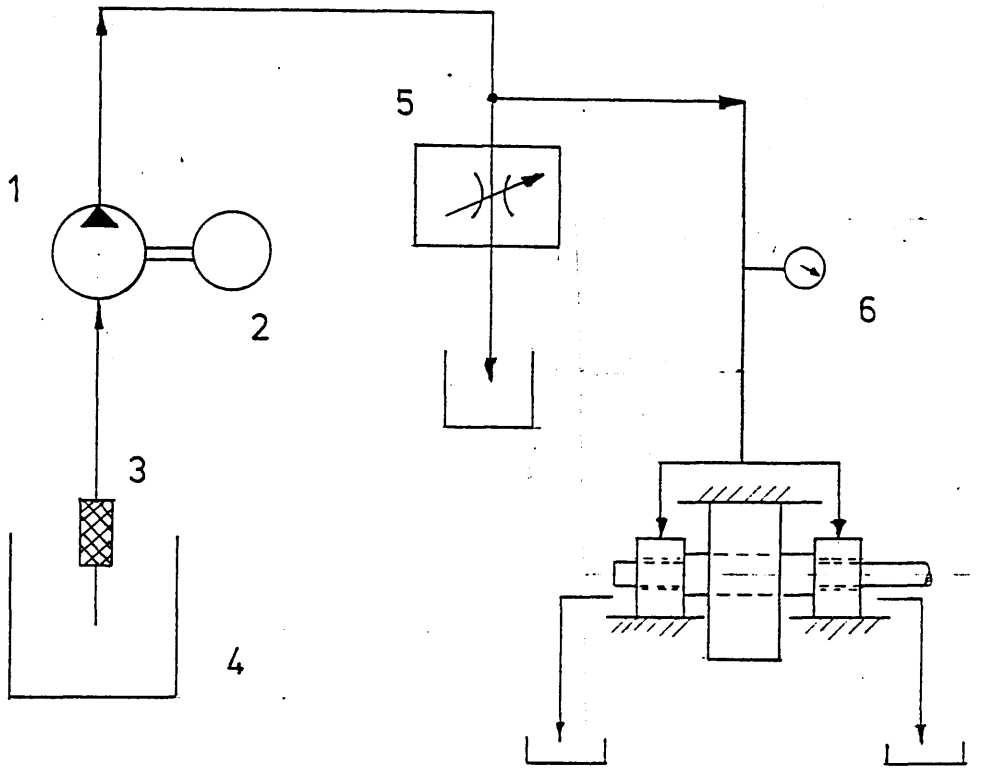

Fig. 4.24 Lubrication system for Hydrodynamic Bearings.

This system permits pressure feed to the test bearings and consists of an oil gear-pump (1) driven by an electric motor(2) directly coupled, and draws oil through a suction filter (3) from a reservoir (4).

The oil pressure from the pump is adjusted by a control valve (5). Pressures from 0 to 20 bar are obtained according to the pressure gauge readings (6).

The oil leaking through the test bearing is collected by a tray and directed back to the reservoir.

The lubrication unit for the hybrid bearings is a high-pressure system of 70 bar, with a very fine filtering facility of 3 μm, to ensure a very clean oil into the bearings, as their configuration, i.e. slot oil entries are very susceptible to blocking.

The circuit and operation of this system are very similar to the one already mentioned, consisting of a motorized gear pump, oil reservoir and their respective valves except for the 3 micron absolute filter.

This circuit is schematically shown in fig. 4.25 below.

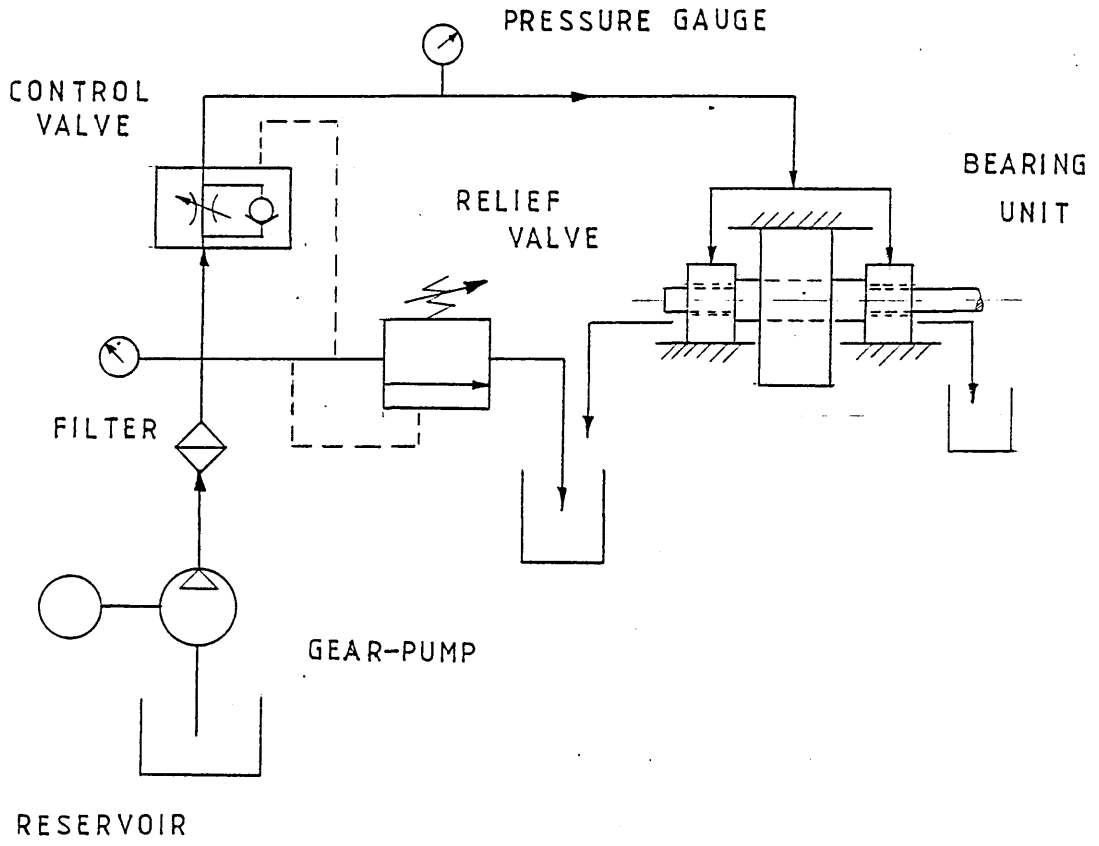

Fig. 4.25 Lubrication system for Hybrid Bearings.

4.2.5 Measurement techniques.

The instrumentation employed was designed to measure and control:

i) The dynamic shaft center displacements
ii) The load applied.
iii) Bearing temperature.
iv) Shaft oscillating motion.
v) The phasing of the applied load and the shaft stroke.

i) Measurement of journal centre displacement.

The coordinate displacements of the journal with respect to the bearing during running were measured by means of two DC miniature inductive displacement transducers, Sangamo-Weston type of 1 mm maximum displacement and linearity 0.3 % . The transducers were fitted in the housing as near as possible to the edge of the test bush. They were positioned in the horizontal and vertical planes, and operated on the test journal.

With this design it was possible to separate the two possible components of bush-journal displacement, such as those due to hydrodynamic action from the bearing unit distortions. Also, the calibration of the system was simple, in situ, and capable of being accomplished rapidly.

As instruments with high sensitivity were used, readings in the order of 0.0025 mm (0.0001 inch) were obtained.

The transducers were connected to either a cathode ray oscillograph (725 - Tektronix type) or an X-Y recorder (Hewlett - Packard - SR - type), so as to enable a continuous record of shaft displacement to be obtained for each testing operation. The circuit used to obtain the eccentricity records is shown diagramatically in fig.4.26 below.

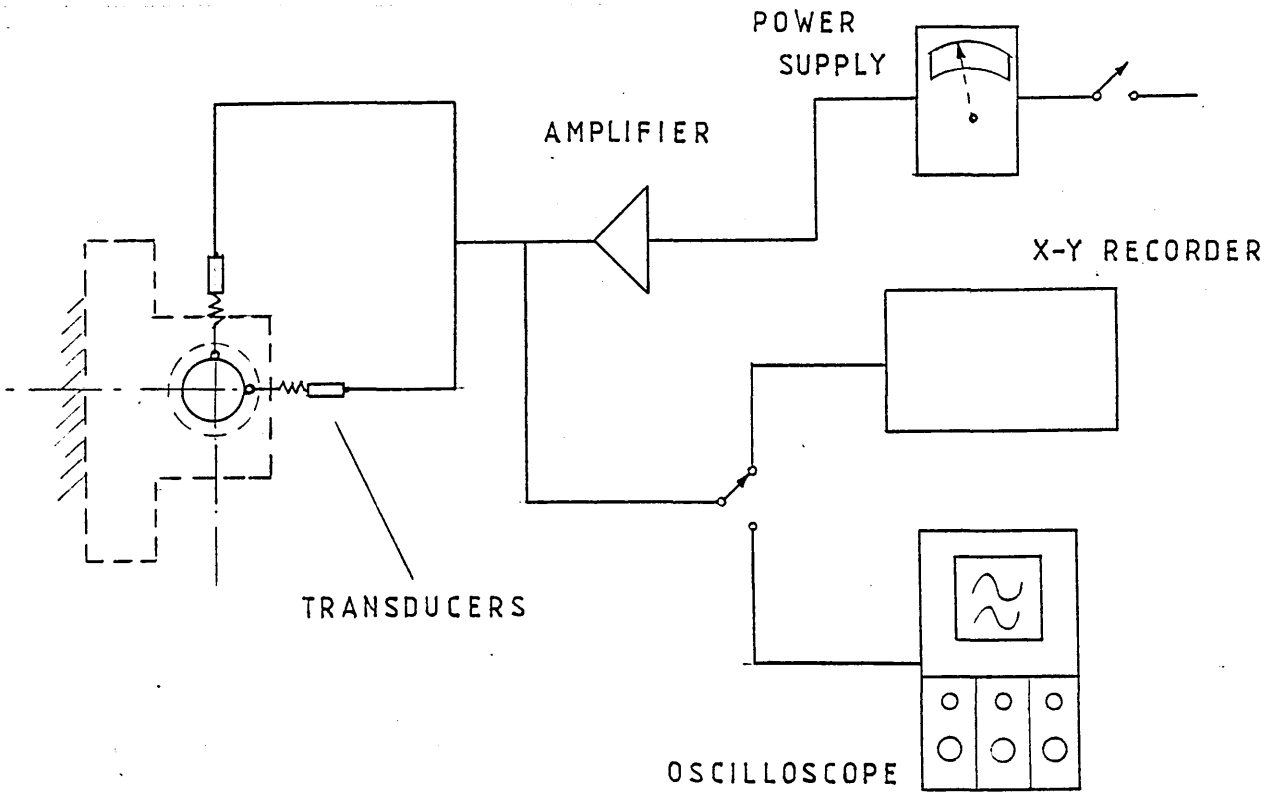

Fig. 4.26 Measurement of the Shaft Locus.

Block Diagram of Circuit.

In operation the electrical power supply is adjusted to give a standard voltage of 25 V through the amplifier to the transducers. Then the output amplified signals are received in the oscilloscope presenting a picture of the locus of the shaft centre, which can be plotted on the X-Y recorder. The input signals to X-Y recorder are modulated by means of filters in order to eliminate any disturbance in the system, providing a quick response and smooth plotting.

ii) Measurement of the load applied.

The vertical load applied to the central bearing, representing double the magnitude of that transmitted to the test bearing is adjusted pneumatically as described in section 4.2 and is measured electrically using a load washer cell (Kistler 902 A, with sensitivity of 4.27 PC/N).

The load cell is connected in series with a minicharge amplifier (Kistler type) and the datum recorded on a U. V. galvanometer recorder (Southern Instruments type) (see fig.4.27).

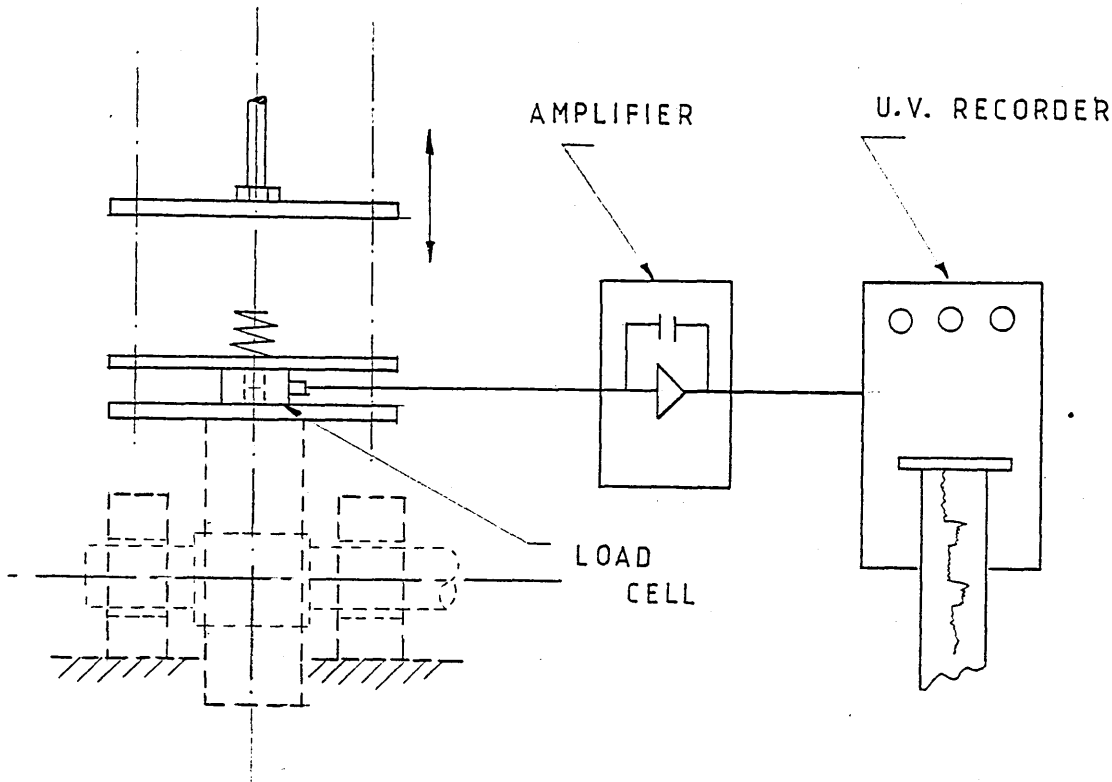

Fig. 4.27 Diagram of the load measurement system.

iii) Bearing temperature.

The bearing temperature is measured by three copper-constantan thermocouples. They are fitted radially in the housing passing through the bearings in the loaded area and connected to an electronic multimeter (Comark - 1231 type).

iv) Measurement of the shaft oscillating motion.

The frequency and the amplitude of the shaft oscillations were measured by means of a potentiometer (Colvern - CLR type) mounted at the end of the secondary shaft. The output put signals were recorded in a U. V. recorder (see fig. 4.28).

v) The phasing of the applied load and the shaft stroke.

The phasing of the load applied relative to the oscillating cycle of the shaft i.e. the stroke, was made by means of a photo-electric cell connected in circuit with a transistor delay and the potentiometer.

This arrangement correlates the peak load either with the half way position of the stroke i.e. when the shaft is at maximum angular speed or with the extremities of the stroke i.e. when the angular speed of the shaft is momentarily zero (see figs. 4.28 and 4.29).

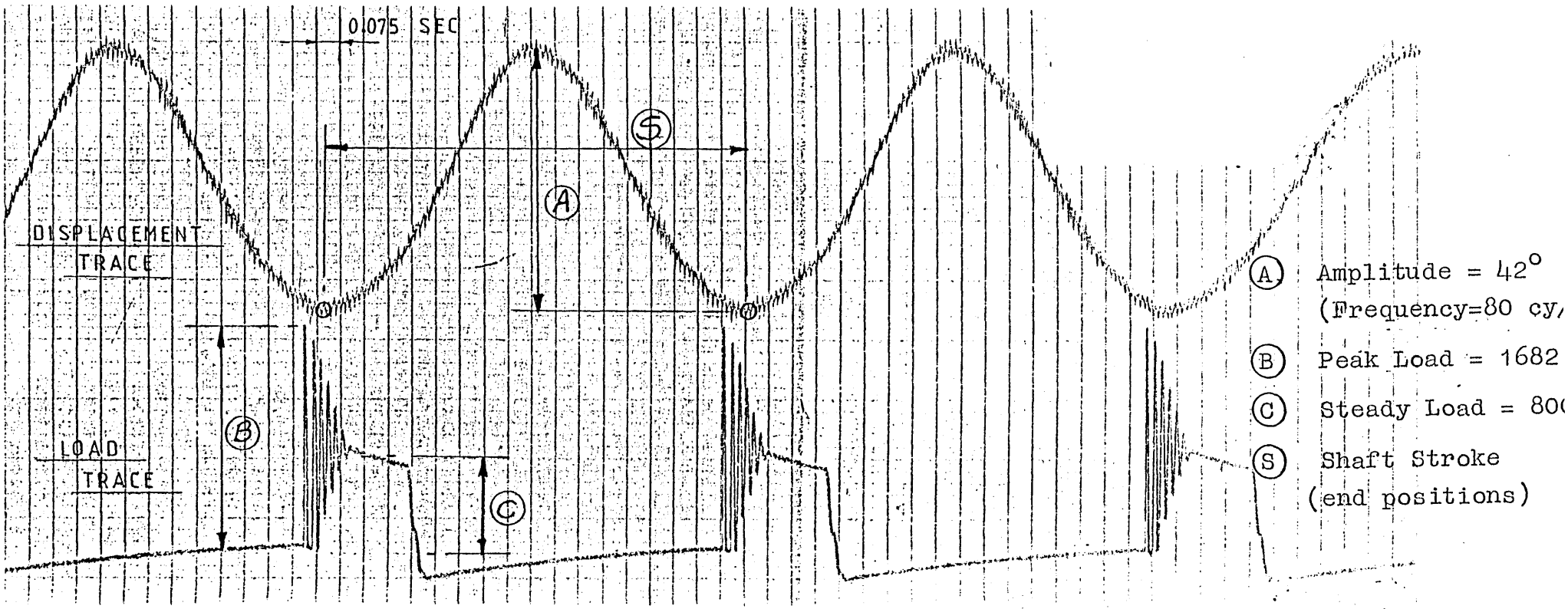

Fig. 4.28 Phasing Shaft Displacement with Impact

Load - Experimental U. V. Traces.

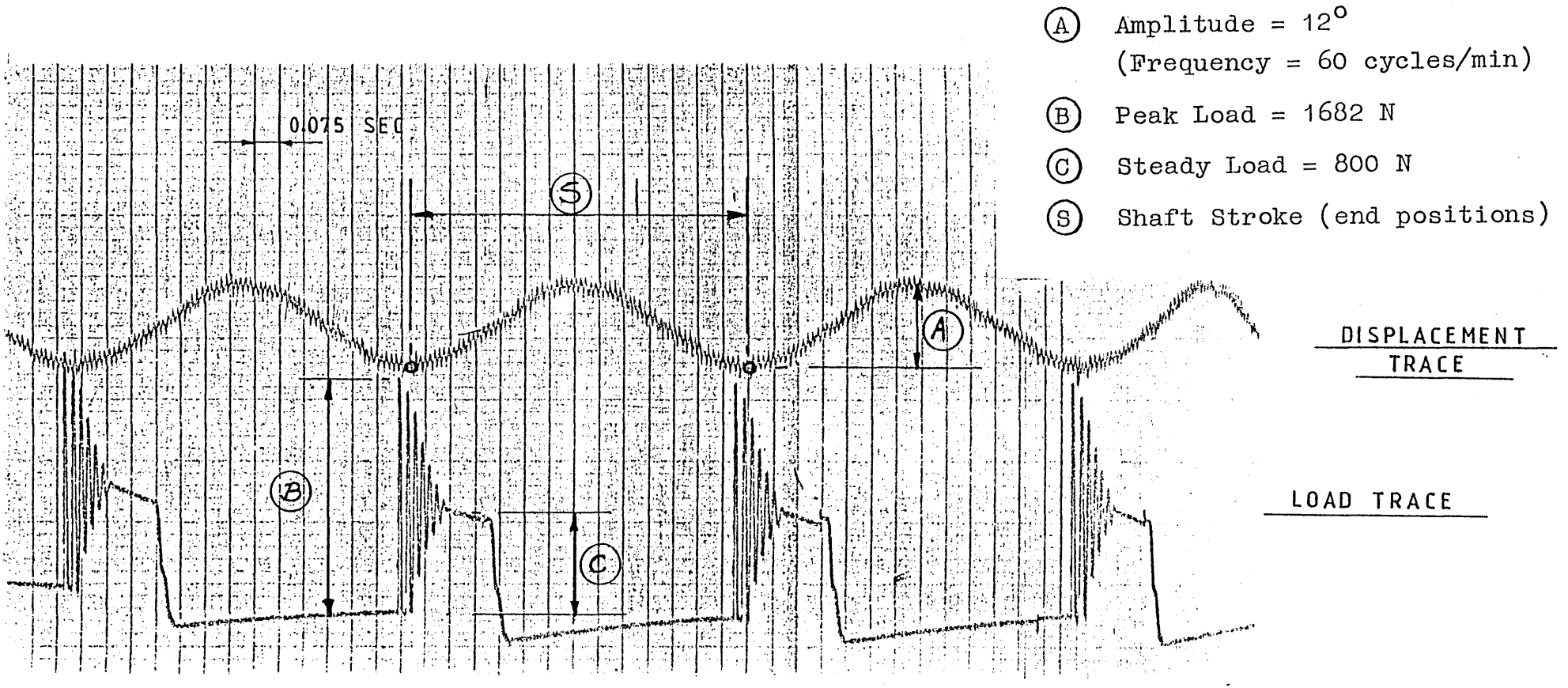

Fig. 4.29 Phasing Shaft Displacement with Impact

Load Experimental U. V. Traces.

4.3 Testing Procedures.

This section describes the tests made on the different bearings and the procedures used to record the required characteristics.

The test procedure varied as the experimental equipment was modified. Two sets of test procedures were adopted, one for the basic hydrodynamic bearings i.e. the grooved bearings, and the other when externally pressurised equipment was used for the hybrid bearings. These will be described in detail in the following sections:

4.3.1 Rig Operation General Procedure.

After the test bearing has been dimensionally checked, it was cleaned and assembled into the apparatus and lubricating system was carefully flushed. The displacement transducers were then set up as follows: each transducer was externally calibrated with a feeler gauge 0.025 mm (0.001 inch). Readings were taken of shaft displacement in the bearing clearance at zero load, by vertical and horizontal movements of the shaft. The channel sensitivities and shifts were adjusted to bring the spot on the oscilloscope to the engraved bearing clearance circle in each of the two directions. Thus, the extreme positions of the shaft centre were found with the shaft stationary, no-oil supply and unloaded. A typical calibration chart is shown in fig. 4.30.

The inductance circuit was set to an inductance corresponding to a film thickness within the expected range. With the shaft running and the oil inlet pressure applied, a continuous record of the shaft displacement was obtained on the X-Y

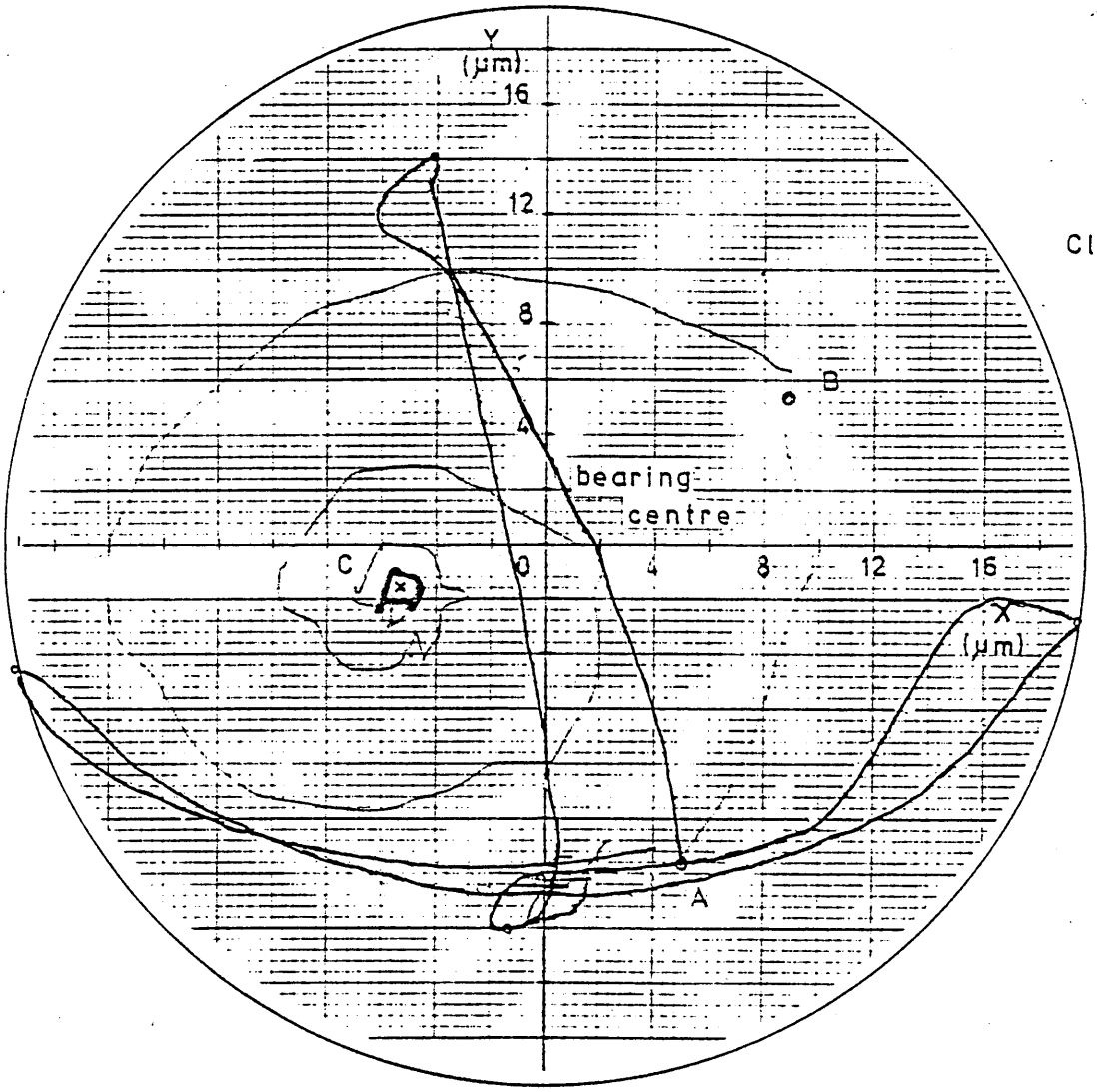

Conditions :

1) No-load

2) No-oil supply

Fig. 4.30 SHAFT CENTRE LOCUS.

(Calibration Chart).

recorder, where the average of the traces representing the location of the journal centre was defined.

From the no-load position of the running shaft, static and dynamic loads were applied and held until a stability condition was reached, then the load was released and the original shaft centre position was re-established. Thus, the locus path of the journal centre was obtained and plotted on the X-Y recorder.

A typical X-Y chart of the shaft eccentricity for a continuous running condition is shown in fig.4.31. It shows two radial displacements;

e_o - Which is the eccentricity from the original centre to equilibrium position after the load is applied (final load).

e_{max} - Which is the maximum eccentricity from the original centre during the time that the load is applied (transient load).

This chart also shows the clearance circle based on the extreme positions of the shaft centre and the position of the shaft at the beginning of the run i.e. when the shaft is at rest.

4.3.2 Experimental Series on the Test Bearings.

The tests on each of the three bearings were grouped in four sections:

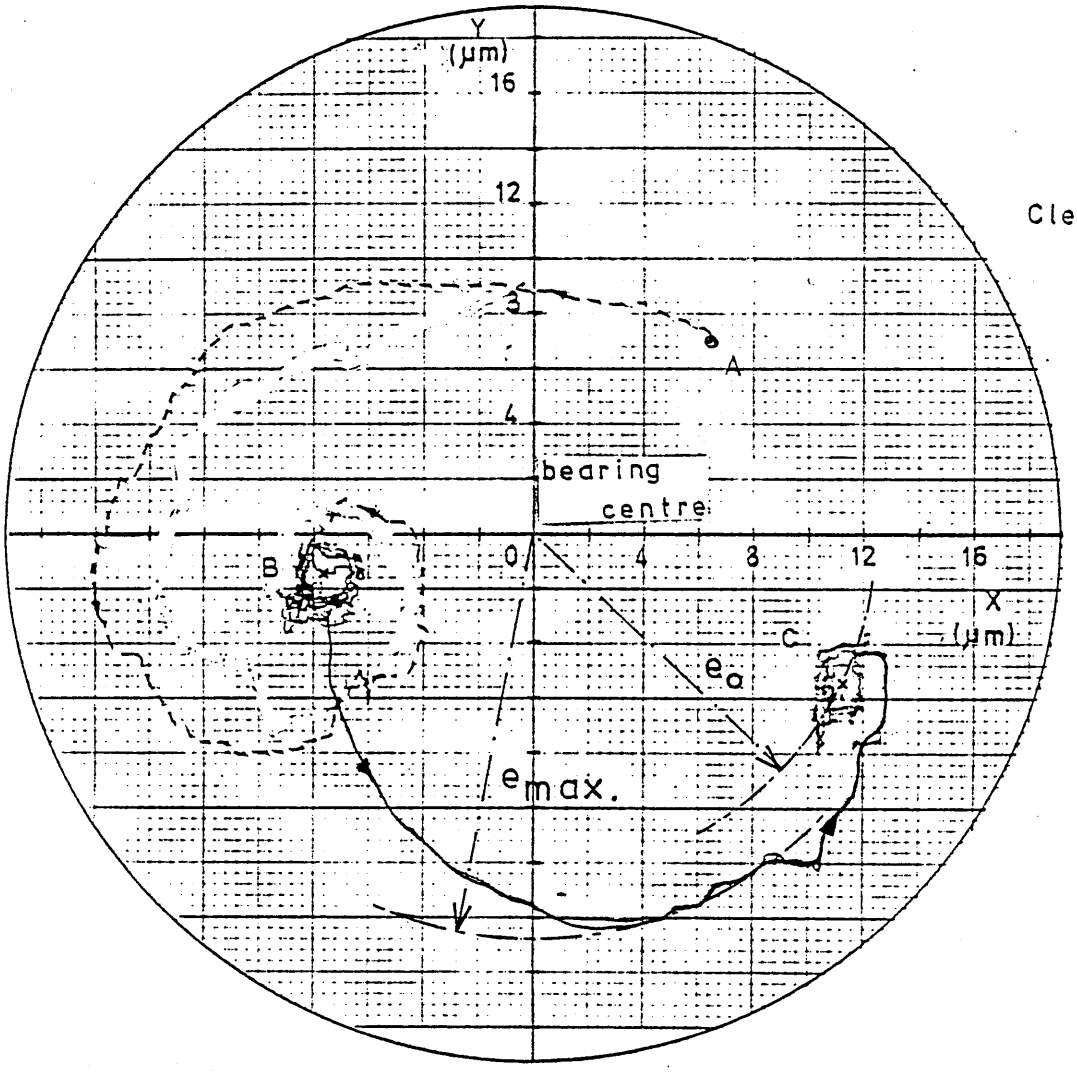

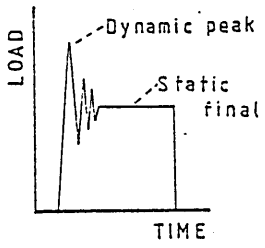

Conditions

N = 40 rev/min

W_{max} = 840 N (peak)

W_o = 420 N (steady)

P_s = 3 bar

Fig. 4.31 SHAFT CENTRE LOCUS.

Series No. 1 : Those tests concerned with the evaluation of the bearing characteristics under static load and continuous motion.

Magnitude of loading : from 158 to 800 N.
Angular velocity : from 40 to 130 rev/min

Series No. 2 : As same as above but those intended to show the characteristics of the bearing under oscillating motion.

Magnitude of loading : from 158 to 800 N.
Oscillating frequency : from 40 to 100 osc/min (0.185 to 0.463 rev/s equivalent).

Series No. 3 : Those intended to show the performance of the bearing under dynamic loading and continuous motion.

Magnitude of loading : from 1180 N to 2200 N
Angular velocity : from 40 to 130 rev/min

Series No. 4 : As same as above but those intended to show the characteristics of the bearing under oscillating motion.

Magnitude of loading : from 1180 N to 2200 N
Oscillating frequency : from 40 to 100 osc/min (0.185 to 0.463 rev/s equivalent).

The experiments were all carried out at a constant speed or frequency of oscillation as specified in each of the series. Different average velocities were obtained by varying the motor shaft angular velocity.

Different loads were obtained by varying the cylinder pressure but keeping the same spring i.e. constant stiffness. The load started at 158 N and increased in steps up to 795 N. The dynamic and static loads applied to the system were measured simultaneously with the shaft centre displacements, using the Kistler load cell as described in section 4.2.

So, in each series of experiments the oil is fed to the bearing, then the load is applied after the shaft is set in motion and test is made for each applied load, then the load is removed before the motor is stopped.

The test conditions which correspond to the series of experiments presented here, and which were chosen for each type of bearings are given in tables in appendix A, B and C. These tables also include the experimental results.

The circumferentially grooved hydrodynamic bearing-type I, was tested with oil supply pressure of 3 bar under the four experimental series above described, but as it will be seen in section 5.2, the tests under oscillating motion proved unsuccesful and the intention to carry out subsequent tests with dynamic loads and oscillating motion was not pursued.

The axially grooved hydrodynamic bearing-type II, was subjected to the same series of tests as the circumferentially grooved bearing, and dynamically loaded with the shaft under oscillating motion. All tests were carried out under three constant oil supply pressures of 3, 7 and 10 bar.

When plotting the results of the oscillating motion tests it was necessary to represent the magnitude of the oscillating motion in the Ocvirk number. Clearly it was not sufficient to use the number of cycles/sec since this would produce differing sliding speeds depending upon the amplitude of the oscillation. Therefore the average equivalent speed in rev/sec was determined as follows:

Average equivalent speed

$$= \frac{2 \text{ angular displacement}^{\circ} \times \text{cycles/min}}{360 \times 60} \quad \text{(rev/s)}$$

and used as $\overline{N}$ in those results for oscillating motion.

For the hybrid bearings-type III, series of tests were carried out in the same manner to the hydrodynamic bearings, but under higher oil supply pressures of 10, 35 and 70 bar, in order to promote a hydrostatic effect in the system.

Bearing temperature was also recorded at intervals during each test for the series of experiments carried out for the circumferentially grooved bearing-type I and axially grooved bearing-type II.

CHAPTER 5. EXPERIMENTAL RESULTS.

5.1 Introduction.

The present section gives the results obtained from the series of experiments carried out for each of the bearings, which were subjected to the different operating conditions described in section 4.5.

A specimen result is explained for each one of the test bearings with the help of photographic traces or X - Y chart recordings and the salient points discussed. Also, X - Y charts covering all the results for each series of tests are included. These are graphically represented by plotting the eccentricity values as a function of duty parameters i.e. Ocvirk number for the hydrodynamic bearings, type I and II and, Fuller number for the hybrid bearing.

On the other hand, the actual numerical results are summarized in tables in the appendix. These also, give the general conditions under which the tests were carried out.

5.2 Experimental Results of the Tests on Bearing Type I - Circumferential Grooved.

5.2.1. Results of Preliminary Tests.

i) Effects of the running speed.

Figures 5.1, 5.2, 5.3 , represent scope traces of the shaft locus when the shaft rotates continuously at speeds of 50, 100 and 130 rev/min. These photographs show

BEARING TYPE I

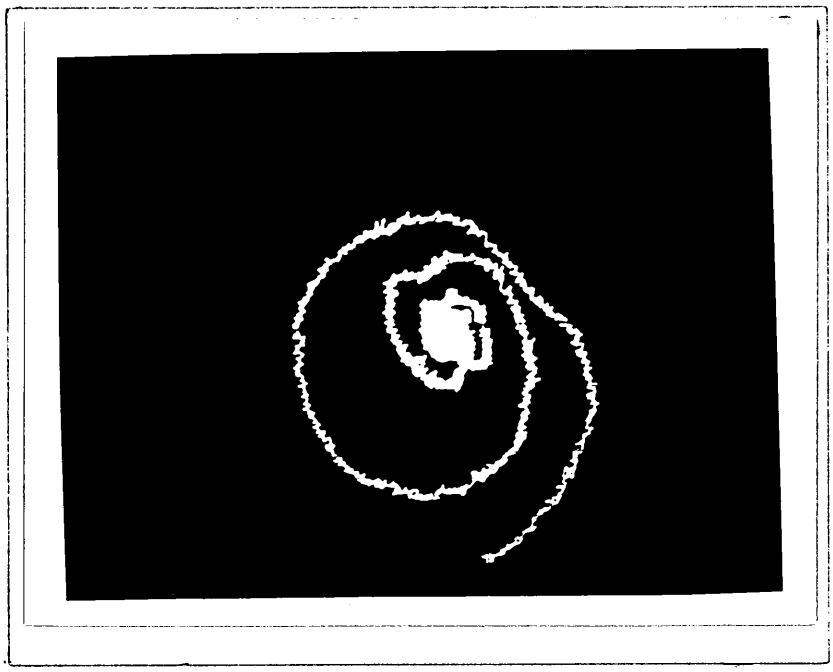

Fig. 5.1 Shaft locus started from rest to running equilibrium position at zero load.

(N = 50 rev/min, P_s = 3 bar)

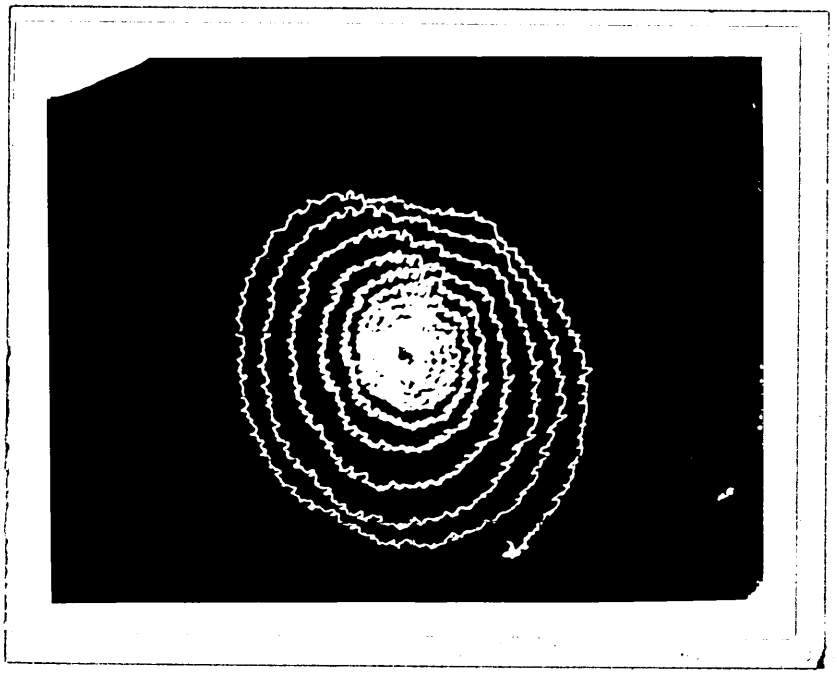

Fig 5.2 Shaft locus started from rest to running equilibrium position at zero load.

(N = 130 rev/min, P_s = 3 bar)

BEARING TYPE I

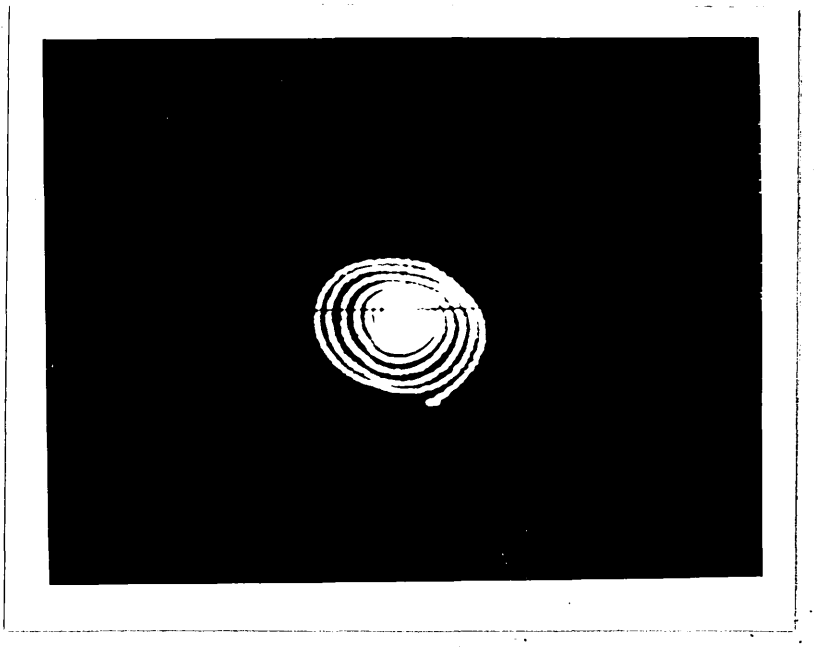

Fig. 5.3 Shaft locus started at zero load up to equilibrium position.

(N = 100 rev/min, P_s = 3 bar)

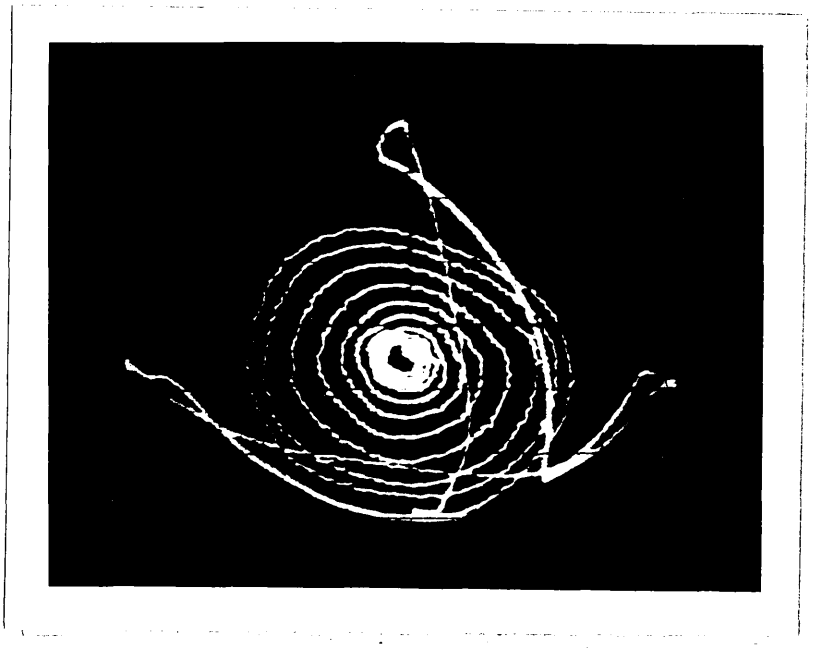

Fig. 5.4 Shaft locus started at zero load up to equilibrium position.
Extreme positions are also indicated.

(N = 100 rev/min, P_s = 3 bar)

the shaft displacement when the bearing started up under no load, and an oil supply pressure of 3 bar. It can be seen that the bearing undergoes a period of semi-instability with a spiral locus. After several revolutions the shaft settles down to a fixed locus. It is also observed that at the highest speed of 130 rev/min, more revolutions take place. In fig. 5.4, the extreme positions of the shaft are also indicated, when it is stationary.

ii) Effect of preloading the bearing.

Figures 5.5, 5.6, are photographs of the scope trace of the shaft locus when it is preloaded at 420 N with oil supply pressure of 3 and 1 bar, before it is run. When it is rotated at 100 rev/min, firstly it goes straight away for a short distance to an equilibrium position without any spiraling at all, then as the load is quickly realeased the shaft follows a spiraling path and after several revolutions, finally stabilizes near to the centre of the bearing.

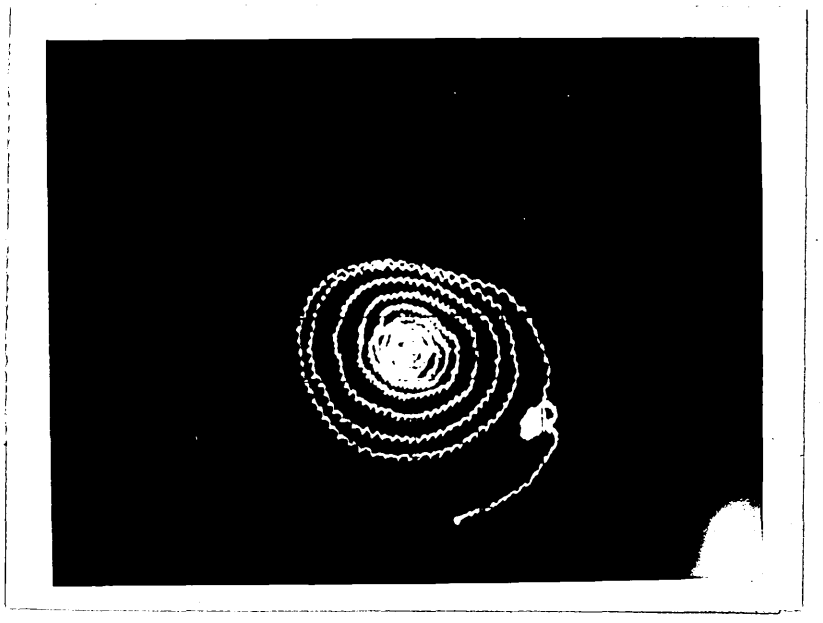

Fig. 5.5 Shaft locus when started at 420 N load, then released to free running.

(N = 100 rev/min, P_S = 3 bar)

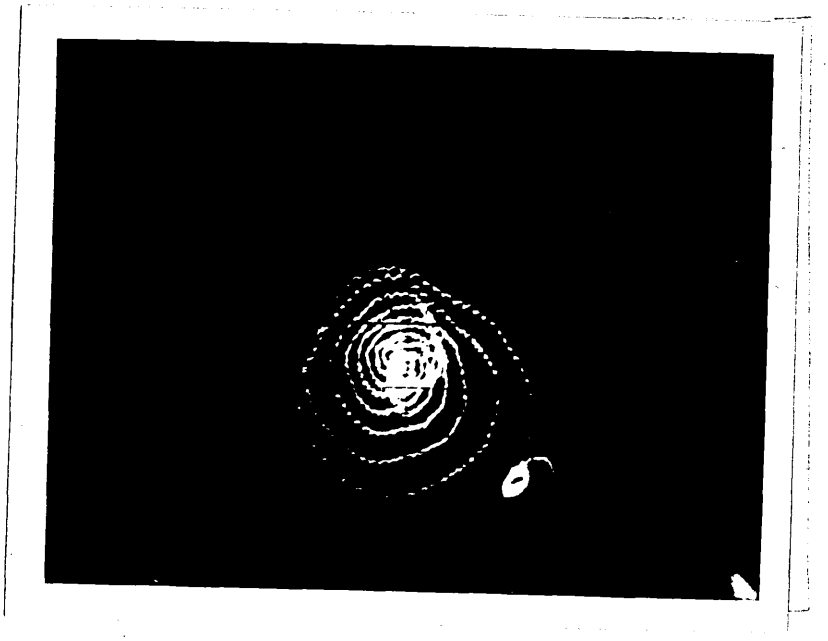

Fig. 5.6 Shaft locus when started at 420 N load, then released to free running.

(N = 100 rev/min, P_S = 1 bar)

5.2.2 Results of Series No 1 Static Load Tests Under Continuous Motion Conditions.

These series of tests were carried out under the conditions described in section 4.3.

Figure 5.7 represents a high speed scope trace of the shaft locus using a simple test set up, static load with speed of 130 rev/min applied to the test bearing.

This photograph clearly illustrates how factors such as the eccentricity displacement and attitude angle of the shaft can be determined.

It shows in the middle the equilibrium position of the shaft centre under continuous motion but unloaded. Then, it gives the momentary path followed by the shaft centre when it is statically loaded until it settles down in another equilibrium position under the effect of the load. No spiraling movement is noted.

Figure 5.8 is another scope trace of the shaft centre locus, when the shaft is subjected to similar conditions as the previous test, except that the running speed has been lowered to 50 rev/min.

It can be seen that the shaft centre follows a different path. First it moves vertically in the direction of the applied load and then for a while along a line normal to the load before it reaches the final loaded equilibrium position. Once again, no spiraling effect is noted.

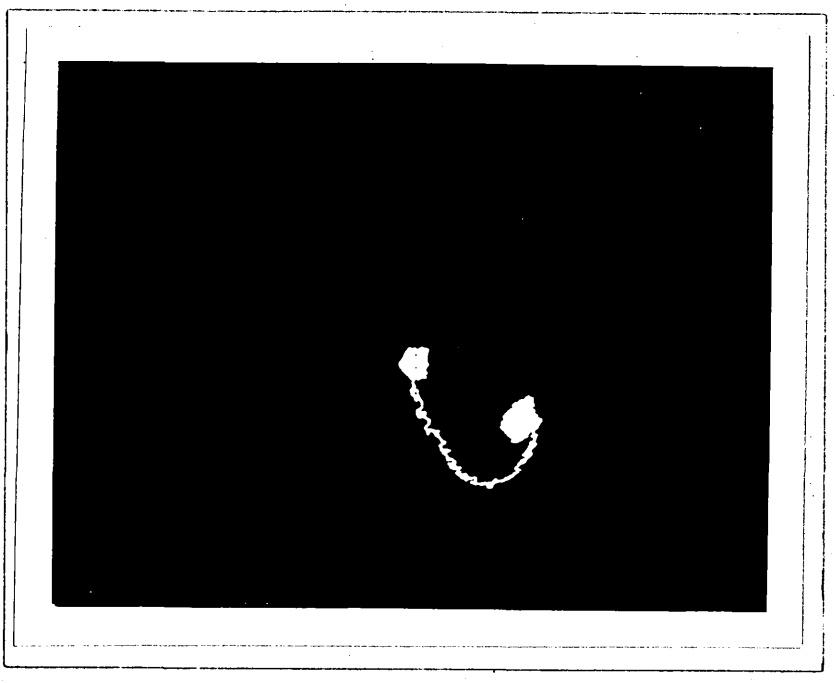

Fig. 5.7 Shaft locus under equilibrium running positions from zero load to test load (static)

(N = 130 rev/min, W = 238 N, P_s = 3 bar)

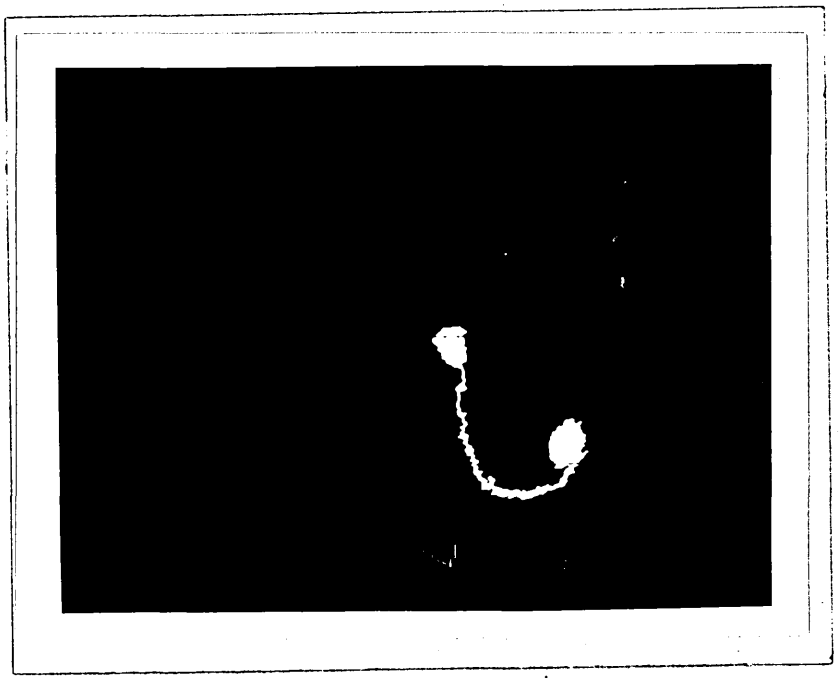

Fig. 5.8 Shaft locus under equilibrium running positions from zero load to rest load (static)

(N = 50 rev/min, W = 238 N, P_s = 3 bar)

These figures are particulary instructive because they offer a graphic verification of the locus of the shaft centre under steady loading and continuous motion.

Figure 5.9, shows a complete series of tests when the shaft is subjected to a set of consecutive loading conditions, stepping gradually from light loads of W = 140 N to heavy loads of W = 720 N with constant speed of 110 rev/min. It is clearly noted that before any change of load is going to be applied, the equilibrium unloaded position, point "A", is established every time, giving a true reference. But the important feature in this case is that the eccentricity of the shaft increases as the load is increased i.e. for light loads much less shaft displacement takes place than for heavy loads.

Figure 5.10 is a similar chart to the above but the tests were carried out at a different running speed of 40 rev/min. It shows that the eccentricities were bigger than the previous ones, getting closer to the metal to metal contact situation

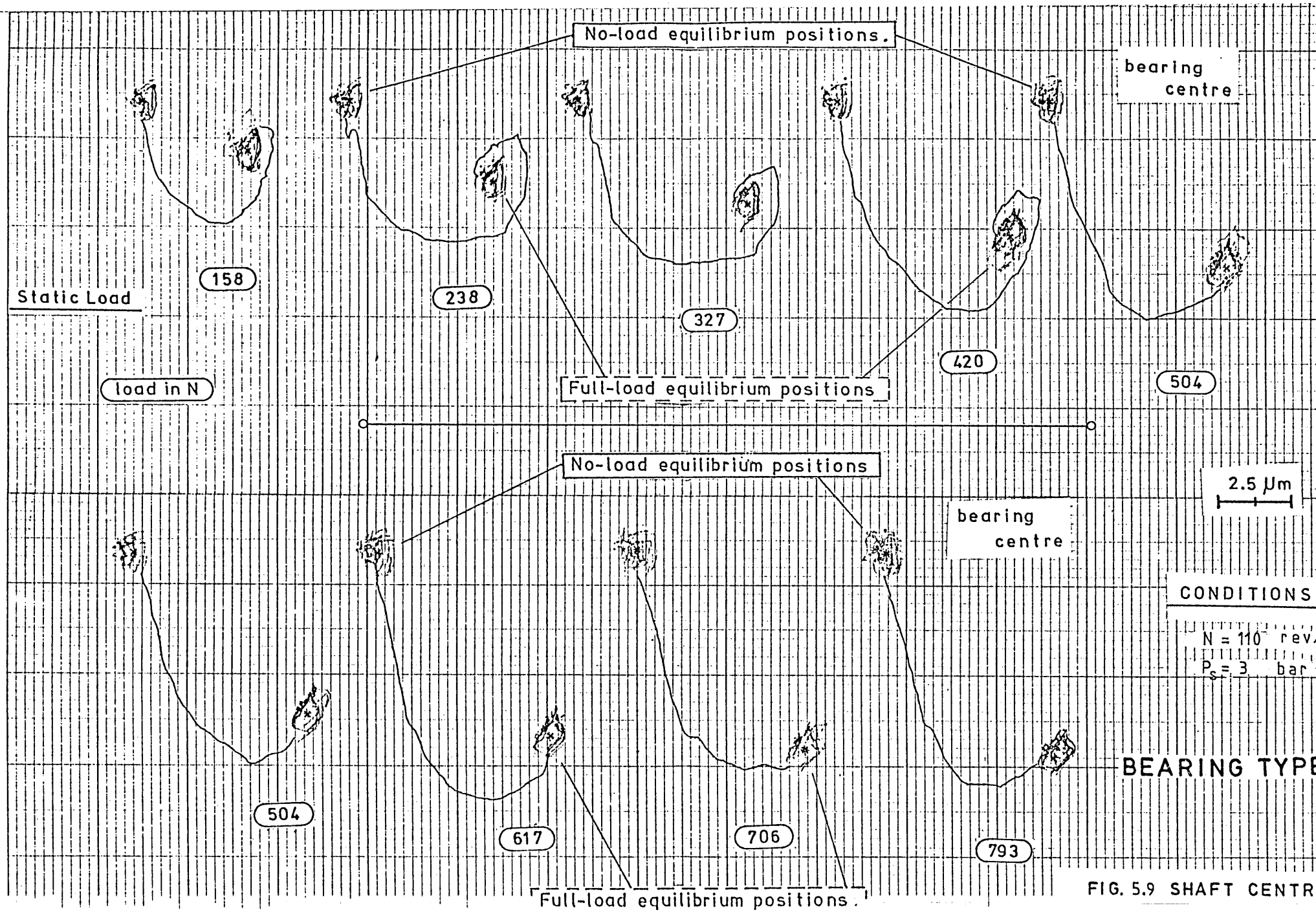

FIG. 5.9 SHAFT CENTR

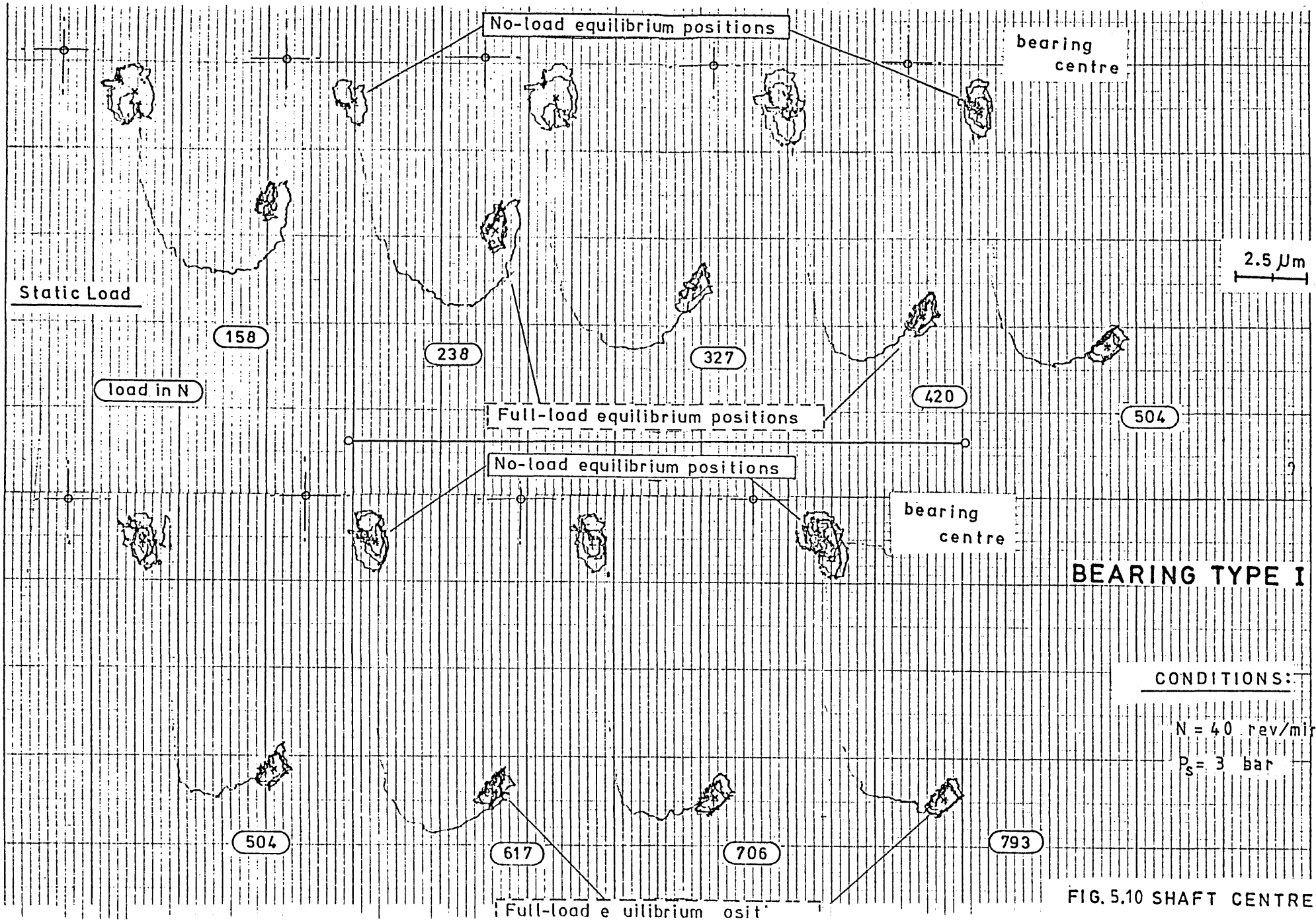

FIG. 5.10 SHAFT CENTRE

5.2.3 Results of Series No. 2 Dynamic Loading Tests Under Continuous Motion Conditions.

These tests were carried out in accordance with the procedures already mentioned in section 4.3 and the following results were obtained.

Figure 5.11 shows scope photographs of shaft centre locus from the unloaded equilibrium position until it has been dynamically loaded, the load magnification factor is given for each test. The shaft is running at a speed of 50 rev/min with constant oil supply pressure of 3 bar. It clearly shows that the shaft centre moves in a more vertical direction until it reaches an equilibrium running position under load. Also, it can be noted that before reaching the equilibrium point, the shaft centre undergoes a maximum eccentricity displacement.

Figure 5.12 shows the shaft centre movement under similar conditions to the previous test but under fast running speed of 130 rev/min. It is noticeable that the shaft follows another path, not as vertical as before and not as far. Also, the final equilibrium position is closer to the unloaded equilibrium position, with the result of a more elongated loop.

Figure 5.13 shows true traces taken directly from the X-Y recorder of the path followed by the shaft centre comparing static and dynamic tests. Again the unloaded equilibrium position of the shaft centre is established before every test is carried out. Variations of the eccentricity are shown as the load is changed.

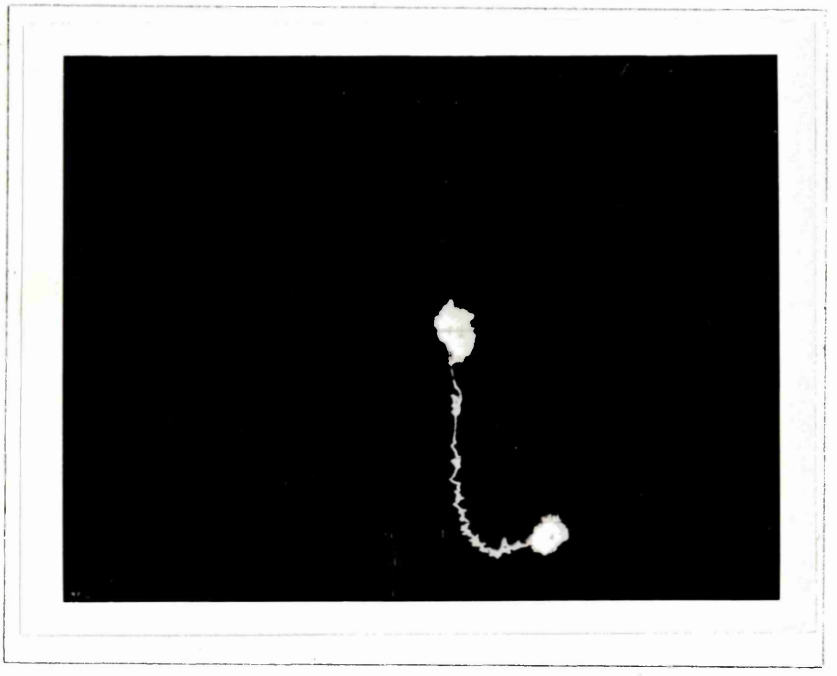

Fig. 5.11 Shaft locus at equilibrium running positions from zero load to test load (dynamic) (N = 50 rev/min, W = 706 N with L.M.F = 1.48, P_s = 3 bar)

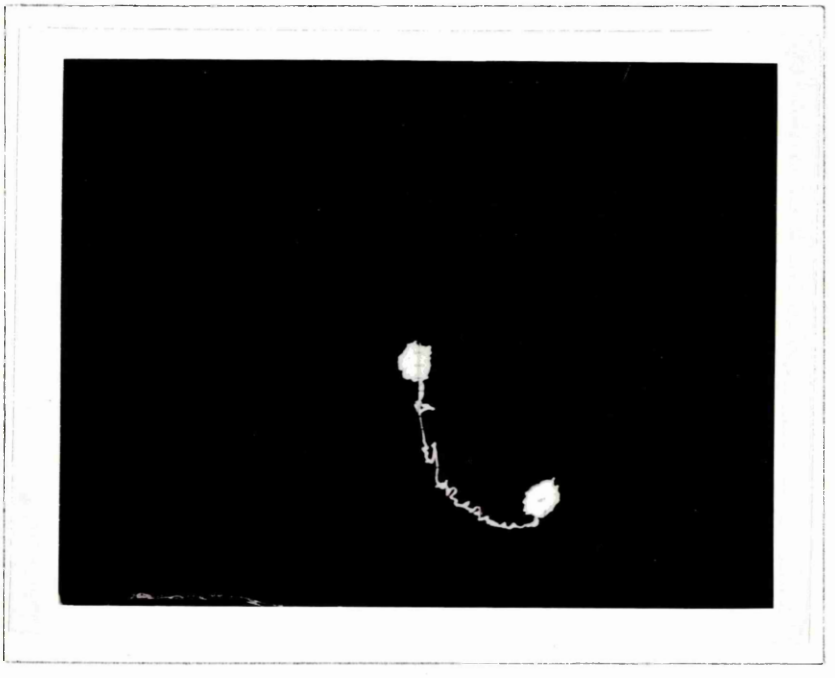

Fig. 5.12 Shaft locus at equilibrium running positions from zero load to test load (dynamic) (N = 130 rev/min, W = 706 N with L. M. F. = 1.48, P_s = 3 bar)

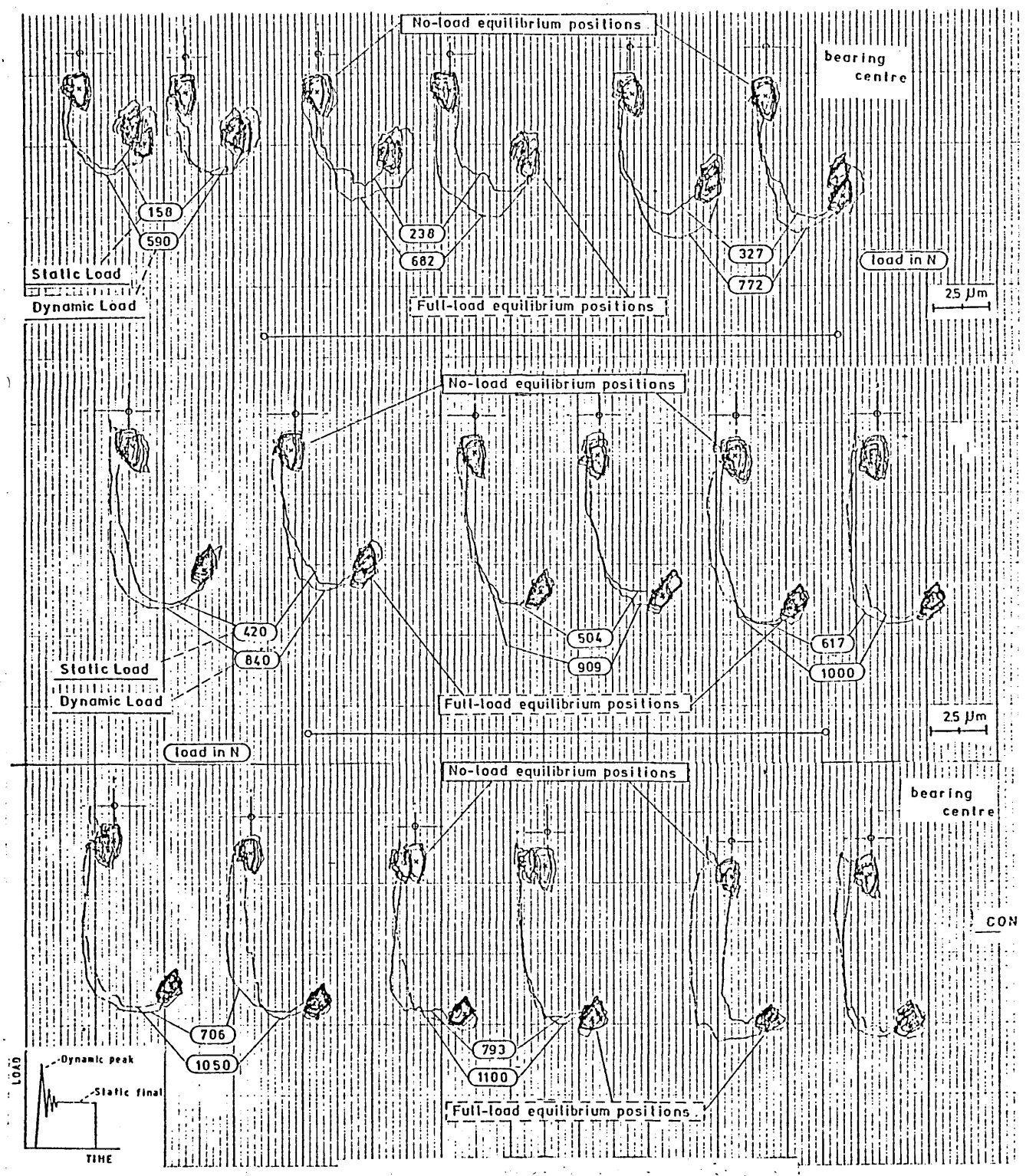

Conditions :

BEARING TYPE I

Dynamic and Static load

N = 100 rev/m

P_s = 3 bar

Fig. 5.13 SHAFT CENTRE LOCUS.

Figure 5.14 shows similar charts to the previous one but in this case the tests were carried out under different running speeds of N = 70 rev/min, for dynamic loads only. From these charts it is noticeable that the shaft eccentricity increased as speed was reduced.

Figure 5.15 is the graphical representation of the results obtained for the above experiments, subjecting the shaft to static and dynamic loading with continuous motion. Graphs from these tests show the variation of eccentricity as the applied load was changed. As the traces of the equilibrium eccentricities for static and dynamic loads were found to be indistinguishable they are plotted as the same values. So only the final eccentricity values for static load, and the maximum and final eccentricities values for dynamic load are shown. Load magnification factors are as indicated. In these graphs it can be seen that the set of results for statically loaded operation of 100 and 70 rev/min follow closely the theoretical curves but at speed of 40 rev/min there is a tendency to an increased eccentricity ratio. The same is true under dynamic loading and in addition, for heavy loads there is no gap between the final and maximum eccentricity positions.

Figure 5.16 is another graphical representation of the above experimental results but plotted on a polar diagram in terms of eccentricity ratio and attitude angle. The effect of speed reduction on eccentricity ratio is seen to become unity at low speed of 40 rev/min when heavy loads are applied. Also, the attitude angle changes as the load increases. Results for 100 rev/min show closest agreement with the theoretical curve, although all results fall greater than those predicted.

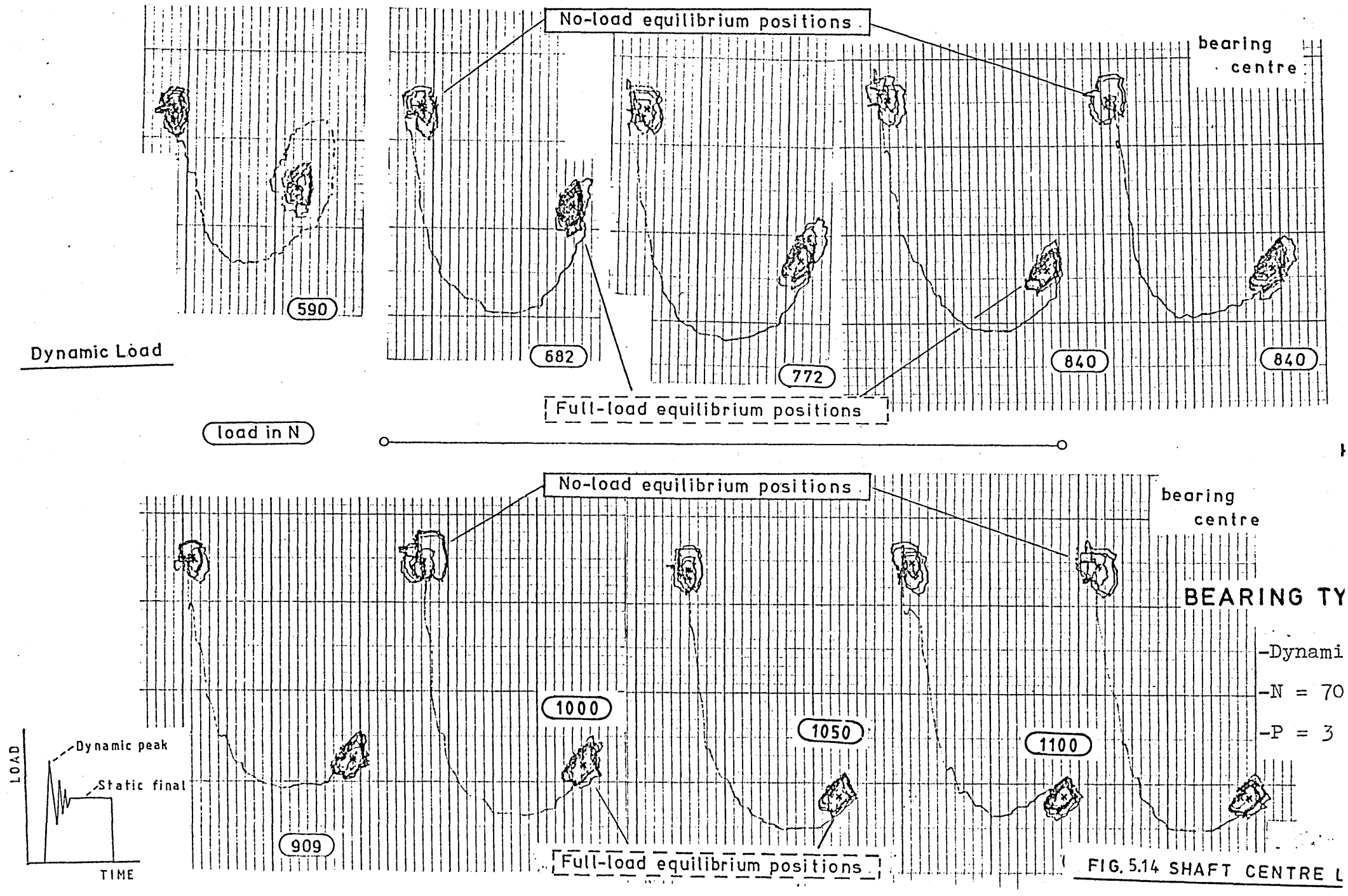

BEARING TY

-Dynami

-N = 70

-P = 3

FIG. 5.14 SHAFT CENTRE L

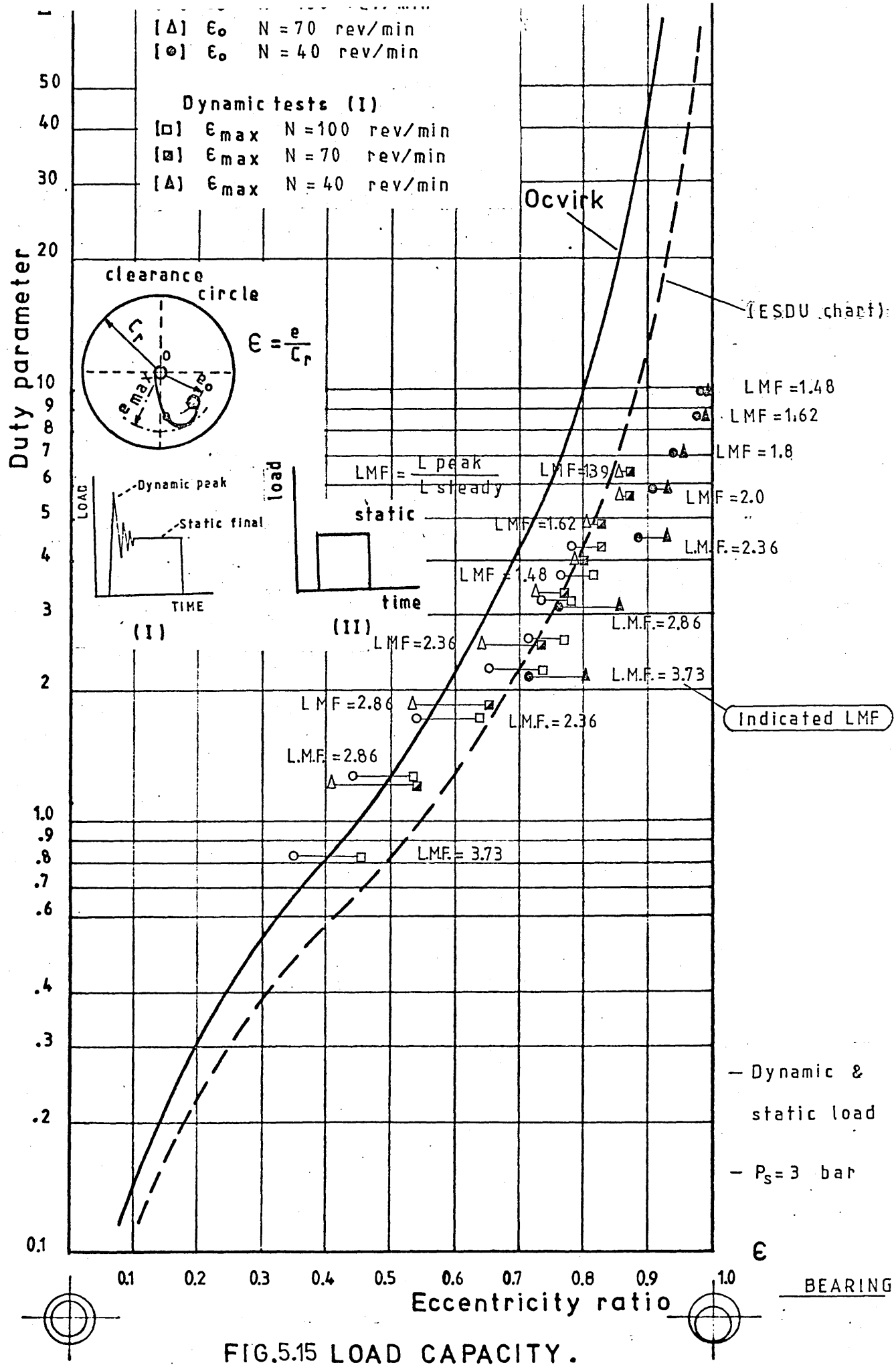

FIG.5.15 LOAD CAPACITY.

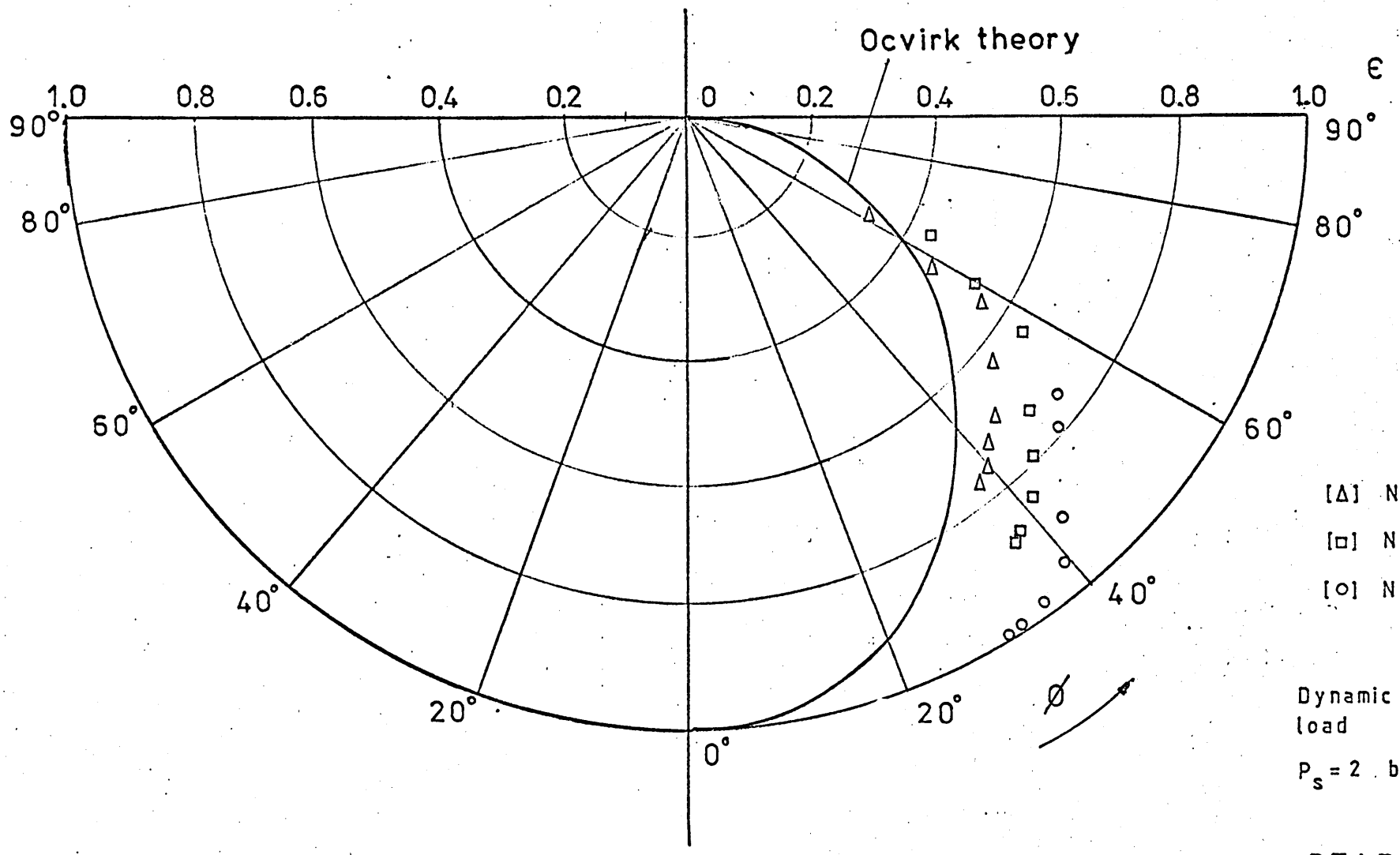

FIG. 5.16 ECCENTRICITY RATIO AGAINST ATTITUDE ANGLE.

5.2.4 Results of Series No. 3 Static Loading Tests Under Oscillating Motion.

These series of tests were attempted but as is shown in fig. 5.17 they were unsuccesful.

It can be noted that no oil film was generated even when the shaft oscillated without load.

Different frequencies were also tried in order to improve the bearing performance but as can be seen in fig. 5.17 it did not help either. So, it was not possible to take any eccentricity variation readings at all and was assumed, that maximum eccentricities took place at any level of the applied load, which were then plotted in graph 5.18.

5.2.5 Results of Series No. 4 Dynamic Loading Test Under Oscillating Motion.

As the previous test proved to be unsuccesful, the intention to carry out tests with dynamic loads and oscillating motion was not pursued.

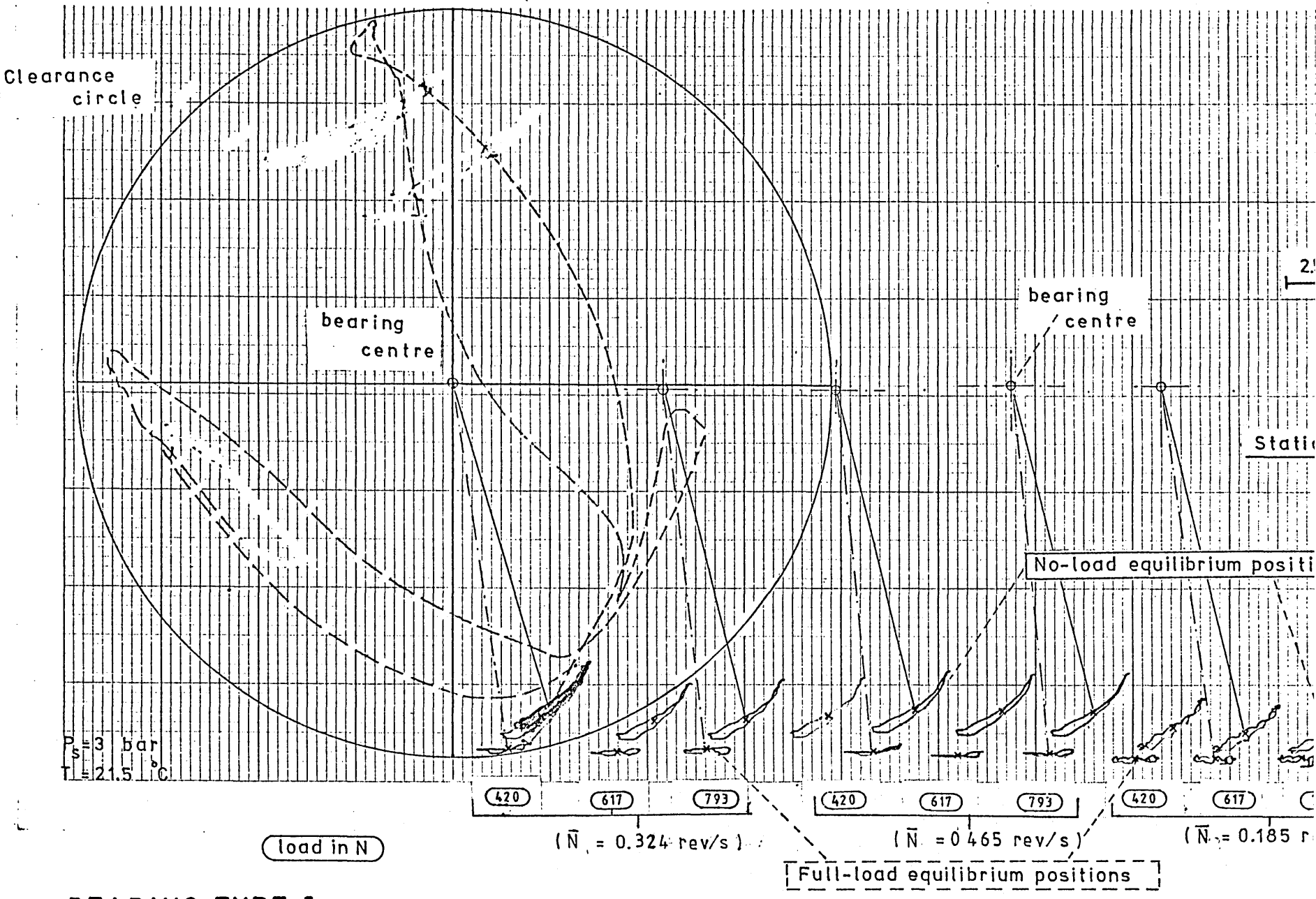

BEARING TYPE I

FIG.5.17 SHAFT CENTRE LOCUS.

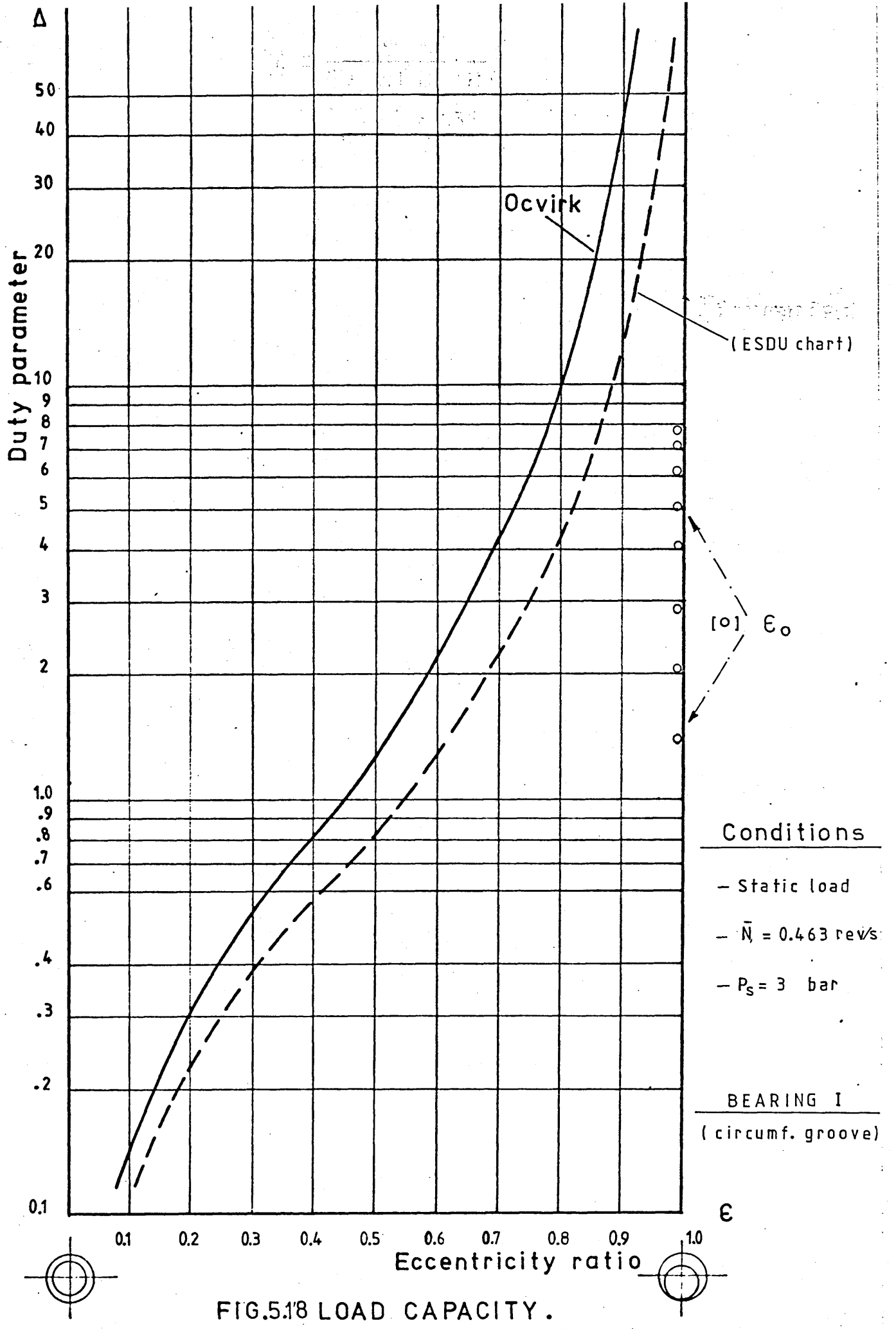

FIG.5.18 LOAD CAPACITY.

5.3 Experimental Results of the Tests on Bearing Type II- Circumferential and axially grooved.

5.3.1 Results of Preliminary Tests.

i) Running characteristics of the shaft under continuous motion and no load.

Figures 5.19 - 20 - 21 are typical traces of the shaft centre running at constant speed of 100 rev/min and under the supply pressures of 3, 7 & 10 bar. Point "A" indicates the shaft at rest position, point "B" also shows the shaft at rest but under the effect of the oil pressure. It is clear ly seen that the oil supply pressure caused the journal to displace upwards.

This effect was more marked as the inlet pressure was further increased. From the rest position "B", the shaft is rotated at constant speed following a spiraling path until it settles down to an equilibrium position, point "C". It can be observed that less spiraling effect takes place as the oil pressure is increased. Also, that the equilibrium running position is displaced to the left from the bearing centre as the pressure is higher.

ii) Oil inlet pressure effect of the shaft running without load and under oscillating motion.

Figure 5.22 shows typical X - Y traces a, b, c and d, which represent the orbits of the shaft centre at equilibrium position under oscillating motion of 0.465 rev/s and oil supply pressures of 4, 7, 10 and 20 bar with no load.

BEARING TYPE II

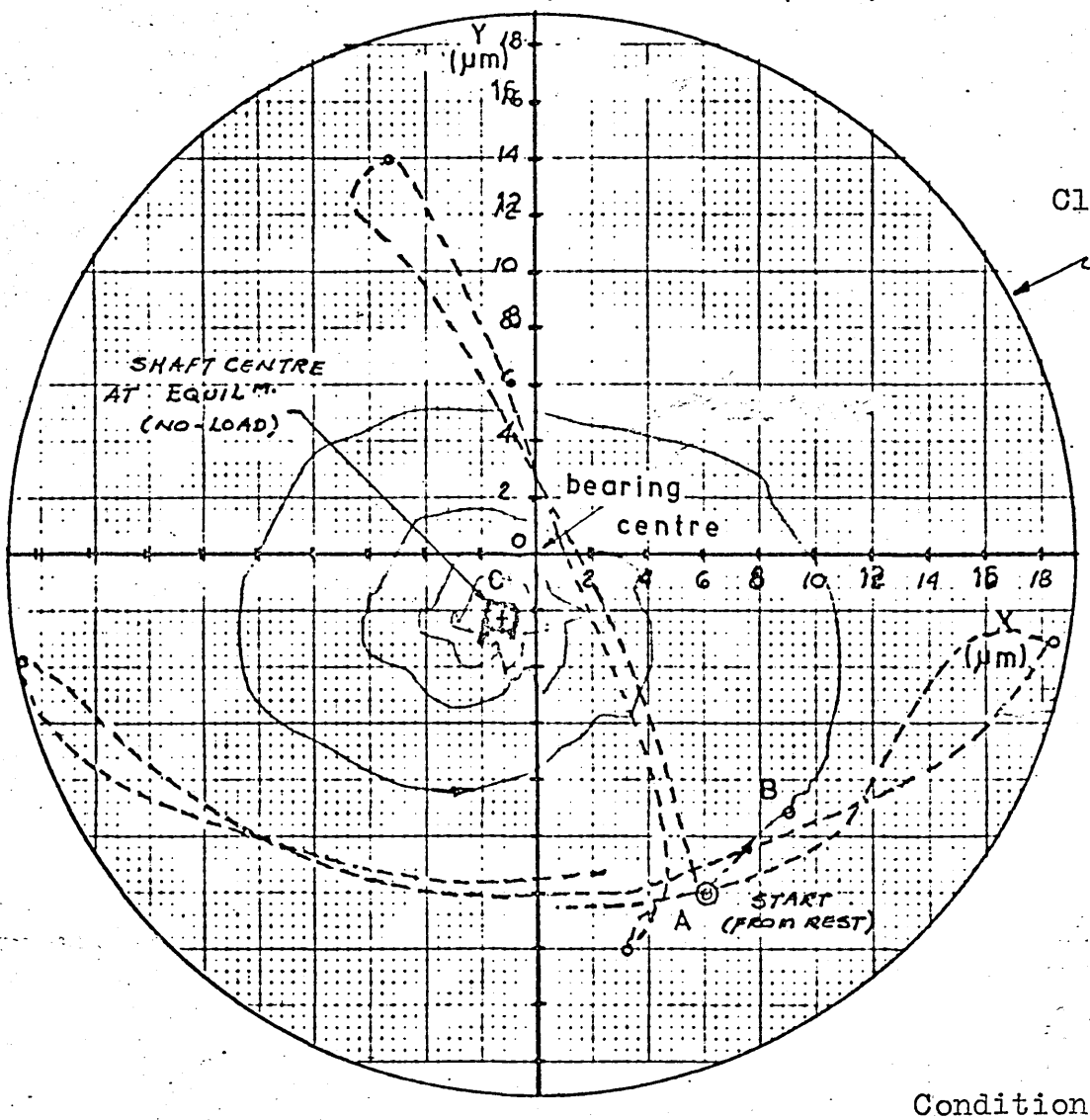

Conditions

N = 100 rev/min

P_s = 3 bar

W = 0 N

Fig. 5.19 SHAFT CENTRE LOCUS.

BEARING TYPE II

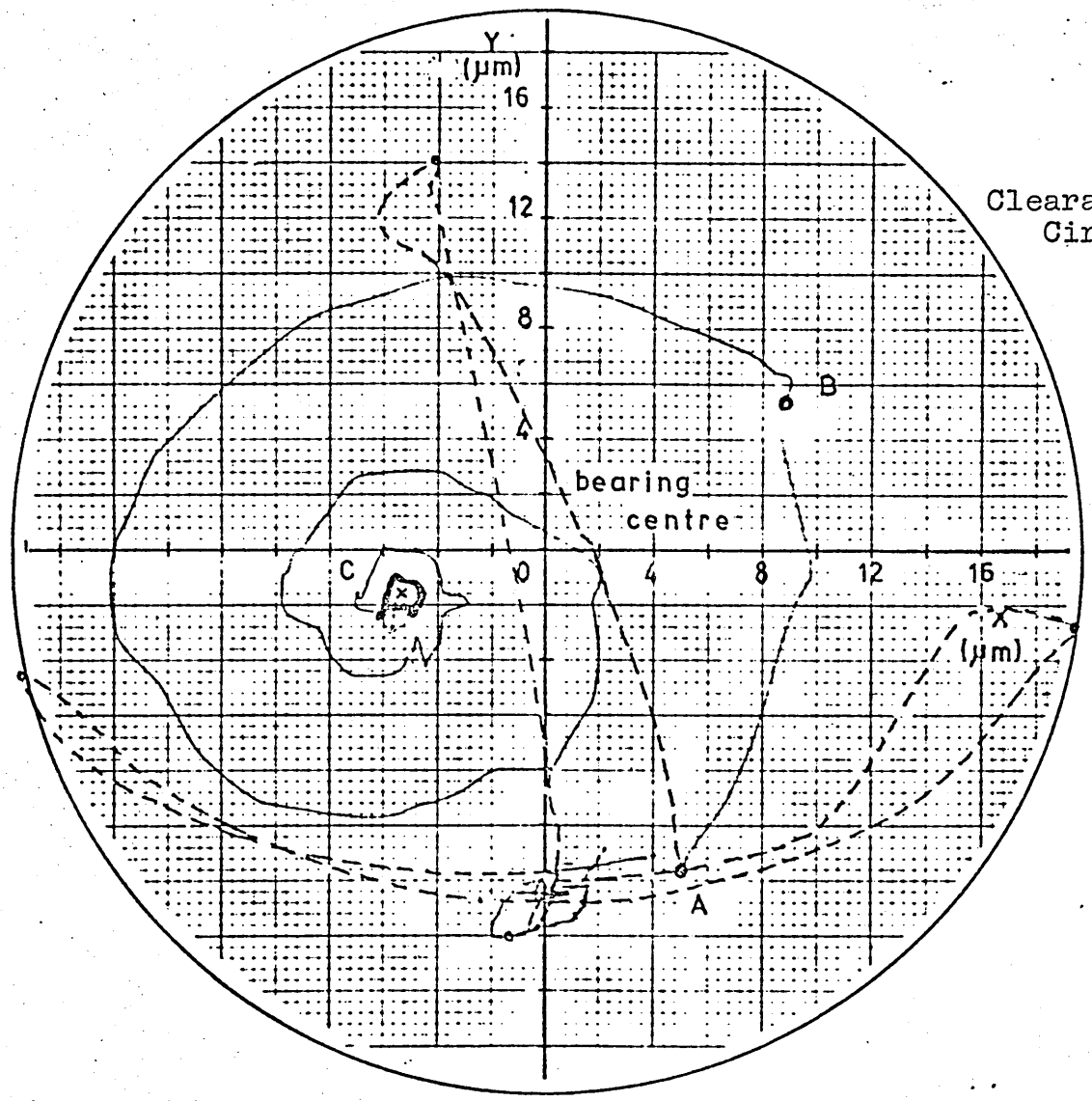

Conditions

N = 100 rev/mi

P_s = 10 bar

W = 0 N

Fig. 5.20 SHAFT CENTRE LOCUS.

BEARING TYPE II

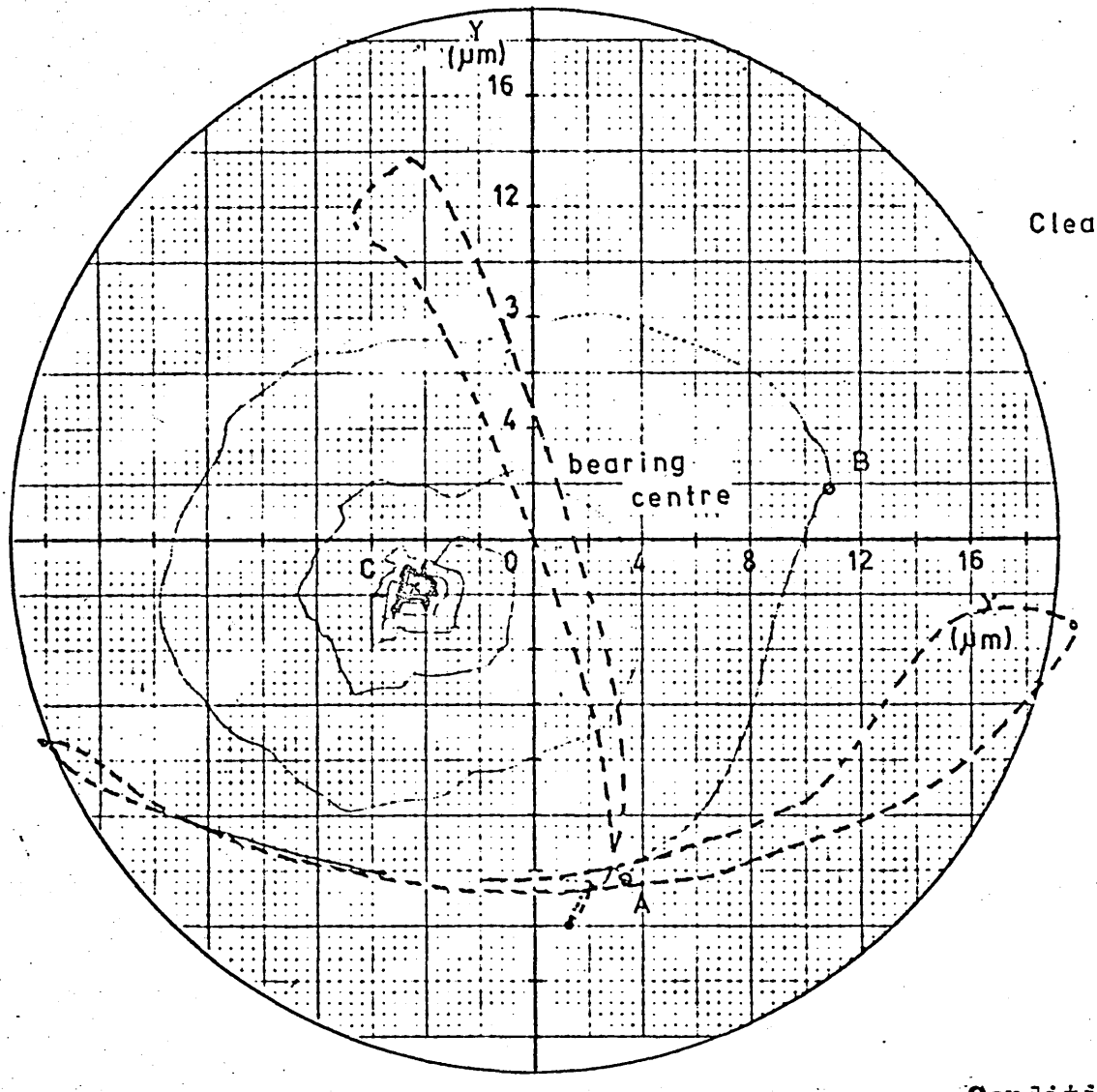

Conditions

N = 100 $\frac{rev}{min}$

P_s = 7 bar

W = 0 N

Fig. 5.21 SHAFT CENTRE LOCUS.

BEARING TYPE II

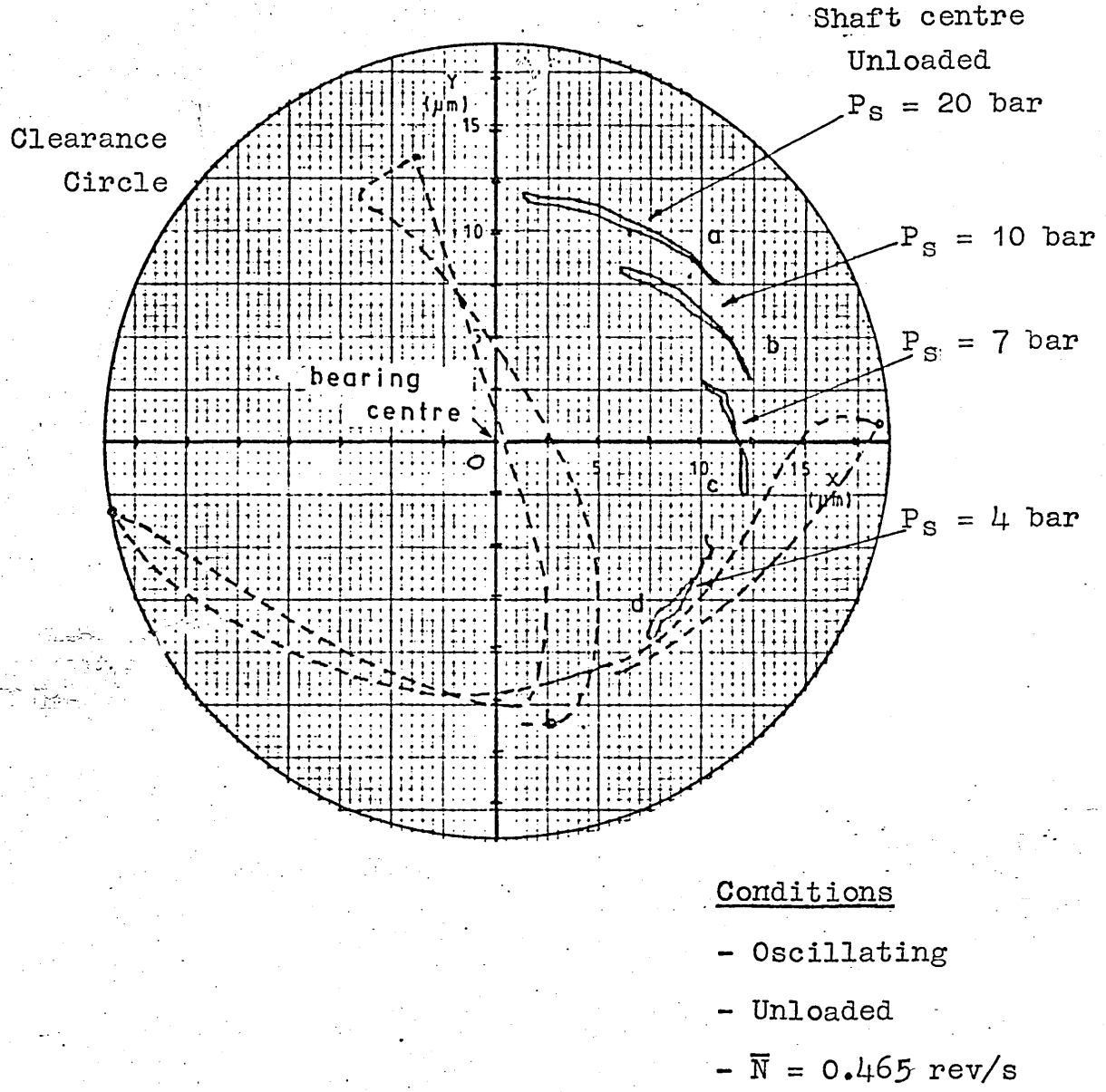

Conditions

- Oscillating
- Unloaded
- $\overline{N}$ = 0.465 rev/s

Fig. 5.22 SHAFT CENTRE LOCUS.

It is noticeable that the eccentricity reduced as oil supply pressure increases as ocurred with bearing I. Also, it can be seen that the orbit traces lie on the right hand side of the clearance circle and they go down and become shorter as the supply pressure is decreased.

The traces of the extreme positions of the shaft centre are also plotted for the shaft stationary. These traces define the clearance circle and are indicated by the broken lines.

iii) Phasing of the stroke position with the applied load.

The purpose of these preliminary experiments was to establish the relation between the applied impact load and the position of the shaft along the stroke when it was under oscillation.

Recordings were obtained, which are shown in figure 5.23 by using a high magnification scale to enable a good visualisation.

It can be noted in these figures, that the unloaded running position always was accurately reached at the same position, trace "a", which lies on the top right hand side from the true centre.

Figure 5.23 clearly shows three points 1, 2 and 3 on the trace "a" which almost correspond to the extreme and centre positions of the shaft oscillating trace. These points represent the starting of the path travelled by the shaft centre when it is dynamically loaded, for each indi-

vidual test, until it reaches the equilibrium loaded position trace "b", showing that this position is equally reached wherever the load has been applied.

Under this criterion the subsequent series of experiments were carried out more confidently without taking into account the position of the shaft when the load was applied.

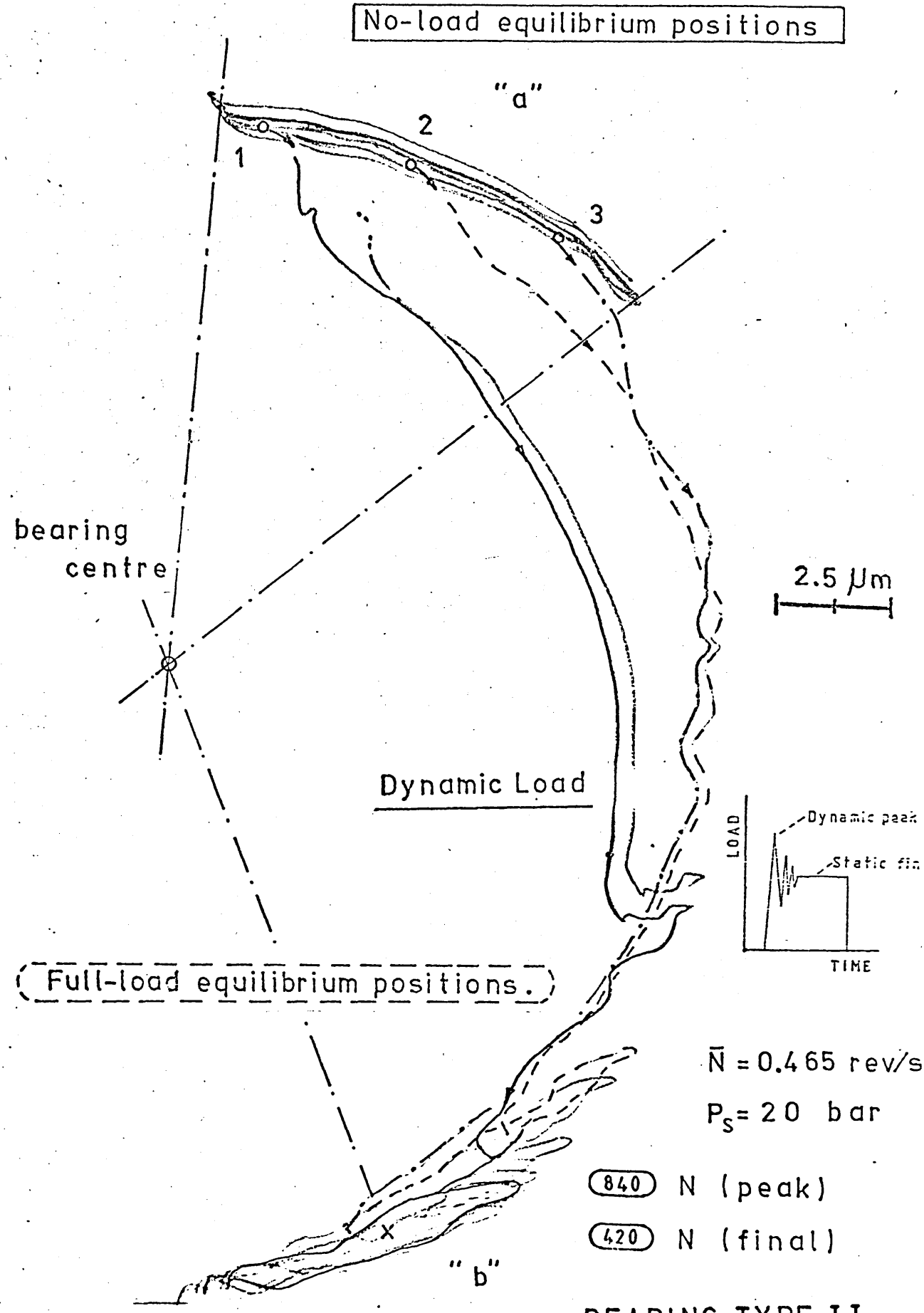

FIG. 5.23 SHAFT CENTRE LOCUS.

5.3.2 Results of Series No. 1 Static Loading Tests Under Continuous Motion.

These series of tests were carried out under the conditions described in section 4.3, and their corresponding results are described as follows:

Figures 5.24 - 25 - 26 show the shaft centre locus under the same static load of 420 N, same continuous speed of 100 rev/min but with different oil supply pressures, of 3, 7 and 10 bar. In these figures it can be noted that the equilibrium unloaded position, point B, moves to the left from the assumed bearing centre as the pressure is increased i.e. at low pressure it is nearer to the centre. Then, when the load is applied, it is clearly noticeable that the path followed by the shaft centre is in the same open loop shape for all of them, but more elongated for the case when high pressure is applied. However, it does not mean that a higher eccentricity of the shaft centre takes place, because the final loaded equilibrium position, point "C", for the three tests have the same eccentricity value, measured from the assumed bearing centre, point "O".

Figures 5.27 - 28 - 29 show further specimen traces of the shaft displacement, under the same static load of 420 N, same oil supply pressures as the previous tests but with different rotational speed of 40 rev/min. These graphs also give the equilibrium running position of the shaft centre and when the load is applied the same loop was obtained.

BEARING TYPE II

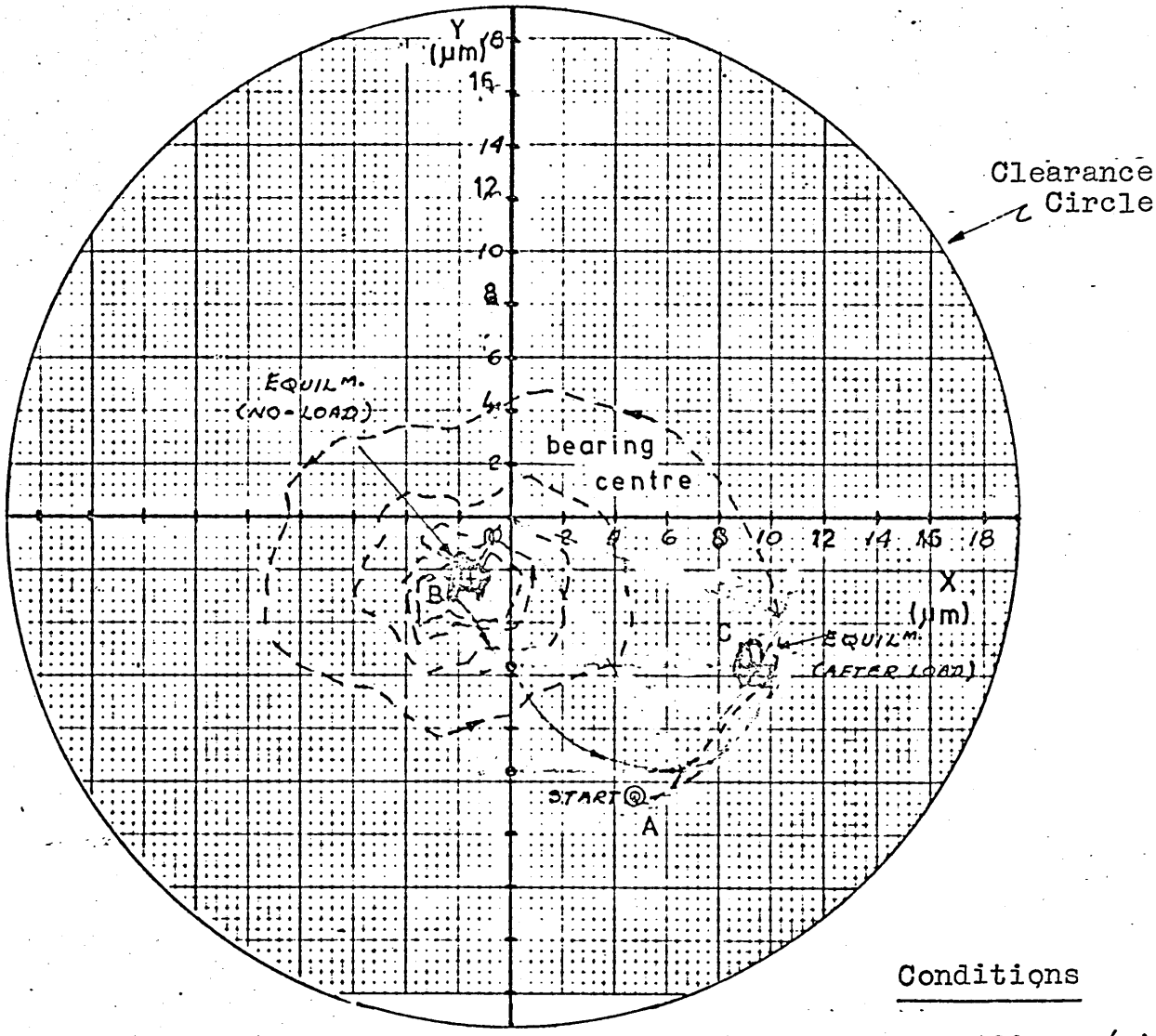

Conditions

N = 100 rev/mi

W = 420 N

P_s = 3 bar

Fig. 5.24 SHAFT CENTRE LOCUS.

BEARING TYPE II

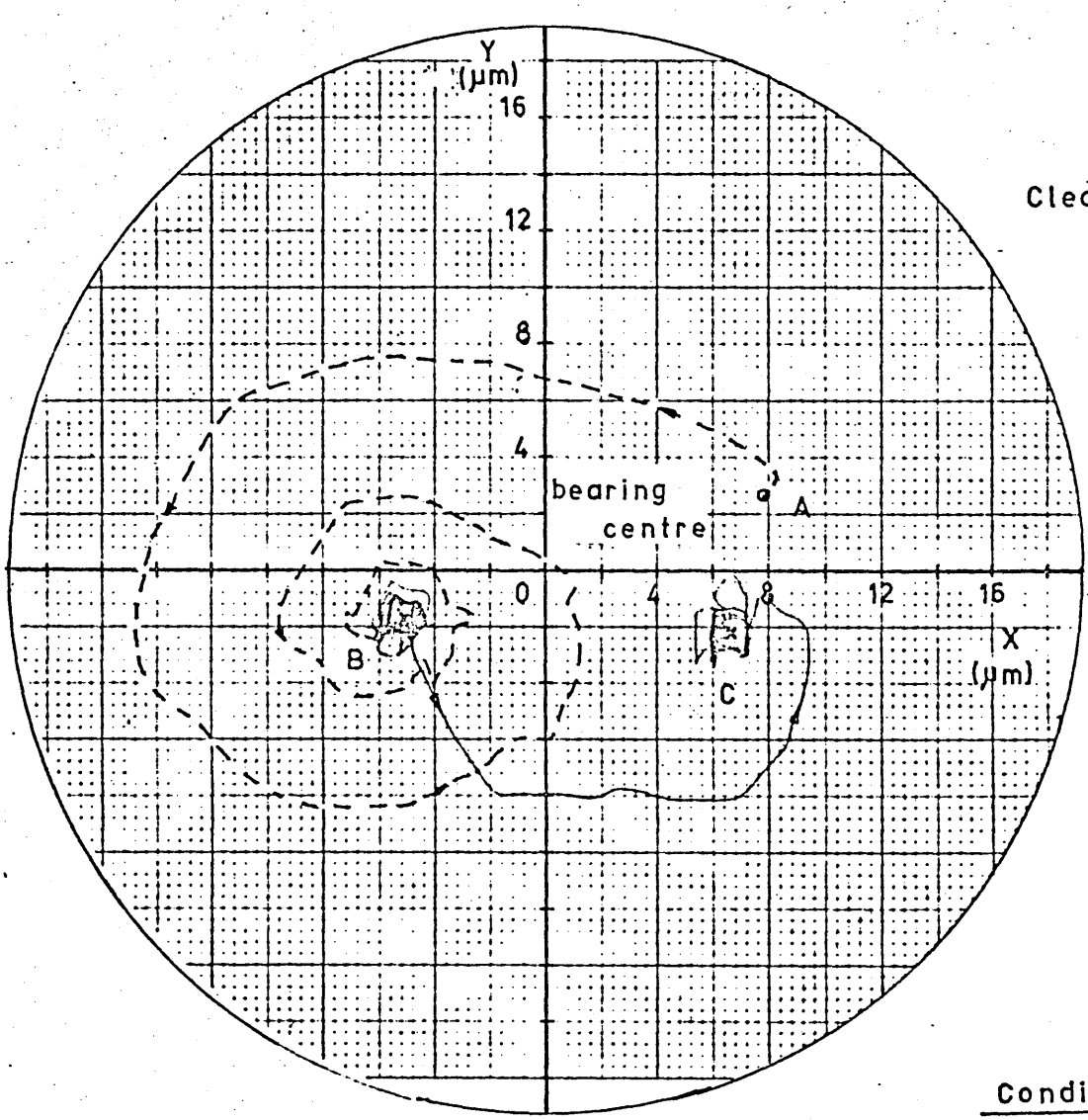

Conditions

$N = 100 \frac{rev}{min}$

$P_s = 7$ bar

$W = 420$ N

Fig. 5.25 SHAFT CENTRE LOCUS.

BEARING TYPE II

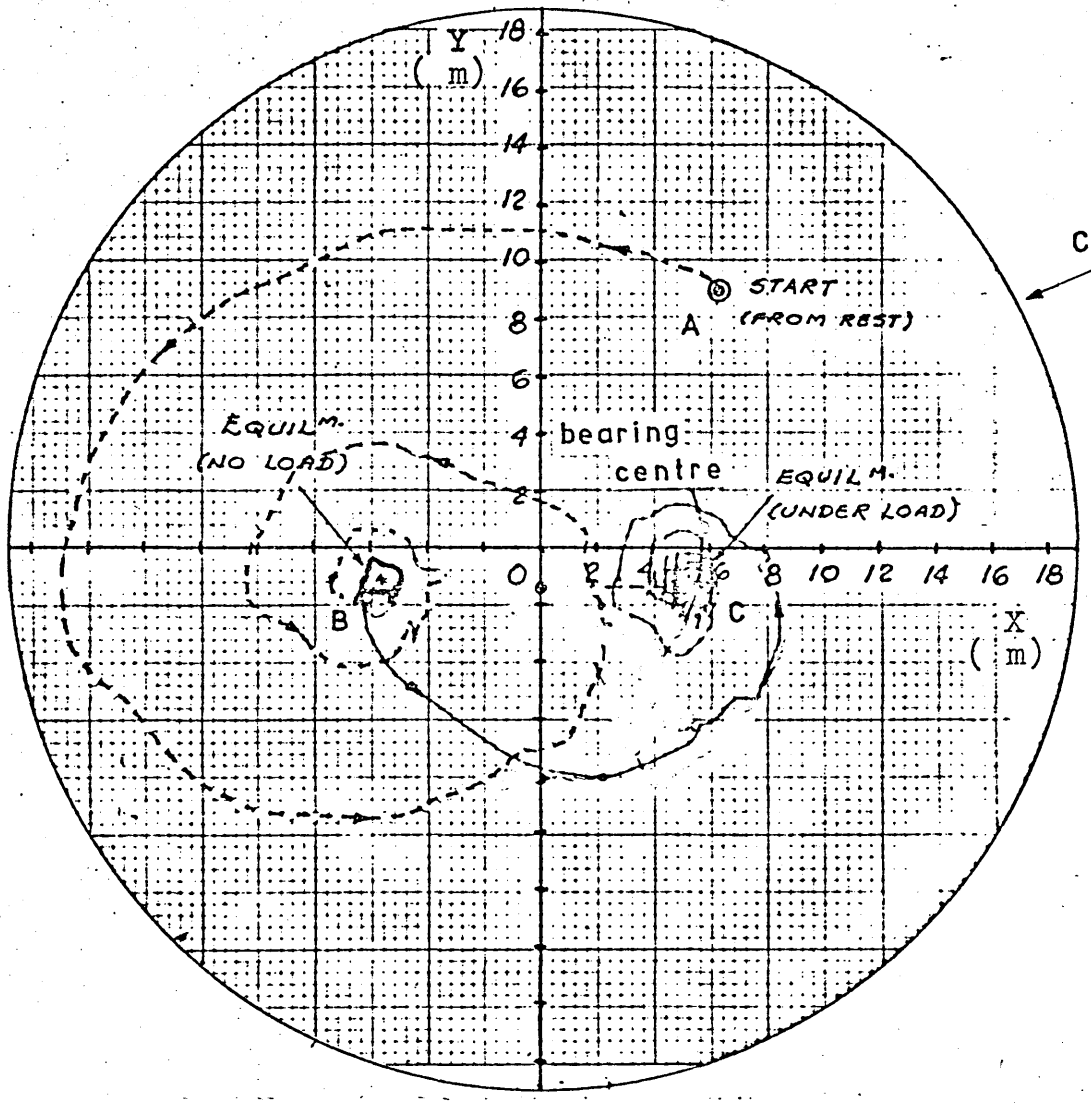

Conditions

N = 100 rev/min

P_s = 10 bar

W = 420 N

Fig. 5.26 SHAFT CENTRE LOCUS.

It can be noted that as the speed was reduced in this case longer shaft centre displacements occured, however the loop shape was about the same for all of them.

The eccentricity values obtained under static load were very similar to the final values for dynamic loading, therefore it was decided to include them in the charts of the series of results for the dynamic tests. These are shown in section 5.3.4.

However, the full results are tabulated in the tables included in appendix B' , and a series of graphs are plotted of capacity number i.e. Ocvirk number, against eccentricity ratio for comparison of experimental data for L/D = 0.65 with analytical curve for short bearing solution.

BEARING TYPE II

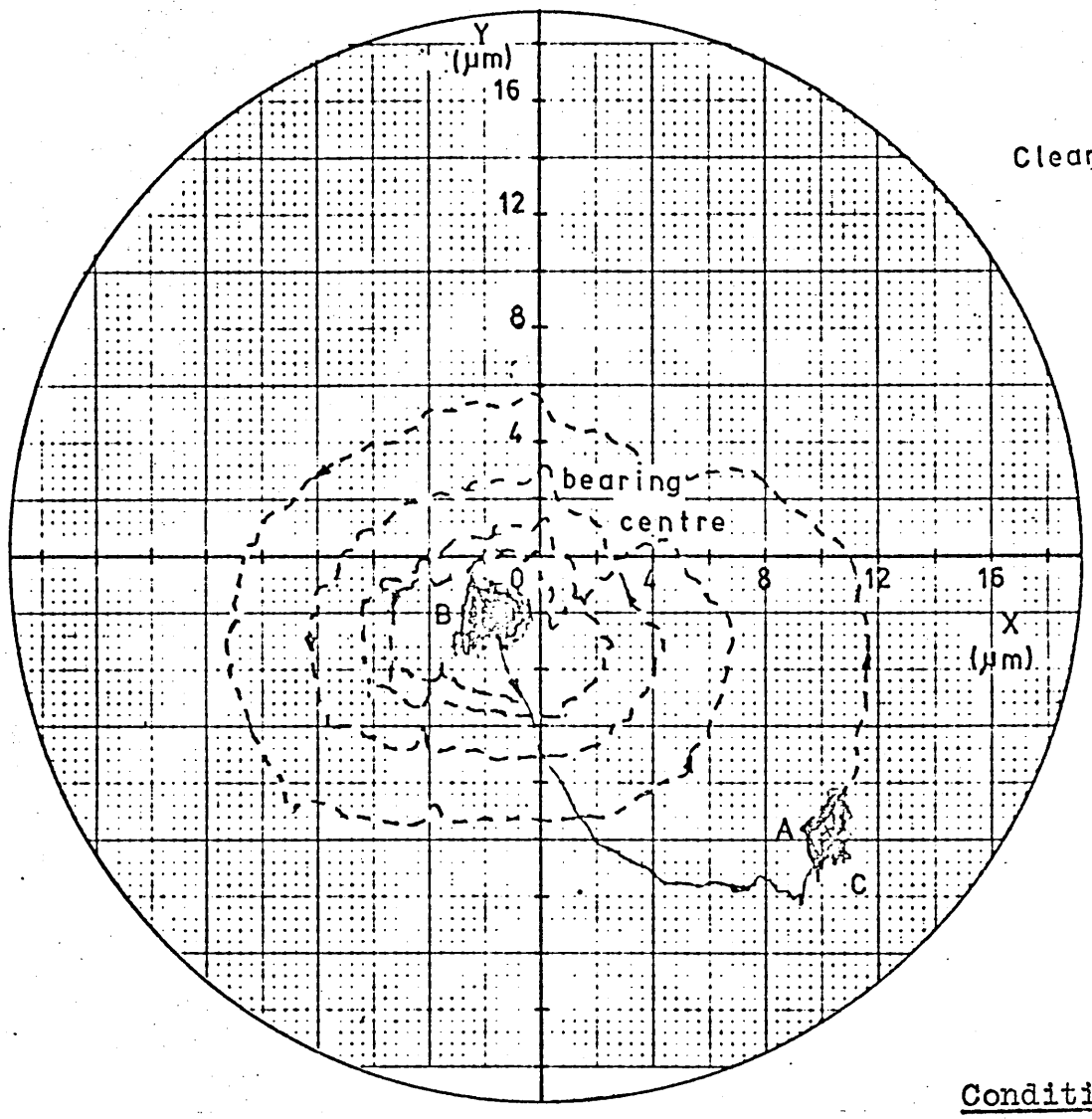

Conditions

N = 40 rev/min

P_s = 3 bar

W = 420 N

Fig. 5.27 SHAFT CENTRE LOCUS.

BEARING TYPE II

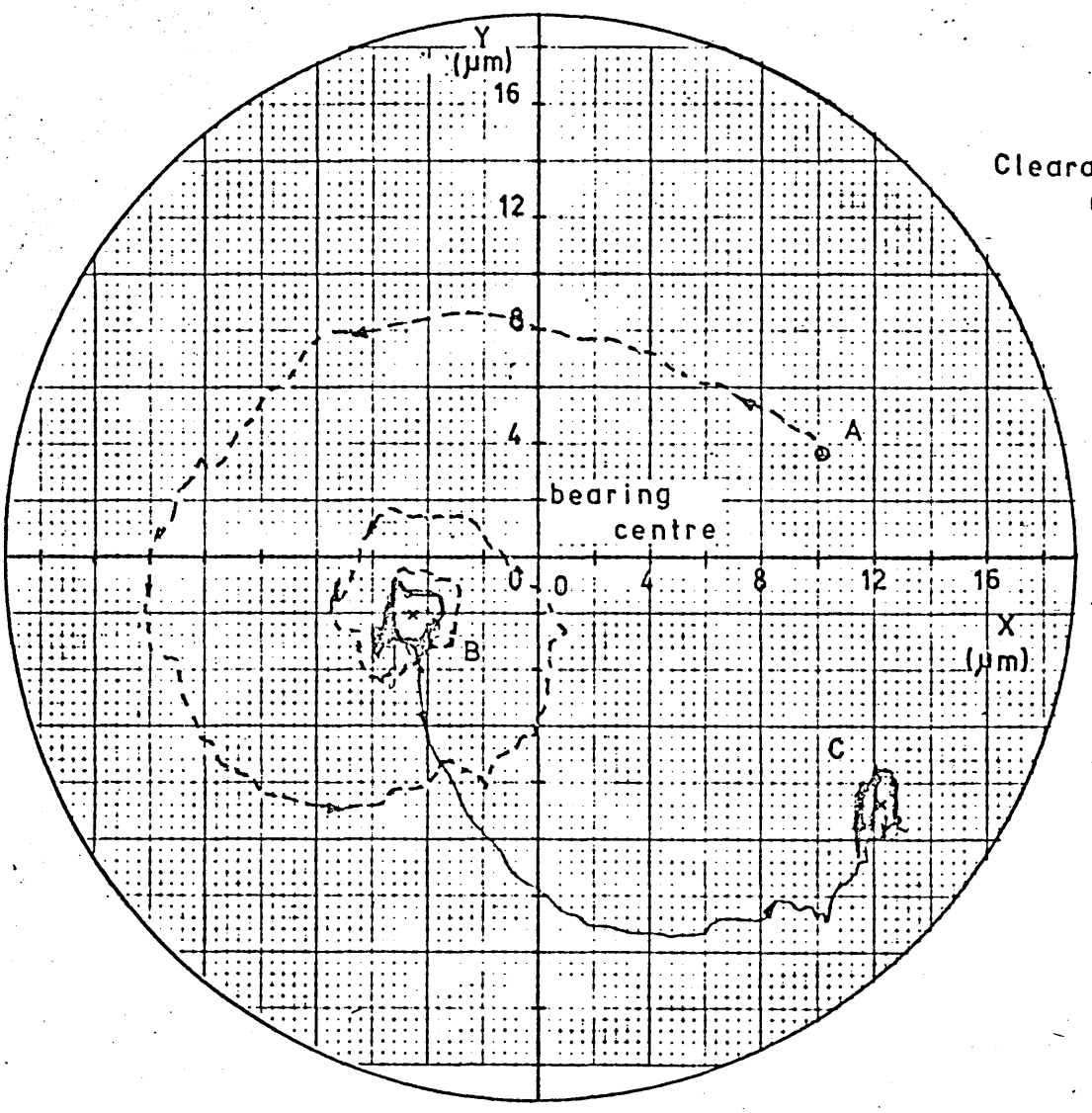

Conditions

N = 40 rev/min

P_s = 7 bar

W = 420 N

Fig. 5.28 SHAFT CENTRE LOCUS.

BEARING TYPE II

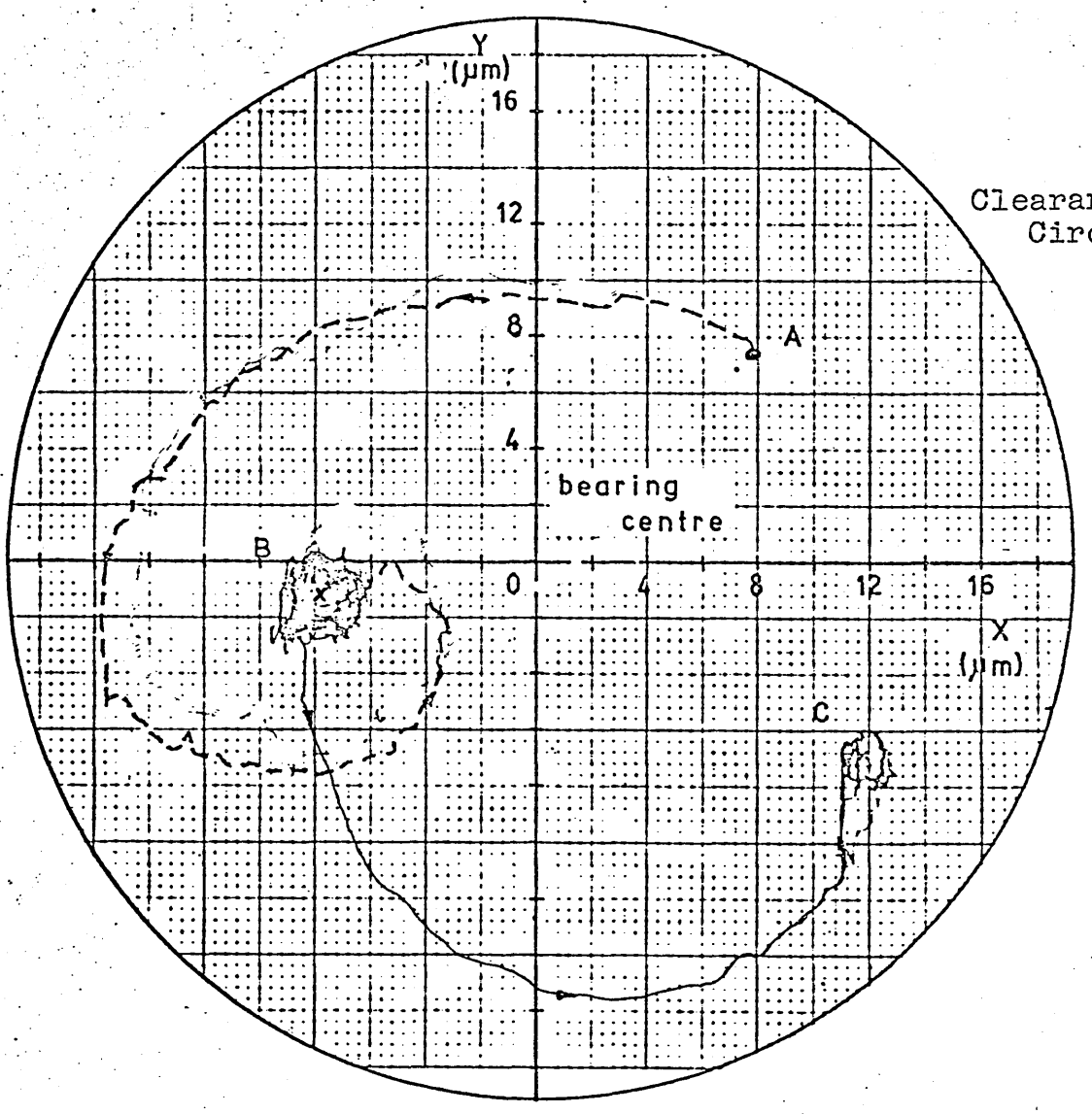

Conditions

N = 40 rev/min

P_s = 10 bar

W = 420 N

Fig. 5.29 SHAFT CENTRE LOCUS.

5.3.3 Results of Series No. 2 Static Loading Tests Under Oscillating Motion.

From the preliminary tests, it was found that this type of bearing was suitable for running under oscillating motion, so a series of tests were carried out under the set of conditions described in section 4.3 and the following results were obtained:

Figures 5.30 - 31 - 32 represent specimen traces of the shaft centre locus, when the shaft is subjected to the same oscillating frequency of 0.465 rev/s, static loads of zero, 238 N and 617 N and different oil supply pressures for each one of 4, 7 and 20 bar.

They show the starting running position of the shaft centre on the right hand side of the clearance circle, which corresponds to the right free side of the bearing assembly. As can be seen these starting positions change as the pressure changes, going down to the bottom half of the clearance circle when the oil pressure is 4 bar, trace A

From these positions the load is applied and only the final equilibrium loaded positions of the shaft centre, trace "B", are plotted to avoid confusion. These correspond to the first applied load of 238 N, from where it can be seen that for high oil supply pressure the shaft centre does not travel as low or as far as it does when low supply oil pressure is applied.

Then, the load was released to bring the shaft back to the starting equilibrium condition in order to apply

the higher load. A new loaded running position was recorded for the shaft centre during each test, as indicated by trace C. These traces show that the eccentricity has become bigger than that for light applied load, although it is almost the same for the three experiments no matter what oil supply pressure has been used.

Again these and other results are plotted as a function of duty parameter in section 5.3.5 in order to provide a comparison with the results of the dynamic tests.

BEARING TYPE II

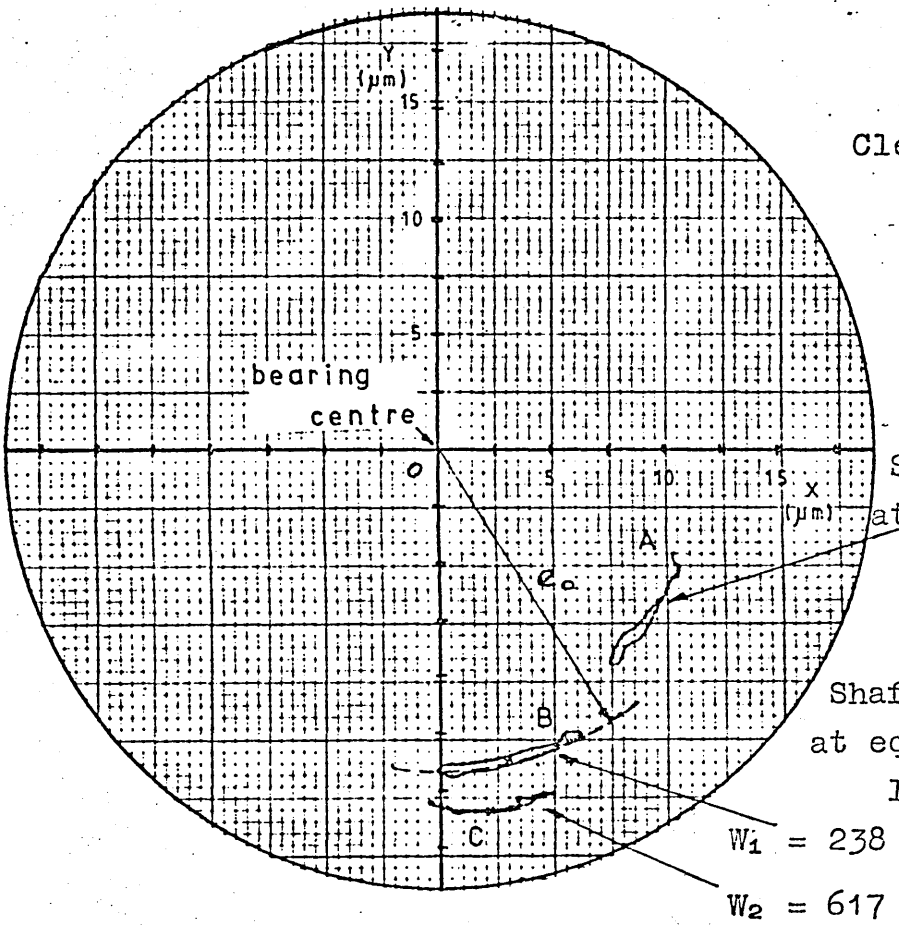

Conditions

Oscillating motion

$\overline{N}$ = 0.465 rev/s

P_s = 4 bar

Fig. 5.30 SHAFT CENTRE LOCUS.

BEARING TYPE II

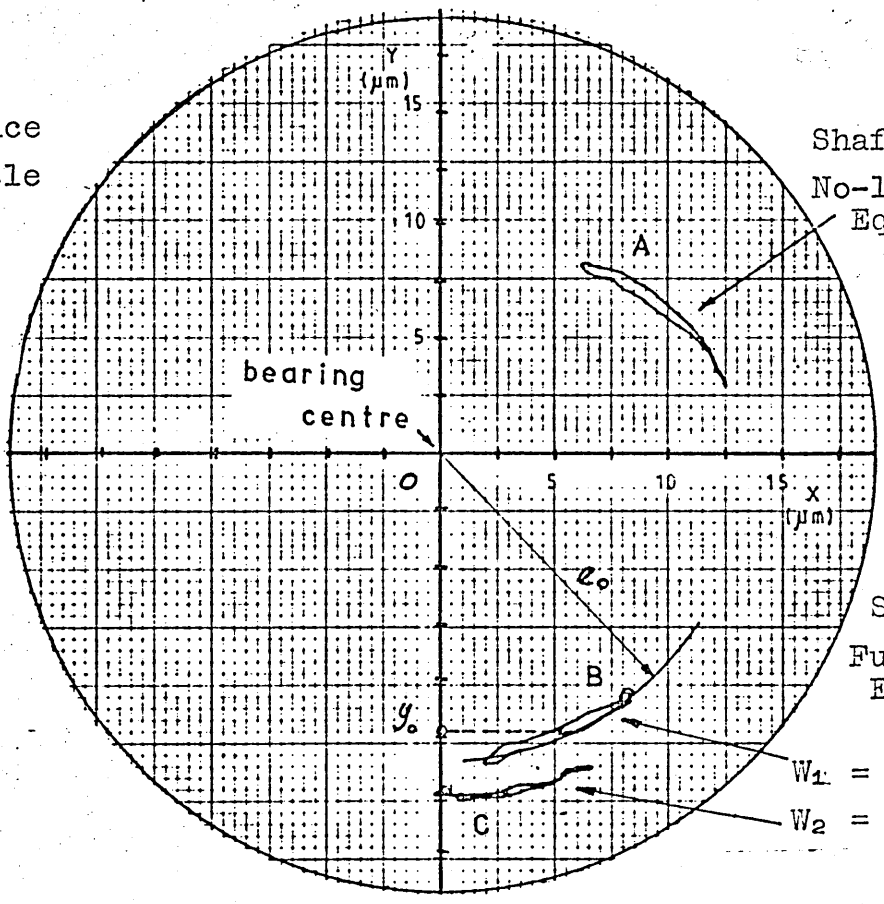

Clearance Circle

Shaft Centre No-load Equilibrium Position

Shaft Centre Full-load Equilibrium Position :

W_1 = 238 N

W_2 = 617 N

Conditions

Oscillating motion

$\bar{N}$ = 0.465 rev/s

P_s = 7 bar

Fig. 5.31 SHAFT CENTRE LOCUS.

BEARING TYPE II

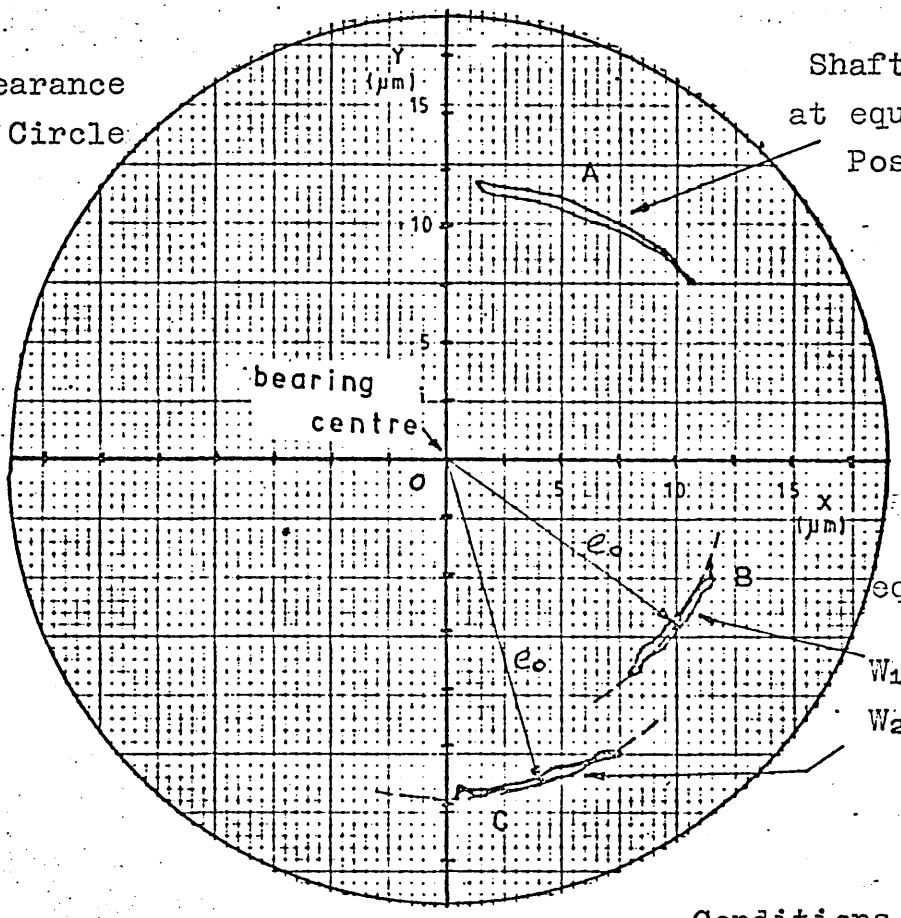

Conditions

- Oscillating motion
- $\overline{N}$ = 0.465 rev/s
- P_S = 20 bar

Fig. 5.32 SHAFT CENTRE LOCUS.

5.3.4 Results of Series No. 3 Dynamic loading Tests Under Continuous Motion.

These series of tests were carried out under the conditions described in section 4.3 and the corresponding results are given below:

From figures 5.33, 5.34 the shaft centre displacement can clearly be seen for a change of the applied load, when the shaft is running at a constant speed of 100 rev/min and the oil supply pressure is also kept constant at 3 bar.

All the traces started by plotting the shaft centre on its rest position and only under the pressure of the inlet oil, which is shown as the point "A". Then, when running, the shaft centre finds its equilibrium position, represented by the orbit "B" which lies on the left hand side of the hypothetical centre. This again shows that all experiments started at the same running position and the spiraling effect was equally reproduced for all of them. When the load was applied the shaft centre moved to the right hand side, until it settled down on a equilibrium loaded running position point "C", which went down as the load was increased in every test.

Figures 5.35 and 5.36 also include the rest and running shaft centre positions without load, points A and B. The test conditions were the same as the previous except that the oil supply pressure was increased at 10 bar. The path followed was of the same shape as previously.

BEARING TYPE II

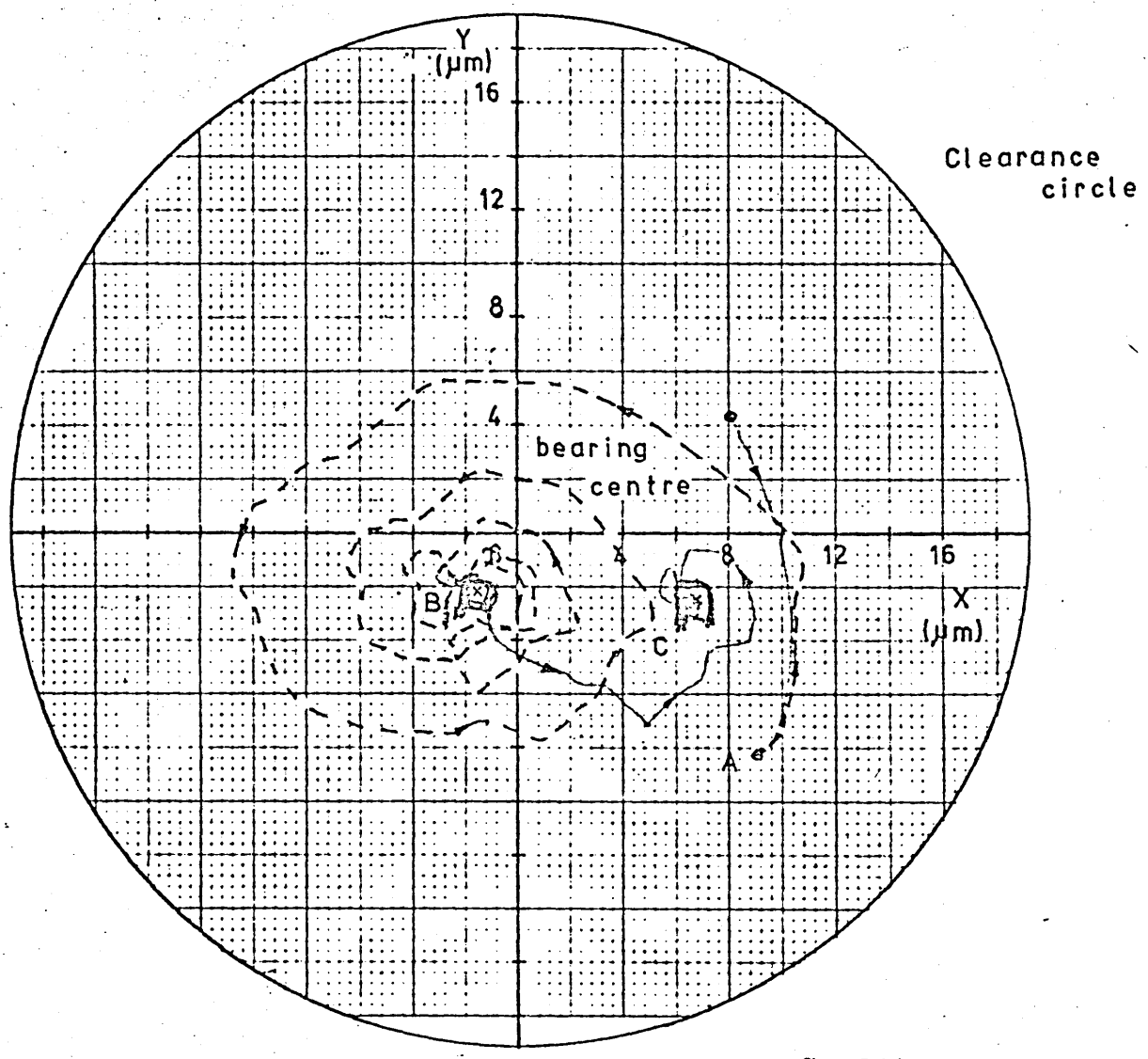

Conditions

N = 100 rev/min

P_s = 3 bar

W_1 = 682 N (peak)

W_2 = 238 N (final)

Fig. 5.33 SHAFT CENTRE LOCUS.

BEARING TYPE II

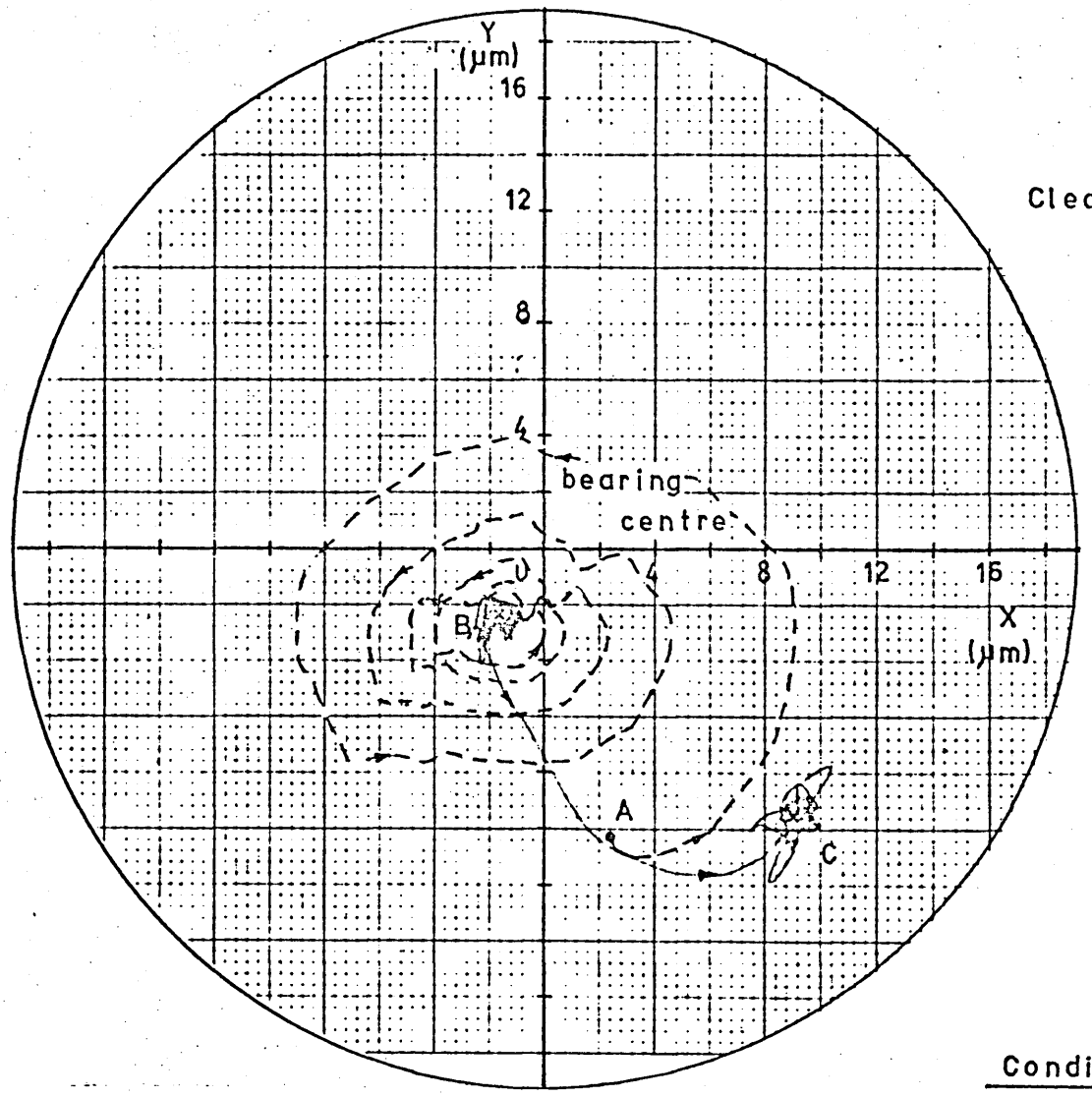

Conditions

$N = 100 \frac{rev}{min}$

$P_s = 3$ bar

$W_1 = 1100N$ (P

$W_2 = 793$ N (F

Fig. 5.34 SHAFT CENTRE LOCUS.

BEARING TYPE II

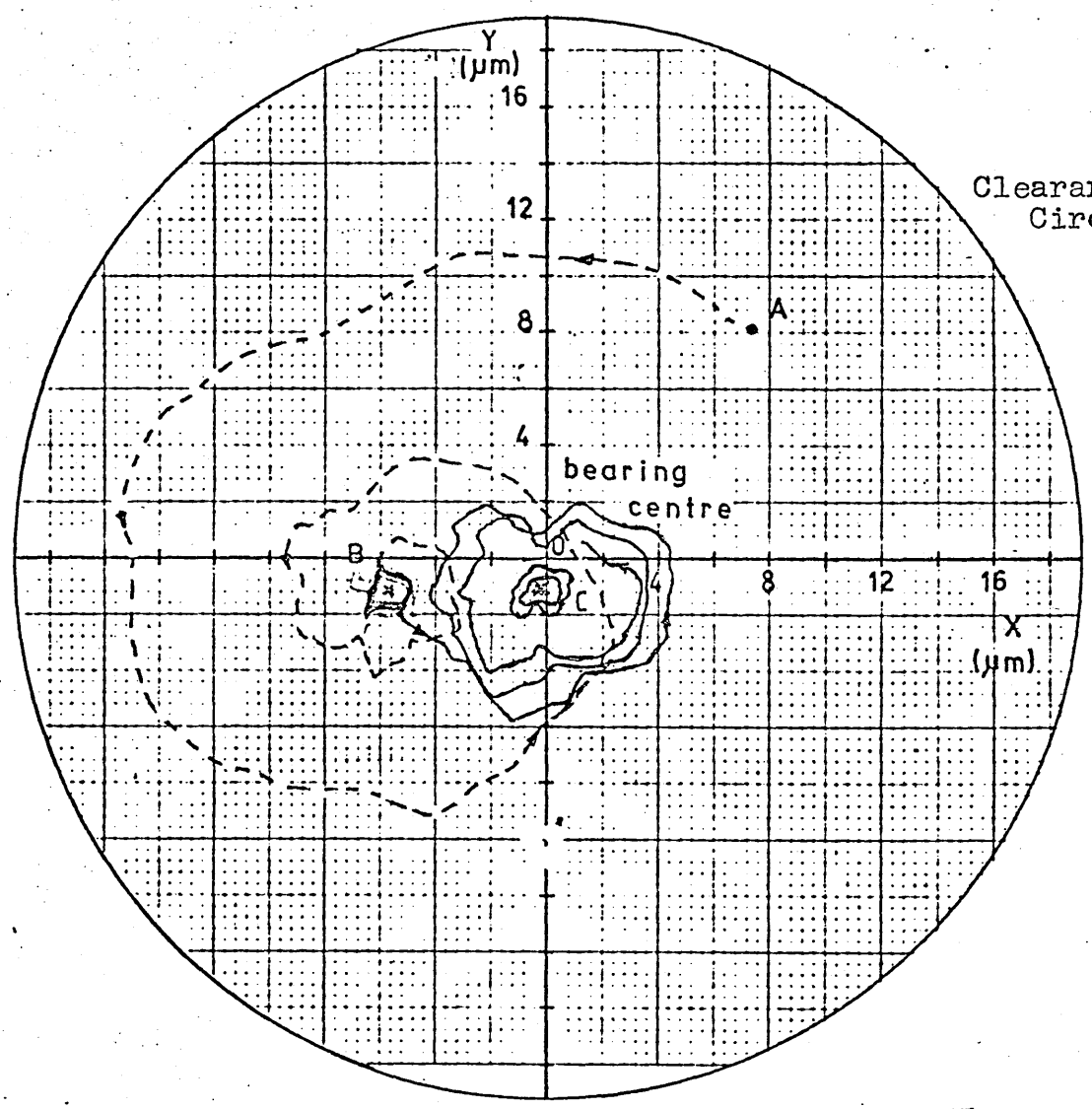

Conditions

N = 100 rev/min

P_s = 10 bar

W_1 = 682 N (peak

W_2 = 238 N (fina

Fig. 5.35 SHAFT CENTRE LOCUS.

BEARING TYPE II

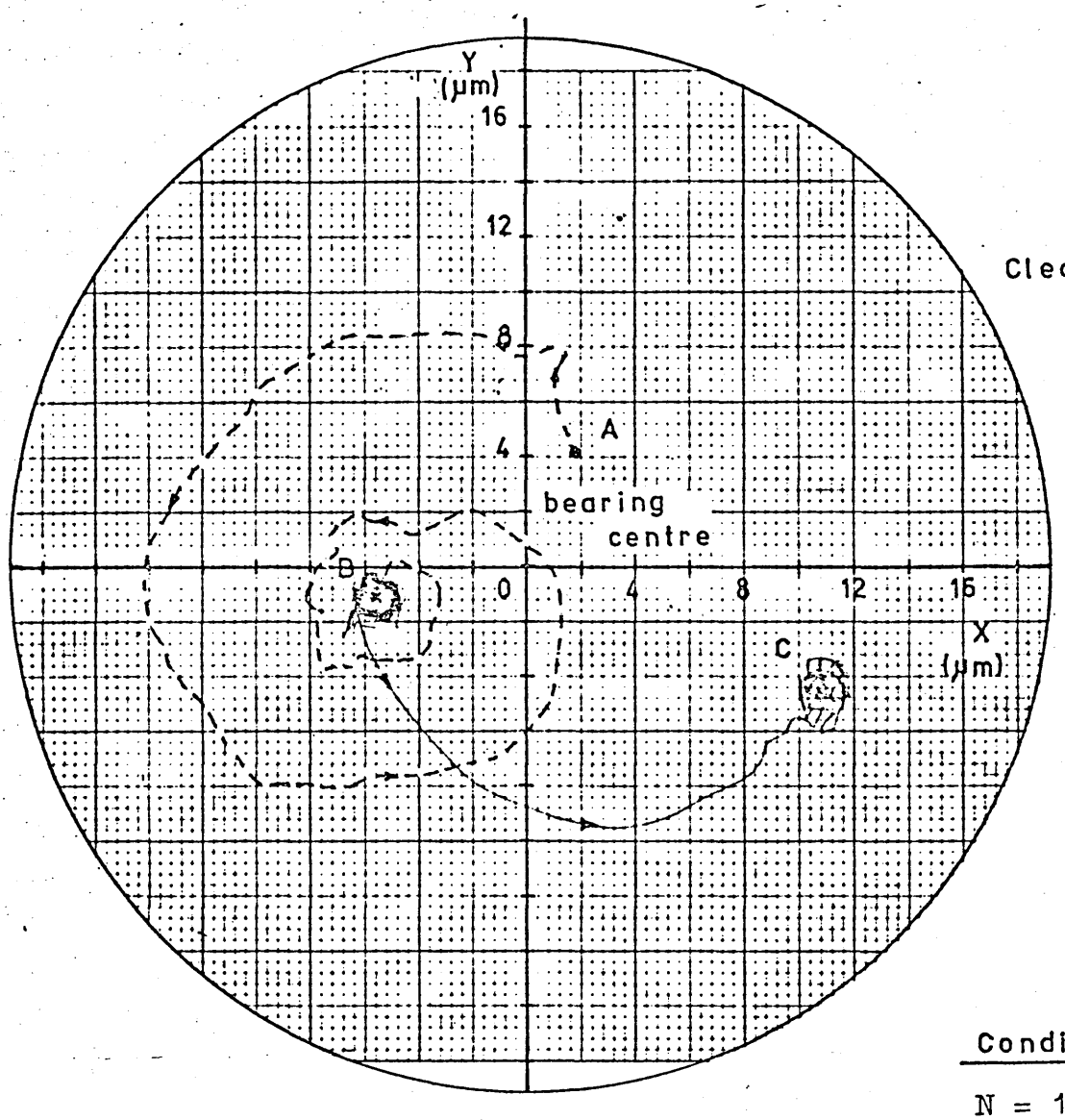

Conditions

N = 100 rev/mi

P_s = 10 bar

W_1 = 1100 N (

W_2 = 793 N (f

Fig. 5.36 SHAFT CENTRE LOCUS.

However, comparing the results apparently longer displacements of the shaft centre took place as the oil pressure was increased. But measuring from the true common centre it can be seen that eccentricities became bigger as the oil supply reduces.

The purpose of the specimen traces in figures 5.37, 5.38 first is to show that the shaft centre travels even closer to the edge of the clearance circle when the speed was slowed down to 40 rev/min under similar conditions to those for high speed. Secondly to prove that indentical paths and eccentricity values of the shaft centre were obtained when the load is either statically or dynamically applied.

A set of graphs are plotted for the series of experimental tests carried out for the shaft centre displacements under continuous motion. As the dynamic, as well as the static loading tests draw out the same eccentricity values for a particular set of experiments, it was decided to plot both series of results on the same graph.

So, figure 5.39 shows the effect of increasing supply pressure by plotting the duty parameter for different loading tests against the experimental eccentricity values. Almost all of the results obtained under continuous motion at 100 rev/min and constant oil pressure of 3 bar, are within the recommended area. It can be seen more clearly that the gap between the final equilibrium and maximum eccentricity is quite large, reducing with increasing duty parameter and reducing load magnification factor.

BEARING TYPE II

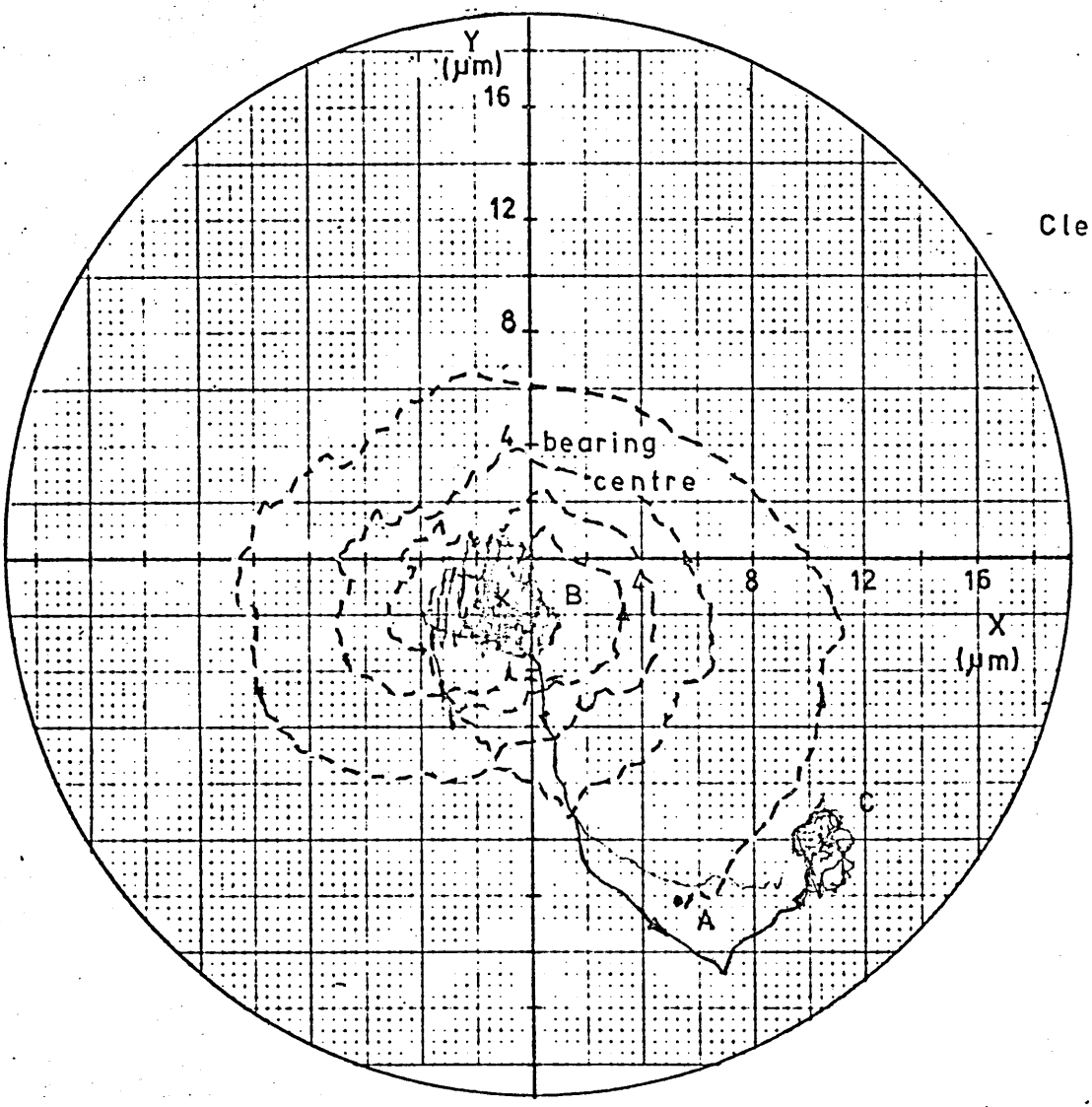

Conditions

N = 40 rev/min

P_s = 3 bar

W_1 = 840 N (peak)

W_2 = 420 N (final)

Fig. 5.37 SHAFT CENTRE LOCUS.

BEARING TYPE II

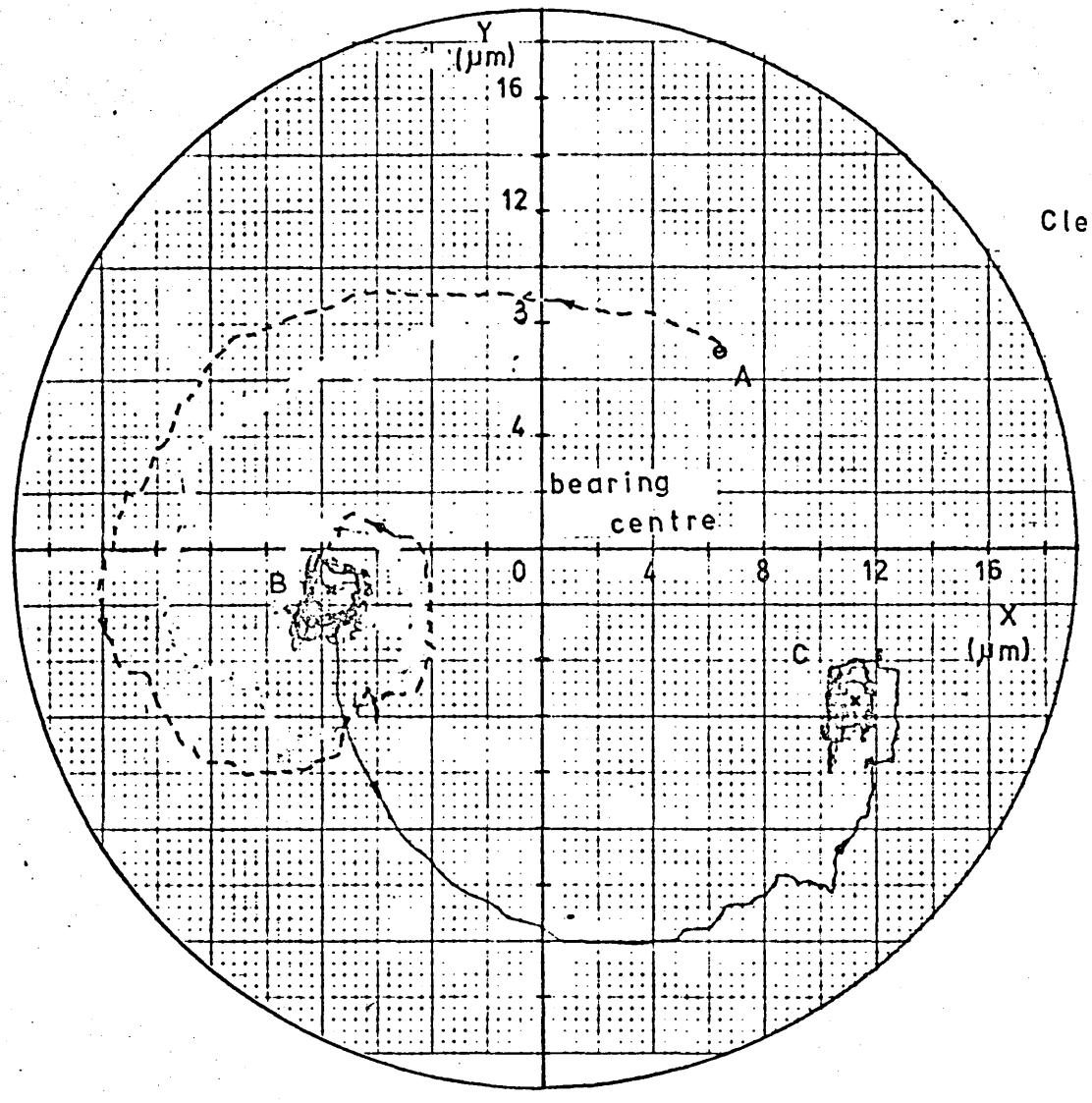

Conditions

N = 40 rev/min

P_s = 10 bar

W_1 = 840 N (peak)

W_2 = 420 N (final)

Fig. 5.38 SHAFT CENTRE LOCUS.

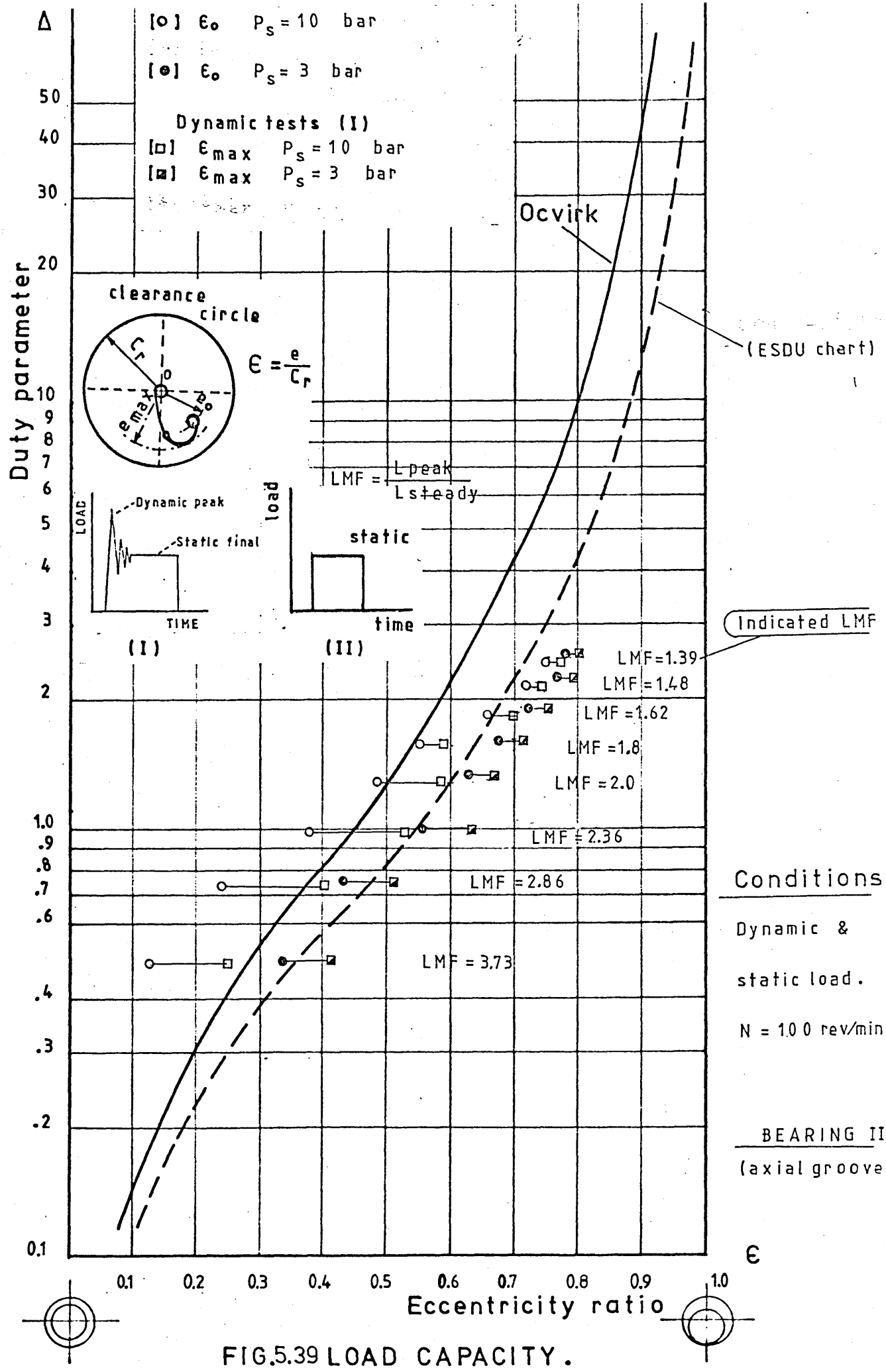

FIG.5.39 LOAD CAPACITY.

However, for supply pressure of 10 bar a hydrostatic effect causes lower eccentricities for low values of the duty parameter. Also, it is observed that the gap between eccenticity values i. e. final and maximum, for each test load, is different, being larger for the light loads than those under heavy loads.

Figure 5.40 is the result of plotting another series of experiments at speeds of 70 and 40 rev/min with supply pressure of 3 bar. Again the points follow closely the recommended area with increases in eccentricity under dynamic loads, being more notable when it is heavily loaded and at low speed of 40 rev/min. Also, it can be seen that at these severe conditions the final and maximum eccenticities have almost the same values.

Figure 5.41 represents the plotting of the final eccentricity values on a polar diagram for both dynamic and static loads. Also, a comparison is made of these experimental values, with those given by the short bearing solution.

So, two sets of results are shown under the same condi tions of loads and speed except that the oil supply pressure is different for each one, 10 and 3 bar.

It can be noted that for the high pressure the eccentri cities corresponding to the lighter loads start nearly from the centre and then as the load was increased the shaft centre went to the right side of the semicircle polar graph, sinking as the load became very heavy. On the other hand the points for the low supply pressure, even

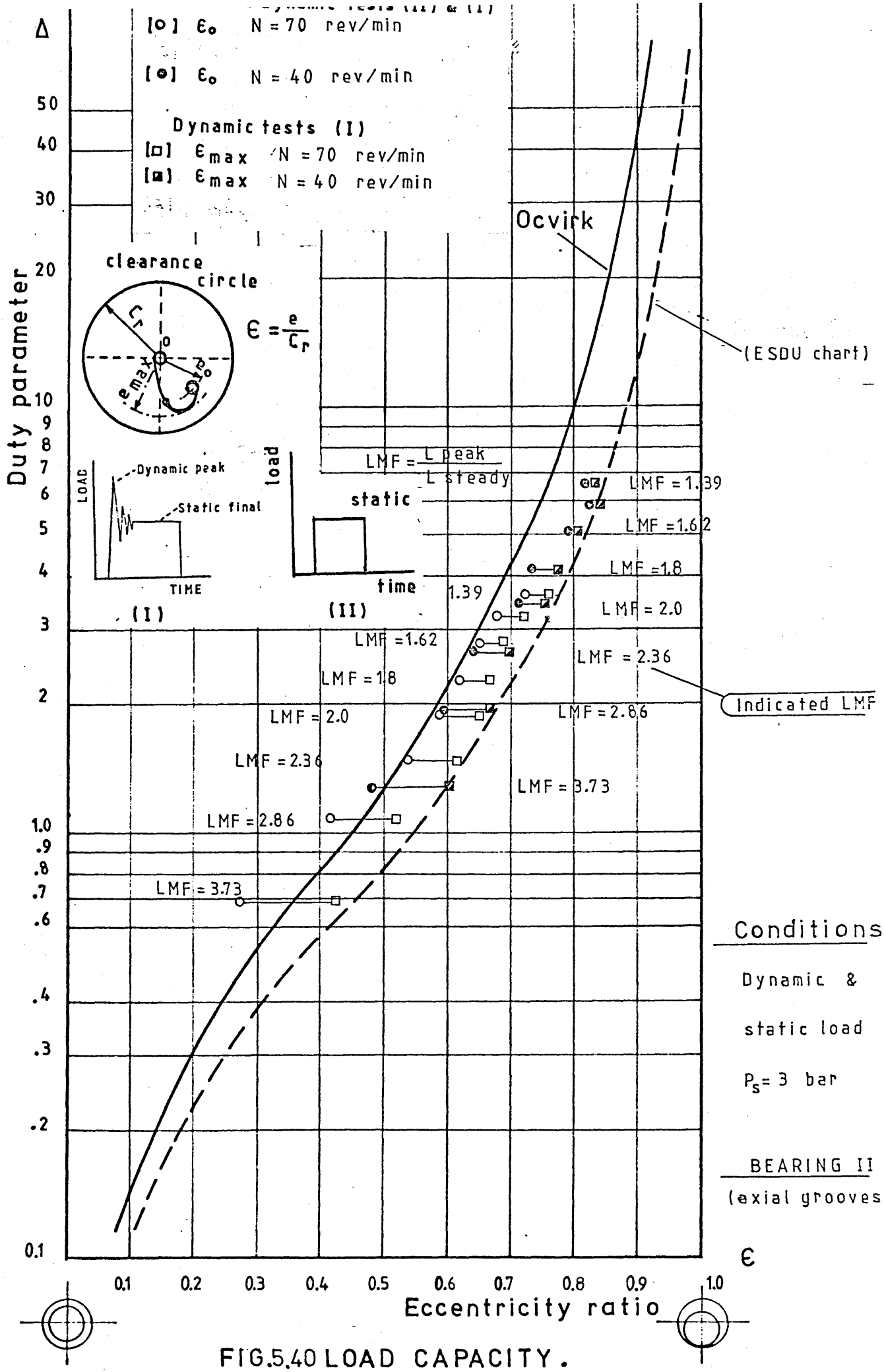

FIG.5.40 LOAD CAPACITY.

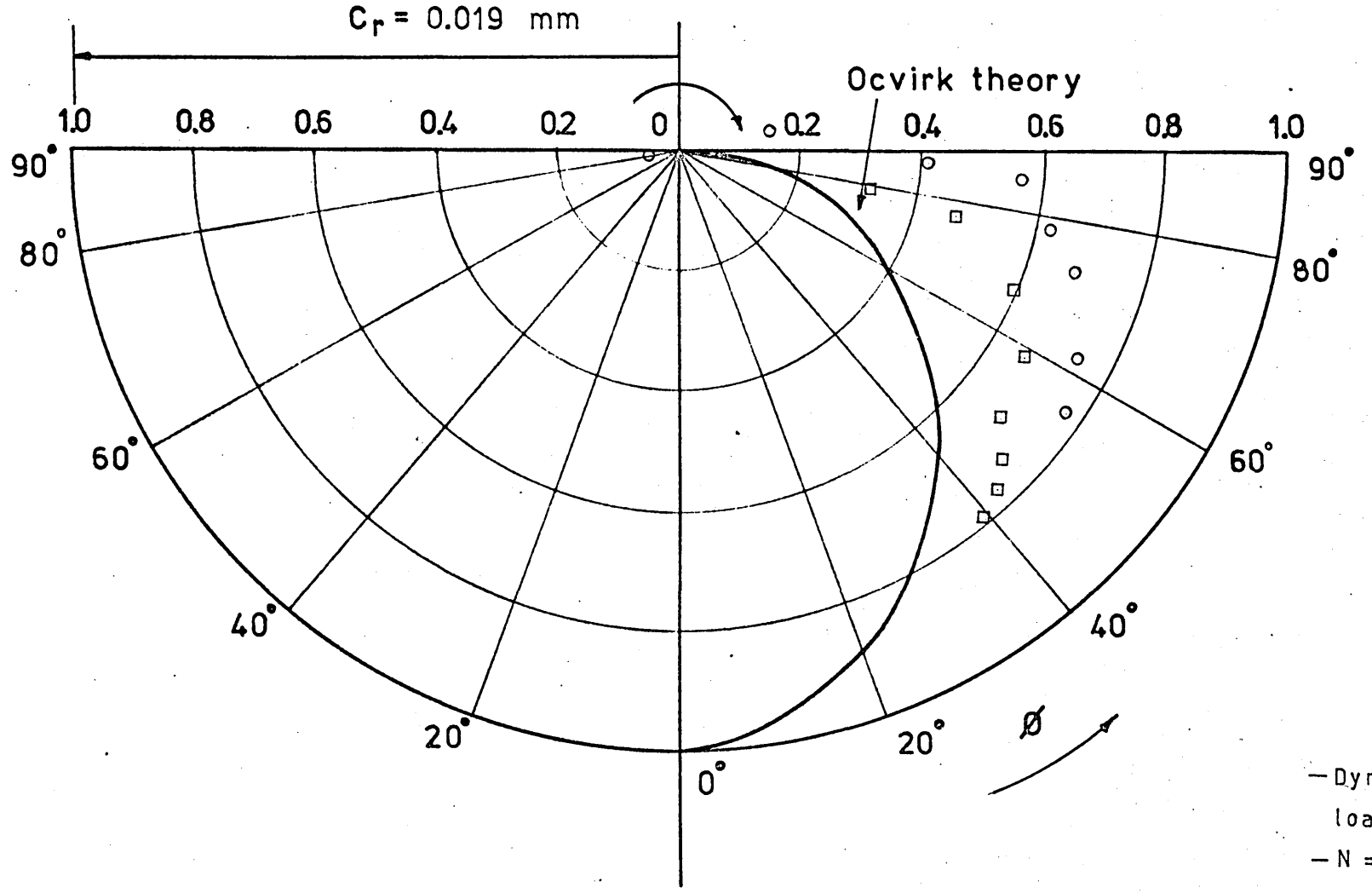

FIG. 5.41 ECCENTRICITY RATIO AGAINST ATTITUDE ANGLE.

those at light loads went to the right straight away and sunk even more getting closer towards the theoretical curve.

Comparing both curves mainly under heavy loads it can be said that the reached eccentricity values were almost the same, however the attitude angles were quite different for each one of the sets of tests.

Figure 5.42, shows results from tests at running speeds of 70 and 40 rev/min.

From figure 5.42 can be noted that shaft eccentricity positions extend as far as those in fig. 5.41, even for a low supply pressure. However, at heavy loads they go closer to the theoretical curve and both have more or less the same eccentricity values.

On the other hand, figure 5.42 illustrates the tendency of the shaft centre to go down, closer to the analytical curve but having high eccentricity ratio values. They also show that the attitude angles are quite different from the previous series of experiments, lower in this case.

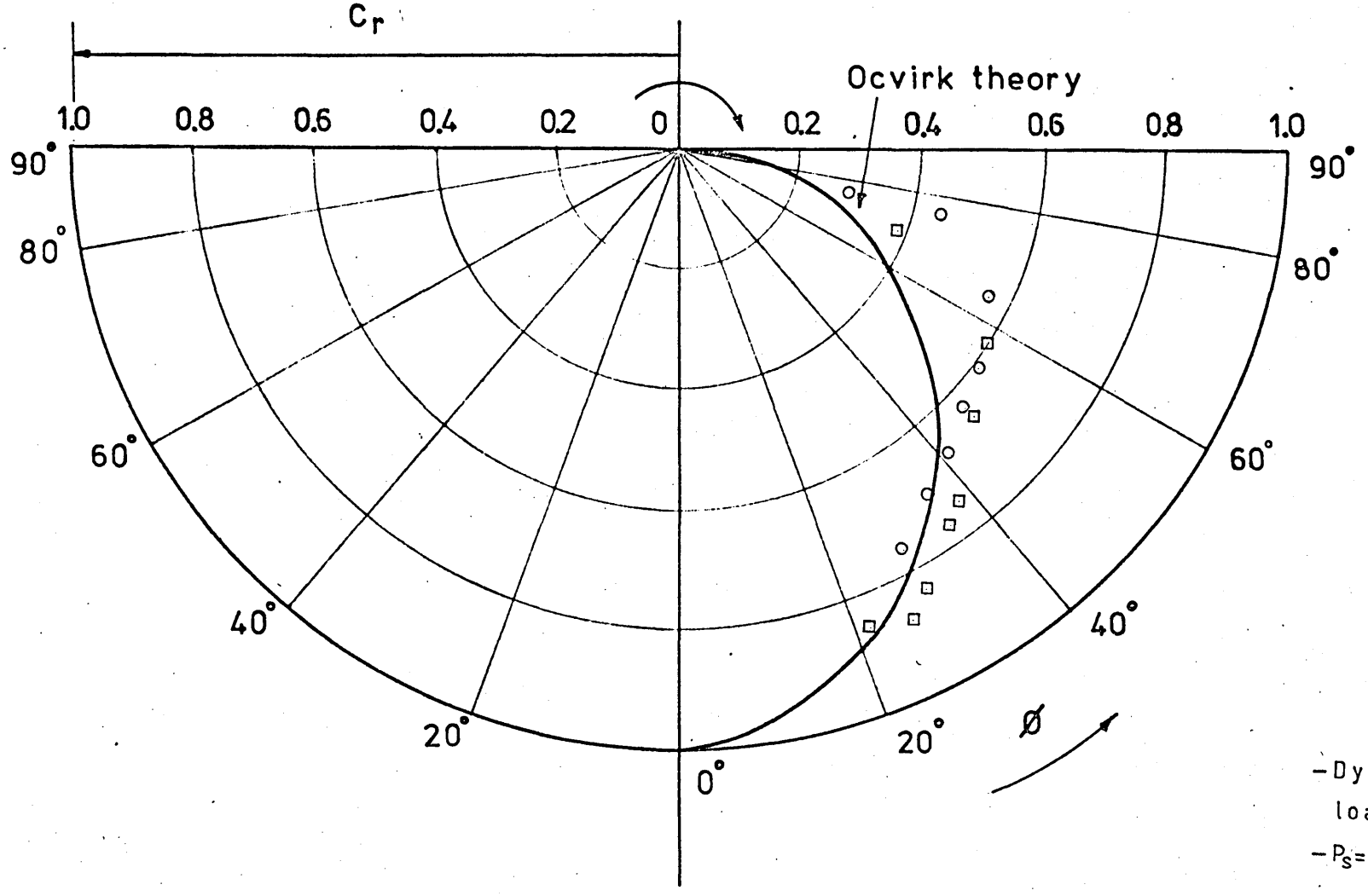

FIG.5.42 ECCENTRICITY RATIO AGAINST ATTITUDE ANGLE.

5.3.5 Results of Series No. 4 Dynamic Loading Tests Under Oscillating Motion.

These series of tests were carried out under the conditions established in section 4.3 and the following results were obtained.

It has been mentioned in section 5.3.3 that similar traces for the dynamic conditions and for those under static loading were obtained. This is shown in figs. 5.43 and 5.44 for 0.465 rev/s oscillating speed, 3 bar supply pressure and a range of applied loads. Only equilibrium positions are shown for the shaft centre running under no-load and loaded respectively, and it is clear that is very little difference between the two sets of results. Figs. 5.45 and 5.46 represent results for both static and dynamic loads with an oscillating speed of 0.185 rev/s and supply pressures of 3 and 10 bar.

It can be seen in fig. 5.45 that there is very little difference in the traces shown in figs. 5.43 and 5.44 even though the oscillating speed is reduced by a factor of 3.

On the other hand, in fig. 5.46. where the oil pressure was higher and the unloaded equilibrium position lies above the horizontal axis, under load the eccentricity ratios were of a similar magnitude but attitude angles were considerably longer for light loads. It can also be noticed that for all conditions, the trace of the shaft centre orbit became more horizontal and shorter as the load was increased.

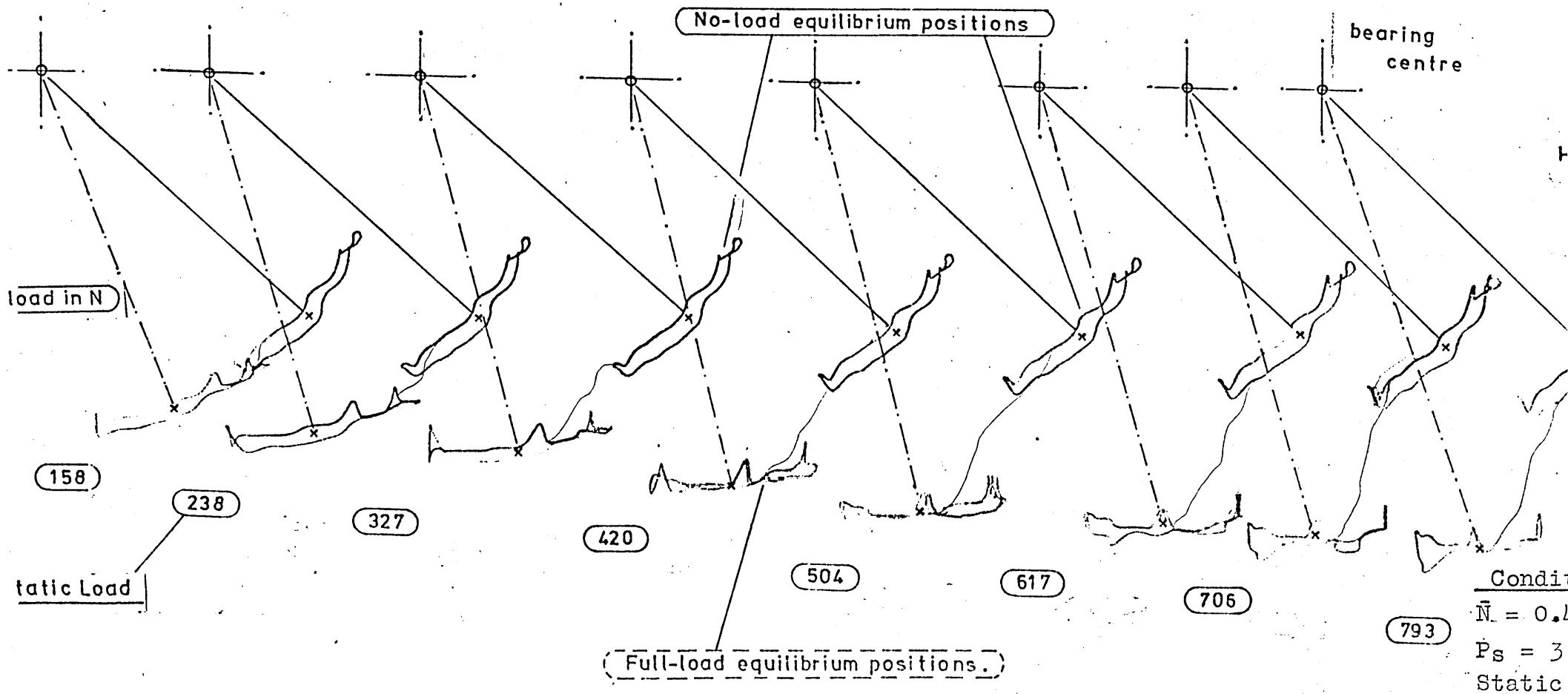

FIG. 5.43 SHAFT CENTRE LOCUS.

BEARING TY

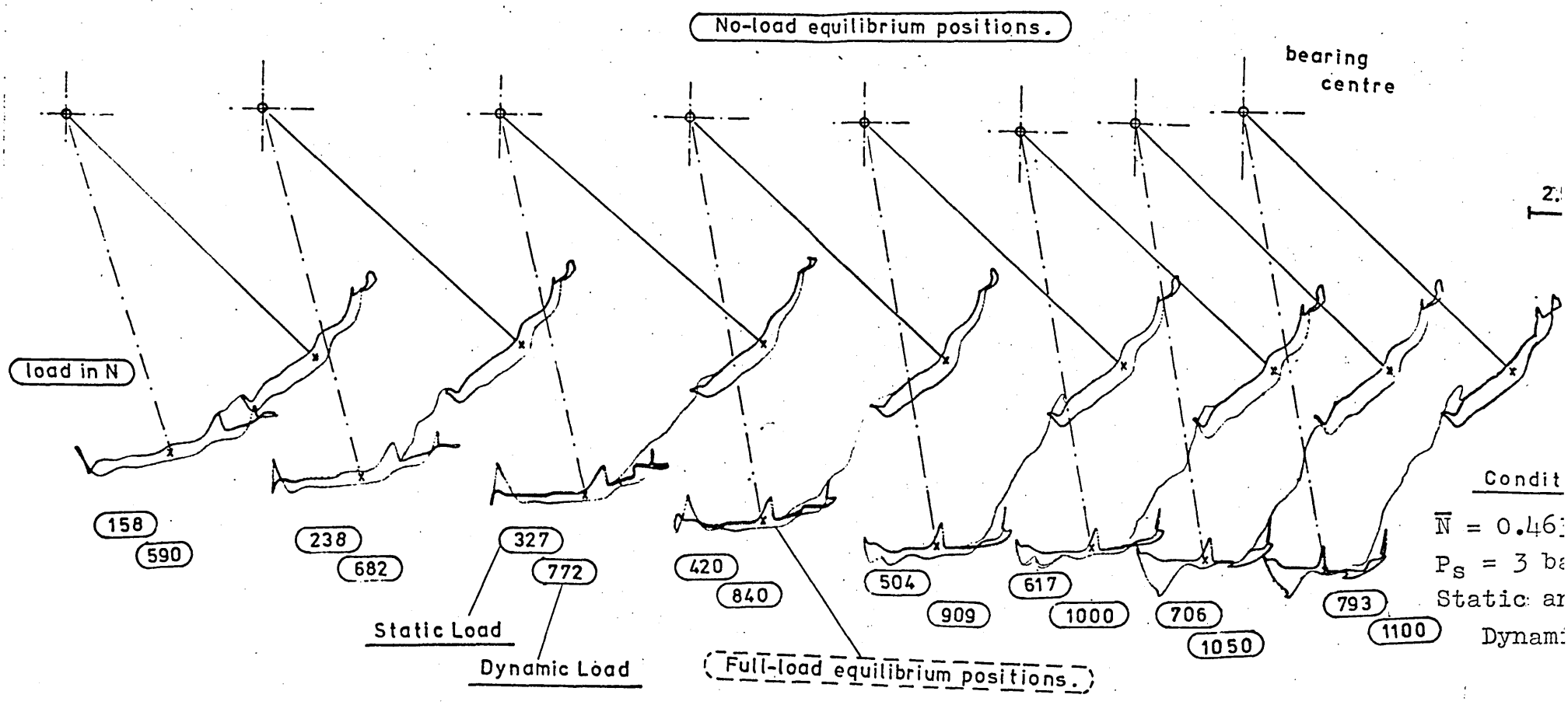

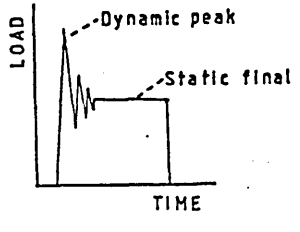

BEARING TYPE

FIG. 5.44 SHAFT CENTRE LOCUS.

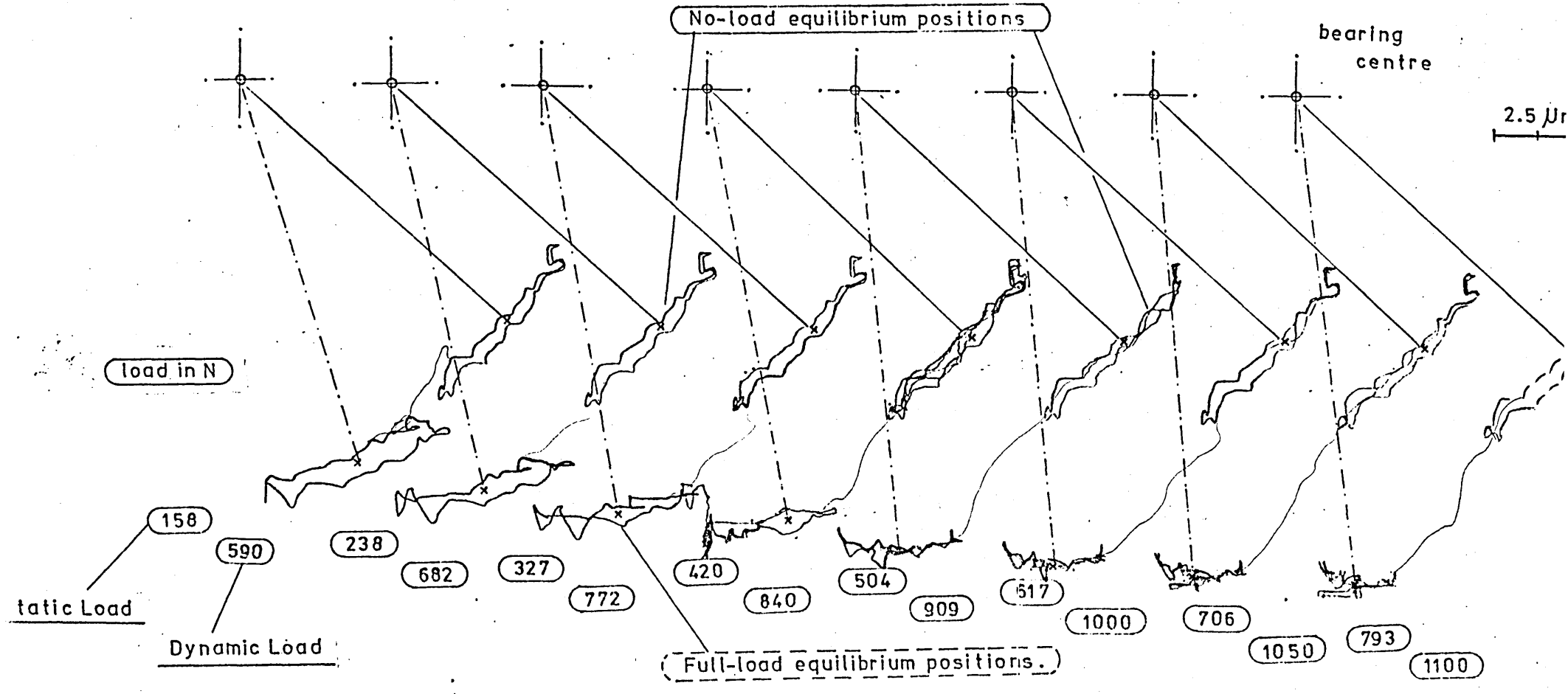

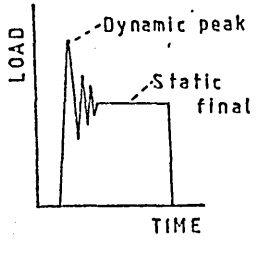

FIG. 5.45 SHAFT CENTRE LOCUS.

Conditions

$\overline{N}$ = 0.185 rev

P_s = 3 bar

BEARING TYPE I

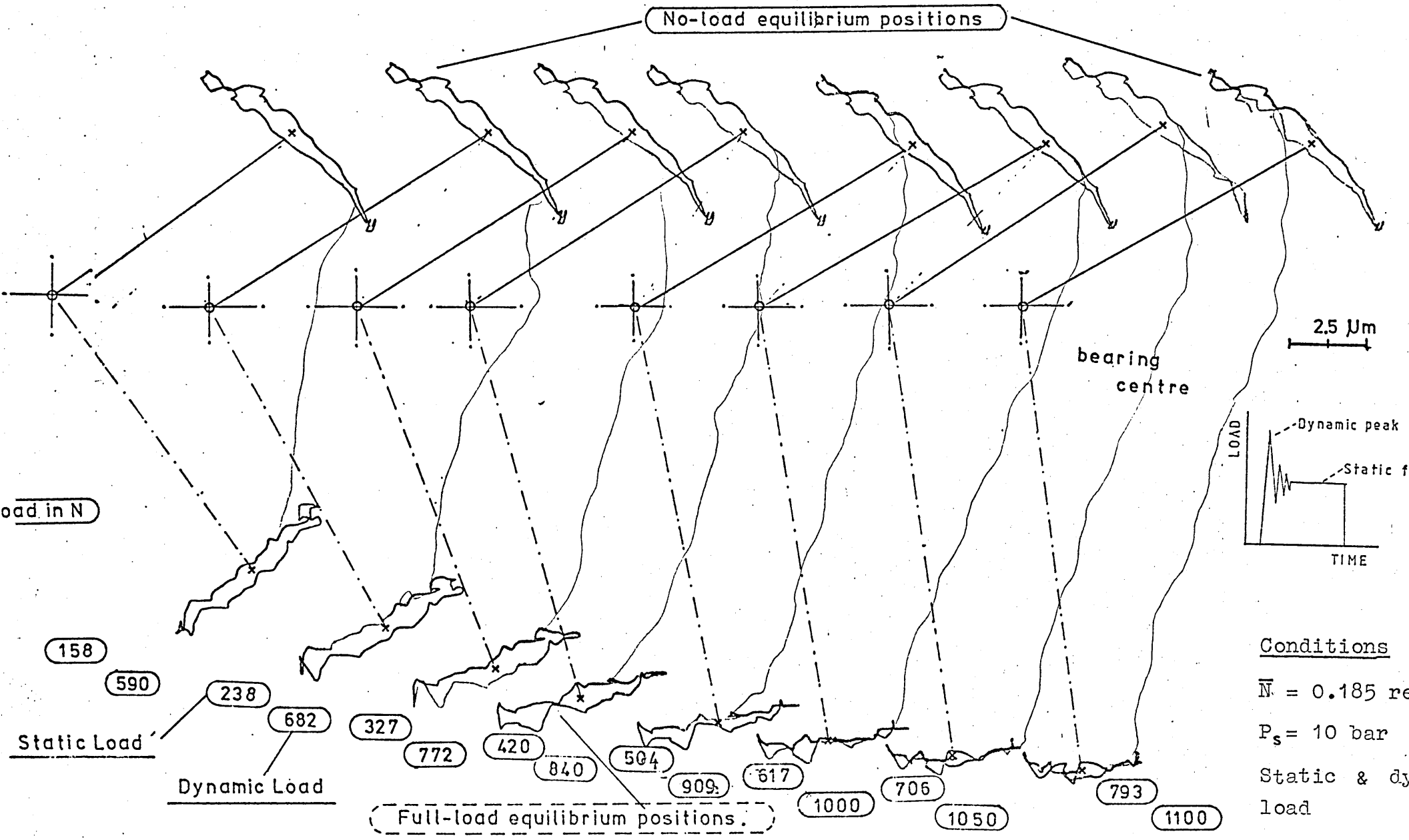

FIG.5.46 SHAFT CENTRE LOCUS.

BEARING TYP

For these results eccentricity ratio was taken at the centre of the locus.

Since it was found that the same equilibrium eccentricity values were obtained with dynamic and static loading conditions for any particular set of experiments it was decided to plot both series of results on the same graph representing eccentricity ratio against Ocvirk Number.

So, the graph in fig. 5.47 illustrates the variation of the duty parameter with eccentricity ratio for the experiments carried out under 0.185 rev/s and oil supply pressures of 3 and 10 bar, with a varying applied load.

The sets of results at 0.185 rev/s follow consistent trends and have almost the same values except that at light load conditions lower eccentricities are obtained for the experiments with high oil supply pressure of 10 bar.

Also, it may be seen that the agreement between experiment and theory is very close for all supply pressures; however the upper points clearly show that the bearing is heavily loaded, as they lie at the limits of the recommended area, where the oil film becomes thinner, indicated by the high eccentricity values.

With respect to the results at high oscillating frequency of 0.463 rev/s, similar trends are obtained. Despite the fact that they show closer agreement to the analytical curve, as the duty parameter has been decreased, the eccentricity values are very much the same as those at low oscillating frequency. For all results, considerable

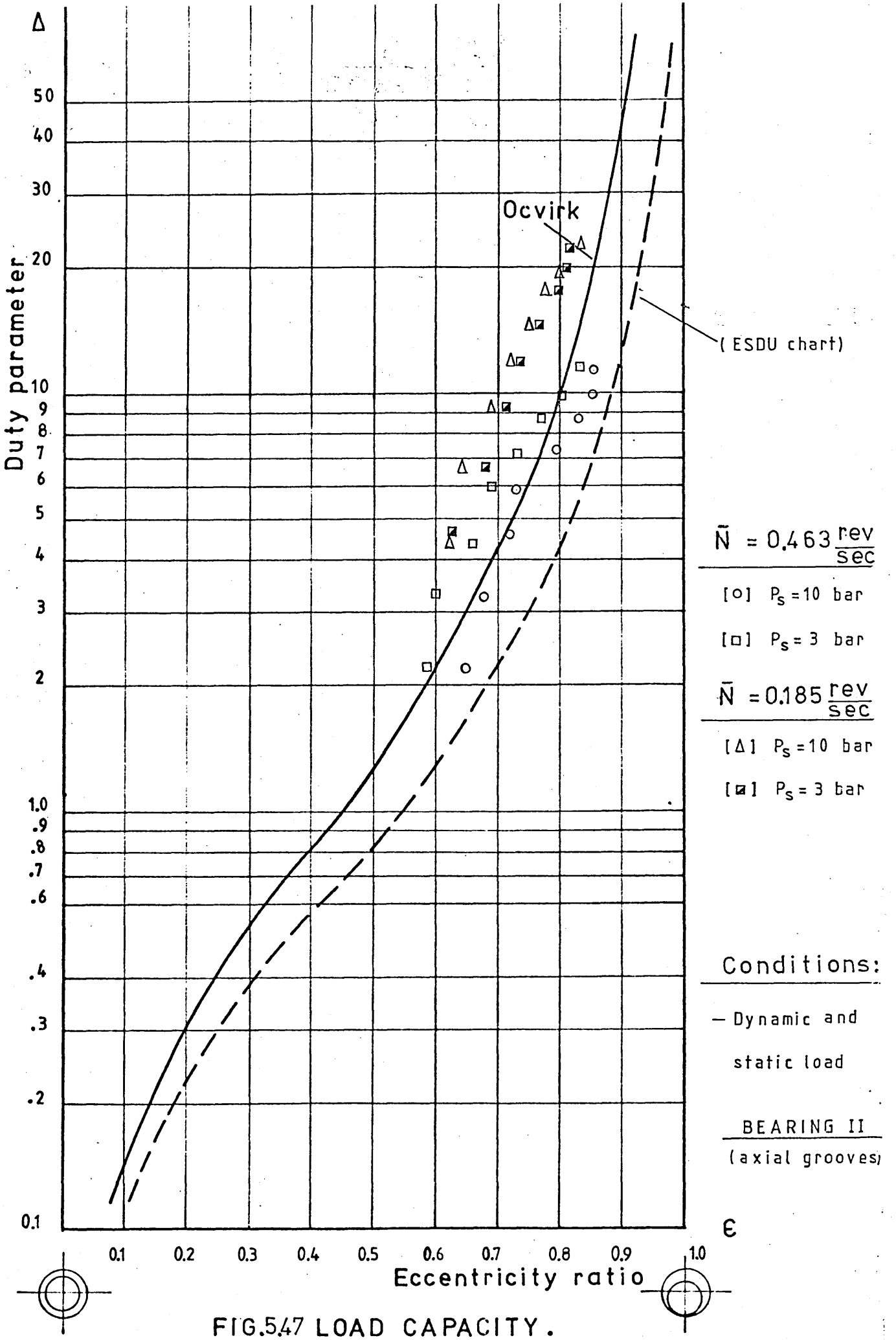

FIG.5.47 LOAD CAPACITY.

eccentricity overshoot occurs at low Ocvirk Number, reducing to virtually no overshoot as the Orvirk Number increases.

Figures 5.48 and 4.49 give a representation of the results of the shaft centre displacements, when the journal runs under oscillating motion and is dynamically and statically loaded, plotted on the polar diagram.

Figure 5.48 shows the results of tests under the same loading conditions and with oscillating frequency of 0.465 rev/s with oil supply pressures at 10 and 3 bar. The starting unloaded condition when the shaft oscillates is indicated by the trace a. It is seen that for the high pressure it lies on the top right hand side of the graph and for the low pressure, trace a", on the bottom right hand side. Then a series of traces "b - c - d - e" are plotted for the shaft centre when it has reached the equilibrium position under various loading conditions.

It can be observed that the traces of the shaft centre move outwards from the centre of the clearance circle as the load is increased, the maximum displacements being almost at the same distance for both sets of oil pressure conditions, but getting closer to the vertical axis for the lower oil supply pressure i.e. the attitude angle is reduced.

Figure 5.49 shows another two series of experiments under similar conditions to the previous ones, except that the frequency of oscillation is lower, 0.185 rev/s.

The shaft eccentricity is plotted in the same way, showing that the traces for each test followed the same pattern, with the difference that they went further out from the centre and closer to the vertical axis, lying between 0^{o} to 20^{o} attitude angle.

Also, it can be noted that the traces of the heavily loaded tests are shorter compared with the experiments under higher oscillating frequency (0.485 rev/s).

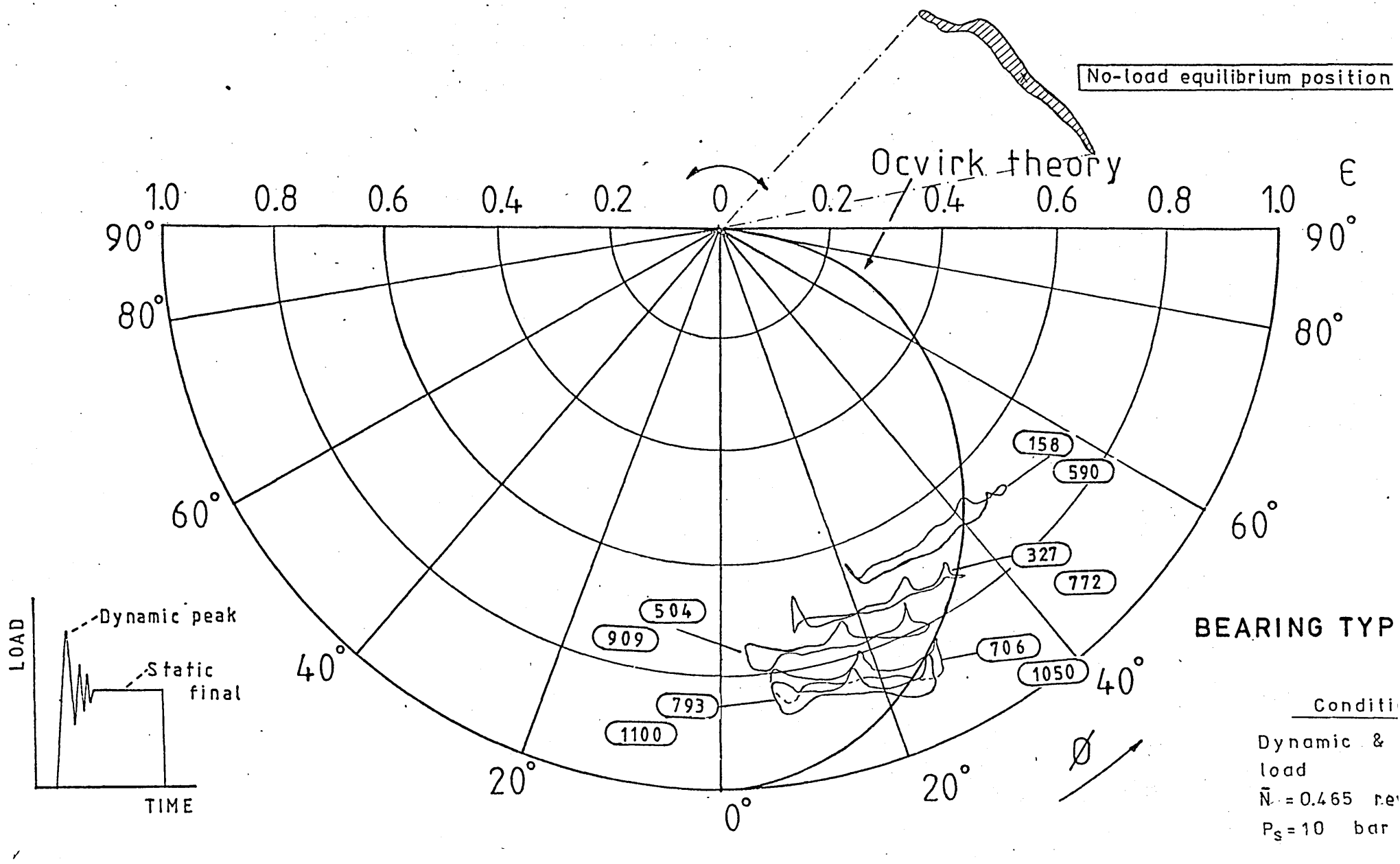

FIG.548a ECCENTRICITY RATIO AGAINST ATTITUDE ANGLE.

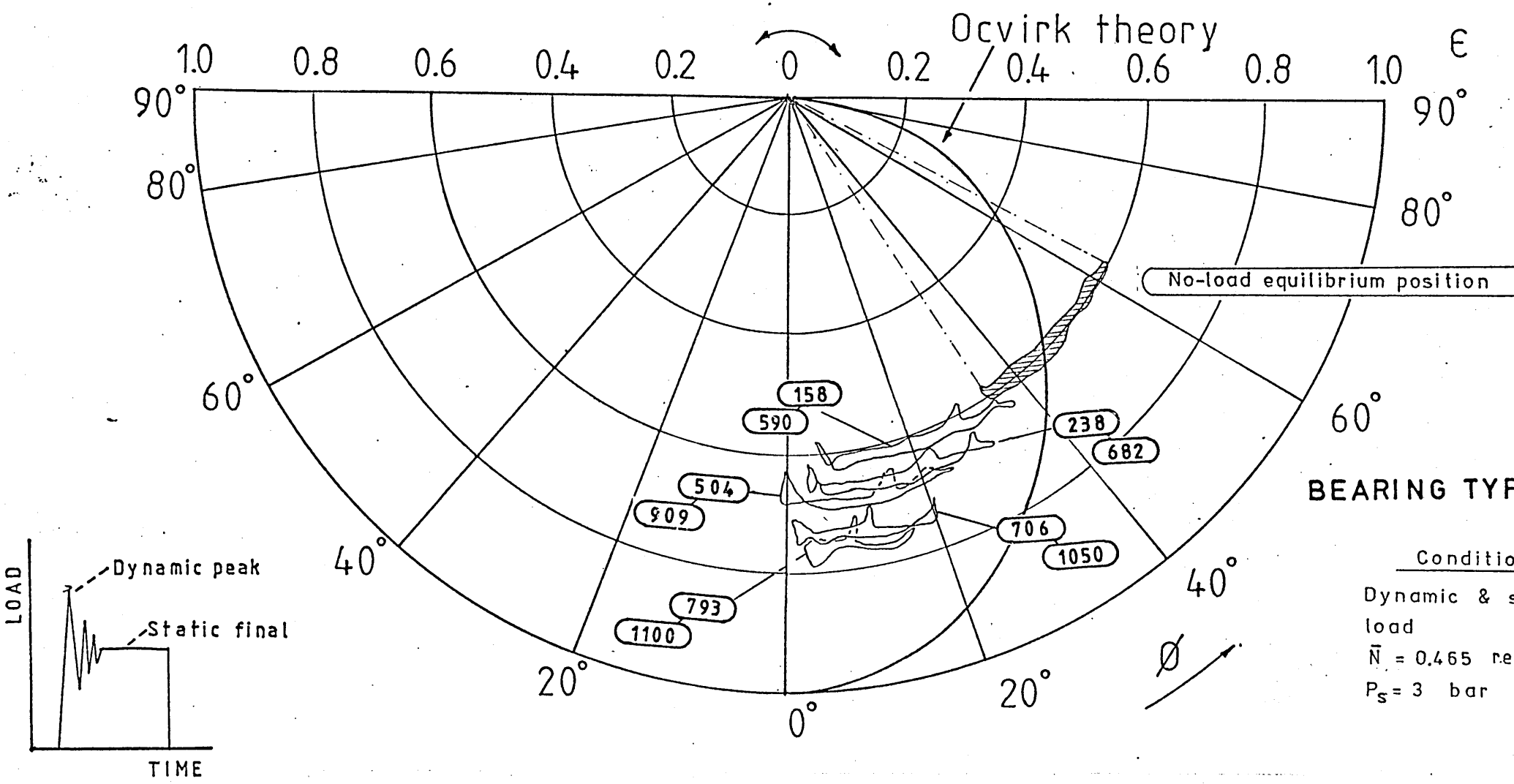

FIG.5.48b ECCENTRICITY RATIO AGAINST ATTITUDE ANGLE.

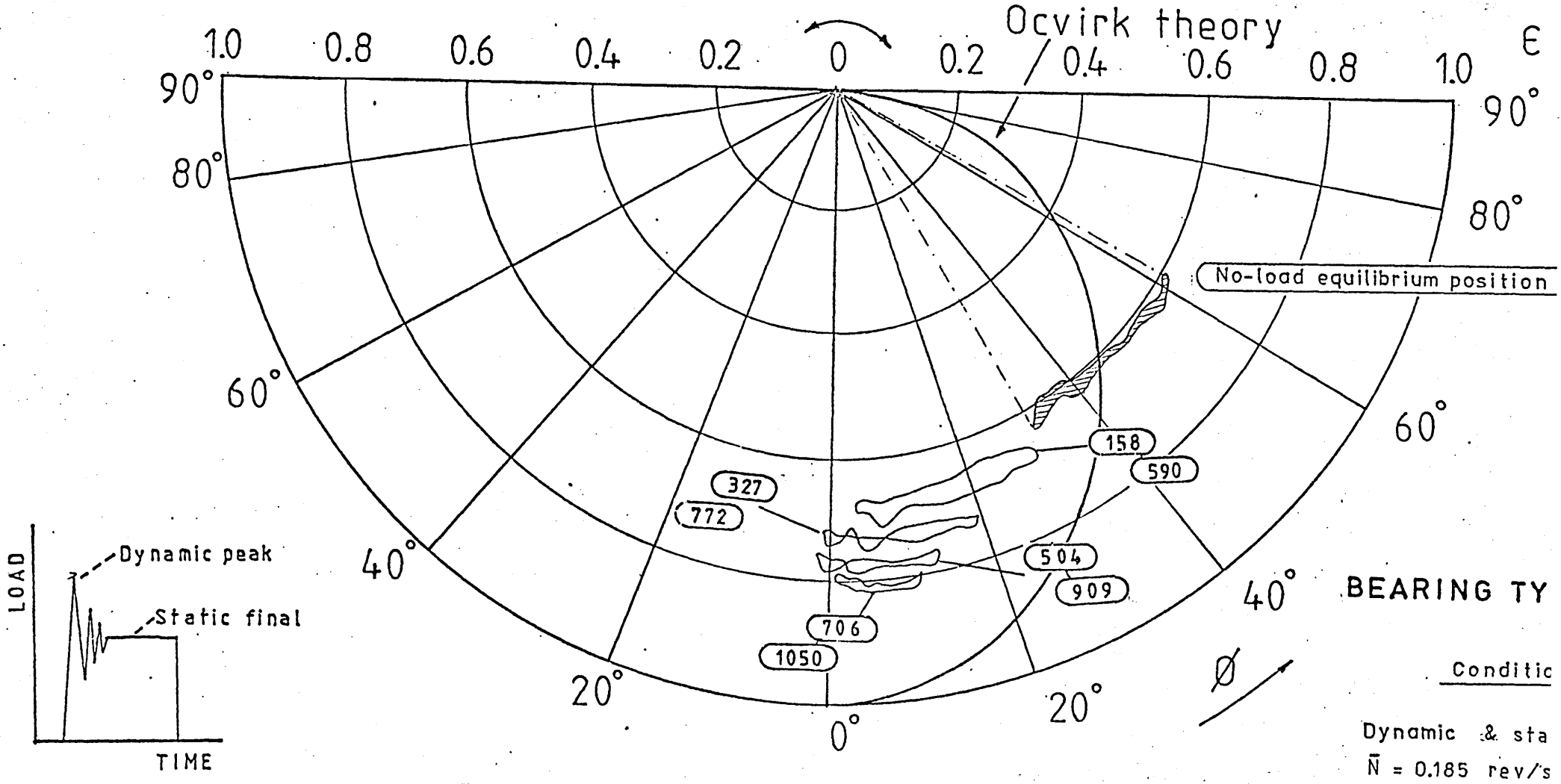

FIG.5.49a ECCENTRICITY RATIO AGAINST ATTITUDE ANGLE.

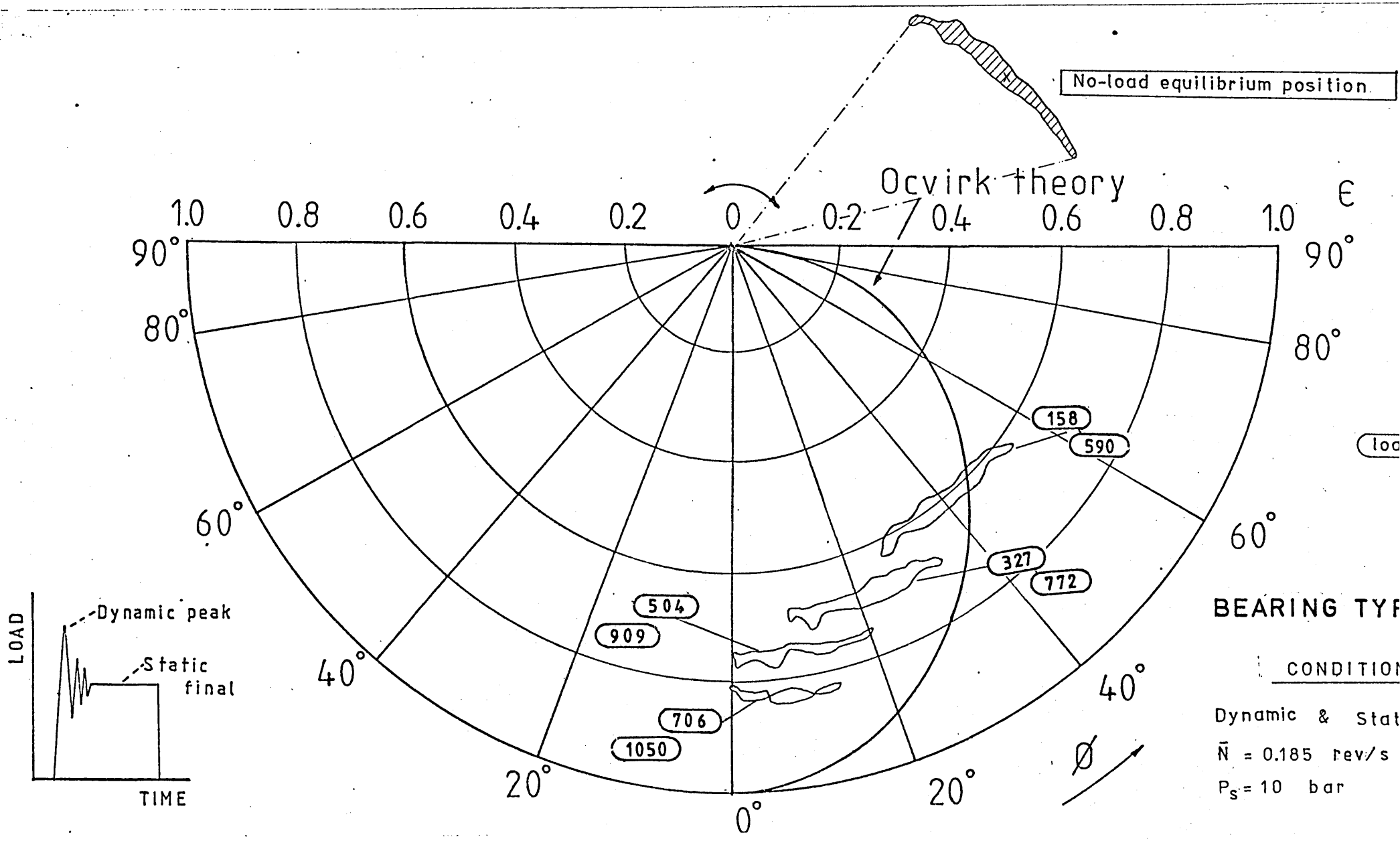

FIG.5.49b ECCENTRICITY RATIO AGAINST ATTITUDE ANGLE.

5.4 Experimental Results of the Tests on Bearing Type III Hybrid Bearing Slot-entry Type.

5.4.1. Results of Series No. 1 and 2 Static and Dynamic Loading tests with the Shaft Rotating Continuously.

These series of tests were carried out under the conditions described in section 4.3. The results of the experiments for both types of loading conditions were plotted on the same chart to illustrate clearly that the effect on the shaft eccentricity is very similar for both conditions.

So, figure 5.50 shows a series of records of the shaft centre displacement for a set of loading conditions with oil supply pressure of 70 bar and constant speed of 100 rev/min In the top part of the charts, the traces under impact loading are shown and the bottom shows those under static loading.

The same plotting procedure was followed as in the previous experiments, starting with the unloading running positions traces "a" and then the loading positions, traces "b", of the shaft centre position.

From this graph, it can be noticed that the traces "a", lie to the left of the bearing centre and when the load is applied, they gradually go down as the load is increased and to the right of the bearing centre, however, even for the heavily loaded conditions the eccentricity values are not very significant. The same picture is also obtained for the static loading conditions.

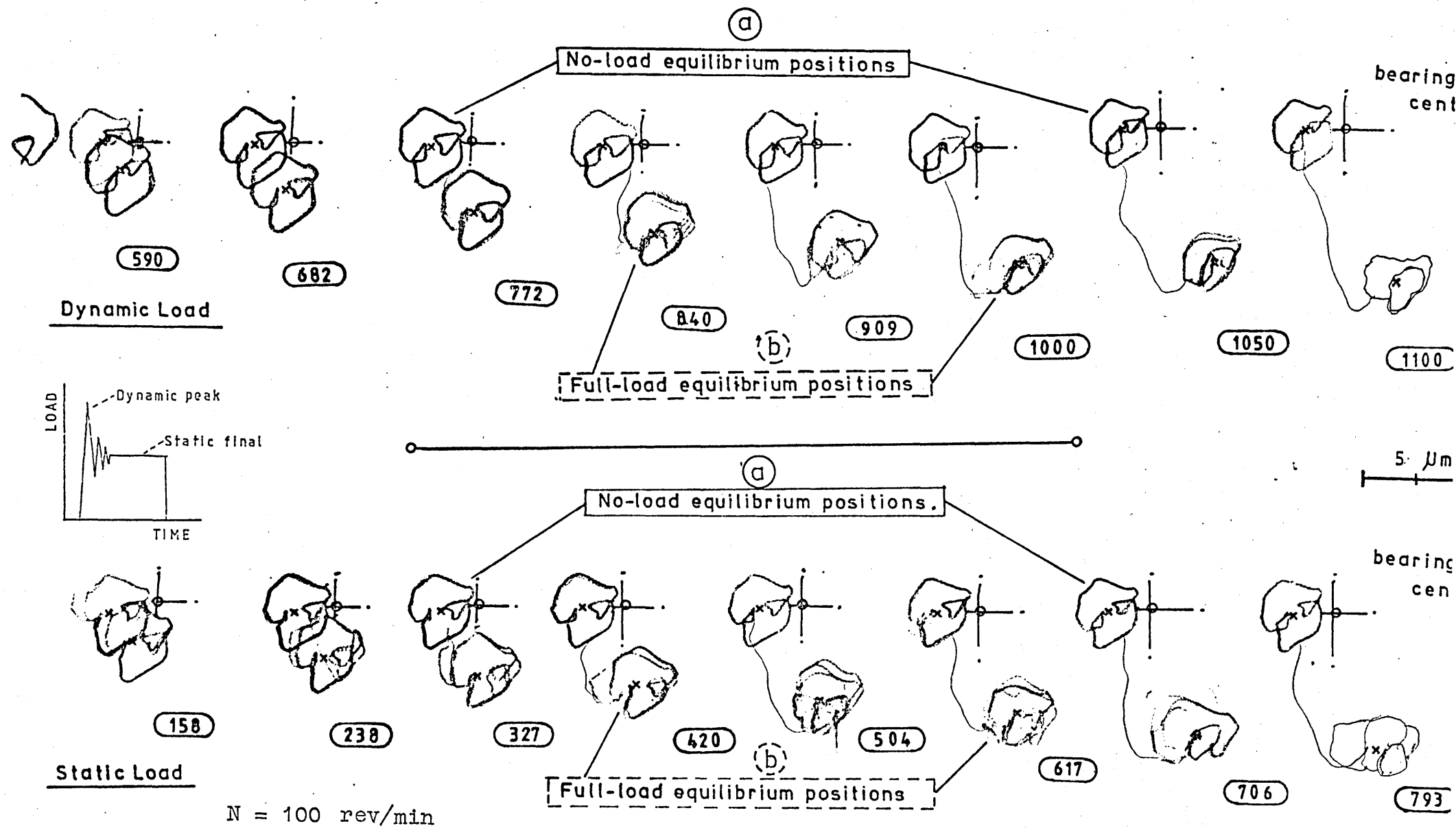

FIG.5.50 SHAFT CENTRE LOCUS.

BEARING TYPE III

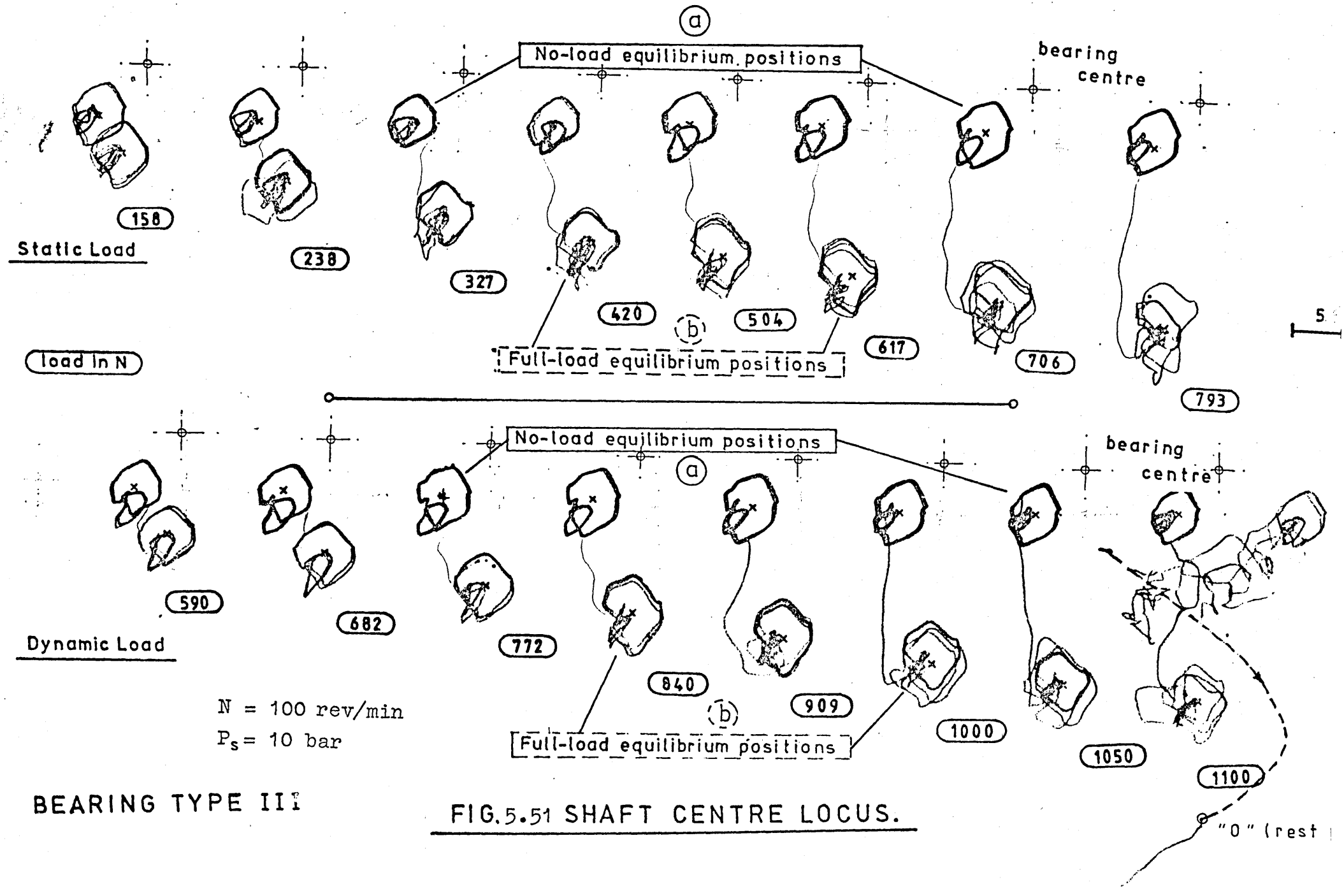

BEARING TYPE III

FIG.5.51 SHAFT CENTRE LOCUS.

Figure 5.51 shows another set of results for conditions very similar to the above except that the oil supply pressure has been reduced to 10 bar. At the top of the chart are the results under static loading and in the bottom half those under impact loading.

These results show a similar pattern as those in fig. 5.50 but in this case larger eccentricity displacements took place. The eccentricities did not go to the limit of the clearance circle, which is indicated by the reference point "0", representing the shaft rest position when the oil supply pressure was switched off.

Figures 5.52 - 53 shows similar tests under the same conditions except that the shaft running speed was reduced to 70 and 40 rev/min. Again, the results compare static and dynamic loading conditions. It can be seen that when the load was applied the shaft centre followed the same patterns as those in fig. 5.50 although with longer eccentricity displacement.

It is quite clear that the eccentricity of the shaft became very big as the load was increased but still not being critical according to reference point "0". Another feature of these series of tests is that when the shaft was loaded it went vertically down, outwards from the bearing centre and as the load increased, they gradually moved to the left of the vertical axis being opposite to the rest of the previous experiments. So, these series of experiments show the "worst" bearing performance so far being obtained for this particular bearing.

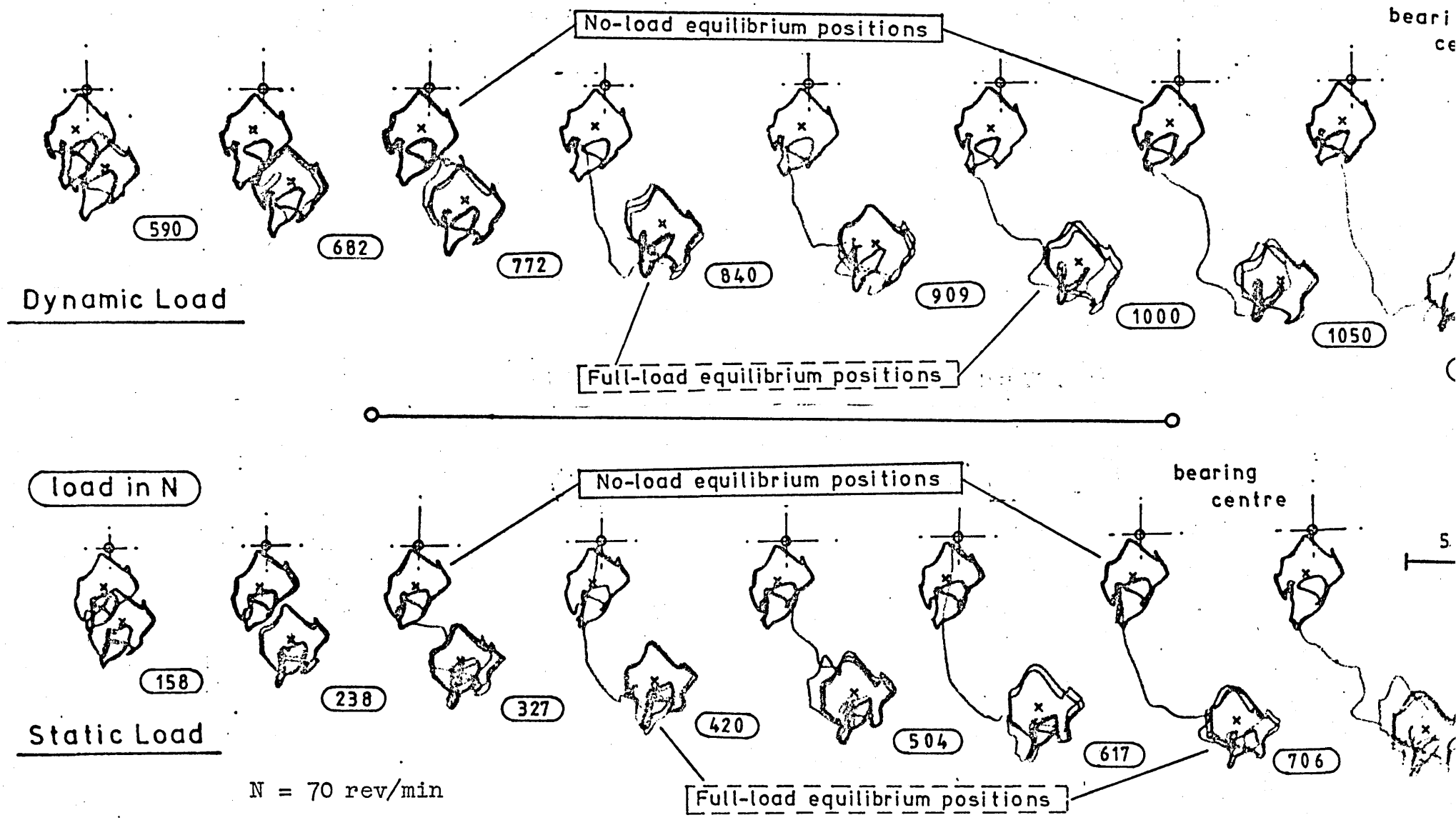

FIG. 5.52 SHAFT CENTRE LOCUS.

BEARING TYPE III

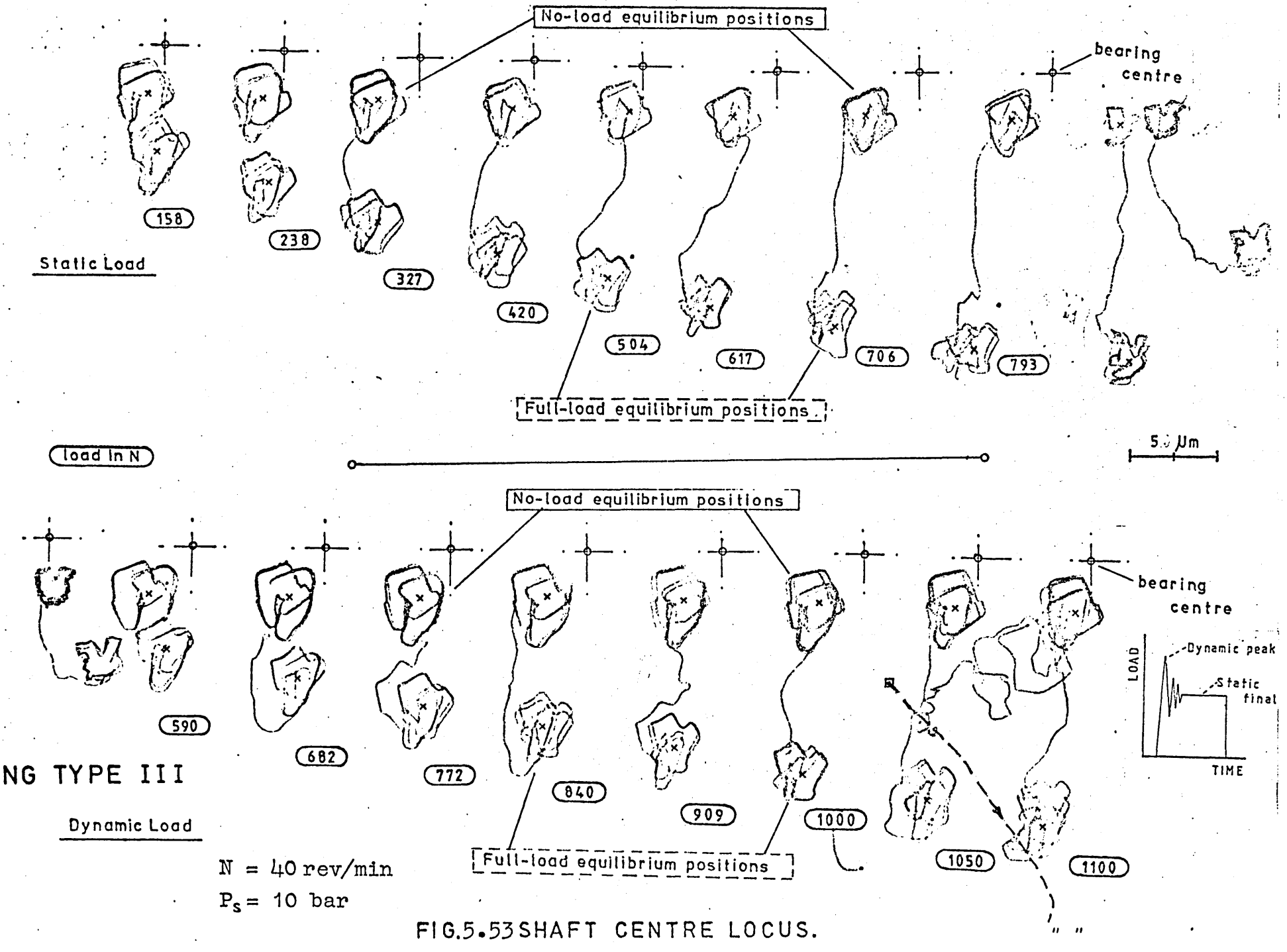

FIG.5.53 SHAFT CENTRE LOCUS.

The previous recorded results are plotted on graphs represented in terms of different duty parameters which give the load capacity and the attitude angle of the bearing. All points indicate equilibrium shaft positions, which are the eccentricities at unloaded and dynamic or statically loaded conditions.

So, figure 5.54 shows the plotting of four series of experiment results as a function of Ocvirk number. It can be noted that the set of results at high speed of 100 rev/min produce eccentricities well below hydrodynamic theory with high oil supply pressures giving particulary low eccentricities.

This graph also shows the results carried out at lower speed of 70 rev/min which at low oil supply pressure clearly indicate that they are very close to the theoretical curve, all of them lying in the recommended area. However for the set of results at high oil pressure they are well to the left hand side of the curve, giving low eccentricity values.

Figure 5.55 represents the full range of results for the hybrid bearing plotted against the Fuller number instead, which takes into account the oil supply pressure.

It can be clearly seen that the results at high oil supply pressure of 70 bar lie on the area of very low values of the duty parameter and eccentricity ratio. On the other hand, those results at low oil supply pressure give very high duty parameter values.

These results seem to follow the same trend for both sets, however it seems that there is slight discontinuity

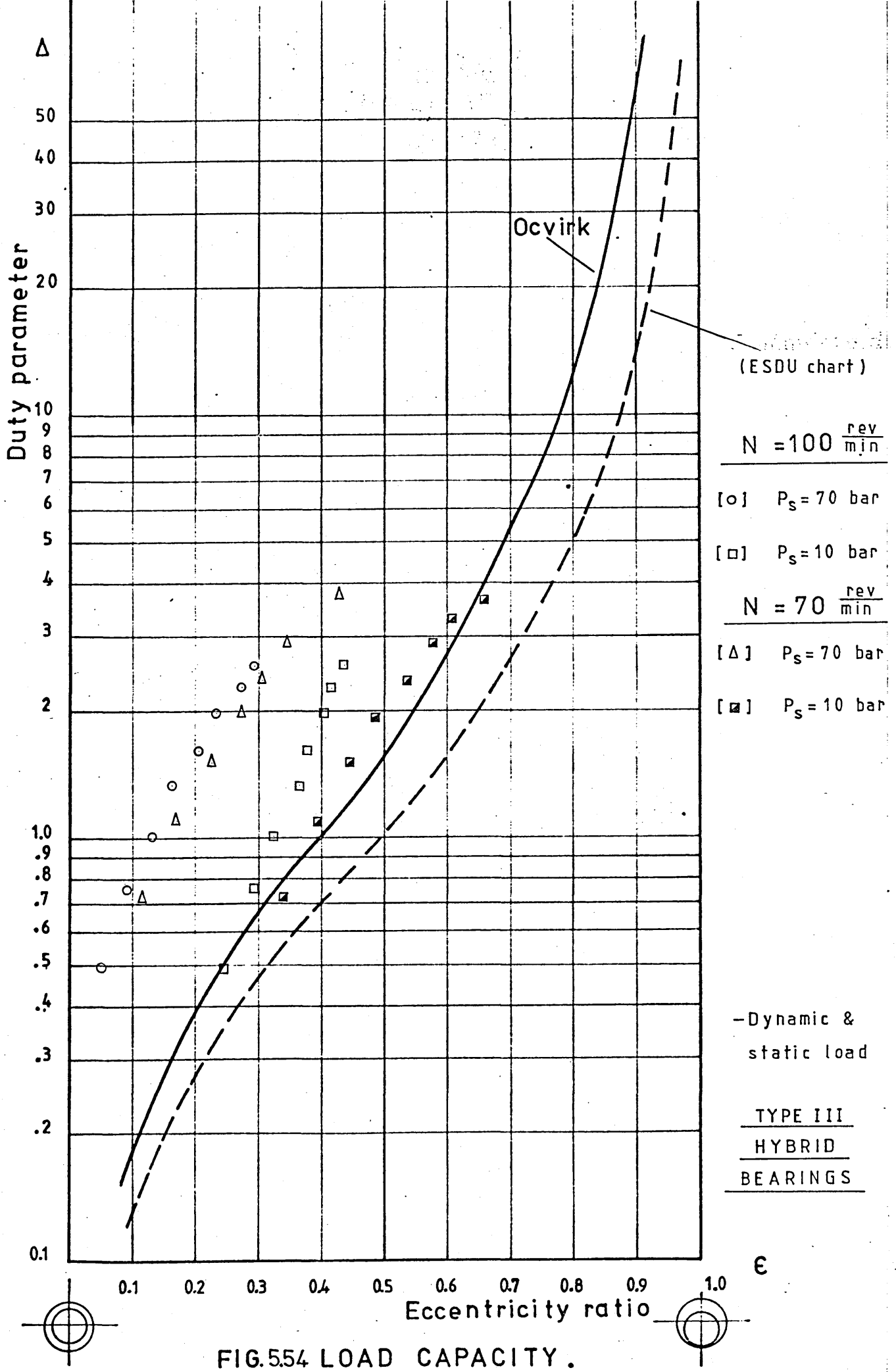

FIG. 5.54 LOAD CAPACITY.

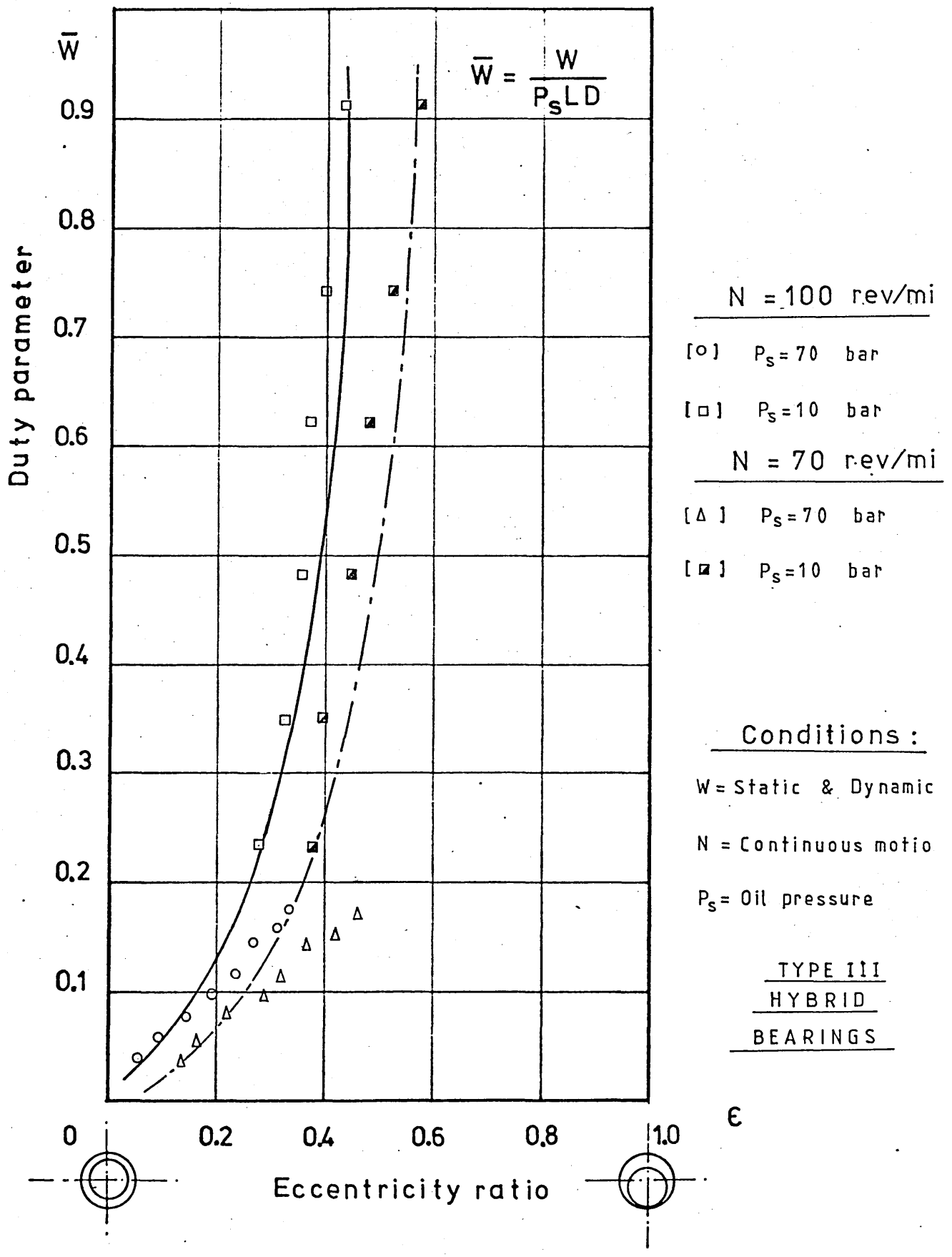

FIG. 5.55 VARIATION OF LOAD PARAMETER WITH ECCENTRICITY RATIO.

between the results obtained at low oil supply pressure with those at high pressure.

Also, it is noted that some hydrodynamic effect is present with the results at a speed of 100 rev/min against those at lower speed of 70 rev/min, as indicated by the small eccentricity values.

Finally, the plotting of the eccentricity results is shown on the polar diagram of figure 5.56 in terms of eccentricity ratio and attitude angle. In this it can be seen that although the unloaded positions are at values of near zero. for all the sets of experiments, as the load is applied, different trends are followed by each set. Those at high oil supply of 70 bar have very low eccentricity value and lie at both sides of the vertical axis between 10^{o} and 20^{o} attitude angle, however those at low oil pressure of 10 bar have bigger eccentricity values and attitude angles of 5^{o} to 20^{o}.

To conclude the graphical representation of the test results under continuous motion, a comparison between the bearings with circumferential and axial grooves type II and the hybrid bearings type III is made, by plotting the eccentricity experimental values against the duty parameter based on the Fuller solution . Bearing in mind that the oil supply pressure is not very high at 10 bar, it does provide a comparison of the performance of each bearing. The results for the hybrid bearing show lower values of eccentricity than those obtained for the axially grooved bearing, particulary as the load becomes heavier (see fig. 5.57).

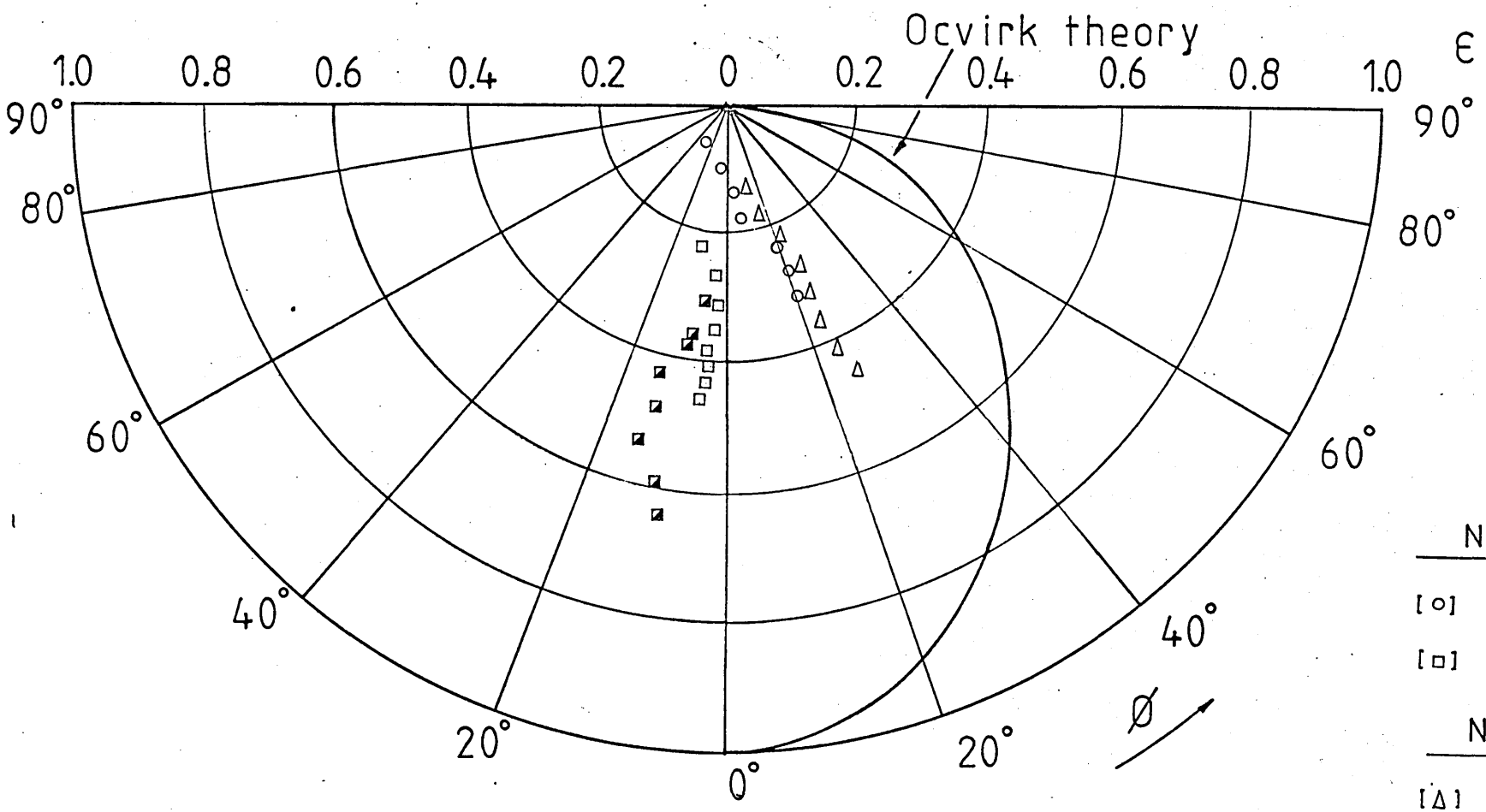

FIG. 5.56 ECCENTRICITY RATIO AGAINST ATTITUDE ANGLE.

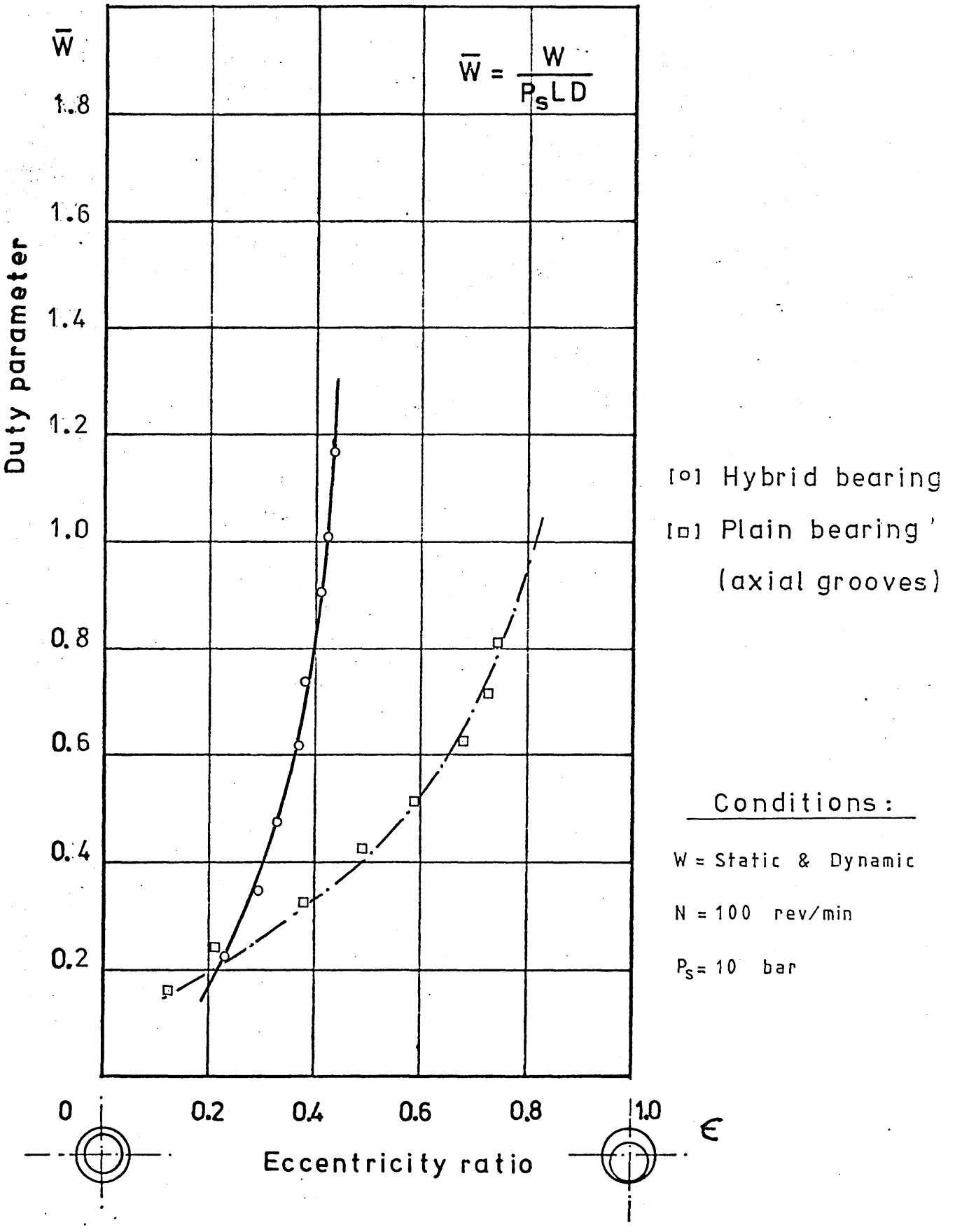

FIG. 5.57 VARIATION OF LOAD PARAMETER WITH ECCENTRICITY RATIO.

5.4.2 Results of Series No. 3 and No. 4 Static and Dynamic Load Under Oscillating Motion.

These series of tests were carried out following the instructions described in section 4.3.

First, some photographic specimens taken from the oscilloscope screen of the shaft centre locus are described.

So, figure 5.58 shows the shaft centre orbit when it has reached an equilibrium stage under oscillating motion of 0.465 rev/s with oil supply pressure of 70 bar. It also gives the momentary path followed by the shaft when it has been dynamically loaded under an impact of 1100 N and finally the equilibrium stage under oscillating motion and static load conditions.

Figure 5.59 shows the result of another experiment under similar conditions as the previous, but in this case the oil supply pressure has been lowered to 10 bar. From this it can be clearly noted that the shaft eccentricity is greater than in the previous test.

Figures 5.60 and 5.61 show further scope results of tests carried out under oscillating frequency of 0.185 rev/s, oil inlet pressure of 10 bar but under different dynamic loading.

Figure 5.61a shows another trace of the shaft centre movement from the unloaded equilibrium position running at 0.185 rev/s, with an oil pressure supply of 70 bar to

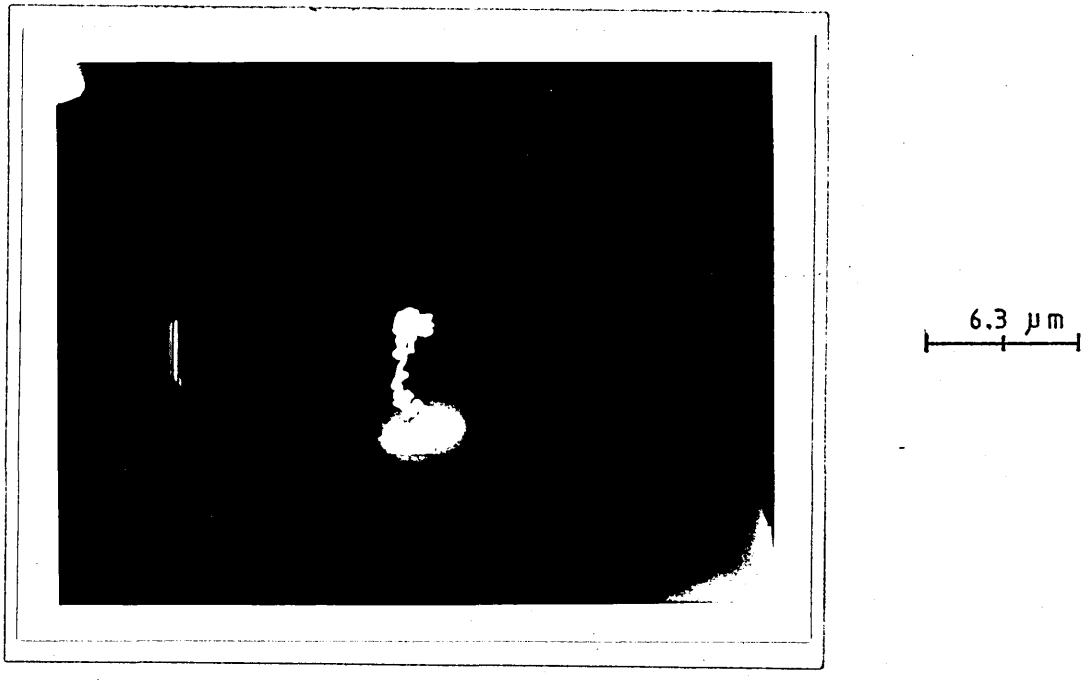

Fig. 5.58 Shaft locus under dynamic load from equilibrium running position.

($\bar{N}$ = 0.465 rev/s, W = 1100 N - peak, P_s = 70 bar)

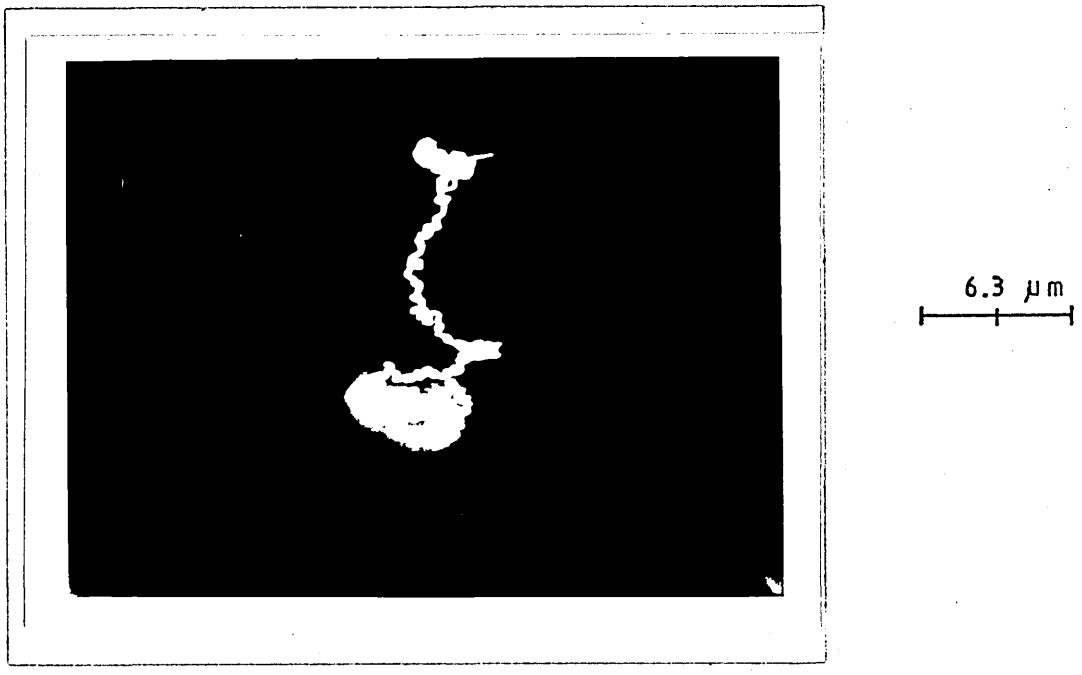

Fig. 5.59 Shaft locus under dynamic load from equilibrium running position.

($\bar{N}$ = 0.465 rev/s , W = 1100 N - peak, P_s = 10 bar)

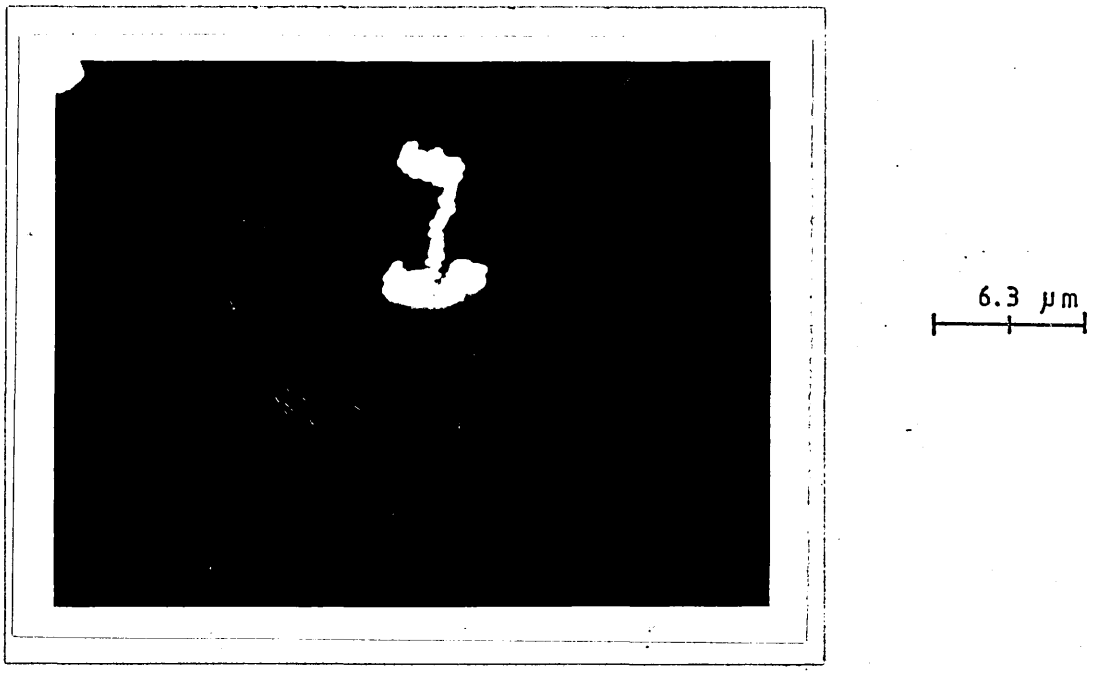

Fig. 5.60 Shaft locus under dynamic load from equilibrium running position.

($\bar{N}$ = 0.185 rev/s , P_s= 10 bar, W = 682 N - peak)

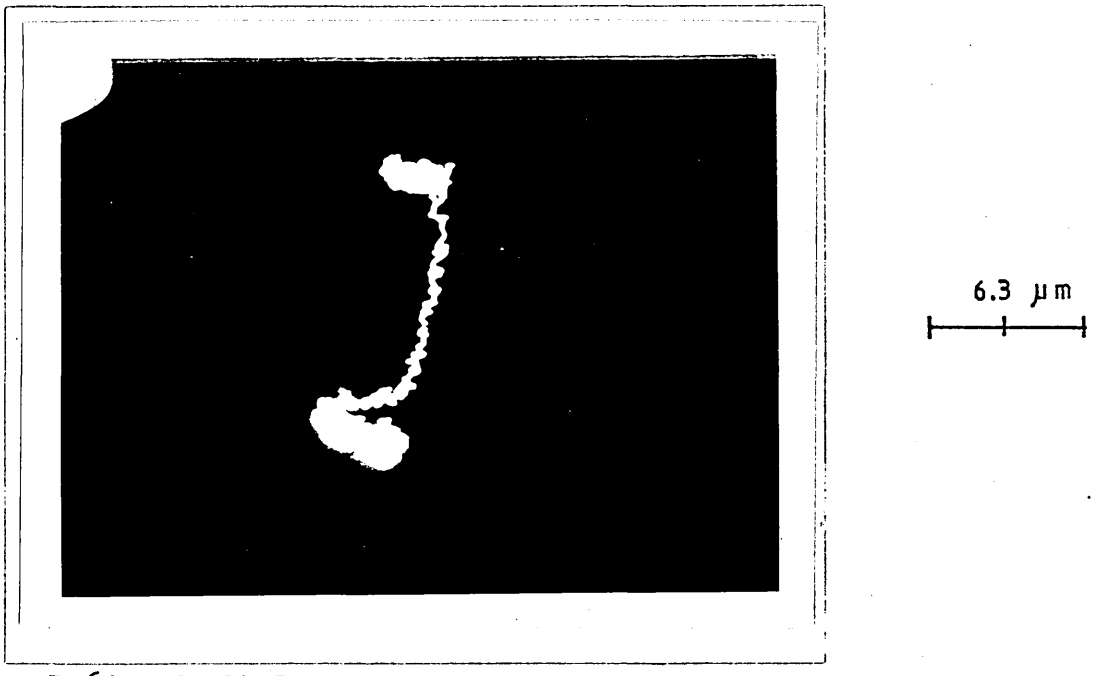

Fig. 5.61 Shaft locus under dynamic load from equilibrium running position.

($\bar{N}$ = 0.185 rev/s ., P_s= 10 bar, W = 1100 N - peak)

BEARING TYPE III

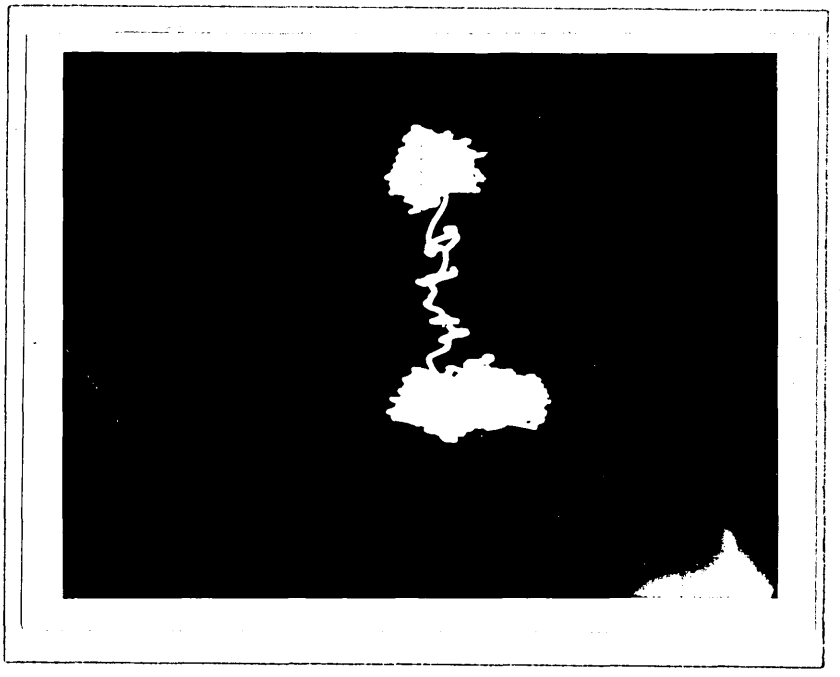

Fig. 5.61a Shaft locus under dynamic load from equilibrium running position.

($\bar{N}$ = 0.185 rev/s, P_s = 70 bar, W = 1100 N - peak)

the heavily loaded position, under 1100 N. This was taken at 2.5 times magnification of the previous photographs, in order to obtain a better resolution of the transient path travelled by the shaft centre.

Also figure 5.60 shows the unloaded position of the shaft centre and its trajectory under dynamic load, until it reaches the final equilibrium position with a static load of 238 N. Figure 5.61 clearly shows longer displacement when the applied load at equilibrium has been increased to 793 N.

Figures 5.62 - 63 - 64 show shaft centre displacements obtained for a series of experiments carried out under oscillating frequency of 0.463 rev/s, and a range of loads and supply pressures.

Once again, the same set of tests is repeated for each loading model, either static or dynamic and, plotted in the same chart, to enable easy comparison.

Figure 5.62 shows the set of results carried out with the highest oil supply pressure obtained in the system, 70 bar. From the chart it can be noticed that the eccentricity has been increased as the load was increased and the final shaft centre went always vertically down in the direction of the load from the unloaded position. The same effect was obtained for the other two series of tests as shown in the recorded charts of figures 5.63 - 64. But it is clearly seen that the shaft eccentricities became bigger as the oil supply pressure was lowered.

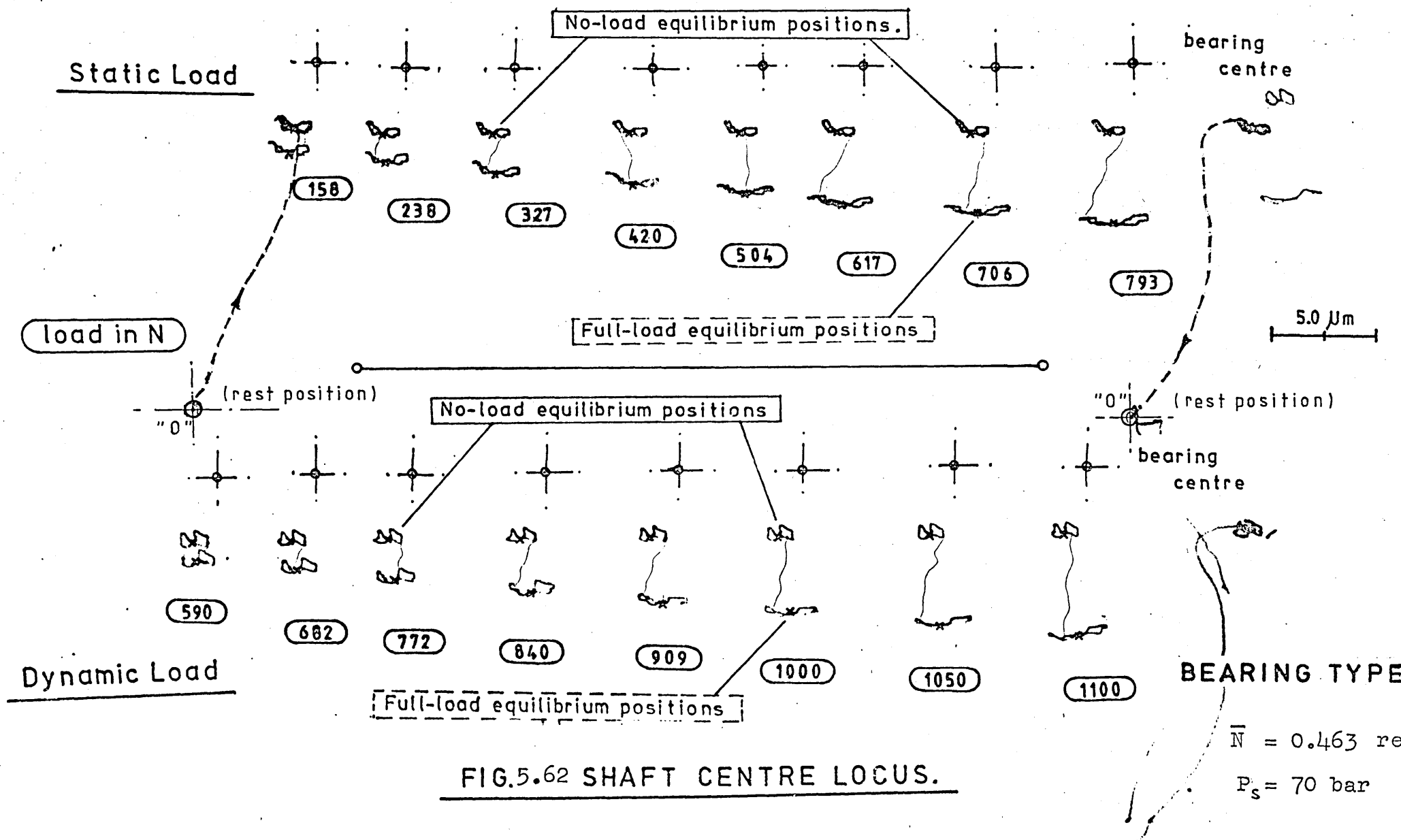

FIG.5.62 SHAFT CENTRE LOCUS.

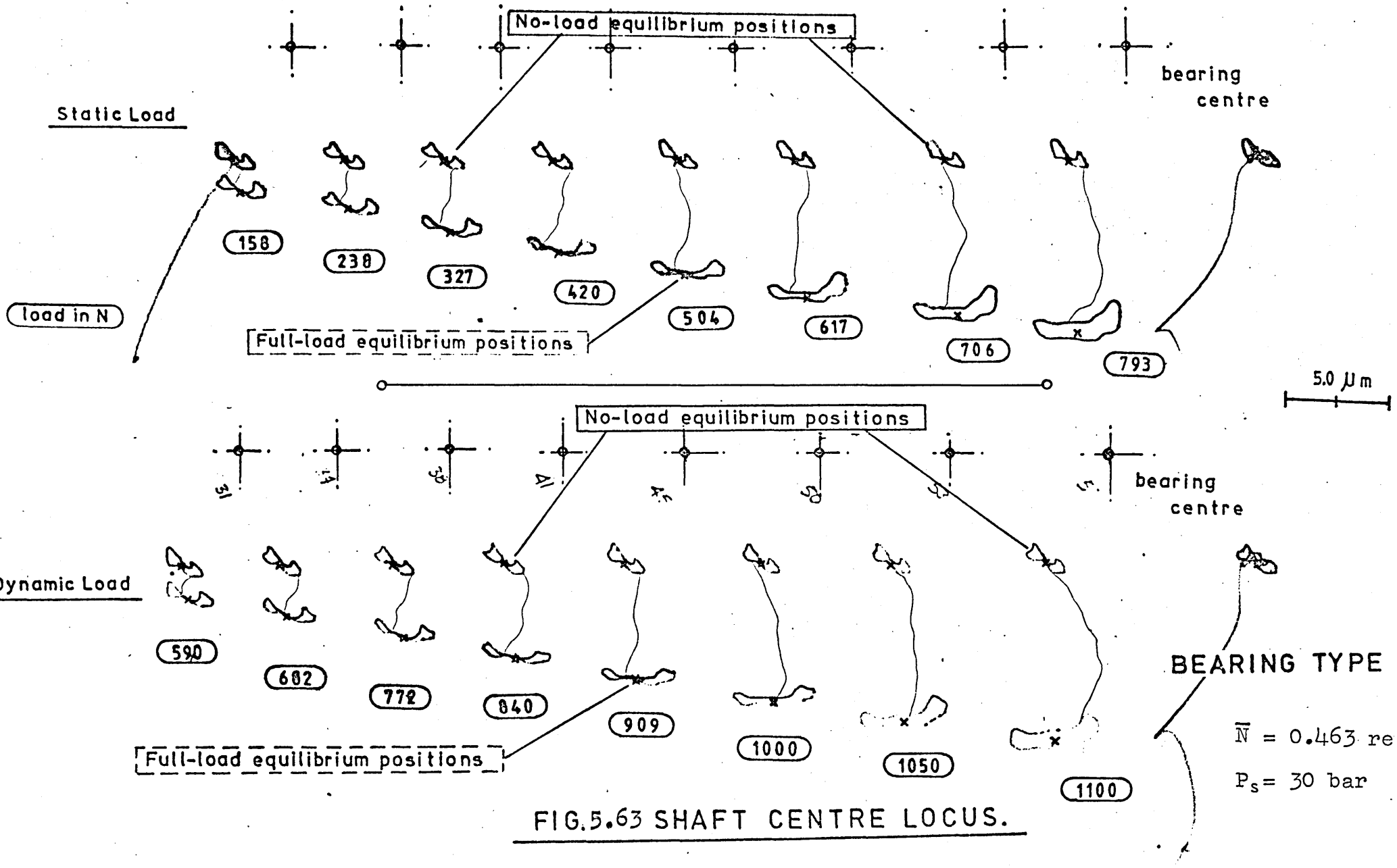

FIG.5.63 SHAFT CENTRE LOCUS.

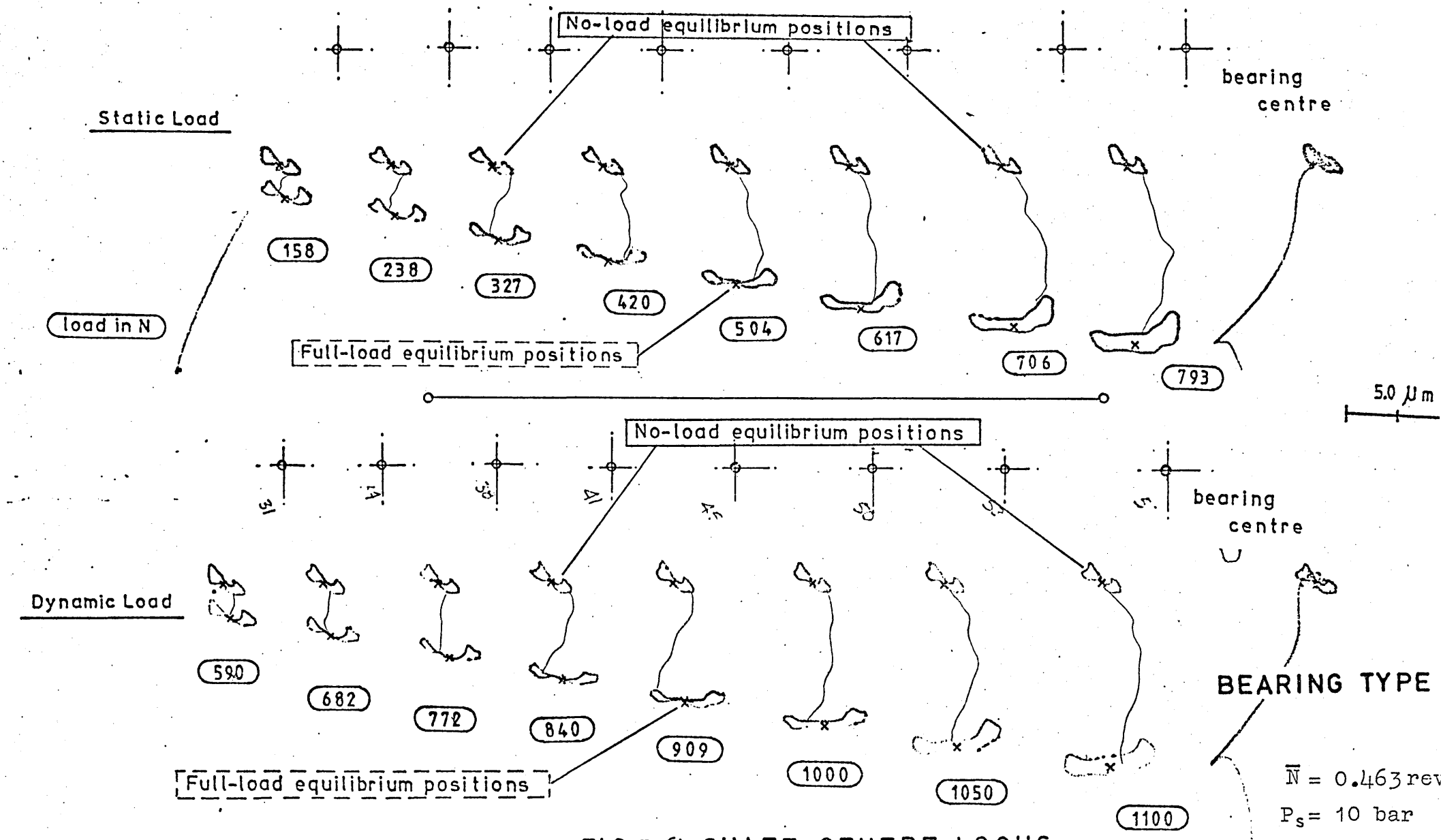

FIG.5.64 SHAFT CENTRE LOCUS.

Another observed feature is that the traces of the orbit described by the shaft when oscillating, become more enlongated as the oil supply pressure drops, being more noticeable in the traces when the load has been already applied.

Figures 5.65 - 66 - 67 represent another series of experimental results of the locus of the shaft centre carried out under similar test conditions to the previous experiments shown in figures 5.62 - 63 - 64 except that in this case the oscillating frequency of the shaft was lowered to a value of less than a half of that used for the other tests, 0.185 rev/s. However, an identical pattern and same eccentricity values were obtained for all the corresponding series of tests carried out, as for those at high oscillating frequency. Once again, the traces of the orbits described by the shaft centre became expanded as the oil supply pressure was dropped.

The basic recorded results are plotted on graphs, which give the journal eccentricity ratio against Ocvirk number or Fuller parameter. All the points represent stable shaft positions, as the values plotted are the eccentricities of the shaft when equilibrium state has been reached after a static or dynamic load has been applied.

Figure 5.68 shows the results for series of shaft eccentricities, plotted against the duty parameter at different oil supply pressure levels of 70, 35 and 10 bar, by varying the applied load and two constant oscillating frequency of 0.465 and 0.185 rev/s.

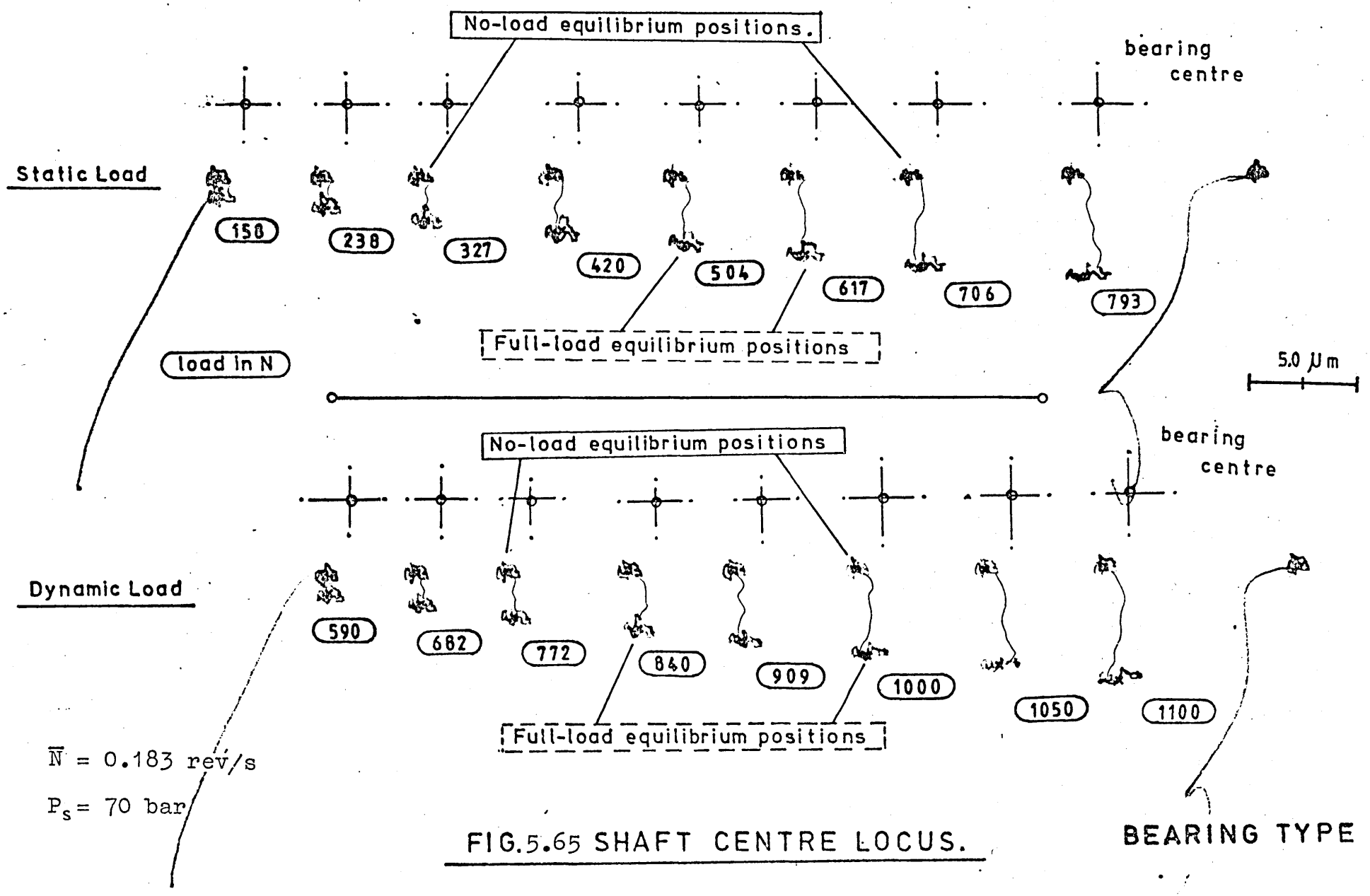

FIG.5.65 SHAFT CENTRE LOCUS.

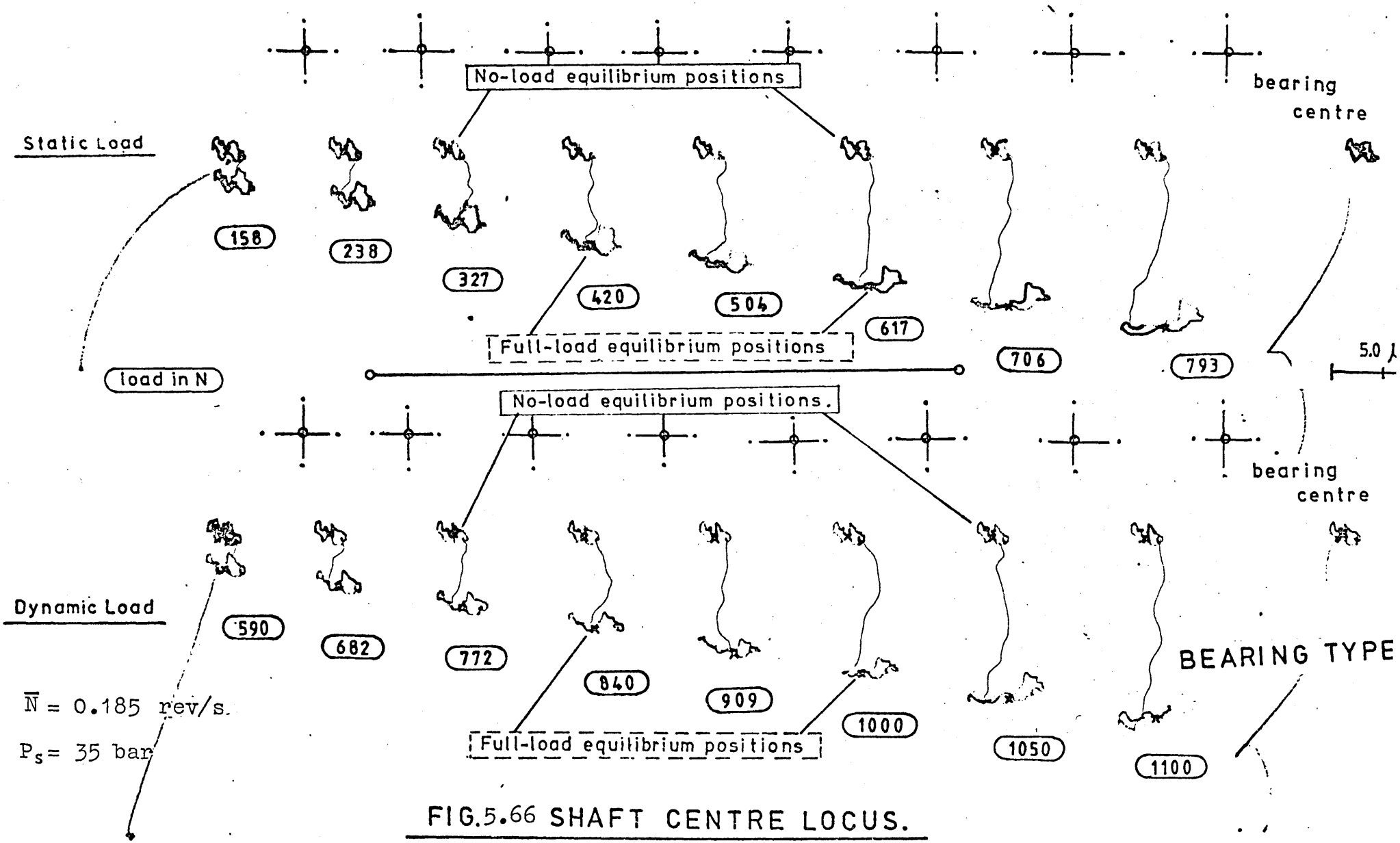

FIG.5.66 SHAFT CENTRE LOCUS.

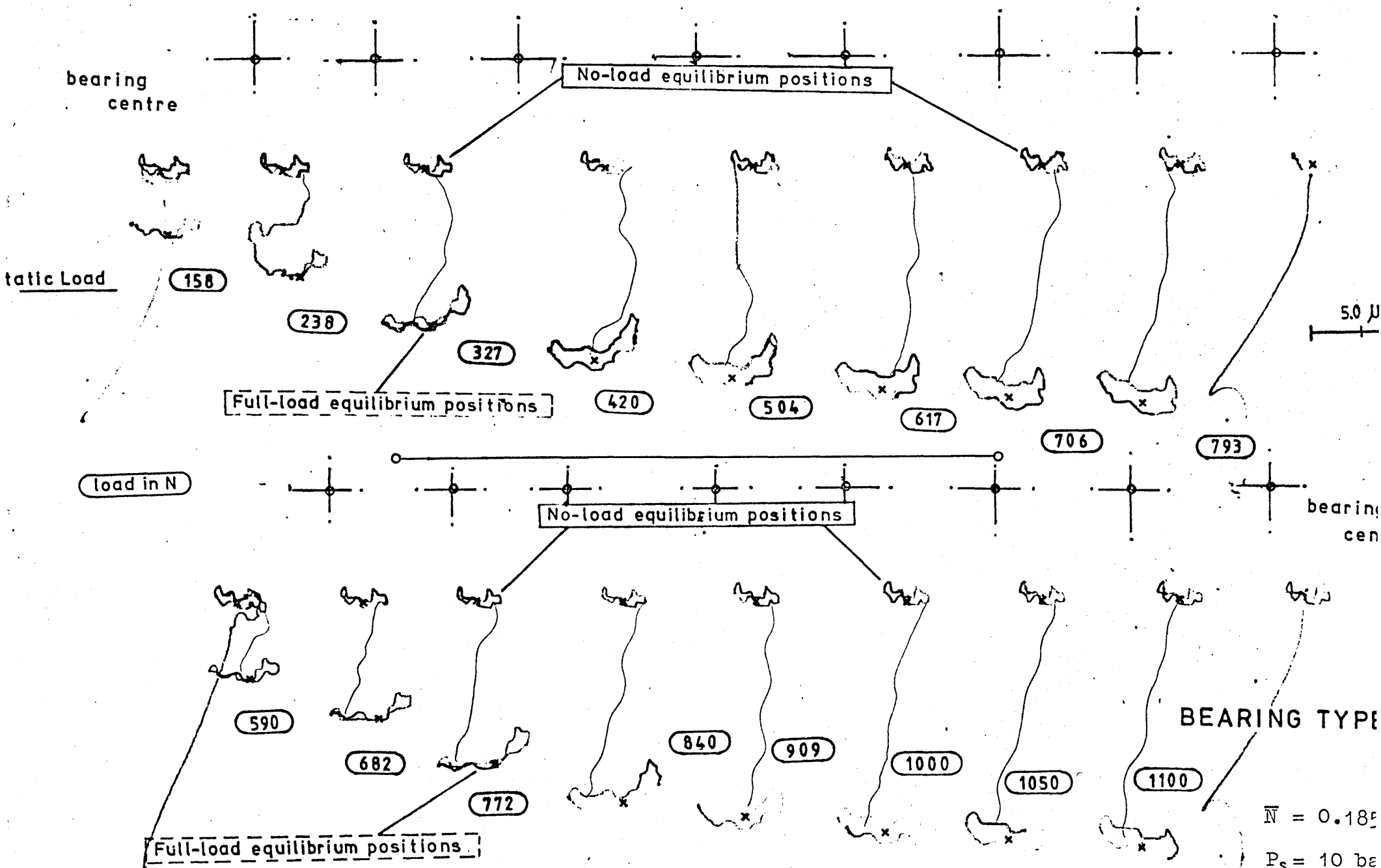

FIG. 5.67 SHAFT CENTRE LOCUS.

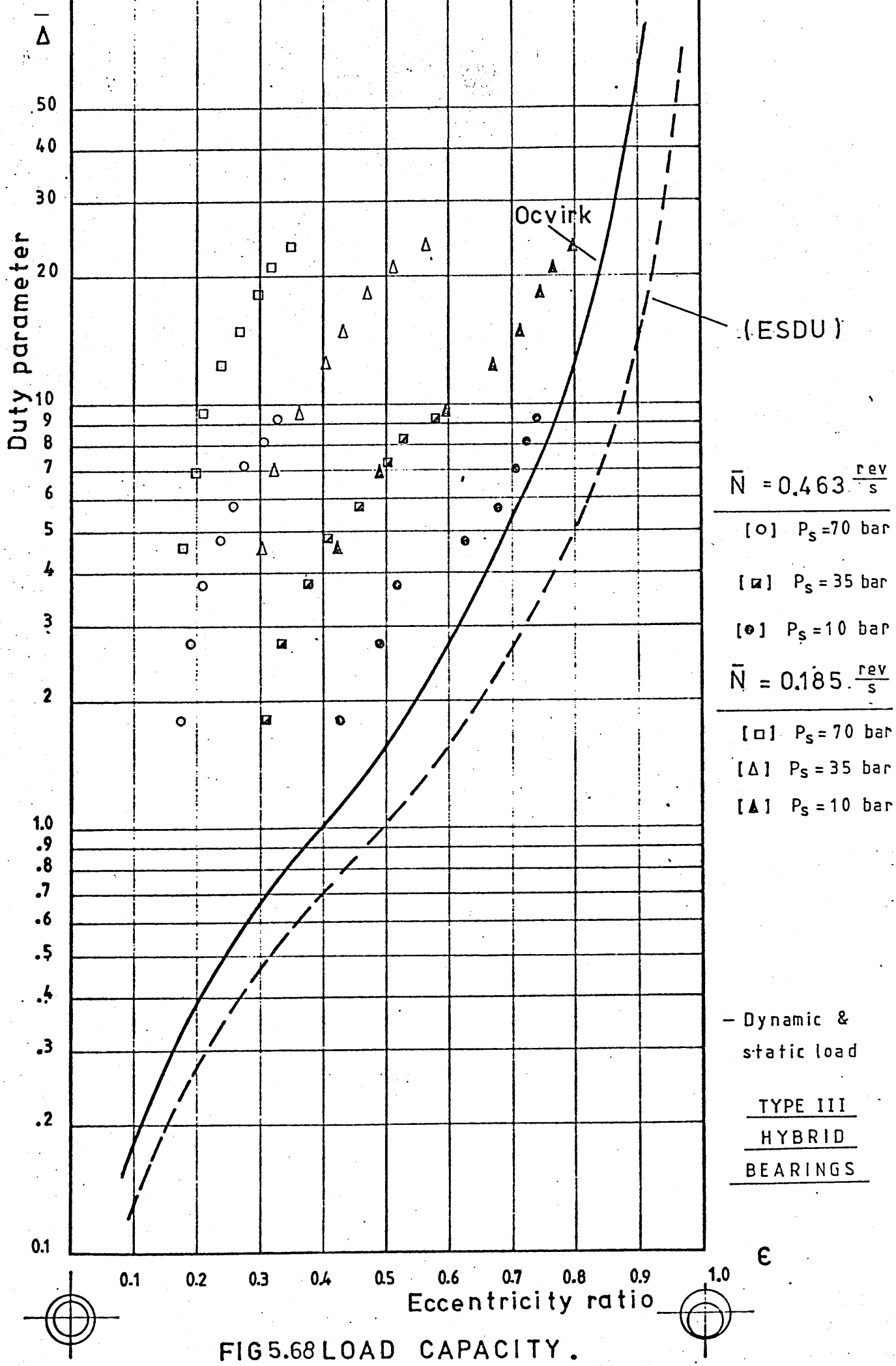

FIG 5.68 LOAD CAPACITY.

It can be noticed that the six sets of results follow almost the same trend and close agreement was found between experimental and the hydrodynamic theoretical curve for the tests at low oil inlet pressure, 10 bar and particulary for those at high oscillating frequency. For the other results it may be seen that a major divergence exists between experimental results and the analysis. In fact the experimental values represent very low eccentricity values at high duty numbers, the greatest divergence being associated with high supply pressure and low oscillating speed.

Figure 5.69 represents the same series of eccentricity results as the previous graph, but plotted against the Fuller Number. Again, both static and dynamic loading conditions are plotted since they correspond to the same point for every test. Another important feature in this case is that almost the same values are obtained for frequencies of 0.465 and 0.185 rev/n, although slight difference is noted for the results at low oil supply pressure, particularly those at low frequency, which have bigger eccentricity values. However, it seems that all the results almost follow the same line, showing small eccentricities with little evidence of a hydrodynamic effect for those bearings under oscillating motion.

The previous shaft displacement results are shown on the polar diagram of figures 5.70 and 5.71 in terms of eccentricity ratio and attitude angle.

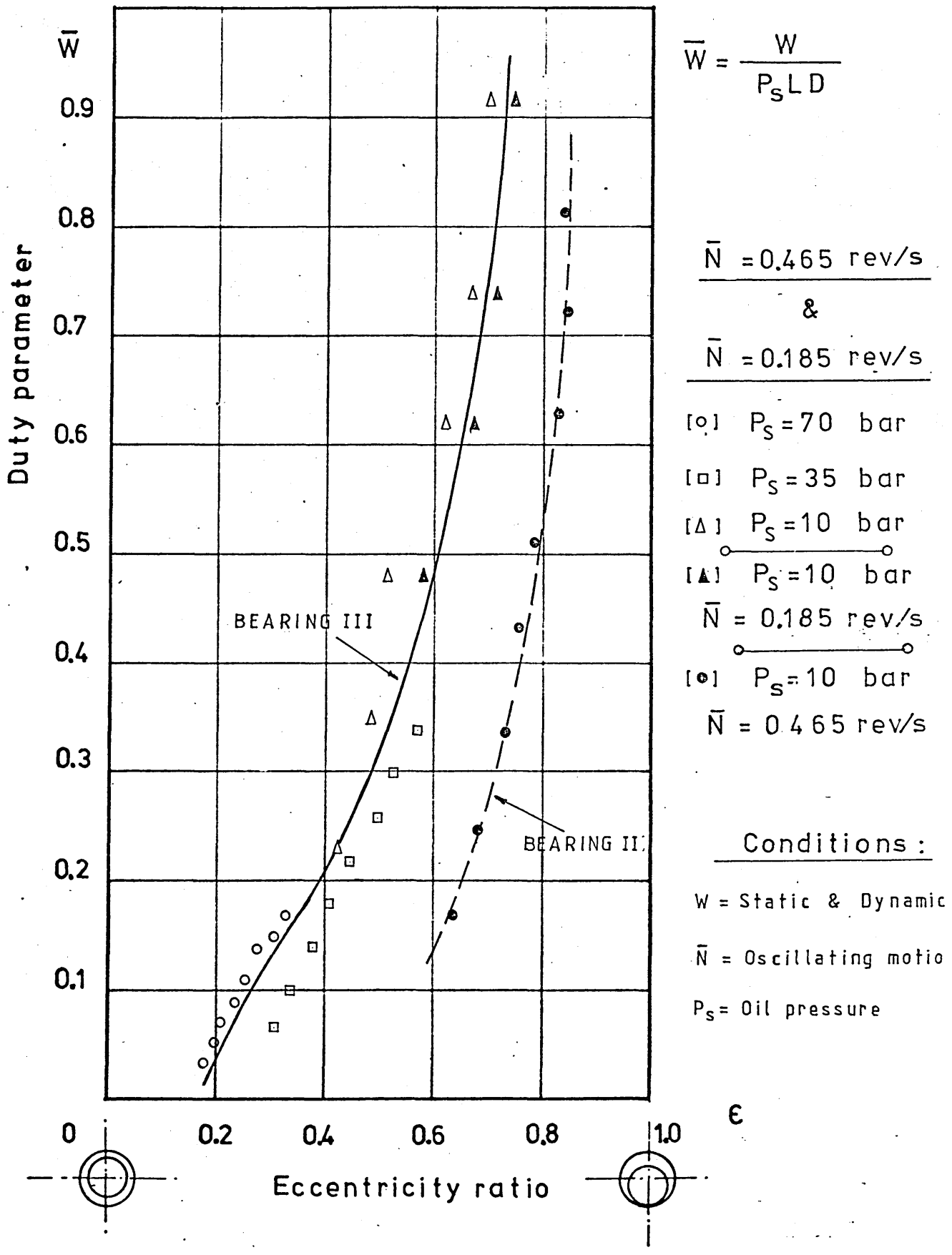

FIG. 5.69 VARIATION OF LOAD PARAMETER WITH ECCENTRICITY RATIO.

The initial unloaded condition, trace "0" is plotted as a reference point for the loaded conditions b, c, d, e and f. From these it can be seen that small displacements are obtained when high oil pressure is applied, 70 bar, even for heavily loaded conditions, and they follow the same trend in a vertically central path, being in line with the applied load. However, when the oil pressure is dropped there is a tendency for all the results to shift gradually to the left hand side and move even lower, giving high eccentricity values at 10 bar oil supply pressure. This clearly shows that the displacements now appear to be more sensitive to oil feed pressures, proving the benefit of the hydrostatic effect.

Figure 5.70 also shows that as the oil pressure was dropped to 35 bar, a shift to the left for all the results was found, although not as much as those for the low oil pressure traces. And it is clearly noted that the eccentricity ratio values are not as big as those obtained at low oil supply pressure.

Figure 5.71, represents a set of experimental results similar to the previous ones, except that the oscillating frequency has been lowered to 0.185 rev/s. Both sets of results follow the same trend, when the oil supply pressure is changed from 70 to 10 bar.

It can also be noted that traces at high oil pressure, 70 bar are in line with the applied load, however as the oil supply is dropped the attitude angles from one set of results to another changed gradually, and slightly bigger

eccentricity ratio values are obtained at 10 bar oil pressure. For both figures the effect of increasing oil supply pressure in reducing the amplitude of oscillations of the shaft is clearly identificable.

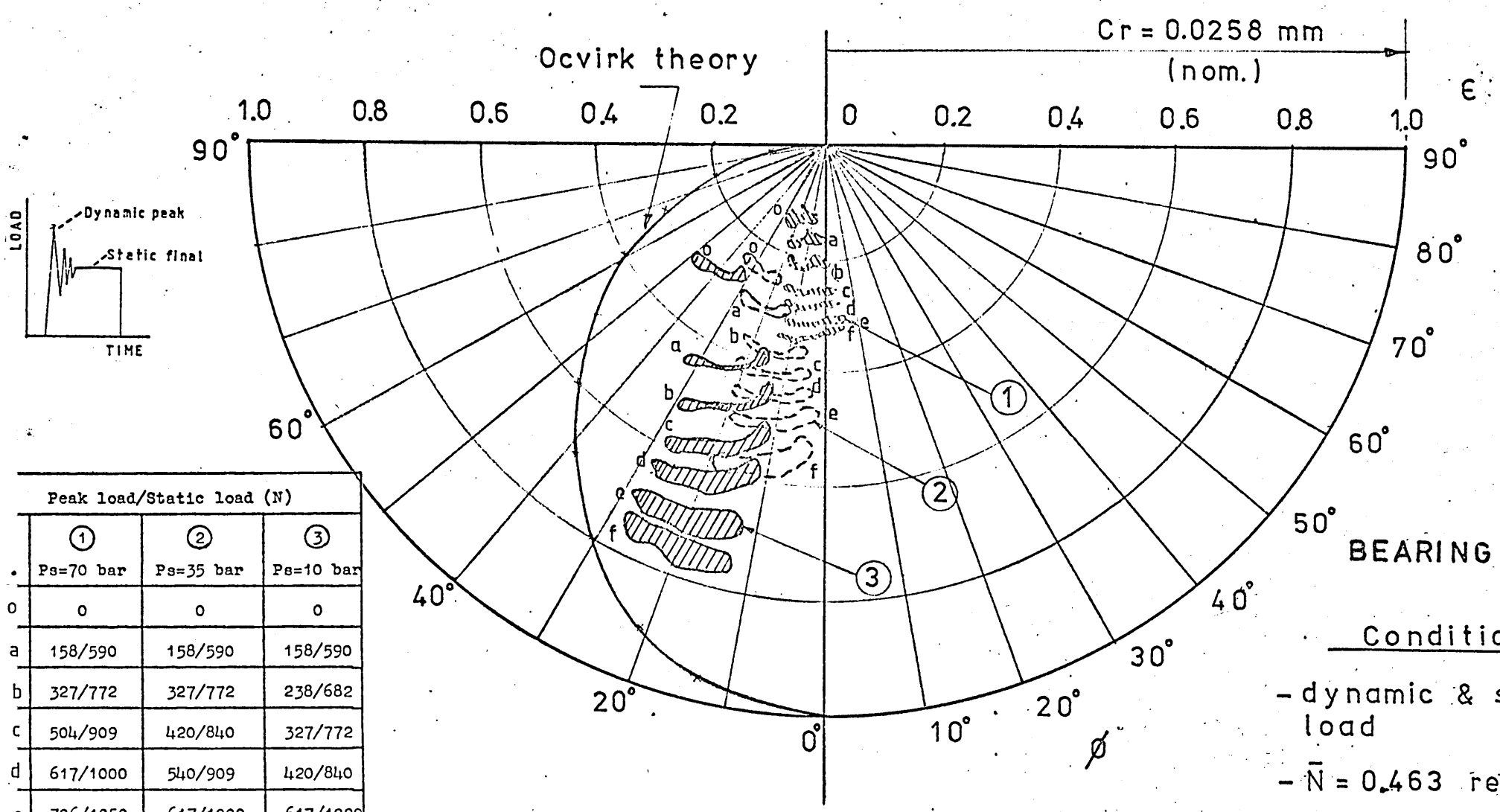

Peak load/Static load (N)			
•	① Ps=70 bar	② Ps=35 bar	③ Ps=10 bar
o	o	o	o
a	158/590	158/590	158/590
b	327/772	327/772	238/682
c	504/909	420/840	327/772
d	617/1000	540/909	420/840
e	706/1050	617/1000	617/1000
f	793/1100	793/1100	793/1100

BEARING TYP

Conditions :

- dynamic & stati load
- $\bar{N}$ = 0.463 rev/s

FIG. 5.70 ECCENTRICITY RATIO AGAINST ATTITUDE ANGLE.

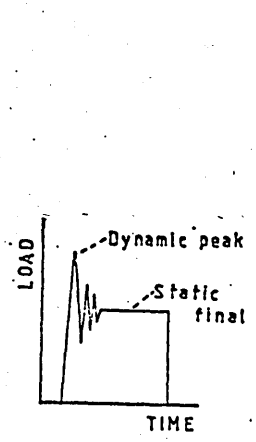

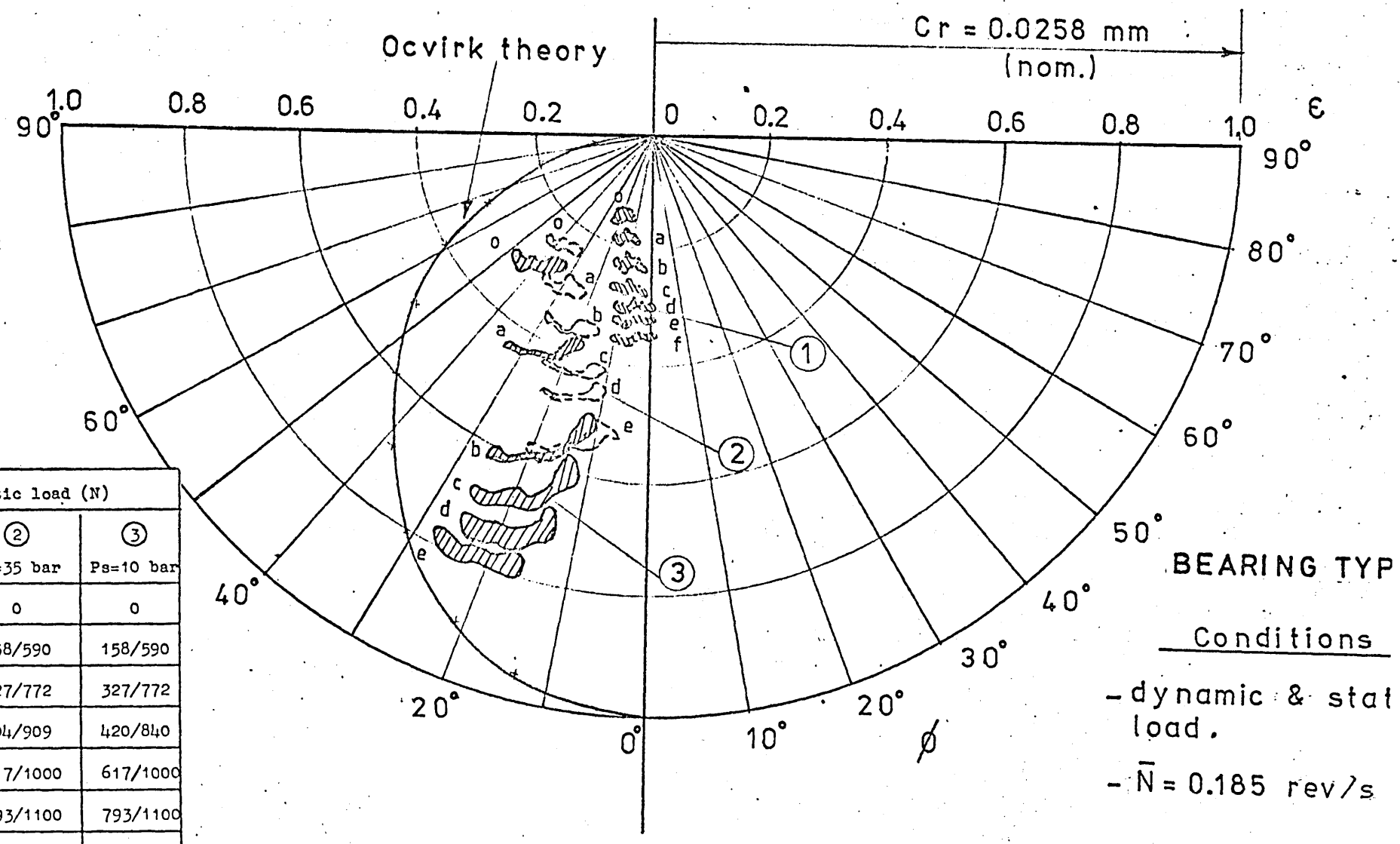

Peak load/Static load (N)			
tn.	① Ps=70 bar	② Ps=35 bar	③ Ps=10 bar
o	0	0	0
a	158/590	158/590	158/590
b	327/772	327/772	327/772
c	504/909	504/909	420/840
d	617/1000	617/1000	617/1000
e	706/1050	793/1100	793/1100
f	793/1100		

BEARING TYP

Conditions

- dynamic & stat load.
- $\bar{N}$ = 0.185 rev/s

FIG.5.71 ECCENTRICITY RATIO AGAINST ATTITUDE ANGLE.

CHAPTER 6. DISCUSSION AND CONCLUSIONS.

6.1 Discussion.

The object of this project has been to assess the performance of oil film bearings under the dynamic and kinematic conditions to be found in the crosspins of heavily loaded universal joints in rolling mill drivelines. Using a scaled down system many experimental results have been obtained for a wide range of operating conditions for three bearing types and represented in non-dimensional form. This section will discuss the results in general terms and also the implications for the possible use of the bearings within a rolling mill universal coupling. Each bearing will be considered in turn.

i) Bearing Type I, hydrodynamic with circumferential groove.

As expected, a bearing having only circumferential oil groove in the pressure zone is unsuitable for use under oscillating motion. This is clearly seen in fig. 5.17 where no oil film was generated at any oscillating frequency under a variety of loads and eccentricities of unity were observed for all results. This observation tends to support the design method by Barwell referred to earlier (7).

Although, boundary conditions had taken place for this type of bearing subjected to oscillating motion it can be said that this type of oil groove has produced a satisfactory oil film when the journal is rotated continuously under both

static and dynamic loads. Figs. 5.13, 5.14 and 5.15 show close agreement between equilibrium eccentricities for those results where the static and final dynamic loads are the same.

When plotted against Ocvirk Number these eccentricities show reasonable correlation with the theoretical curves, with a tendency to low eccentricities at low Δ and higher eccentricities at higher Δ. It is noticeable that the results produced at the lowest speed of 40 rev/min show eccentricities which are quite large and deviate from theory.

Figure 5.15 also shows the extent of the eccentricity overshoot found in the bearings under dynamic loads. Maximum overshoot of 30% is seen for low capacity number results having high load magnification factor (>3) on a low load (<300 N). The eccentricity overshoot reduces as bearing capacity number increases to the point where very little overshoot occurs for load magnification factors of less than 2 on static loads greater than 600 N.

Although the final positions of the bearing journal are very similar for both static and dynamic tests, the trajectories shown in fig. 5.13 do suggest a more vertical path for the dynamically loaded bearings than for those which were statically loaded. This seems to support the idea of a squeeze film effect with a pressure build up in the oil film at the early stages of the impact element of the dynamic load being sufficient to slow down the journal to a point where the equilibrium position is similar to that produced by a static load.

ii) Bearing Type II, hydrodynamic with axial grooves in the pressure zone and a circumferential groove.

Very similar results are observed for this bearing as for bearing I for continuous rotation. The bearing performed reasonably closely to the theoretical curves for static loads, with the eccentricity overshoot for dynamic load conditions, being somewhat greater than for the previous bearing. Figs. 5.39 and 5.40 show 100% overshoot for lightly loaded bearings with magnification factors in excess of 3 reducing to zero for heavily loaded bearings with magnification factors less than 2. However under oscillating motion the type II bearing was seen to perform reasonable well, the performance for both static and dynamic loads being summarised in fig. 5.47.

It is noticeable that the oscillating motion results always produce locus whose orbit is a closed loop which suggests that the shaft centre position is varying as the motion changes direction.

From fig. 5.47 can be seen that no eccentricity overshoot ocurred with the dynamically loaded oscillating motion tests irrespective of the load or the magnification factor. Another interesting feature of this oscillating bearing is the apparent insensitivity of eccentricity ratio to supply pressure variations which were seen to be significant when the bearing was rotating continuously. The only effect of supply pressure on the results with oscillating motion was to increase attitude angle at low loads (figs. 5.48, 5.49). The results also support the use of the average oscillating speed in formulating the duty parameter, since they correlate

quite well with the theoretical curves. This is true despite the fact that the theoretical prediction of bearing performance is based on the assumption of steady state conditions, which are not appropriate in this case.

On the other hand, when the bearing is under oscillating motion there is a tendency of some oil film generation as summarised in fig. 5.47 for both static and impact loads. It is interesting to see that no overshoot on eccentricity is noticeable when the shaft is under oscillating motion.

As it has already been shown that the duty parameter for a rolling mill universal coupling may be far in excess of the capabilities of the hydrodynamic bearing we cannot anticipate the use of this type of bearing in this application. However for the less severely loaded couplings it seems possible that such a bearing may be useful. In particular it does emphasize the importance of axial grooving in hydrodynamic bearings and illustrates that even in a bearing in which the relative motion between the journal and bearing is of an oscillatory nature, it is possible to obtain hydrodynamic conditions of lubrication,

iii) Bearing Type III, Slot-entry Hybrid Bearing.

As was expected from the literature survey this bearing proved to be superior in performance to the hydrodynamic bearings. In general terms the eccentricity ratios for equivalent loading conditions were much less with the hybrid bearing than with the other two..

For both continuous and oscillating motion for any particular combination of load, speed and supply pressure

no significant difference in eccentricity ratio was found between tests with static and dynamic loads.

Dealing with continuous motion results first, it is clear from fig. 5.54 that eccentricities increased marginally as the bearing speed reduced. Also an increase in supply pressure from 10 to 70 bar is seen to produce a reduction in eccentricity ratio ranging from around 70 % at low Ocvirk Number to about 40 % at high Ocvirk Number. It is also quite clear that this method of representation of the experimental information is inappropriate as most of the eccentricities are considerably lower than predicted. This is also true of the attitude angle results shown in fig. 5.56 which are considerably lower than those predicted by the hydrodynamic analysis.

Using the Fuller Number to represent the bearing variables (fig 5.55) produces a more consistent effect with regard to supply pressure. However some evidence of the hydrodynamic action of this bearing is shown within this graph as a reduction in eccentricity ratio with increase in speed. In comparing the hybrid with the hydrodynamic bearing type II for the same operating conditions, Fuller Number representation has been used in fig. 5.57 and shows clearly the benefits obtained with the hybrid bearing. A 50 % reduction in eccentricity ratio is obtained for a Fuller Number of 1.0 but perhaps more significant the rate of increase of the eccentricity ratio with the hydrodynamic bearing is far greater than with the hybrid bearing where the results tend towards a maximum eccentricity ratio for Fuller Numbers in excess of 1.0.

The results for tests with oscillating motion showed the reduction of eccentricity ratio with increasing supply pressure as summarised in fig. 5.68, but as with the hydrodynamic bearing type II, oscillating speed variation produced no discernible effect on eccentricity ratio for the hybrid bearing. One additional feature of this bearing was the small amplitude of oscillation of the shaft, which reduced significantly as the supply pressure increased. This is shown in figs. 5.70 and 5.71. In addition the low attitude angles shown in these figures together with the wide variations of the results contained in fig. 5.68 suggest again that the hydrodynamic analysis is inappropriate for the hybrid bearing.

The usefulness of the Fuller Number is shown for oscillating motion in fig. 5.69 where a single coherent curve is produced for all results having both speed and supply pressure variation. The advantage of the hybrid over the hydrodynamic type II bearing is also demostrated in this diagram with 25 % reduction in eccentricity ratio being evident. Comparing this graph with fig, 5.55 illustrates the deterioration of the hybrid bearing performance between continuous and oscillatory motion. Eccentricities are seen for continuous motion ranging between 55 % and 75 % of those found for oscillating motion.

It would appear therefore that the hybrid bearing offers genuine posibilities of satisfactory use within large rolling mill driveline universal couplings. In order to support the massive loads involved a large supply pressure would be required but the dynamic nature of the loads and the oscillating motion should be accomodated satisfactorily by the hybrid bearing.

6.2 Conclusions.

A test rig capable of simulating the parameters found in dynamically loaded oil-film bearings under both oscillating and continuous motion has been designed, built and used. For the operating conditions described in section 4.3. the following conclusions may be drawn from the experimental programme carried out for the three different oil film bearings:

1. Single circumferential groove hydrodynamic bearings have been unable to support either static or dynamic loads under oscillating motion.

2. Single circumferential groove hydrodynamic bearings running at constant speed have supported dynamic loads with some transient overshoot in eccentricity ratio, compared with equilibrium values.

3. Axial groove hydrodynamic bearings have supported static loads with oscillating motion and with the load parameter determined using the average cyclic velocity, comparisons with theoretical predictions based on continuous rotation are good.

4. Axial groove hydrodynamic bearings have supported dynamic loads under constant speed with transient overshoot in eccentricities.

5. Axial groove hydrodynamic bearings have supported both static and dynamic loads which when combined with oscillating motion give very similar eccentricities with no transient overshoot.

6. Slot-entry hybrid bearings have supported any combination of static and dynamic load under constant and oscillating motion with no transient overshoot of eccentricity ratio.

FURTHER WORK.

Extended trials of universal couplings in real rolling mill drive lines using hybrid or axially grooved hydrodynamic bearings is the appropriate next stage of development. It is probably better to use the latter, for a low capacity application, because of the low supply pressures involved. Suitable modification of a standard coupling should be straight-forward.

With regard to the experimental equipment used in the work described in this thesis, it would be useful to extend the range of operating conditions. This would enable the determination of the general limitations of the bearings under oscillating and dynamic loads. Consideration should be given to the effect of angle and speed of oscillation, impact compared with dynamic load and oil viscosity variation.

CHAPTER 7. LIST OF REFERENCES.

1. Kamii N. and Okuda H.: Universal joints applied to hot strip mill drives. Iron and Steel Eng. Dec.1975.

2. Society of Automotive Engineers: Universal joint and Driveshaft Design Manual, advances in Engineering series No. 7 1979.

3. Potgieter F. M. : Cardan universal joints applied to steel (industry) mill drives. Iron and Steel Eng. v 46 n3 Mar 1969.

4. Raimondi A. A. and Boyd J. : A solution for the finite journal bearing and its application to analysis and design: I, II, III. Trans. Ame. Soc. Lub. Engrs. 1958.

5. Dubois G. B. and Ocvirk F. W. : Short bearing approximation for full journal bearings. N.A.C.A. Technical note 2808, Oct, 1952.

6. Cole J.A. and Hughes C. J. : Oil flow and film extent in complete journal bearings. Proc. Conf. on Lubrication and Wear, paper 87 London 1957. Inst. Mech. Engrs.

7. Barwell F. T., Milne A. A. : Some experiments on oscillating bearings. The Institution of Engineers and Shipbuilders in Scotland, vol. 98, 1954 - 55.

8. Handbook on torsional vibration. Cambridge B. I. C. E. R. A.

9. Bigden J. : Universal joint design basics. Power Transm. Des. V 20 N 5, May 1978.

10. Potgieter F. M. : Germans develop unique universal joints. SAE Journal, Sept 1958.

11. Porter B. : The efficiencies of transmissions incorporating Hooke's joint. Engineer, 213, June 1962.

12. Hall A. S., Holowenko A. R.,: Shaum's outline of theory and problems of machine design, New York, Shaum Publishing Co., 1961.

13. Larke E. : The rolling of strip sheet and plate, 2nd. edition, Chapman & Hall, 1963.

14. Tzelikov A. Y. and Smirnov V. : Rolling mills, Pergamon Press, 1965.

15. Starling C. W. : The theory and practice of flat rolling, London Univ. Press 1962.

17. Furuya T., Kitashima S. : A newly developed 6 - high cold mill to solve shape problems. Proc. Conference, Cardiff, Sept. 1978. The Metals Society.

18. Fletcher J. : Universal joints applied to rolling mill main drives. M. Eng. Thesis, University of Sheffield, 1980.

19. Ford H., Hessenberg W. C. F. : Research on the rolling of strip. A symposium of selected papers, 1948 - 1958. The British Iron and Steel Research Association.

20 Thomas C. W. : Torque amplification and torsional vibration in large reversing mill drives. Iron and Steel Engineer V 46 n S May 1969.

21. Kashay A. M., Voelker F. C. : Dynamic Shock phenomena in rolling mills. Trans. ASME, Journal of Engineering for Industry, May 1979.

22. Molnar J. A. : Torque amplification factor (TAF) analyses and tests on two bar mill stands. Iron and Steel Engineer, Jan 1981.

23. Howard D. R. : Analysis of the rolling load traces of a 4 high hot reversing mill. Swiss aluminium AG. Davy - Loewy Internal report, 1967.

24. Rollet P. : The possibility of using bearing universal joints on rolling mill drives at Rotherham Works, B.S.C.- (internal report). 1978.

25. Koyo Seiko Catalogue : New heavy duty drive shaft. No. 231 E, 1976.

26. Patterson C., Fletcher J. D. : Vibration aspects of rolling mill horizontal drives with reference to recent coupling development. 2nd. Int. Conf. on Vibrations in Rotating Machinery. Cambridge, U. K. I. Mech. Eng. 1980.

27. Howard D. R. : Study of universal joints for Anchor secondary blooming mill, Davy - Loewy Internal report Feb. 1979.

28. Reynolds O. : Philosophical Transactions of the Royal Society, London, Vol. 177. 1886.

29. Czichos H., Tribology : A systems approach to the science and technology of friction, Lubrication and Wear. Elsevier SCI. Pub. Co. 1978.

30. Barwell F. T. : Bearing Systems, Principles and Practice. Oxford Univ. Press, 1979.

31. Sommerfeld A. : The earlier history of the hydrodynamic theory of lubrication friction. Proc. Gen. Disc. of Lubrication and Lubricants. Inst. of Mech. Engrs. London, 1937.

32. Gumbel L. and Everling E. : Reinbug und Schmierung im Maschinenbau, M. Krain, 1925.

33. Michell A. G. N. : Progress in fluid film lubrication, Trans. ASME. 51, 1929.

34. Swift H. W. : Fluctuating loads in sleeve bearings, journal of the Instn. of Civil Engrs. Vol.5 1937.

35. Burwell J. T. : The calculeted performance of dynamically loaded sleeve bearings, J. Appl. Mech. Vol 69 1947.

36. Burwell J. T. : The calculated performance of dynamically loaded sleeve bearings II, J. Appl. Mech. Vol 71, 1949.

37. Burwell J. T. : The calculated performance of dynamically loaded sleeve bearings III, J. Appl. Mech. Vol. 73, 1951.

38. Hahn H. W. : Dynamically loaded journal bearing finite length, Proc. Conf. on Lubrication and Wear P. 100 (Instn. Mech. Engr., London, 1957.)

39. Hornsnell R. and Mc Callion H. : Prediction of journal bearing characteristics under static and dynamic loading,

Proc. Conf. on Lubrication and Wear, 1963 (Instn. Mech. Engrs. London).

40. Lloyd T., Horsnell R. and Mc Callion H. : An investigation into the performance of dynamically loades journal bearings : Theory Proc. Instn. Mech. Engrs. 1966 - 1967 Vol. 181 pt. 3B.

41. Middleteon V., Dudley B. R. and Mc Callion H. : An investigation into the performance of dinamically journal bearing : Experiment. Proc. Instn. Mech. Engrs. 1966 - 1967. Vol. 181 pt.3B.

42. Archibald F. : Load capacity and time relations for squeeze films. Trans. ASME vol. 78, 1956.

43. Radermacher K. : Experimental investigation into cylindrical plain bearing under loads varying in magnitude and direction, Lubrication and Wear Conv. 1964 (Instn. Mech. Engrs. London).

44. Carl Th. E. : An experimental investigation of a cylindrical journal bearing under constant and sinusoidal load, Lubrication and Wear Conv. 1964 (Instn. Mech. Engrs. London).

45. Simons E. M. : Hydrodynamic lubrication of cydically loaded bearings. Trans. ASME, 72, 1950.

46. White D. C. : Squeeze film journal bearings, Ph. D. Thesis, Cambridge University, 1970.

47. Jakobsen K. and Christensen H. : Performance of oscillating bearings, Proc. Instn. Mech. Engrs. 1968. Vol. 183 Pt. 3P.

48. Blount E. and De Guerin D. : The importance of surface finish, loaded area conformity, and operating temperature in small end plain bearings for high duty two-stoke engines, Conf. Lubrication and Wear 1957. (Instn. Mech. Engrs. London).

49. Glaeser W. A. and Dufrane K. F. : Performance of heavily loaded oscillatory journal bearings, ASLE. Trans. Vol 20, 4, 1976.

50. Fogg A. and Jakeman C. : The friction of oscillating bearing. Dept. of Scientific and Industrial Research 3. Lubrication Research. (1935).

51. Wilcock D. F. and Booser E. R. : Bearing design and application. Mc Graw Hill, N. Y. 1957.

52. Rowe W. R., Koshal D., Stout K. J. : Slot - entry bearings for hybrid operation. J. Mech. Engrg. Science, 18, 2, 1976.

53. Sir W. B. Hardy : The analysis of commercial lubricating oils by physical methods. Lubrication Research Technical paper No. 1.

54. Neale M. J. (editor) : Tribology Handbook, Butterworths, London 1973.

55. Cameron A. : The principles of lubrication, Longmans, London 1966.

56. Woolacott R. G. : Hydrodynamic journal bearing performance at high speed under steady load. Proc. Instn. Mech. Engrs. Vol 180, pt. 3 K, 1966.

57. Fuller D. D. : Hydrostatic Lubrication Machine Design, Pt 1 (July 1947). Pt 2 (July 1947), Pt 3 (Oct 1947).

58. Rowe W. B. : Hydrostatic bearing design. Tribology 2, No. 1, Feb 1969.

59. Pinkus O. and Sterlincht : Theory of hydrodynamic lubrication, Mc Graw Hill, 1961.

60. Dee, C. W. and Shires G. L. : The current state of the art fluid bearings with discrete slot inlets. Trans. ASME J. Lub. Tech. paper 71 - lub - L, 1971.

61. Anon : Calculation methods for steadily loaded pressure fed hydrodynamic journal bearings. Engng. Sciences Data Unit, item 66023, Instn. Mech. Engrs. 1966.

62. Horstmann Gouge Ltd., catalogue : Fluid bearings externally pressurized journal and journal thrust.

63. Ransome Hoffmann Pollard Ltd. (RHP) catalogue : Roller bearing technical information.

64. Reich K.: Universal coupling analysis, graphic computer program, Sheffield Polytechnic, undergraduate report, 1980.

65. Mobil Oil Co. Ltd, catalogue : Mobil product data sheet. Mobil DTE named and double lettered oils, code No. 8530, Oct 1976.

APPENDICES

(A) Results of tests on bronze-bearings.

Bearing Type I.

(B) Results of tests on bronze-bearings.

Bearing Type II.

(C) Results of tests on hybrid-bearings.

Bearing Type III.

(D) Detail drawings.

(D1) Oscillating bearing test rig.

(D2) Test rig frame.

(D3) Test shaft.

(D4) Test bearing.

(D5) Bearing housing.

(D6) Sliding plates.

(D7) Cylinder base plate.

(D8) Column.

(D9) Column-support.

(D10) Bush.

(D11) Secondary shaft.

(D12) Pillow-blocks base.

(D13) Rocker arm.

(D14) Connecting rod.

(D15) Crank.

(D16) Plan location.

TABLE A 1

RESULTS OF TESTS ON BRONZE - BEARINGS.

Parameters:

1) Load: Dynamic & Static

2) Motion: Continuous N = 100 (rev/min)

3) Geometry: Cd = 0.050 mm (0.002 inch)
Type of grooves: Circumferential

4) Lubrication: Mobil-oil "DTE" (viscosity 300 cS at 25° C)
Inlet oil Pressure: P_s = 2 (bar)

Load W (N)	Capacity Number 1/Δ	Δ	Shaft Displacement (μm) Static e_o	Dynamic e_c	Dynamic e_{max}	Eccentricity Ratio Static ϵ_o	Dynamic ϵ_o	Dynamic ϵ_{max}
158	1.15	0.87	8.9	8.9	11.2	0.35	0.35	0.45
238	0.76	1.31	11.2	11.2	13.5	0.44	0.44	0.54
327	0.56	1.79	13.7	13.7	16.9	0.54	0.54	0.67
420	0.43	2.3	16.5	16.5	18.5	0.65	0.65	0.73
504	0.37	2.7	18.0	18.0	19.5	0.71	0.71	0.77
617	0.29	3.4	18.5	18.5	19.8	0.73	0.73	0.78
706	0.26	3.8	19.3	19.3	20.6	0.76	0.76	0.81
795	0.23	4.4	19.8	19.8	19.3	0.78	0.78	0.76
(Temperature:		21.2°C)						

TABLE A 2

RESULTS OF TESTS ON BRONZE - BEARINGS.

Parameters:

1) Load: Dynamic & Static

2) Motion: Continuous N = 70 (rev/min)

3) Geometry: Cd = 0.050 mm (0.002 inch)

Type of grooves: Circumferential

4) Lubrication: Mobil-oil "DTE" (viscosity 300 cS at 25° C)

Inlet oil Pressure: P_s = 2 (bar)

Load W (N)	Capacity Number 1/Δ	Δ	Shaft Displacement (μm) Static e_o	Dynamic e_o	Dynamic e_{max}	Eccentricity Ratio Static ϵ_o	Dynamic ϵ_o	Dynamic ϵ_{max}
158	0.80	1.25	10.4	10.4	13.7	0.41	0.41	0.54
238	0.53	1.88	13.5	13.5	16.5	0.53	0.53	0.65
327	0.39	2.58	16.3	16.3	18.5	0.64	0.64	0.73
420	0.30	3.32	18.5	18.5	19.5	0.73	0.73	0.77
504	0.25	3.98	19.8	19.8	19.8	0.78	0.78	0.78
617	0.20	4.87	20.3	20.3	20.8	0.80	0.80	0.82
706	0.18	5.57	21.8	21.8	21.8	0.86	0.86	0.86
795	0.16	6.30	21.1	21.1	20.8	0.83	0.83	0.82
(Temperature:		21.5° C)						

T A B L E A 3

RESULTS OF TESTS ON BRONZE - BEARINGS.

Parameters:

1) Load: Dynamic & Static

2) Motion: Continuous N = 40 (rev/min)

3) Geometry: Cd = 0.050 mm (0.002 inch)
Type of grooves: Circumferential

4) Lubrication: Mobil-oil "DTE" (viscosity 300 cS at 25° C)
Inlet oil Pressure: P_s = 2 (bar)

Load W (N)	Capacity Number 1/Δ	Δ	Shaft Displacement (μm) Static e_o	Dynamic e_o	Dynamic e_{max}	Eccentricity Ratio Static ϵ_o	Dynamic ϵ_o	Dynamic ϵ_{max}
158	0.45	2.21	18.3	18.3	20.3	0.72	0.72	0.80
238	0.30	3.3	19.5	19.5	21.8	0.77	0.77	0.86
327	0.22	4.6	22.6	22.6	23.6	0.89	0.89	0.93
420	0.17	5.9	23.1	23.1	23.6	0.91	0.91	0.93
504	0.14	7.1	23.9	23.9	24.0	0.94	0.94	0.94
617	0.12	8.6	24.9	24.9	25.4	0.98	0.98	1.0
706	0.10	9.8	25.4	25.4	25.4	1.0	1.0	1.0
795	0.09	11.1	25.4	25.4	25.4	1.0	1.0	1.0
(Temperature:		21.4° C)						

TABLE A4

RESULTS OF TESTS ON BRONZE - BEARINGS.

Parameters:

1) Load: Dynamic & Static

2) Motion: Oscillating N = - (rev/min)

$\bar{N}$ = 0.463 (rev/s)

3) Geometry: Cd = 0.050 mm (0.002 inch)

Type of grooves: Circumferential

4) Lubrication: Mobil-oil "DTE" (viscosity 300 cS at 25° C)

Inlet oil Pressure: P_s = 3 (bar)

Load W (N)	Capacity Number $1/\bar{\Delta}$	$\bar{\Delta}$	Shaft Displacement (μm) Static		Shaft Displacement (μm) Dynamic		Eccentricity Ratio Static		Eccentricity Ratio Dynamic	
			e_o	e_{max}	e_o	e_{max}	ϵ_o	ϵ_{max}	ϵ_o	ϵ_{max}
140	0.69	1.43	25.9				1.0			
210	0.46	2.14	25.9				1.0			
290	0.34	2.96	25.9				1.0			
410	0.24	4.18	25.9				1.0			
500	0.19	5.1	25.9				1.0			
620	0.16	6.3	25.9				1.0			
700	0.14	7.14	25.9				1.0			
770	0.12	7.91	25.9				1.0			
(Temperature:		21.8° C)								

TABLE B 1

RESULTS OF TESTS ON BRONZE - BEARINGS.

Parameters:

1) Load: Dynamic & Static

2) Motion: Continuous N = 100 (rev/min)

3) Geometry: Cd = 0.038 mm (0.00153 inch)

Type of grooves: Circumferential & Axial

4) Lubrication: Mobil-oil "DTE" (viscosity 300 cS at 25° C)

Inlet oil Pressure: P_s = 3 (bar)

Load W (N)	Capacity Number 1/Δ	Δ	Shaft Displacement (μm) Static e_o	Dynamic e_o	Dynamic e_{max}	Eccentricity Ratio Static ϵ_o	Dynamic ϵ_o	Dynamic ϵ_{max}
158	2.0	0.50	6.6	6.6	7.8	0.34	0.34	0.41
238	1.31	0.76	8.3	8.3	10.1	0.43	0.43	0.53
327	1.0	1.00	10.7	10.7	12.2	0.55	0.55	0.63
420	0.75	1.34	11.9	11.9	12.9	0.63	0.63	0.67
504	0.62	1.61	12.9	12.9	13.9	0.66	0.66	0.72
617	0.51	1.87	13.7	13.7	14.4	0.73	0.73	0.75
706	0.44	2.26	14.4	14.4	15.0	0.76	0.76	0.79
795	0.39	2.54	14.8	14.8	15.0	0.78	0.78	0.79
(Temperature:		22.1° C)						

RESULTS OF TESTS ON BRONZE - BEARINGS.

Parameters:

1) Load: Dynamic & Static

2) Motion: Continuous N = 100 (rev/min)

3) Geometry: Cd = 0.038 mm (0.00153 inch)

Type of grooves: Circumferential & Axial

4) Lubrication: Mobil-oil "DTE" (viscosity 300 cS at 25° C)

Inlet oil Pressure: P_s = 10 (bar)

Load W (N)	Capacity Number $1/\Delta$	Δ	Shaft Displacement (μm) Static e_o	Dynamic e_o	Dynamic e_{max}	Eccentricity Ratio Static ϵ_o	Dynamic ϵ_o	Dynamic ϵ_{max}
158	2.0	0.50	2.5	2.5	4.8	0.13	0.13	0.25
238	1.31	0.76	4.3	4.3	7.9	0.22	0.22	0.40
327	1.0	1.00	7.4	7.4	10.4	0.38	0.38	0.53
420	0.75	1.34	9.6	9.6	11.2	0.49	0.49	0.59
504	0.62	1.61	10.4	10.4	11.2	0.55	0.55	0.59
617	0.51	1.97	12.8	12.8	13.2	0.67	0.67	0.69
706	0.44	2.26	13.9	14.0	13.9	0.72	0.72	0.72
795	0.39	2.54	14.4	14.4	14.4	0.76	0.76	0.76
(Temperature:		22.4° C)						

TABLE B 3

RESULTS OF TESTS ON BRONZE - BEARINGS.

Parameters:

1) Load: Dynamic & Static

2) Motion: Continuous N = 70 (rev/min)

3) Geometry: Cd = 0.038 mm (0.00153")

Type of grooves: Circumferential & Axial

4) Lubrication: Mobil-oil "DTE" (viscosity 300 cS at 25° C)

Inlet oil Pressure: P_s = 3 (bar)

Load W (N)	Capacity Number 1/Δ	Δ	Shaft Displacement (μm) Static e_o		Dynamic e_o	e_{max}	Eccentricity Ratio Static ϵ_o		Dynamic ϵ_o	ϵ_{max}
158	1.39	0.72	5.3		5.3	8.4	0.28		0.28	0.43
238	0.91	1.1	8.1		8.1	10.2	0.42		0.42	0.52
327	0.66	1.5	10.4		10.4	11.9	0.54		0.54	0.62
420	0.52	1.9	11.4		11.4	12.7	0.59		0.59	0.65
504	0.43	2.3	11.9		11.9	12.6	0.62		0.62	0.66
617	0.36	2.8	12.7		12.7	13.2	0.65		0.65	0.69
706	0.31	3.2	13.2		13.2	14.0	0.68		0.68	0.73
793	0.27	3.6	14.5		14.5	10.4	0.72		0.72	0.76
(Temperature:		22.7°	C)							

RESULTS OF TESTS ON BRONZE - BEARINGS.

Parameters:

1) Load: Dynamic & Static

2) Motion: Continuous N = 40 (rev/min)

3) Geometry: Cd = 0.038 mm (0.00153 inch)
Type of grooves: Circumferential & Axial

4) Lubrication: Mobil-oil "DTE" (viscosity 300 cS at 25° C)
Inlet oil Pressure: P_s = 3 (bar)

Load W (N)	Capacity Number 1/Δ	Δ	Shaft Displacement (μm) Static e_o		Dynamic e_o	Dynamic e_{max}	Eccentricity Ratio Static ϵ_o	Dynamic ϵ_o	Dynamic ϵ_{max}
158	0.79	1.26	9.4		9.4	11.7	0.48	0.48	0.60
238	0.52	1.9	12.4		12.4	12.9	0.64	0.64	0.67
327	0.38	2.6	12.4		12.4	13.5	0.64	0.64	0.69
420	0.29	3.36	13.7		13.7	14.5	0.71	0.71	0.75
504	0.25	4.0	14.0		14.0	14.0	0.72	0.72	0.72
617	0.20	4.9	15.2		15.2	15.2	0.79	0.79	0.79
706	0.18	5.6	16.0		16.0	16.0	0.83	0.83	0.83
795	0.16	6.3	15.7		15.7	15.7	0.81	0.81	0.81
(Temperature:		22.5° C)							

TABLE B 5

RESULTS OF TESTS ON BRONZE - BEARINGS.

Parameters:

1) Load: Dynamic & Static

2) Motion: Oscillating $\bar{N}$ = 0.465 rev/s

3) Geometry: Cd = 0.038 mm (0.00153 inch)
Type of grooves: Circumferential & Axial

4) Lubrication: Mobil-oil "DTE" (viscosity 300 cS at 25° C)
Inlet oil Pressure: P_s = 10 (bar)

Load W (N)	Capacity Number $1/\bar{\Delta}$	$\bar{\Delta}$	Shaft Displacement (μm) Static e_o	Static e_{max}	Dynamic e_o	Dynamic e_{max}	Eccentricity Ratio Static ϵ_o	Static ϵ_{max}	Dynamic ϵ_o	Dynamic ϵ_{max}
158	0.45	2.2	12.7		12.7		0.65		0.65	
238	0.30	3.3	13.2		13.2		0.68		0.68	
327	0.22	4.6	14.0		14.0		0.72		0.72	
420	0.17	5.8	14.5		14.5		0.73		0.73	
504	0.14	7.1	15.2		15.2		0.79		0.79	
617	0.11	8.6	16.0		16.0		0.83		0.83	
706	0.10	9.8	16.5		16.5		0.85		0.85	
795	0.09	11.1	16.5		16.5		0.85		0.85	
(Temperature: 21.8° C)										

TABLE B 6

RESULTS OF TESTS ON BRONZE - BEARINGS.

Parameters:

1) Load: Dynamic & Static

2) Motion: Oscillating $\bar{N}$ = 0.185 rev/s

3) Geometry: Cd = 0.038 mm (0.00153 inch)

Type of grooves: Circumferential & Axial

4) Lubrication: Mobil-oil "DTE" (viscosity 300 cS at 25° C)

Inlet oil Pressure: P_s = 10 (bar)

Load W (N)	Capacity Number $1/\bar{\Delta}$	$\bar{\Delta}$	Shaft Displacement (μm) Static e_o	Static e_{max}	Dynamic e_o	Dynamic e_{max}	Eccentricity Ratio Static ϵ_o	Static ϵ_{max}	Dynamic ϵ_o	Dynamic ϵ_{max}
158	0.23	4.4	11.7		11.9		0.62		0.62	
238	0.15	6.6	12.2		12.4		0.64		0.64	
327	0.11	9.1	13.5		13.5		0.69		0.69	
420	0.08	11.8	14.0		14.0		0.72		0.72	
504	0.07	14.1	14.6		14.6		0.75		0.75	
617	0.06	17.3	15.0		15.0		0.77		0.77	
706	0.05	19.7	15.5		15.5		0.80		0.80	
795	0.04	22.3	16.0		16.0		0.83		0.83	
(Temperature:		22.1° C)								

TABLE C 1

RESULTS OF TESTS ON HYBRID - BEARINGS.

Parameters:

1) Load: Dynamic

2) Motion: Continuous N = 100 (rev/min)

3) Geometry: Cd = 0.050 mm (0.002 inch)

Type of bearing: Slot - Entry

4) Lubrication: Mobil-oil "DTE" (Viscosity 300 cS at 25° C)

Inlet oil Pressure: P_1 = 70 (bar)

P_2 = 35 (bar)

P_3 = 10 (bar)

Load W (N)	Capacity Number $\bar{W}$	Δ	Shaft Displacement (μm) e_1	e_2		Eccentricity Ratio ϵ_1	ϵ_2	
158	2.0	0.5	1.5	7.1		0.06	0.28	
238	1.31	0.76	2.5	8.1		0.10	0.32	
327	1.0	1.0	3.8	8.9		0.15	0.35	
420	0.75	1.34	5.1	9.1		0.20	0.36	
504	0.62	1.61	6.1	9.9		0.24	0.39	
617	0.51	1.97	6.8	10.6		0.27	0.42	
706	0.44	2.26	7.9	10.9		0.31	0.43	
793	0.39	2.54	8.6	11.4		0.34	0.45	

TABLE C 2

RESULTS OF TESTS ON HYBRID - BEARINGS.

Parameters:

1) Load: Dynamic

2) Motion: Continuous N = 70 (rev/min)

3) Geometry: Cd = 0.050 mm (0.002 inch)

Type of bearing: Slot - Entry

4) Lubrication: Mobil-oil "DTE" (Viscosity 30 cS at 25° C)

Inlet oil Pressure: P_1 = 70 (bar)

P_2 = 35 (bar)

P_3 = 10 (bar)

Load W (N)	Capacity Number		Shaft Displacement (μm)			Eccentricity Ratio		
	$\bar{W}$	Δ	e_1	e_2		ϵ_1	ϵ_2	
158	1.37	0.73	3.5	9.4		0.14	0.37	
238	0.91	1.1	4.3	9.9		0.17	0.39	
327	0.66	1.5	5.6	11.2		0.22	0.44	
420	0.52	1.93	7.3	11.9		0.29	0.47	
504	0.43	2.32	8.1	12.9		0.32	0.51	
617	0.35	2.84	9.4	14.2		0.37	0.56	
706	0.31	3.25	10.6	15.2		0.42	0.60	
795	0.27	3.66	11.7	16.5		0.46	0.65	

T A B L E C 3

RESULTS OF TESTS ON HYBRID - BEARINGS.

Parameters:

1) Load: Dynamic & Static

2) Motion: Oscillating $N =$ (rev/min)

$\bar{N} = 0.463$ (rev/s)

3) Geometry: $Cd = 0.050$ mm (0.002 inch)

Type of bearing: Slot - Entry

4) Lubrication: Mobil-oil "DTE" (Viscosity 300 cS at 25° C)

Inlet oil Pressure: $P_1 = 70$ (bar)

$P_2 = 35$ (bar)

$P_3 = 10$ (bar)

Load W (N)	Capacity Number $\bar{W}$	$\bar{\Delta}$	Shaft Displacement (μm) e_1	e_2	e_3	Eccentricity Ratio ϵ_1	ϵ_2	ϵ_3
158	0.55	1.81	4.5	7.9	10.9	0.18	0.31	0.43
238	0.36	2.72	5.1	8.6	12.4	0.20	0.34	0.49
327	0.27	3.74	5.3	9.6	13.2	0.21	0.38	0.52
420	0.21	4.8	6.1	10.4	15.7	0.24	0.41	0.62
504	0.17	5.76	6.6	11.4	17.0	0.26	0.45	0.67
617	0.14	7.06	7.1	12.7	17.8	0.28	0.50	0.70
706	0.12	8.08	7.9	13.5	18.3	0.31	0.53	0.72
793	0.11	9.1	8.4	14.5	18.8	0.33	0.57	0.74

T A B L E C 4

RESULTS OF TESTS ON HYBRID - BEARINGS.

Parameters:

1) Load: Dynamic

2) Motion: Oscillating $N = -$ (rev/min)

$\bar{N} = 0.185$ (rev/s)

3) Geometry: Cd = 0.050 mm (0.002 inch)

Type of bearing: Slot - Entry

4) Lubrication: Mobil-oil "DTE" (Viscosity 300 cS at 25° C)

Inlet oil Pressure: $P_1 = 70$ (bar)

$P_2 = 35$ (bar)

$P_3 = 10$ (bar)

Load W (N)	Capacity Number $\bar{W}$	$\bar{\Delta}$	Shaft Displacement (μm) e_1	e_2	e_3	Eccentricity Ratio ϵ_1	ϵ_2	ϵ_3
158	0.22	4.52	4.6	7.6	10.7	0.18	0.30	0.42
238	0.15	6.8	5.1	8.1	12.4	0.20	0.32	0.49
327	0.11	9.3	5.6	9.1	14.7	0.22	0.36	0.58
420	0.08	12.0	6.1	10.2	17.0	0.24	0.40	0.67
504	0.07	14.4	6.8	10.9	18.0	0.27	0.43	0.71
617	0.057	17.6	7.6	11.9	18.8	0.30	0.47	0.74
706	0.049	20.2	8.1	12.9	19.3	0.32	0.51	0.76
793	0.044	22.7	8.9	14.2	20.0	0.35	0.56	0.79

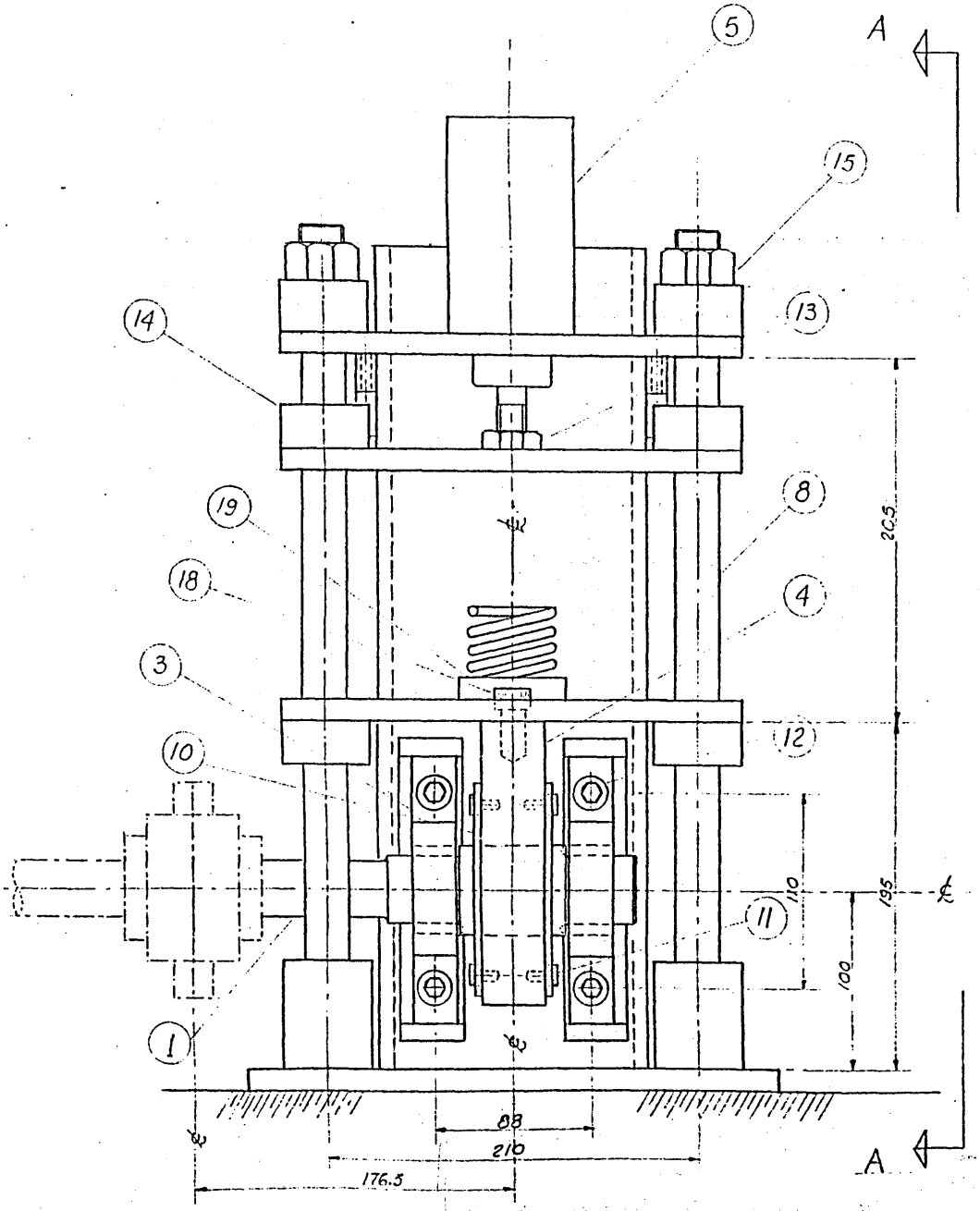

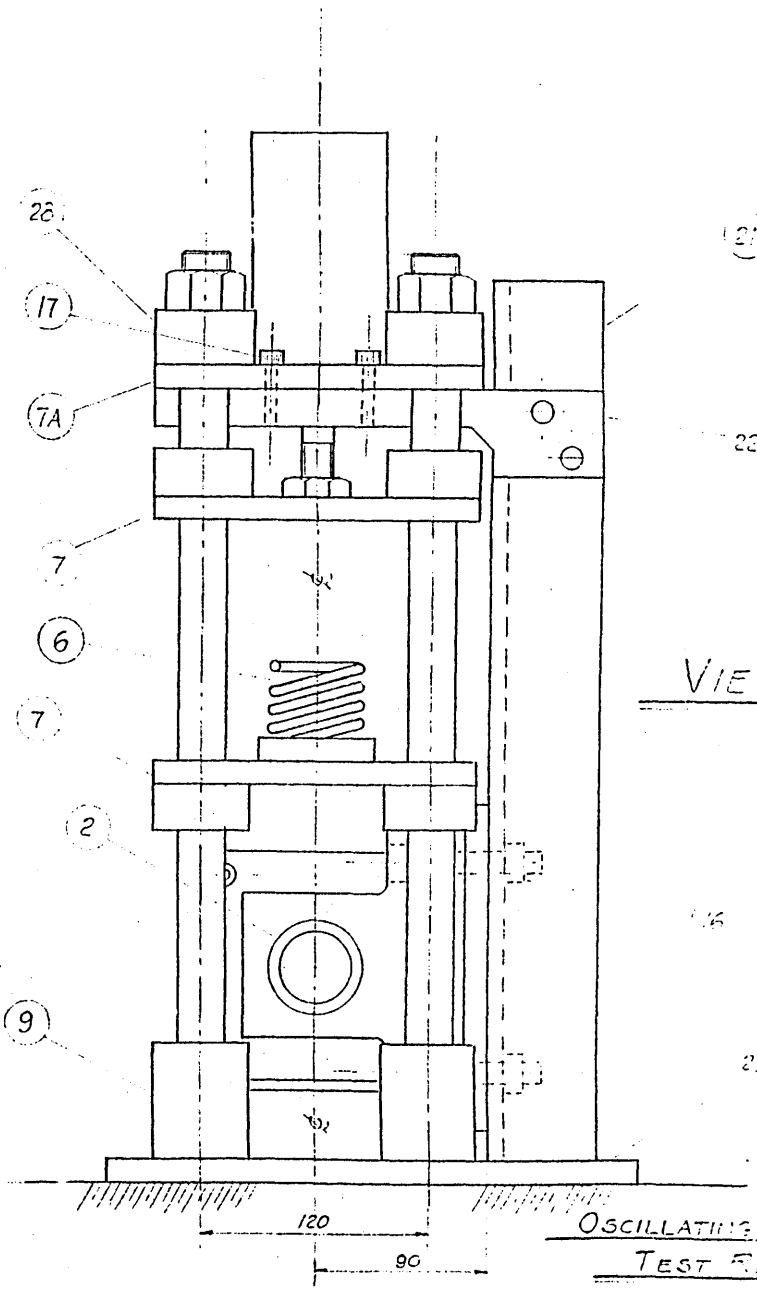

VIEW A

OSCILLATING BEAM TEST RIG.

SCALE: 1:2

DIMENSIONS: mm

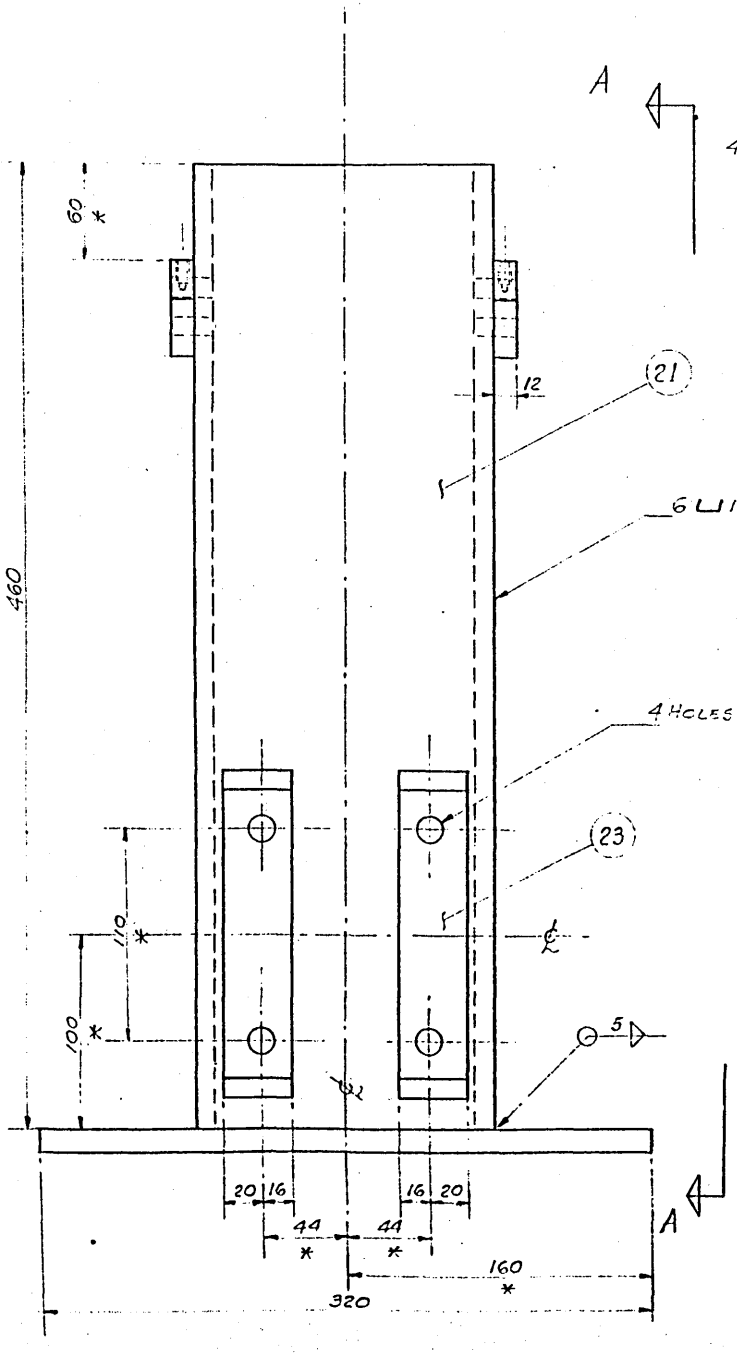

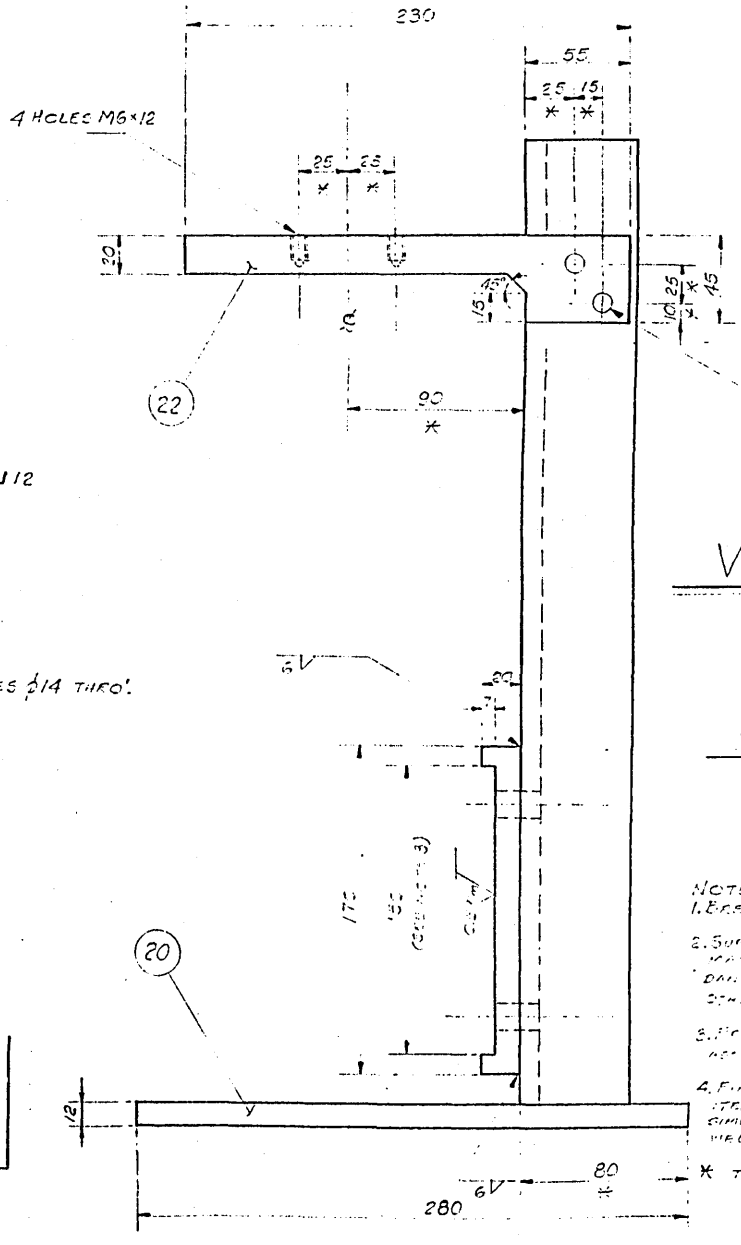

TEST RIG

SCALE : 1 : 2

DIMENSIONS : m

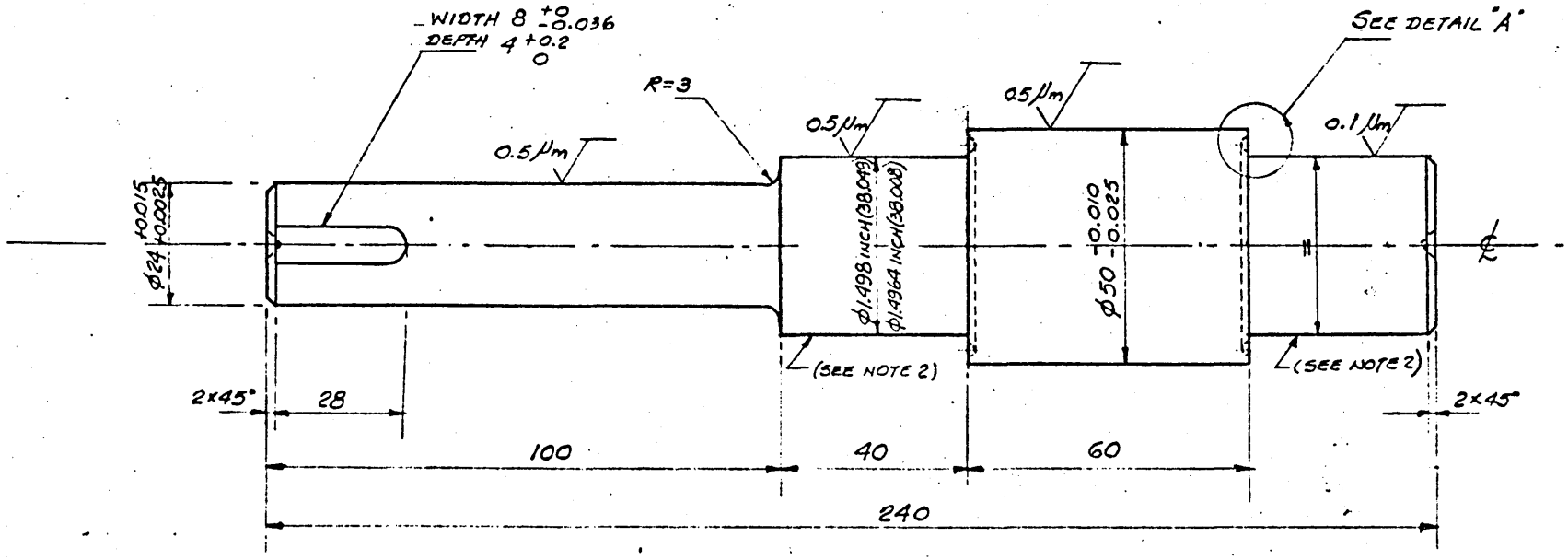

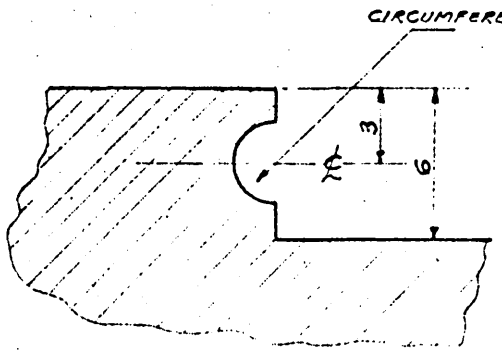

DETAIL "A"

MATL. EN-8

NOTE:

1. BREAK ALL CORNER
2. CASE - HARDENED 260-290 BHN.

PART 1 - TEST SHAFT.

(1 REQ.)

DIMENSIONS : mm

J. PEREZ - JU

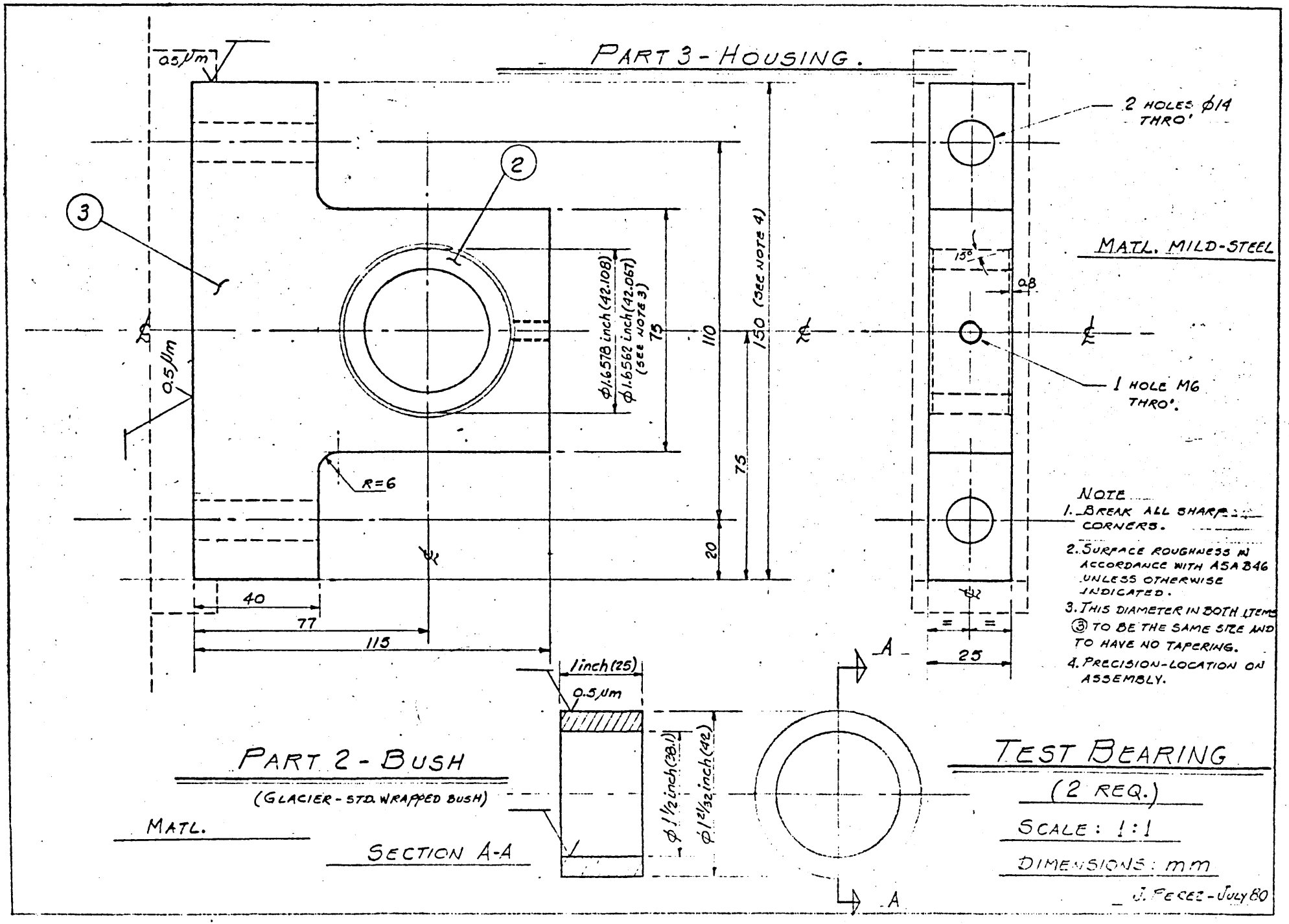
PART 3 - HOUSING.
0.5 µm
2
3
Φ1.6578 inch (42.108)
Φ1.6562 inch (42.067)
(SEE NOTE 3)
75
110
150 (SEE NOTE 4)
75
20
0.5 µm
R=6
40
77
115
2 HOLES Φ14 THRO'
15°
Φ8
1 HOLE M6 THRO'.
25
MATL. MILD-STEEL
NOTE
1. BREAK ALL SHARP CORNERS.
2. SURFACE ROUGHNESS IN ACCORDANCE WITH ASA B46 UNLESS OTHERWISE INDICATED.
3. THIS DIAMETER IN BOTH ITEMS (3) TO BE THE SAME SIZE AND TO HAVE NO TAPERING.
4. PRECISION-LOCATION ON ASSEMBLY.
A
A
1 inch (25)
0.5 µm
Φ1 1/2 inch (38.1)
Φ1 21/32 inch (42)
PART 2 - BUSH
(GLACIER - STD. WRAPPED BUSH)
MATL.
SECTION A-A
TEST BEARING
(2 REQ.)
SCALE : 1:1
DIMENSIONS : mm
J. FECEZ - July 80

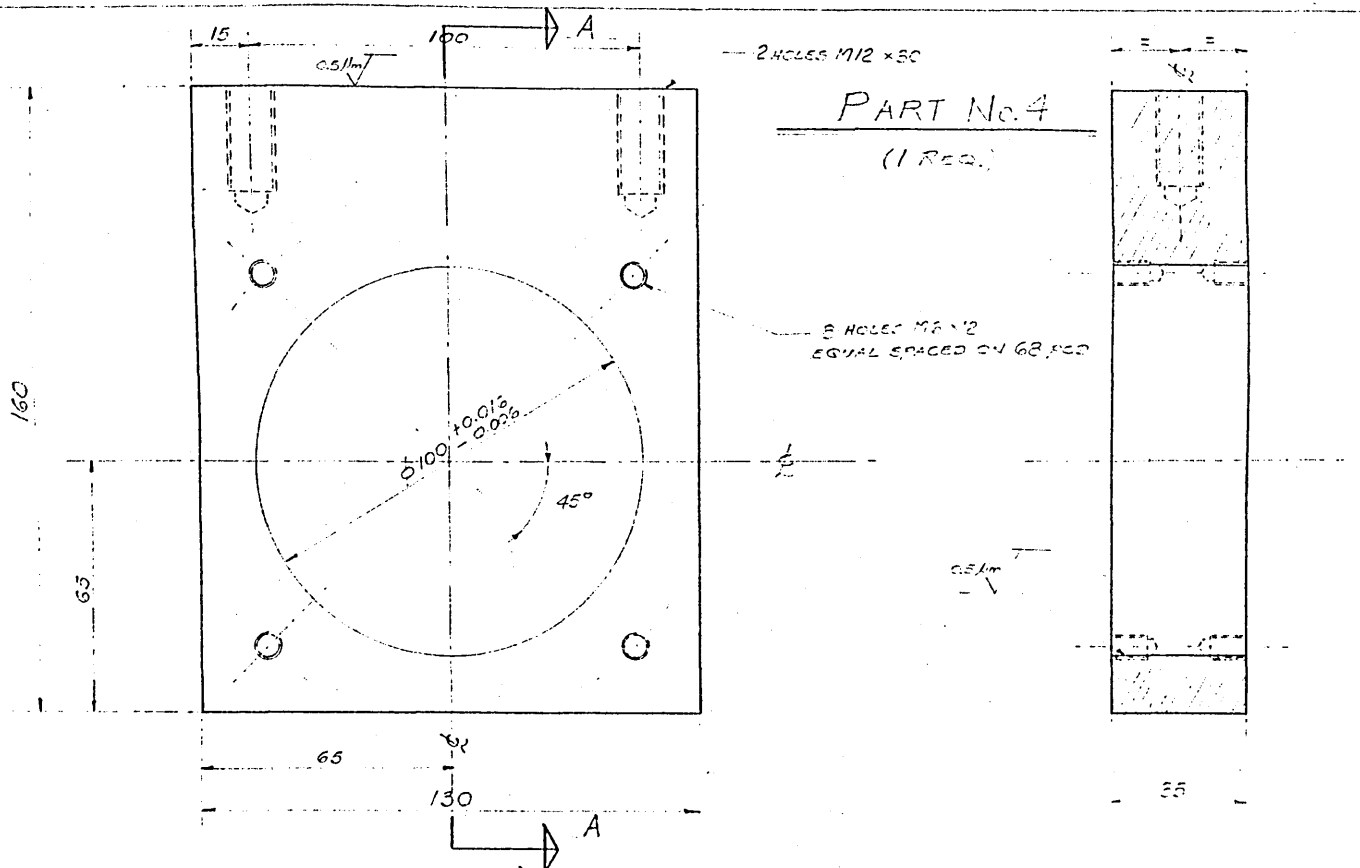
15
100
A
0.5/1m
2 HOLES M12 × 30
PART No. 4
(1 REQ.)
8 HOLES M8 × 12
EQUAL SPACED ON 68 P.C.D
160
Ø100 +0.01 -0.02
45°
65
0.5/1m
SECTION
65
130
35
A
B
PART No. 10
(2 REQ.)
4 HOLES 5.8 THRO'
EQUAL SPACED ON 68 P.C.D
120
Ø70
Ø33
45°
Ø12
60
60
120
5
12
B
SECTION B-B
BEARING HOUSING
SCALE : 1:1
DIMENSIONS IN MM

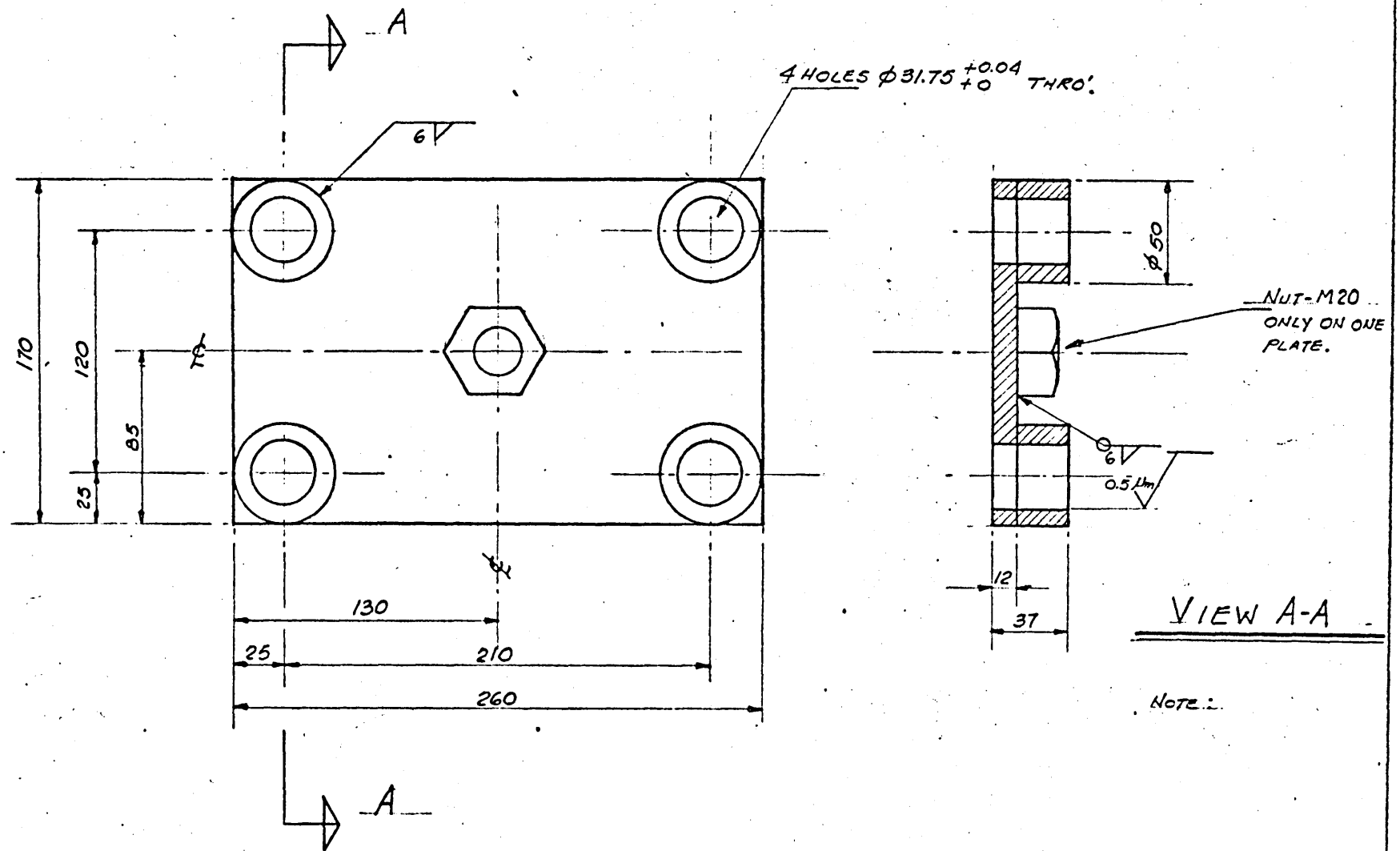

VIEW A-A

Note :-

MATL. MILD-STEEL

PART 7 - SLIDING PLATES

(2 REQ.)

SCALE : 1 : 2

DIMENSIONS : mm

J. PEREZ - July 80

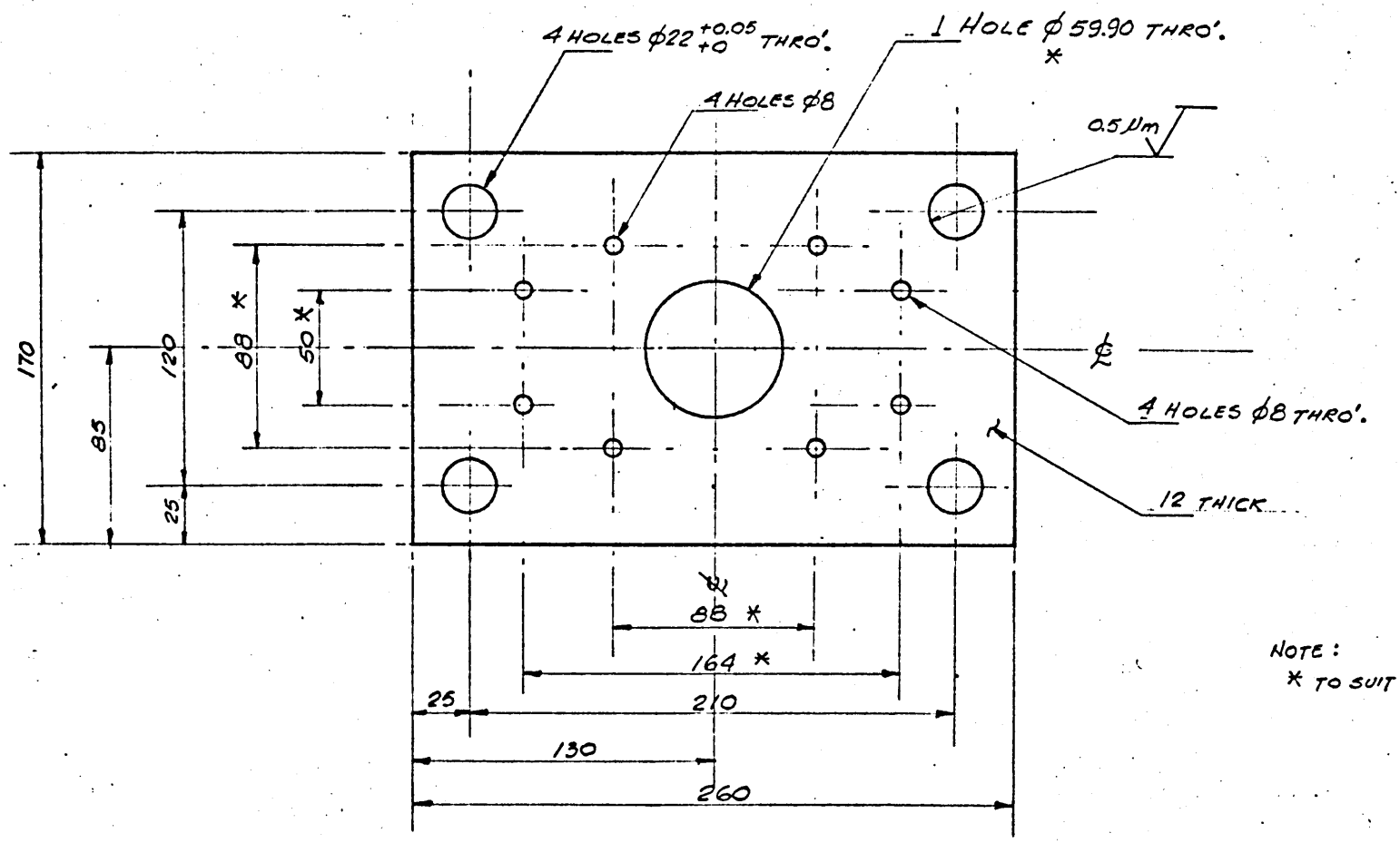

NOTE :
* TO SUIT ON ASSEMBLY.

MATL. MILD-STEEL

PART 7' - CYLINDER BASE PLATE.

(1 REQ.)

SCALE : 1:2

DIMENSIONS : mm

J. PEREZ - JULY 80

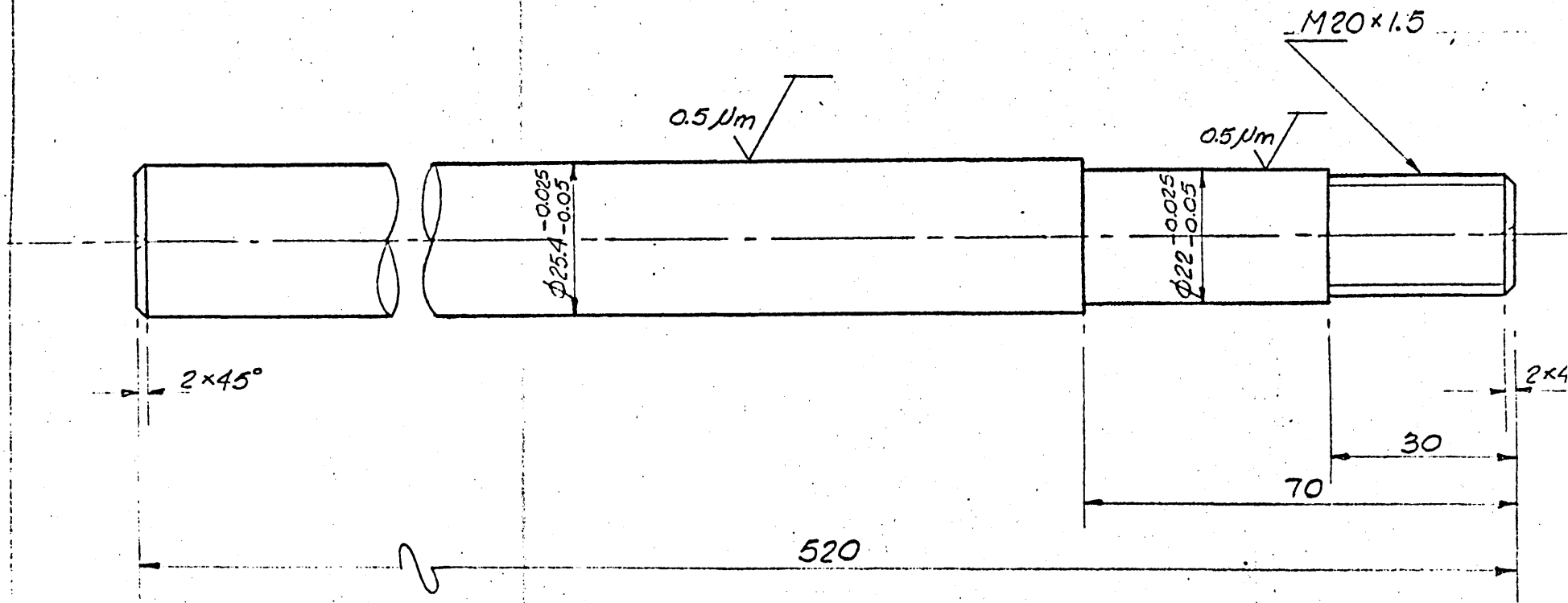

MATL. MILD-STEEL

PART 8 - COLUMN.

(4 REQ.)

SCALE : 1 : 1

DIMENSIONS : mm

J. PEREZ-JUL

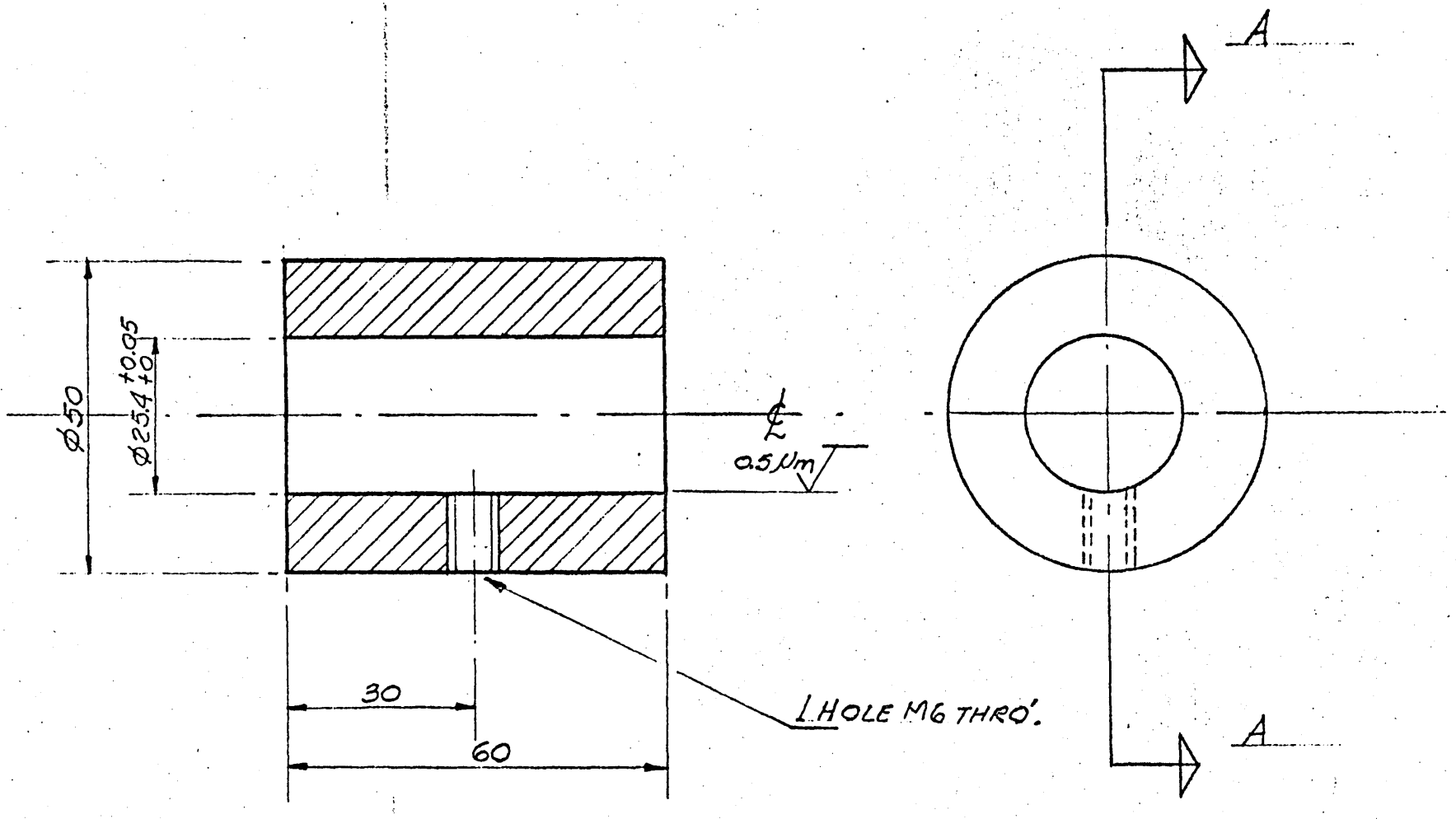

VIEW A-A

PART 9 - COLUMN-SUPPORT

(4 REQ.)

MATL. MILD-STEEL

SCALE : 1 : 1

DIMENSIONS : mm

J. PEREZ-JU

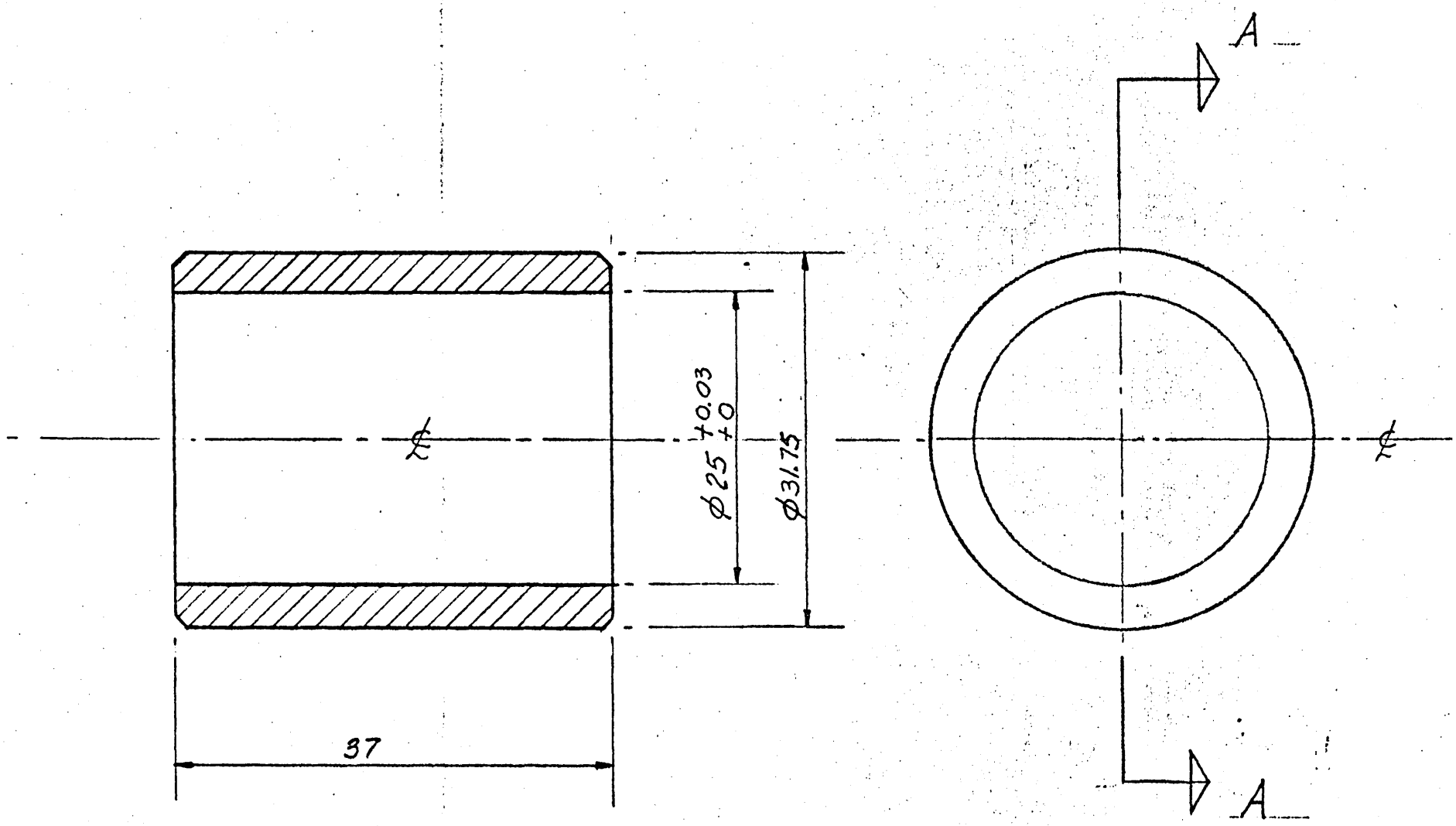

SECTION A-A

MATL. BRONZE

PART 14A - BUSH

(8 REQ.)

SCALE : 2 : 1

DIMENSIONS : mm

J. PEREZ - OCT.

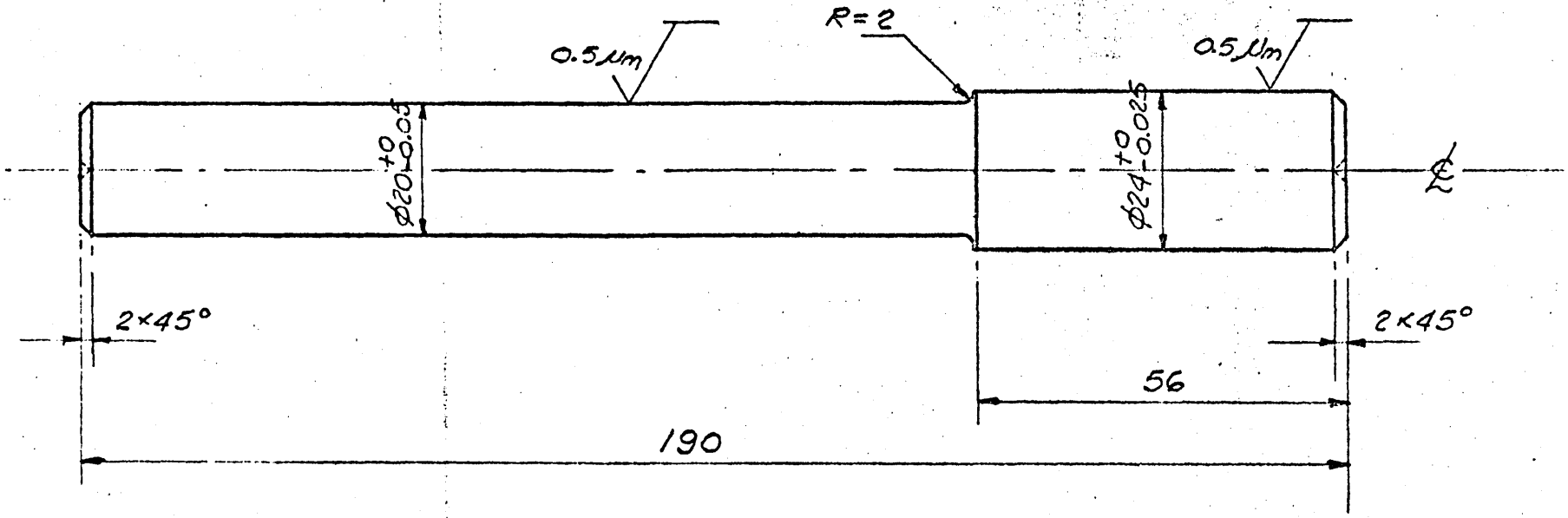

MATL. MILD-STEEL

PART 24 - SECONDARY SHAF

SCALE: 1:1

DIMENSIONS: mm

J. PEREZ - JULY

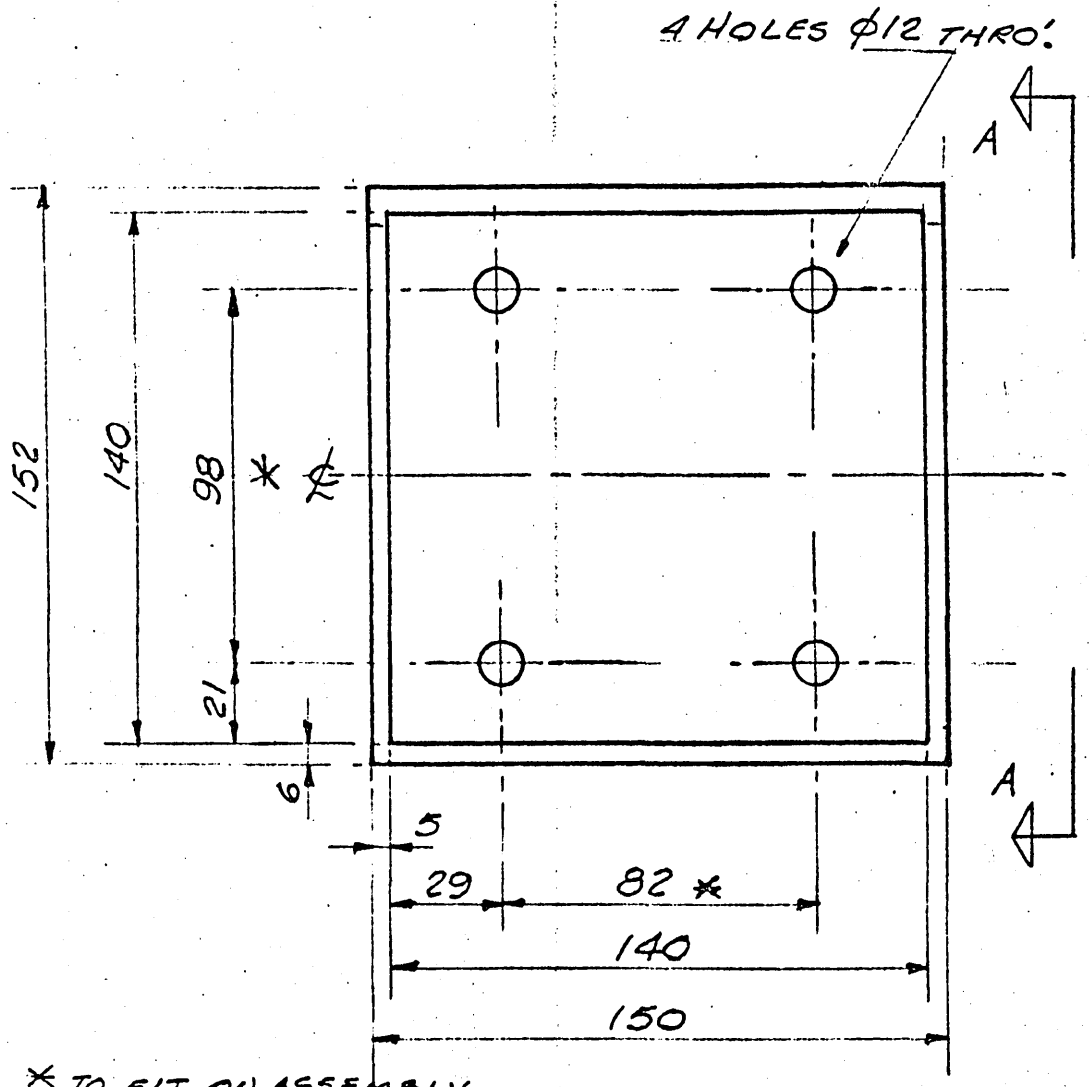

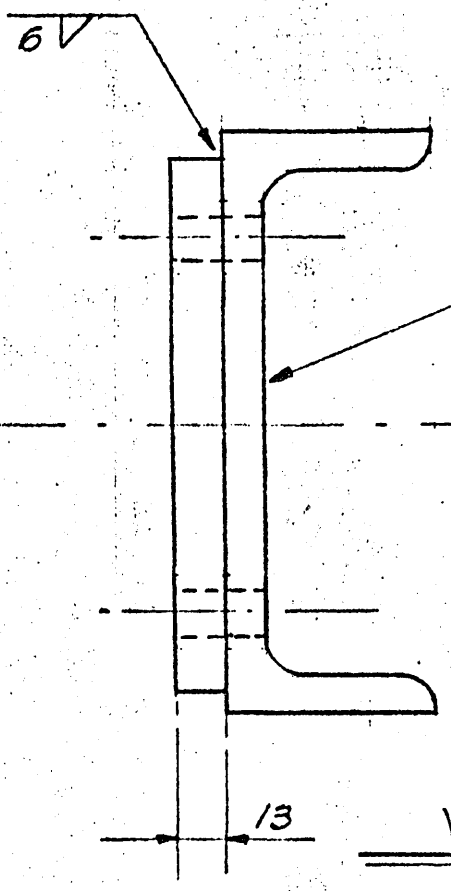

VIEW A-A

PART 25-PILLOW-BLOCKS BAS

MATL. MILD-STEEL

SCALE: 1:2

DIMENSIONS: mm

J. PEREZ-JU

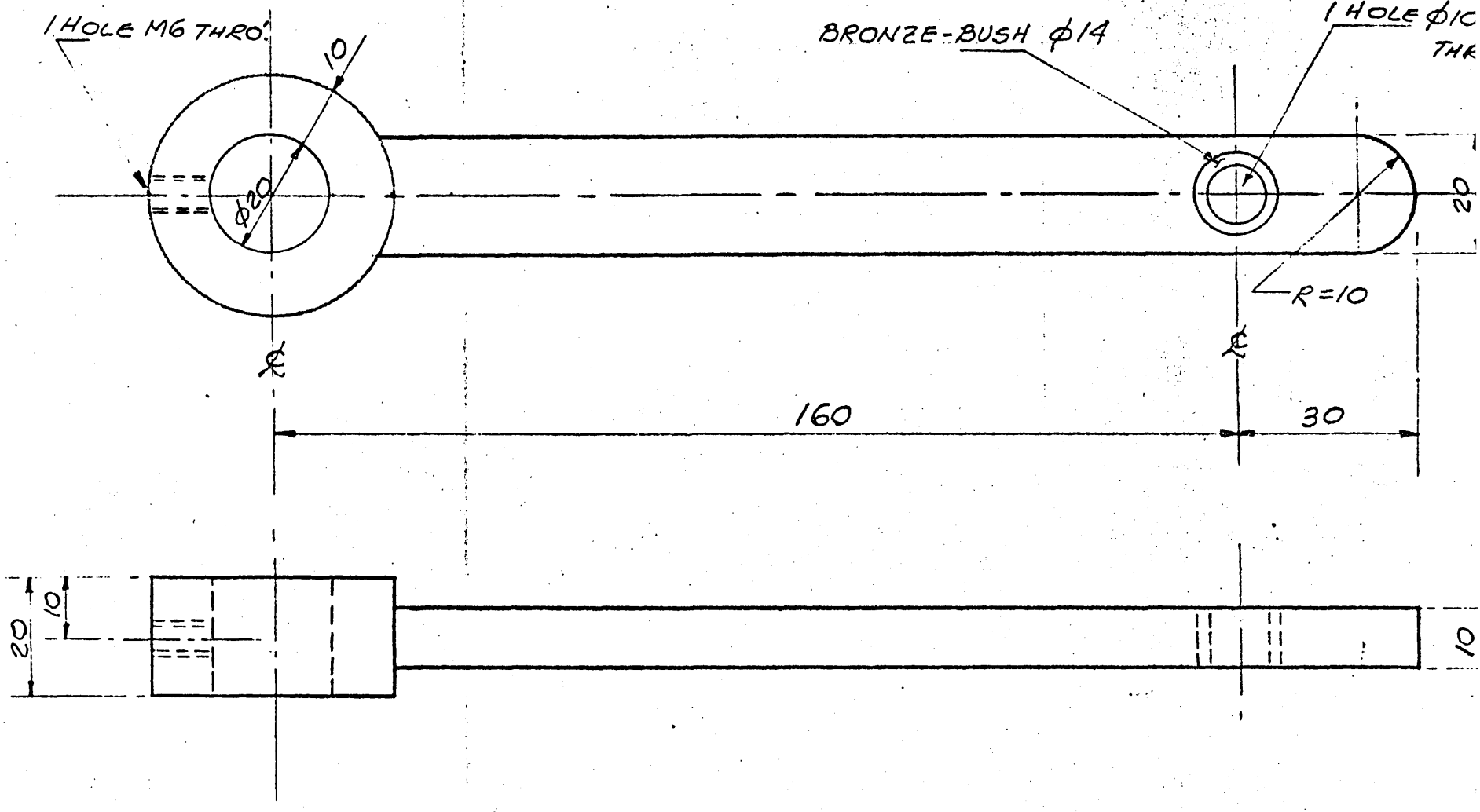

MATL. MILD-STEEL

PART 26 - ROCKER A

SCALE : 1:1

DIMENSIONS : mm

J. PEREZ-JU

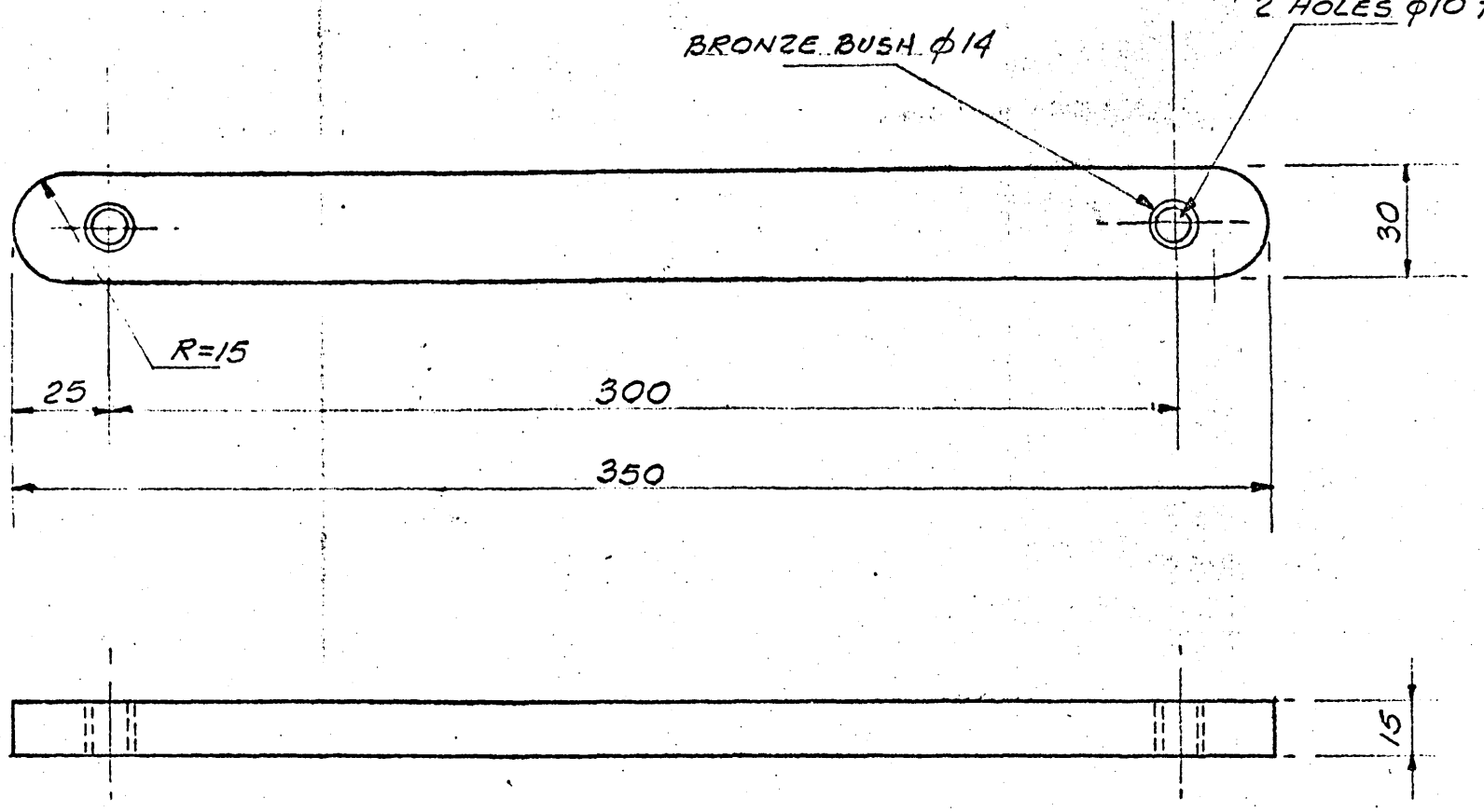

MATL. MILD-STEEL

PART 27 - CONNECTING RO

SCALE: 1:2

DIMENSIONS: mm

J. PEREZ-JUL

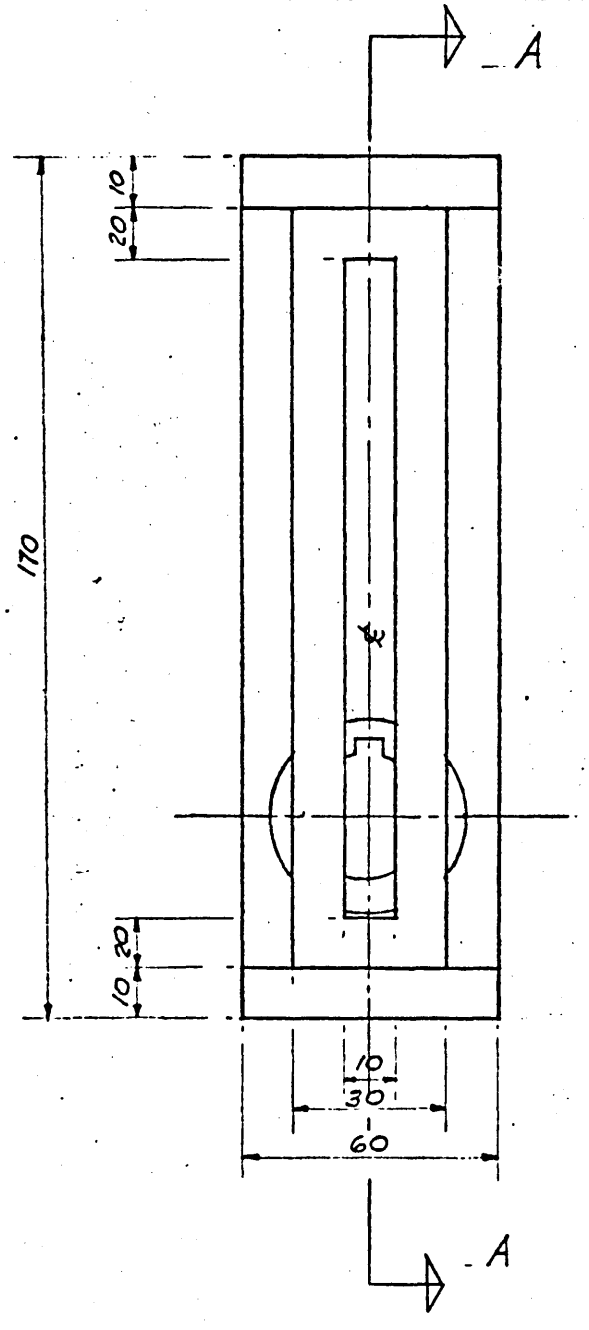

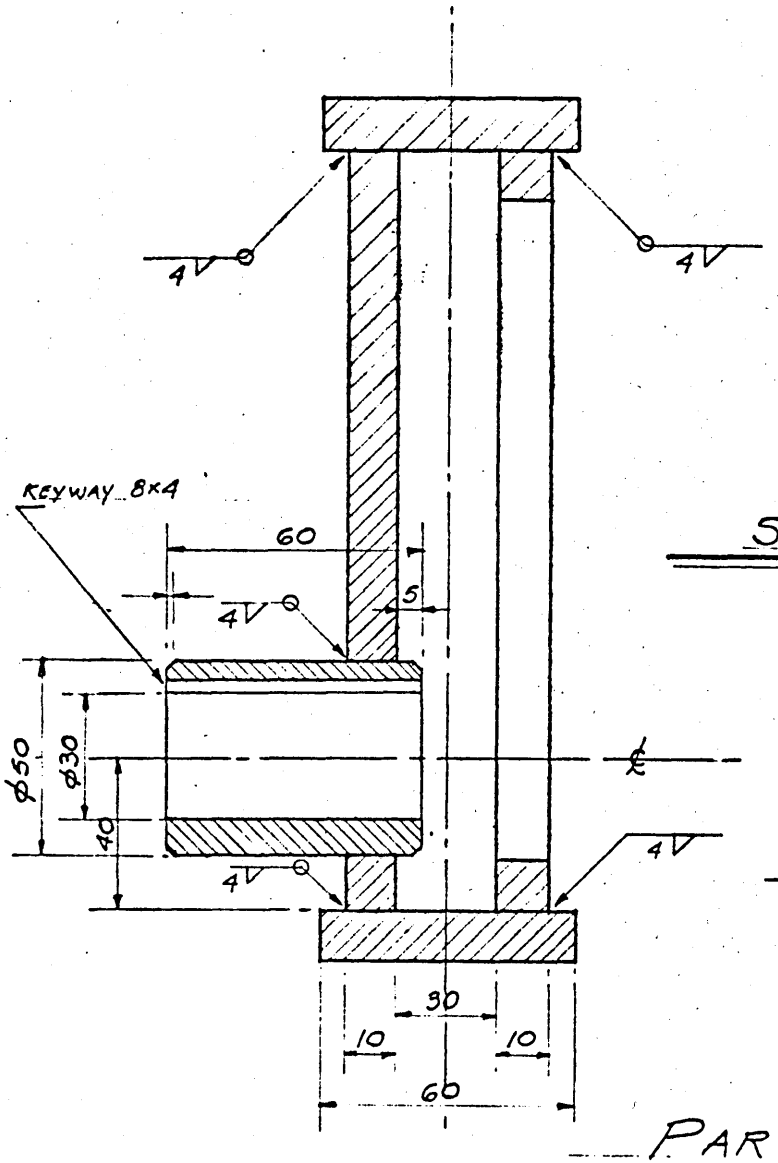

SECTION A-A

MATL. MILD-STEEL

PART 28-CRANK

SCALE: 1:1

DIMENSIONS: mm

J. PEREZ-OCT. 80

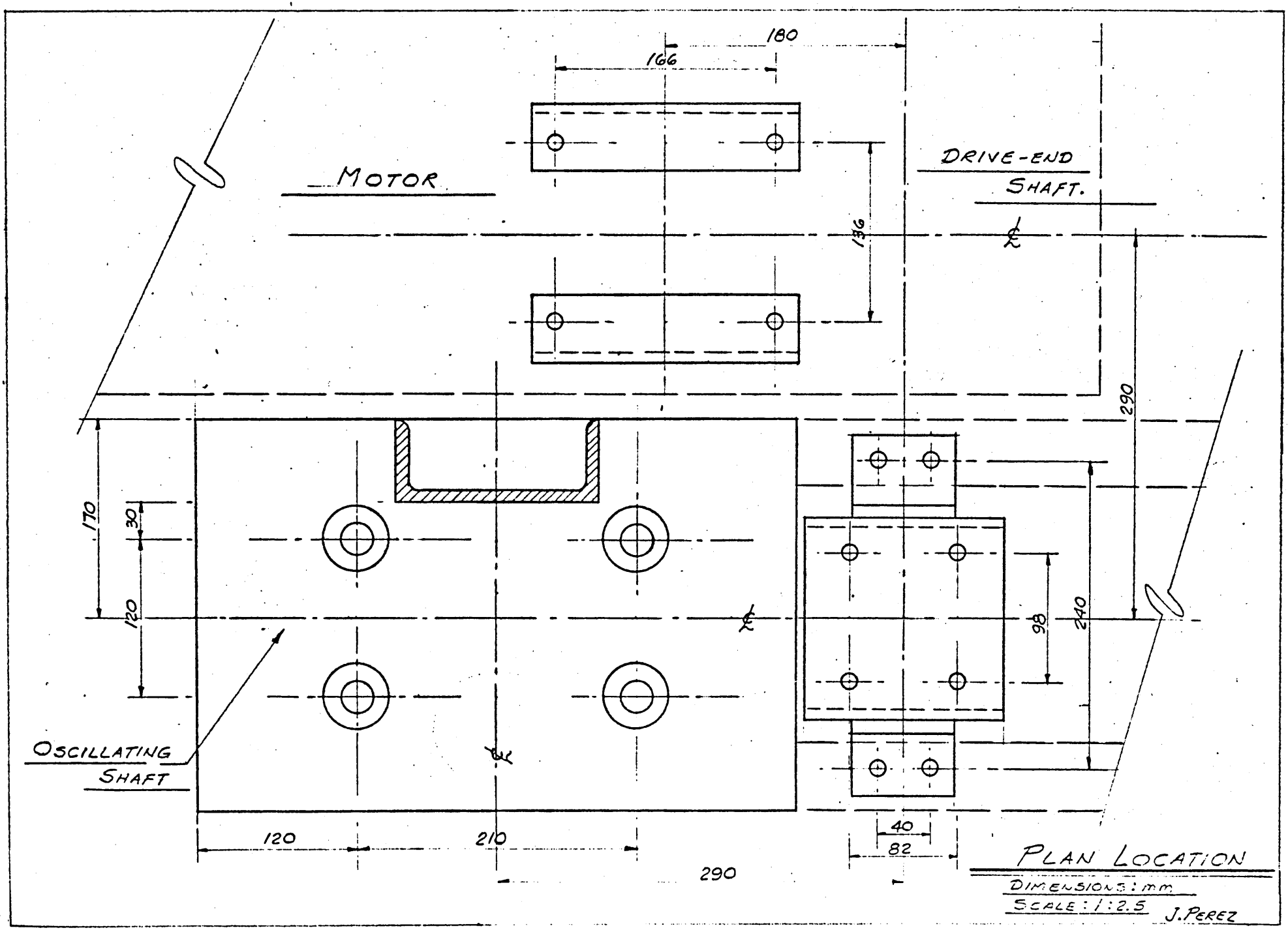
180
166
MOTOR
DRIVE-END
SHAFT.
136
290
170
30
120
98
240
OSCILLATING
SHAFT
120
210
290
40
82
PLAN LOCATION
DIMENSIONS: mm
SCALE: 1:2.5
J. PEREZ

Record of courses attended during period of research.

1. Steel Plant Design module of Post Graduate Diploma in Engineering. Sheffield City Polytechnic. Nov. 1979.

2. Selected lectures on Tribology - course given by G. R. Symmons. Department of Mechanical and Production Engineering. Sheffield City Polytechnic. Jan. 1981.